NUMERICAL LINEAR ELASTIC INVESTIGATION OF STEEL ROOF DECK DIAPHRAGM BEHAVIOUR ACCOUNTING FOR THE CONTRIBUTION OF NON-STRUCTURAL COMPONENTS

By

Simon Mastrogiuseppe

McGill

Department of Civil Engineering and Applied Mechanics

McGill University, Montréal, Québec, Canada

February, 2006

A thesis submitted to the Faculty of Graduate and Postdoctoral Studies in partial fulfillment of the requirements of the degree of Master of Engineering

Your file Votre référence
ISBN: 978-0-494-24996-3
Our file Notre référence
ISBN: 978-0-494-24996-3

ABSTRACT

Dynamic analysis programs and empirical formulae are often used to compute the period of vibration of single-storey steel buildings. Recent ambient vibration tests of buildings in Québec and British Columbia have shown that the predicted period of vibration is typically much longer than that measured. Software and empirical formulae do not usually take into account the stiffening effects of the non-structural components; this could be the source of the discrepancy between the results in the field and the results obtained by computational methods.

This research project concentrates on the roof diaphragm system of single-storey steel buildings and the contribution of the non-structural components to diaphragm stiffness. It is believed that the non-structural components, roofing materials such as gypsum board and fibreboard, add to the overall stiffness of the system. A roofing system called AMCQ SBS-34 consisting of gypsum board, ISO insulation board and fibreboard, all hot bitumen adhered, was studied. The full roof system, as well as its individual components and connections, were first studied through laboratory testing. The flexural and shear stiffness of the fibreboard and gypsum panels, as well as the shear stiffness and equivalent flexural stiffness of the complete roof system and shear stiffness of the roofing connections were determined.

Linear elastic finite element models, using the SAP2000 software, were developed to replicate the behaviour of bare sheet steel and clad diaphragm test specimens. The test based properties of the roofing components and connections were incorporated into the definition of the elements. The models were then calibrated based on the results of large-scale diaphragm tests by Yang. Once the elastic behaviour of the diaphragms had been matched, a parametric study was performed in order to assess the importance of the contribution of the roofing assembly relative to the roof deck panel thickness.

It was shown that as the deck thickness increases, the relative contribution of the non-structural components decreases on a percentage basis, but does not become non-negligible. The increase in shear stiffness of the diaphragm ranges from 58.6% for the 0.76 mm deck panel to 4.7% for the 1.51 mm roof deck panel, dependent on the sidelap and deck-to-frame connection configuration.

RÉSUMÉ

Les programmes d'analyse dynamique et les formules empiriques sont souvent utilisés pour calculer la fréquence naturelle de vibration de bâtiments à un étage en acier. De récents résultats expérimentaux au Québec et en Colombie-Britannique démontrent que ces analyses donnent des périodes beaucoup plus longues qu'avec des tests in-situ. Les programmes d'analyse dynamique et les formules empiriques ne prennent pas en considération les effets de renforcement des éléments non-structuraux : ces éléments pourraient être la source de la différence entre les résultats in-situ et les analyses numériques.

Ce projet porte sur le diaphragme de toit et la contribution des éléments non-structuraux à la rigidité du diaphragme. On croit que les éléments non-structuraux – tels que les matériaux de toiture du type panneaux de gypse ou fibre de bois – ajoutent à la rigidité du système. Une combinaison de toiture appelée AMCQ SBS-34, composée de panneaux de gypse, d'isolant en polyisocyanurate et de fibre de bois, a été étudiée. Les rigidités en flexion et en cisaillement des composantes ont été déterminées séparément; de plus, la rigidité en cisaillement et la rigidité équivalente en flexion de la combinaison de toiture ont été déterminées.

Des modèles éléments finis, bâtis avec le logiciel SAP2000, ont été développés afin de reproduire le comportement du diaphragme de toit sans et avec les composantes non-structurales. Les modèles, une fois bâti, ont été calibrés à partir des données expérimentales obtenues par Yang. Une fois le modèle calibré, une étude paramétrique est effectuée afin de déterminer la contribution relative des éléments non-structuraux à la rigidité totale du diaphragme selon l'épaisseur du tablier métallique.

Il a été démontré que la contribution relative des composantes non-structurales diminue lorsque l'épaisseur du tablier d'acier augmente, mais elle ne devient pas non-négligeable. L'augmentation de la rigidité varie de 58.6% pour le tablier de 0.76 mm d'épaisseur à 4.7% pour le tablier de 1.51 mm, dépendamment de la configuration des connecteurs à la structure et des connecteurs de couture.

ACKNOWLEDGEMENTS

First off, I would like to thank Professor Colin A. Rogers. Without your support, kindness, guidance and constant input, this thesis would never have been completed. Your constant presence during the whole two years of this project made is not only possible, but thoroughly enjoyable. Thank you.

I would also like to mention Professor Robert Tremblay from École Polytechnique de Montréal. Your help in determining the direction of this study as well as for your input along the way were much appreciated.

I would also like to thank the following people:

- Steve Kecani and Eddie Del Campo from the Department of Physics machine shop. Thanks for helping me keep my fingers.
- Ronald Sheppard, Damon Kiperchuk, Marek Przykorski and John Bartczak. Without your help, I would not have finished.
- Denis Fortier for helping me decipher the ASTM drawings.
- Dr. William Cook, for saving my hard drive.
- Everybody in the civil administrative staff.

Special thanks to Camelia Dana Nedisan for your help. It was a pleasure working with you.

The following organizations and companies are highly appreciated for their contributions on this project: the Natural Sciences and Engineering Research Council of Canada (NSERC); The Canam Group Ltd.; Hilti Limited; André at Toitures Couture Inc.; André at Anica Steel Inc.

Last but not least, I would like to thank my family and Caroline for their support and their belief in me.

TABLE OF CONTENTS

LIST OF FIGURES

LIST OF TABLES

LIST OF SYMBOLS

CHAPTER 2

b	Width of diaphragm
E	Young's modulus
g	Acceleration constant, 9.81 m/s^2
G'	Roof diaphragm shear stiffness
h	Height of building
h_n	Height of building above ground level
I	Moment of inertia
K_B	Lateral load resisting system (LLRS) stiffness
K_D	Roof diaphragm stiffness
L	Length of roof diaphragm
l	Width of building
L_d	Diaphragm length perpendicular to the direction of seismic loading
N	Number of stories
W	Seismic weight

CHAPTER 3

Section 3.2

t	Average thickness of shear area
b	Width of specimen
d	Thickness of specimen
F^*	Multiplication factor to compensate for non-uniform stress distribution in small specimens, 1.19
G	Shear modulus
L	Length of specimen
P	Compressive load
r	Measured displacement

Section 3.3

c	distance from neutral axis to extreme fibre
E	Young's Modulus
I	Moment of inertia
L	Span
P	Load
P/Δ	Slope
Sb	modulus of rupture or maximum fibre stress

Section 3.4

n	Speed of crosshead
L	Length of side of shear area
Z	Shear strain rate, taken as 0.005 (mm/mm/min)
K_{iso}	Shear stiffness of polyisocyanurate panel
K_{fb}	Shear stiffness of fibreboard panel
K_{gyp}	Shear stiffness of gypsum board panel
K_{full}	Shear stiffness of non-structural sandwich

CHAPTER 4

L	Model length, 6096 mm
A	Model width, 3657.6 mm
P	Unit point load
S	Unit shear force, P/L
Δ	Y-direction deflection due to P
γ	Shear distortion, Δ/A
G'	Diaphragm shear stiffness
Δ_S	Shear displacement
Δ_D	Diaphragm warping displacement
Δ_C	Connection displacement
E	Young's modulus
t	Base metal thickness
C	Connector slip parameter
s	Girth of corrugation per rib
d	Corrugation pitch
ϕ	Reduction factor based on number of equal spans

CHAPTER 1
INTRODUCTION

1.1 General

Single-storey steel buildings make up a large percentage of the building stock in the light industrial and commercial industry. These buildings can be located in regions of moderate or active seismicity levels, such as the west coast of British Columbia and the St. Lawrence and Ottawa River valleys. The lateral force resisting system is often composed of concentrically braced frames (CBFs) placed on the perimeter of the building and a flexible steel roof deck diaphragm. When these structures undergo wind or earthquake loading, the forces flow from the roof diaphragm into the braced frames and are then transferred to the footings (Figure 1.1). Roof diaphragms are made of corrugated steel deck panels, which are connected to the main structure and to one another. The deck-to-frame connections are typically made with welds, powder actuated nails or screws, whereas the sidelap fasteners are normally clinches, screws or welds. In Canada, non-structural components are then installed above the roof diaphragm to provide fire protection, insulation and a resistance to water penetration (Figure 1.2). The behaviour of roof deck diaphragms has been studied to great extent, starting with Nilson in the 1960s *("Shear Diaphragms of Light Gage Steel", Nilson, 1960).*

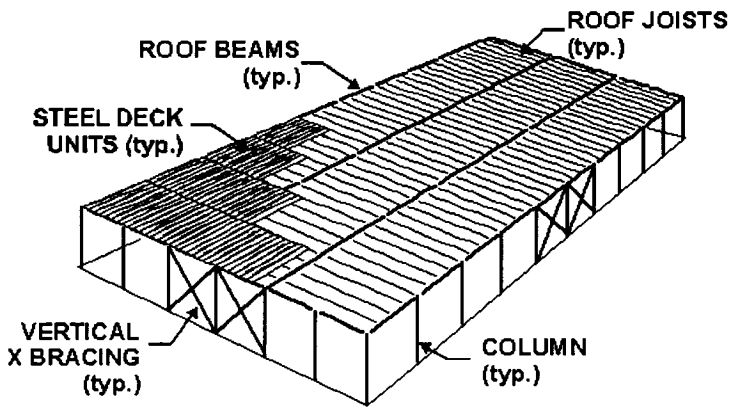

Figure 1.1: Typical structural arrangement of a single storey steel building ***(Rogers & Tremblay, 2000)***

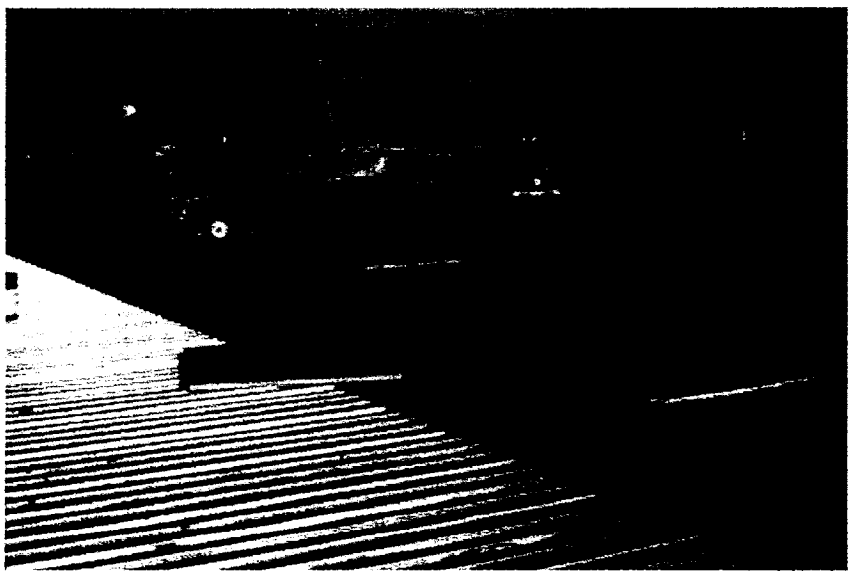

Figure 1.2: Non-structural roofing components

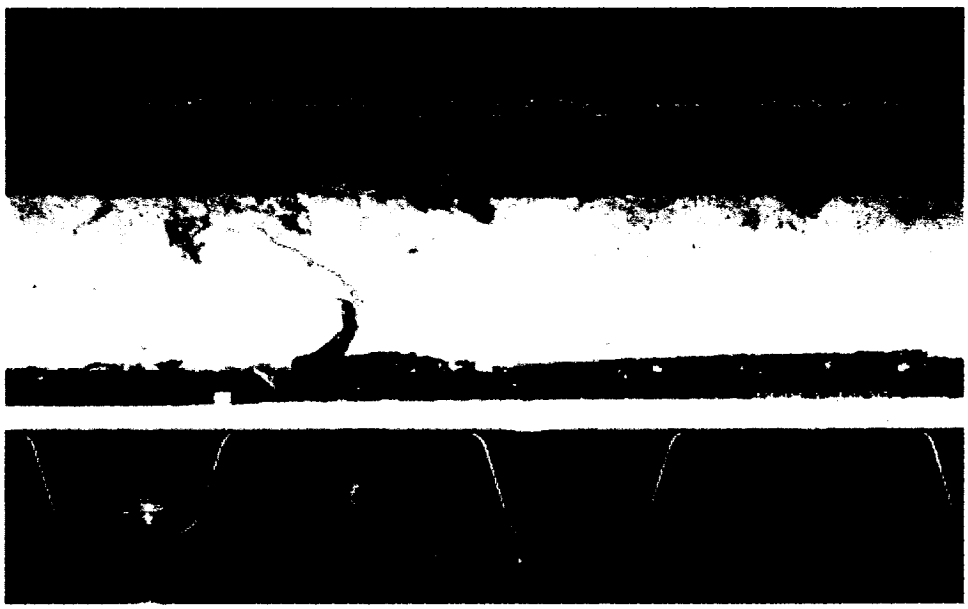

Figure 1.3: Roofing cross-section as tested by Yang (2003)

A research program on the behaviour of roof deck diaphragms under seismic loading has been underway since 1999 at École Polytechnique of Montreal and McGill University. Numerous bare steel diaphragm specimens featuring different connection configurations and deck thickness have been tested to evaluate their inelastic performance (Essa et al. (2001), Martin (2002), Yang (2003)). Yang also carried out tests of two diaphragms that

were constructed with non-structural components (Figure 1.3). It has been shown that there is a significant difference in stiffness, strength and ductility depending mainly on the connection detailing. However, the contribution of the non-structural components to the roof diaphragm stiffness and strength is also of importance. These components cause an increase in both the stiffness and strength according to Yang. Additional studies to identify the period of vibration of low-rise buildings have been completed at the University of Sherbrooke (Lamarche, 2005) and at the University of British Columbia (Turek and Ventura, 2005). These ambient vibration tests have revealed that there exists a discrepancy between the building period used for seismic design, as obtained from the 2005 National Building Code of Canada (NBCC) (NRCC, 2005) and from dynamic analyses, compared with that which the buildings actually possess. It is possible that the non-structural roofing components are, in part, responsible for a shortening of the natural period of vibration.

1.2 Statement of Problem

The opportunity for engineers to carry out dynamic analyses has increased with the advent of powerful analysis tools. In many design situations, it has become necessary to use software to estimate the dynamic characteristics of buildings with non-symmetrical geometry and stiffness discontinuities because they are outside the scope of the building code (NRCC, 2005). However, recent studies have shown that dynamic analyses of single-storey concentrically braced frame (CBF) buildings generate results that differ from in-situ testing.

Analytical studies have found the periods of vibration of low-rise steel buildings to be much longer than in-situ testing: for example, the period of an actual building as obtained from field testing measurements by Ventura (1995) was found to be shorter than that predicted analytically by Medhekar (1997) (Figure 1.4). This difference is usually attributed to the contribution of non-structural components. Single-storey buildings are probably more sensitive to the stiffening effects of architectural components because of their inherent flexibility and lightness. Furthermore, the flexibility of the structure

originates largely from the roof diaphragm. Medhekar and Yang have shown that non-structural roofing components reduce diaphragm flexibility.

Furthermore, in the NBCC, the magnitude of the seismic loads at a given site depends on the fundamental period of vibration of the structure, which is often estimated using the empirical equations that are provided in the building code. These equations have typically been derived for multi-level buildings with rigid floor and roof diaphragms; therefore they do not necessarily represent the behaviour of low-rise steel buildings with flexible roof diaphragms.

At this stage, there remains doubt as to the ability of an engineer to accurately predict the fundamental period of vibration of a low-rise steel building, and hence to determine appropriate seismic loads, because of the influence of flexible roof deck diaphragms and non-structural components.

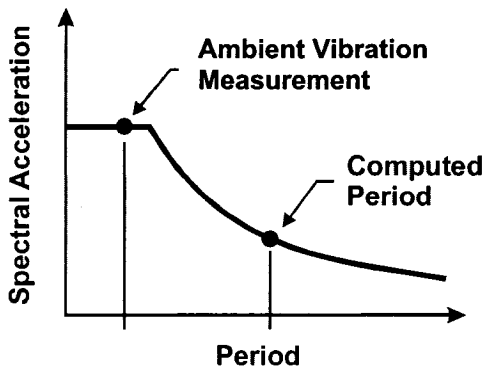

Figure 1.4: Periods of vibration

1.3 Objectives

The overall goal of this research is to provide a better understanding of the effect of non-structural roofing components on the performance of single-storey steel buildings subjected to seismic loading.

The project can be divided into a series of specific objectives as listed below:

a) Determine the material properties for the non-structural roofing components, such as gypsum board and fibreboard, from ASTM standard laboratory tests.
b) Determine the increase in shear stiffness of the diaphragm due to the non-structural roofing materials, adhered together with hot bitumen.
c) Determine the connection properties between the non-structural roofing materials and the steel deck diaphragm, as well as the connection stiffness for deck-to-frame and sidelap connections for different deck thicknesses.
d) Develop a linear elastic finite element model of a roof deck diaphragm that accounts for both the steel panels and non-structural components.
e) Compare the analytical results with the findings of Yang (2003) and Essa et al. (2001) and stiffness values obtained with the Steel Deck Institute (SDI) equations. Using the model, carry out a parametric study of diaphragm systems with different deck thickness and connection patterns to establish the contribution of the non-structural elements to initial shear stiffness.

1.4 Scope and Limitation of Study

The scope of this project is limited to the materials typically used in the construction of roof deck diaphragms in Canada. The non-structural roofing components are those used in the construction of an AMCQ SBS-34 roof as tested by Yang. The gypsum board is 12.7 mm (½") type X, produced by *CGC* under the brand name *Sheetrock*, and the fibreboard is *Cascade Securpan* 1". The steel roof deck panels specified for study were those most commonly found in Canada. Four thicknesses of a 38 mm deep deck were considered: 0.76 mm, 0.91 mm, 1.22 mm and 1.51 mm. The deck-to-frame fasteners were Hilti X-EDNK-22 THQ 12M powder actuated nails. The gypsum-to-deck connectors used were SFS intec *#12 hex with round galvalume plates*, produced under the Deckfast™ trademark. Hilti S-MD 12-14 X 1 HWH #1 screws were used for the sidelap connections.

The SAP2000 finite element model was developed to reproduce the diaphragm tests, 3658 mm wide by 6096 mm long (12' X 20'), conducted by Yang, Essa and Martin. Analyses of the model were conducted in order to obtain the initial linear elastic response

of the roof deck diaphragm as opposed to the inelastic performance as studied by Essa, Martin and Yang. Furthermore, the SDI design method for deck diaphragm stiffness (1991) was used to evaluate the stiffness of models for which no test results existed.

1.5 Thesis Outline

This thesis is concerned with the contribution of non-structural components to roof diaphragm shear stiffness in single-storey concentrically braced frame (CBF) steel structures. It is divided into three main parts:

Chapter 2 is a review of previously completed research on roof diaphragm behaviour and on dynamics of low-rise steel buildings.

Chapter 3 focuses on the experimental programs conducted to identify the material properties of the non-structural roofing components, as well as the stiffness of the diaphragm connections.

Chapter 4 describes the development of the finite element model and the numerical analyses of roof deck diaphragms with and without non-structural components. A comparison of the analytical results with the full-scale diaphragm tests conducted by Yang (2003) and Essa et al. (2001), as well as with the computed SDI values is also provided. A parametric study of the contribution to shear stiffness of non-structural components is also carried out, for which various diaphragm configurations are considered.

Chapter 5 lists the conclusions of the study and highlights recommendations for further research in this field.

CHAPTER 2
LITERATURE REVIEW

2.1 General

Johnson and Converse (1947) were the first to carry out the testing of cold formed steel diaphragms. Since then, an important and large body of work has been compiled. This Chapter will review some of the research on cold formed steel deck diaphragms that has been completed over the years. Emphasis is placed on the previous studies by Rogers and Tremblay (2000, 2003a,b), Essa *et al.* (2001, 2003), Martin (2002) and Yang (2003) that form the initial phases of the single-storey steel structure / flexible roof diaphragm research project at École Polytechnique and McGill University.

2.2 Nilson

Nilson's publication "Shear Diaphragms of Light Gage Steel" (1960) was the first substantial test program on steel deck diaphragms. He developed two test approaches (cantilever and simple beam) that are still used by researchers to this day. Both test setups are now included in the ASTM E455 (2002) Standard.

Nilson carried out 39 monotonic tests of bare sheet steel diaphragms. He wrote that *"diaphragm strength of floor and roof elements can be utilized to resist horizontally applied loads"* and *"be effective as shear diaphragms"*. However, Nilson declared that the analysis of steel deck diaphragms is not feasible, as it is made up of many small parts and stress concentrations at the welded connections. He also suggested using the cantilever test frame rather than the simple beam. Nilson concluded that full-scale tests are still the most reliable method to evaluate diaphragm behaviour.

2.3 Luttrell

Luttrell has been involved in the study of steel deck diaphragm design since the sixties and has been technical advisor to the Steel Deck Institute (SDI) since 1965. A large proportion of his research has been the testing of roof deck diaphragms and their connections, from which he derived the SDI design method for light gauge steel roof diaphragms *(SDI, 1981, 1991)*. The SDI method is commonly used by structural

engineers in North America for the design of diaphragms. The overall in-plane shear stiffness of a bare sheet steel diaphragm depends on the type of panel, the number of panels, the number of fasteners per panel, the stiffness of the fasteners (both deck-to-frame and sidelap), as well as the dimensions of the diaphragm. For a full review of the SDI design method by Luttrell the reader is referred to the thesis of Nedisan (2002).

Luttrell also mentions that non-structural members may increase in-plane shear stiffness and strength. He states that "*systematic attachment of rigid flat panels to the top corrugations of a diaphragm can increase both diaphragm strength and stiffness. [...] Properly located attachments through the panels and into the tops of the deck corrugation, particularly on the diaphragm perimeter, limit warping and increase shear stiffness" (Luttrell, 1995).*

2.4 Tremblay and Stiemer

The non-linear response of 36 rectangular single-storey steel buildings subjected to historical earthquake ground motion records was examined by Tremblay and Stiemer (1996). The lateral load resisting systems of these structures were made up of a flexible metal roof diaphragm and vertical bracing located along the exterior walls. Periods of vibration of these buildings were computed firstly by assuming that the roof diaphragm was perfectly rigid and secondly, by assuming that a flexible roof diaphragm existed. Tremblay and Stiemer noted that the influence of the diaphragm is very clear: the period of vibration of the structures increased dramatically. The period of vibration, when accounting for the flexible diaphragm, was on average 1.5 times longer than with a rigid diaphragm in the short direction of the building, and between 2 and 3 times longer in the other direction. The study showed that diaphragm flexibility influenced the overall lateral stiffness of a structure, and hence, should be taken into account when computing the period of vibration of steel single-storey buildings.

2.5 Medhekar

Medhekar's thesis entitled "Seismic evaluation of steel building with concentrically braced frames" contained the findings of an investigation into the behaviour of single-

storey and two-storey steel buildings with concentrically braced frames (CBFs) designed according to the 1995 NBCC (NRCC, 1995) provisions and the S16.1-94 Standard (CSA, 1994). Medhekar also reviewed a seismic design method based on displacement limits rather than force limits (Medhekar, 1997; Medhekar and Kennedy, 1999).

His study of single-storey CBF steel buildings showed that the roof diaphragm flexibility has a significant impact on the overall period of vibration of the building. Based on Medhekar's work, Tremblay et al. (2000) established the following equations to determine the period based on a combination of the bracing and diaphragm stiffness:

$$T = 2\pi\sqrt{\frac{(K_B + K_D)}{K_B K_D}\frac{W}{g}} \qquad (2\text{-}1)$$

where:

$$K_D = \frac{\pi^2}{\frac{L^3}{\pi^2 EI} + \frac{L}{G'b}} \qquad (2\text{-}2)$$

where:

K_B = lateral load resisting system (LLRS) stiffness,

K_D = roof diaphragm stiffness,

W = seismic weight,

L = length of roof diaphragm,

G' = roof diaphragm shear stiffness,

E = modulus of elasticity of steel deck,

I = steel deck equivalent inertia,

b = diaphragm width.

Furthermore, Medhekar accounted for the contribution of non-structural components to overall building stiffness, and more specifically, included the shear stiffness of the gypsum board to the in-plane roof diaphragm shear stiffness. He evaluated the in-plane shear stiffness of the gypsum board to be 1.1 kN/mm. This value was based on a tangent modulus of rigidity of 69 MPa.

2.6 Rogers and Tremblay

Rogers and Tremblay (2000, 2003a, b) conducted 189 steel deck connection tests, 45 of which were sidelap connections (16 screws, 20 button punches, 9 welds) and 144 deck-to-frame connections (47 screws, 71 powder actuated fasteners (nails), 26 welds). Five loading protocols were used: monotonic, quasi-static, 0.5Hz cyclic, 3Hz cyclic and simulated earthquake motion.

Table 2.1: Connection stiffness values *(Rogers and Tremblay, 2003)*

Connection Type	Computed (kN/mm)	SDI (kN/mm)
Sidelap		
0.76 X 38 - button punch	0.35	1.00
0.91 X 38 - button punch	0.71	1.06
0.76 X 76 - button punch	0.16	1.00
0.76 X 76 - button punch	0.25	1.06
0.76 X 38 - 10-14x7/8" screw	1.35	9.90
0.91 X 38 - 10-14x7/8" screw	2.26	10.6
0.76 X 38 - weld	1.26	23.9
Deck-to-Frame		
PAF		
0.76 X 3mm plate - Hilti X-EDNK22-THQ12	23.2	23.9
0.76 x 3mm PLATE - Buildex BX12	28.2	23.9
0.91 X 3mm plate - Hilti X-EDNK22-THQ12	23.9	25.5
0.91 x 3mm PLATE - Buildex BX12	30.5	25.5
0.76 X 20mm plate - Hilti X-ENPH2-21-L15	13.0	23.9
0.76 x 20mm PLATE - Buildex BX14	14.6	23.9
0.91 X 20mm plate - Hilti X-EDNK22-THQ12	23.8	25.5
0.76 x 3mm PLATE - Buildex BX14	18.7	25.5
0.76[1] X 3mm plate - Hilti X-EDNK22-THQ12	11.8	23.1
Screw		
0.76 X 3mm plate - 12-14 X 1"	25.7	23
0.76 X 3mm plate - 12-24 X 7/8"	43.3	23
0.91 X 3mm plate - 12-14 X 1"	21.4	24.5
0.91 X 3mm plate - 12-24 X 7/8"	36.6	24.5
Weld		
0.76 X 3mm plate	25.5	26
0.91 X 3mm plate	31.8	27.7
0.76 X 20mm plate	38	26

The obtained data revealed that the type of fastener influences the ultimate capacity, stiffness and energy dissipating characteristics of the connection. For sidelaps, the welded connections could absorb the greatest amount of energy, followed by button punched connections and finally screwed connections. For the deck-to-frame connections, the nailed connections proved to be the most effective energy dissipating connector, followed closely by the screwed connections. The welded connections showed significant ultimate capacities but very low ductility, failing at small displacements when subjected to repeated loads, thus exhibiting low energy dissipation.

The data obtained from these tests is critical in the building of a finite element model that will accurately recreate the actual behaviour of steel deck roof diaphragms. Although tests were performed on connection specimens for this research project, this data was used to build preliminary models. Some of the values obtained from their tests are presented in Table 2.1.

2.7 Essa *et al.*

The main objective of the research program was to investigate the overall behaviour of the shear diaphragm, focussing on the energy dissipating capability, ductility, stiffness and ultimate capacity. Other than overall behaviour of the diaphragm, connection stiffness was also investigated: comparisons of SDI (1991) and CSSBI (1991) diaphragm strength, S_u, and shear stiffness, G' as defined previously, predictions were made with test based values (Essa et al., 2001, 2003).

Eighteen full-scale (3.66 x 6.09 m) cantilever bare steel diaphragm tests were conducted: 16 of which were constructed of 0.76 mm panels and 2 with 0.91 mm panels. Both standard (interlock) and B-deck (nestable) panels with a 38 mm deep profile were used. A variety of connections were placed; for sidelap connectors, welded, button punched and screwed connections were installed and for the deck-to-frame connectors, welds, welds with washer, screws and nails were used. Of each connection configuration, two specimens were tested: one loaded monotonically and the other with a quasi-static reversed cyclic load protocol.

The test results showed that diaphragms with welded deck-to-frame fasteners have low ductility and cannot sustain cyclic loading at relatively large displacement amplitudes. Strength and failure modes are loading dependent. Nailed, screwed and welded-with-washer connections increase strength, stiffness and energy dissipation characteristics of the diaphragm considerably (Table 2.2).

Table 2.2: Test series results conducted by Essa *et al. (2001, 2003)*

Test	Sidelap	Frame	Deck Profile	S_u (kN/m)	G' (kN/mm)
38-76-6-WB-M-1	B.P.	Welded	Standard	8.05	2.328
38-76-6-WB-Q-2	B.P.	Welded	Standard	7.53	2.342
38-76-6-SS-M-3	Screwed	Screwed	B	14.2	4.169
38-76-6-NS-M-4	Screwed	Nailed (H)	B	12.3	3.782
38-76-6-BS-M-5	Screwed	Nailed (B)	B	11.5	3.968
38-76-6-SS-Q-6	Screwed	Screwed	B	12.7	3.965
38-76-6-NS-Q-7	Screwed	Nailed (H)	B	12.2	3.479
38-76-6-NS-Q-8	Screwed	Nailed (B)	B	12.3	3.651
38-76-6-WW-M-9	Welded	Welded	Standard	12.1	2.958
38-76-6-W'W-M-10	Welded	Welded	Standard	14.7	3.423
38-76-6-WS-M-11	Screwed	Nailed (H)	B	18.2	3.144
38-76-6-WW-Q-12	Welded	Welded	Standard	11.4	2.763
38-76-6-W'W-Q-13	Welded	Welded	Standard	13.2	3.197
38-76-6-WS-Q-14	Screwed	Welded	B	13.1	3.015
38-76-6-W'S-M-15	Screwed	Welded	B	19.0	4.322
38-76-6-W'S-Q-16	Screwed	Welded	B	18.8	4.084
38-91-6-NS-M-17	Screwed	Nailed (H)	B	14.6	4.442
38-91-6-NS-Q-18	Screwed	Nailed (H)	B	15.6	5.011

2.8 Martin

The objective of Martin's (2002) research project was to evaluate the ductile performance of roof deck diaphragms depending on the type of deck-to-frame and sidelap connector used. The chosen deck-to frame connectors were the following: welded, welded with washer, screwed, nailed with Hitli and Buildex nails. Sidelaps were either screwed, welded or button punched. Nineteen full-scale (3.66 x 6.09 m) cantilever bare steel diaphragm tests were conducted; 17 with 0.76 mm deck and 2 with 0.91 mm deck. There were two loading protocols, monotonic and reversed cyclic quasi-static.

The experimental data showed that roof diaphragms made with button punched sidelap and welded deck-to-frame connections must remain in the elastic range to resist seismic loading. However, roof diaphragms with nailed deck-to-frame connections and screwed sidelaps can undergo inelastic deformation while maintaining enough capacity to resist the seismic loads. The results of the tests conducted by Martin are shown in Table 2.3.

Table 2.3: Large-scale diaphragm test series by Martin *(2002)*

Test	Sidelap	Frame	Deck Profile	S_u (kN/m)	G' (kN/mm)
38-91-6-NS-M-19	Screwed	Nailed (H) (1)	B	16.7	4.13
38-76-6-WB-SD-20	B.P.	Welded (2)	Standard	9.81	2.44
38-91-6-WB-SD-21	B.P.	Welded (2)	Standard	13.8	3.16
38-91-6-W'W-M-22	W.W.W. (3)	W.W. washer (4)	B	32.1	4.54
38-91-6-W'W-SD-23	W.W.W. (3)	W.W. washer (4)	B	34.6	4.60
38-91-6-W'W-LD-24	W.W.W. (3)	W.W. washer (4)	B	33.2	4.36
38-91-6-NW-M-25	W.W.W. (3)	Nailed (H) (5)	B	22.5	4.33
38-91-6-NW-SD-26	W.W.W. (3)	Nailed (H) (5)	B	26.5	4.09
38-91-6-NW-LD-27	W.W.W. (3)	Nailed (H) (5)	B	26.2	3.64
38-76-6-NS-SD-28	Screwed	Nailed (H) (1)	B	14.1	2.45
38-76-6-NS-LD-29	Screwed	Nailed (H) (1)	B	13.6	2.37
38-76-6-NS-M-30 (6)	Screwed	Nailed (H) (1)	B	23.4	13.5
38-76-6-NS-SD-31 (6)	Screwed	Nailed (H) (1)	B	26.5	15.0
38-76-6-NS-LD-32 (6)	Screwed	Nailed (H) (1)	B	34.4	18.3
38-91-6-NS-SD-33 (6)	Screwed	Nailed (H) (1)	B	35.2	18.4
38-91-6-NS-SD-34	Screwed	Nailed (H) (1)	B	17.0	4.01
38-91-6-NS-LD-35	Screwed	Nailed (H) (1)	B	17.3	3.90
38-76-6-WB-SD-36	B.P.	Welded (2)	Standard	5.80(7a) 5.69(7b)	2.40(7a) 0.94(7b)
38-91-6-WB-M-37	B.P.	Welded (2)	Standard	12.6	3.32

(1): Used Hilti (H) X-EDNK22-THQ12 fastener for nailed frame connection and 12-14-7/8" fastener for screwed sidelap connections.
(2): Welded frame connections were made with 16 mm diameter arc spot welds.
(3): Welded sidelap connection with washers
(4);: Welded frame connections with washers.
(5): Used Hilti (H) X-EDNK22-THQ12 fastener for nailed frame connections.
(6): All fasteners spaced at 152 mm o/c in both directions, spacing in all others tests equal to 305 mm.
(7): 200 cycles at 0.4 γ_u (a) and 2 cycles at 0.6 γ_u (b) prior to short duration loading protocol.

Martin looked at the inelastic performance of the seismic force resisting system when the diaphragm was selected as the energy dissipating element by means of dynamic analyses with the software Ruaumoko (Carr, 2000). He showed that only certain connection

configurations (nail & screw) could be relied on to obtain the ductility needed to specify force modification factors greater than one for seismic design. However, the diaphragm element used in the non-linear time history dynamic analyses was calibrated from the results of the tests by Essa *et al.*. No account of the effect of the non-structural roofing components was made.

2.9 Nedisan

The objective of this project was to conduct numerical analyses of single-storey steel buildings with flexible diaphragms (Nedisan, 2002). The first stage of this project was to develop a better understanding of the SDI equations for the calculation of roof diaphragm stiffness and strength. As a second stage, periods of vibration were calculated for structures using three methods: a DRAIN-2D analysis model, the formula developed by Medhekar (1997) and the FEMA273 (1994) equation. All methods gave similar results for six buildings, while using both the 1995 NBCC and the 2005 NBCC (NRCC, 2005). Nedisan, using the equations developed by Medhekar (1997), then calculated periods of vibration of buildings and compared the values obtained to shake table tests conducted by Tremblay and Bérair (1999). The results obtained by the equations were very similar to the test results obtained by Medhekar.

2.10 Yang

Yang (2003) conducted 12 large-scale roof diaphragm tests under both monotonic and reversed cyclic quasi-static loading. A total of 10 specimens consisted of bare steel roof deck; however two of the diaphragms were constructed with the non-structural roofing components. Roof construction can vary significantly from one project to another, thus after conducting an extensive literature review and consulting with the Ontario Industrial Roofing Contractors Association (OIRCA) and the Association des Maîtres Couvreurs du Québec (AMCQ), the AMCQ SBS-34 roofing system was chosen. It is a common and conventional system composed of the following layers:

- Two layers (4 mm + 2.2 mm) of SBS waterproof membrane;

- One layer of 25 mm (1") thick 1219.2 mm by 1219.2 mm (4'x4') non-flammable wood fibreboard, hot bitumen adhered;
- One layer of 63.5 mm (2.5") thick polyisocyanurate (ISO) insulation, hot bitumen adhered;
- Two layers of paper vapour retarder (No. 15 asphalted felts), hot bitumen adhered;
- One layer of 12.7 mm (½") thick 1219.2 mm by 2438.4 mm (4'x8') type X gypsum board, 12 screws per panel mechanically fastened;
- Steel deck.

The bitumen used was Type 2 asphalt conforming to CSA A123.4 (Baker, 1980). A cross-section of the final roof diaphragm specimen tested by Yang is shown in Figure 2.1.

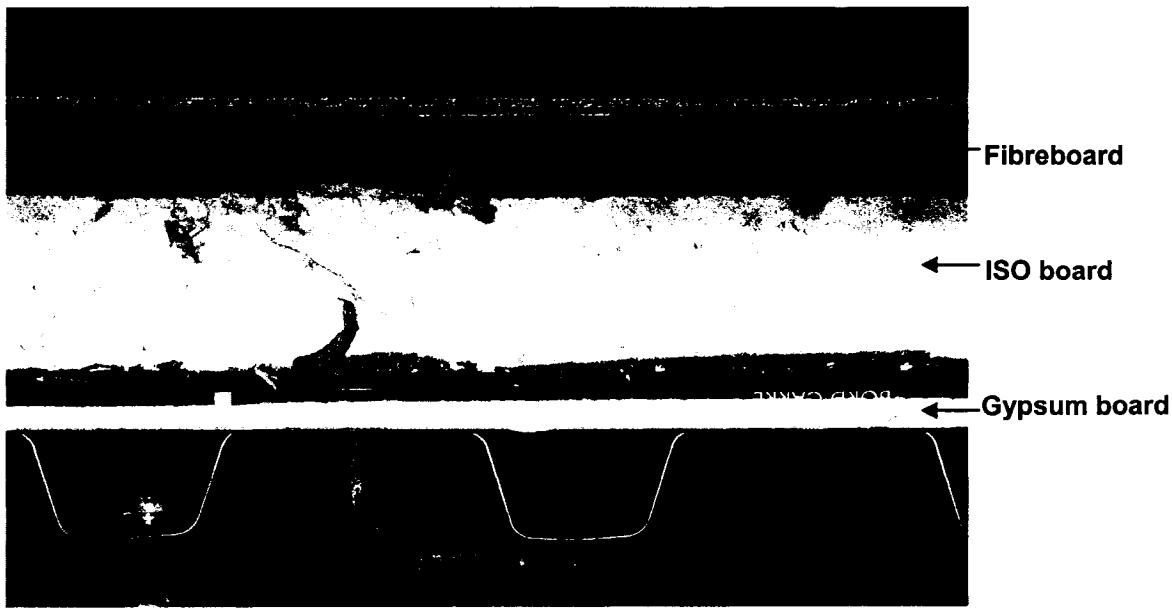

Figure 2.1: Roof cross-section tested by Yang *(2003)*

Test specimens were constructed with various connection detailing, end lap conditions, loading and deck thickness / height. The deck-to-frame connectors consisted of Buildex powder actuated fasteners, Hilti powder actuated fasteners or welds. The sidelap connections consisted of screwed fasteners (Hilti or Buildex screws) or button punches.

Three loading protocols were used: monotonic, seismic short duration loading or a cyclic load protocol followed by a monotonic loading.

The test specimens were divided into four groups. Group 1 consisted of a single test, specimen 38, which had screwed sidelap connections, Buildex powder actuated fasteners (PAF) for the deck-to-frame connectors and P3615-B 0.91 mm thick steel deck. It underwent the short duration seismic loading developed by Martin (2002), which lasts 25 seconds.

Group 2 contained four test specimens, tests 39 to 42. The defining characteristic was that there was a longitudinal overlap at the mid-point of the specimens. Two specimens had screwed sidelap connections and Hilti PAF deck-to-frame connections. The first of the two was tested with a monotonic loading protocol; the second with a short duration seismic loading protocol. The two others had button punched sidelap connections and welded deck-to-frame connections. As with the two previous specimens in Group 2, the first specimen was loaded monotonically and the second underwent a short duration seismic loading protocol. All specimens were constructed with P3615-B 0.76 mm steel deck.

Tests 43 to 46 made up Group 3. All tests had screwed sidelap connectors and Hilti PAFs for the deck-to-frame connectors and used a P3615-B 0.76 mm sheet steel deck. Tests 43 and 44 were bare sheet steel, whereas tests 45 and 46 had the non-structural roofing components added. Tests 43 and 45 were loaded monotonically and tests 44 and 46 were loaded using a cyclic loading protocol followed by a monotonic loading. These tests were done in order to determine the contribution of the non-structural components to overall in-plane strength and stiffness.

The three final tests were compiled in Group 4. All were button punched for sidelap and all had welded deck-to-frame connections. Tests 47 and 48 had P2436 0.76 mm deck whereas test 49 was made of P2436 0.91 mm deck. Tests 47 and 49 were tested with a

monotonic load protocol, while specimen 48 was tested with a short duration seismic loading protocol.

The main topic of research was the inelastic behaviour of steel roof deck diaphragms. In testing, it was found that the non-structural components, if appropriately fastened to the steel roof deck, increased both the in-plane shear strength and stiffness of the diaphragm. In this test model, gypsum board fastened by screws to the steel deck was found to influence the diaphragm properties to the greatest extent. An increase of the mean strength of approximately 26% was realised, in addition to a mean stiffness increase of near 46% for the tested diaphragms.

The stiffness results obtained from this series of tests are the basis of the numerical study that is carried out in this project. The results of the test series are provided in Table 2.4.

Table 2.4: Large-scale diaphragm test series by Yang *(2003)*

Group	Test	Sidelap	Frame	Deck Profile	S_u (kN/m)	G' (kN/mm)
1	38-91-6-NS-SD-38	Screwed (3)	Nailed (1)	B	15.25	3.52
2	38-76-3-NS-M-39	Screwed (3)	Nailed (2)	B	11.28	1.73
	38-76-3-NS-SD-40	Screwed (3)	Nailed (2)	B	12.68	1.58
	38-76-3-WB-M-41	B.P.	Welded	Standard	9.14	1.65
	38-76-3-WB-SD-42	B.P.	Welded	Standard	10.29	1.55
3	38-76-6-NS-M-43	Screwed (3)	Nailed (2)	B	13.4	2.58
	38-76-6-NS-C-44	Screwed (3)	Nailed (2)	B	10.47	2.85
	38-76-6-NS-M-R-45	Screwed (3)	Nailed (2)	B	15.6	4.17
	38-76-6-NS-C-R-46	Screwed (3)	Nailed (2)	B	15.9	3.9
4	75-76-6-WB-M-47	B.P.	Welded	Standard	7.27	0.8
	75-76-6-WB-SD-48	B.P.	Welded	Standard	7.02	0.72
	75-91-6-WB-M-49	B.P.	Welded	Standard	8.58	1.06

(1): Buildex BX-14 nail fastener
(2): Hilti X-EDNK22-THQ12 (3): Welded sidelap connection with washers
(3): Hilti 12-14X1 screws
(4): Welded 16 mm diameter arc spot welds.

In addition to the laboratory testing, Yang built a SAP2000 (Yang, 2003) linear elastic finite element model of the roof deck diaphragm tests that he had conducted, both bare

steel and clad versions (Figure 2.2). The model was 914.4 mm wide by 3048 mm long, representing a single width of roof deck that was half as long as the actual diaphragm test specimen. A cantilever analysis model was selected in an attempt to adequately recreate the test conditions. Yang built models with different numbers of elements, dividing the deck into 500, 1596 and 3192 elements, to identify the effect of the finite element mesh. The gypsum board was also divided into firstly 40 shell elements and was later divided in 1596 shell elements. The linear elastic model was able to adequately recreate the warping that the cross-section underwent under loading; as well, the results obtained became more accurate as the number of shell elements was increased. The 1596 element model was deemed sufficient to obtain outputs that were consistent with the experimental results.

For the model that included the non-structural components, the stiffness of the gypsum was unknown at that point. Three values were assumed for flexural stiffness: 2.0 GPa, 1.0 GPa, and 0.293 GPa and Poisson's ratio was chosen to be 0.3. With respect to connection stiffness, values were taken from Rogers and Tremblay (2000, 2003a,b) for both the sidelap and deck-to-frame connectors.

Figure 2.2: Underformed shapes of bare sheet steel deck (left) and deck with gypsum elements (right) (Yang, 2003).

The results of the linear elastic analyses conducted by Yang are presented in Table 2.5. Based on test results the desired values were 2.58 kN/mm for the bare sheet steel and 4.17 kN/mm for the model with the roofing components. As can be seen, Yang was not able to precisely replicate the measured stiffness of the test diaphragms using the finite element analyses. The 1592 shell element model is an adequate mesh density as the

stiffness value is relatively close to the 2.58 kN/mm value obtained from physical testing. Yang was not able to properly reproduce the measured stiffness of the model due to lack of information and inaccurate modelling parameters. It is further discussed in Chapter 4.

Table 2.5: Shear stiffness *(Yang, 2003)*

Bare sheet	**G' (kN/mm)**
SDI	1.70
500 shell element case (sheet thickness 0.76 mm and 7.6 mm*)	1.52
1596 shell element case (sheet thickness 0.76 mm)	2.31
3192 shell element case (sheet thickness 0.76 mm)	2.24
With roofing (with 12.7 mm thick Gypsum board)	
SDI + (Test 45 – Test 43)	3.29
Gypsum board 40 shell element case: Layout 1, E_g=2.0 GPa	1.96
Gypsum board 40 shell element case: Layout 2, E_g=2.0 GPa	1.92
Gypsum board 1596 shell element case: Layout 1, E_g=1.0 GPa	4.13
Gypsum board 1596 shell element case: Layout 1, E_g=0.293 Gpa	3.31
Stiffening (ΔG')	
(Test 45 – Test 43)	**1.59**
Gypsum board 40 shell elements, Layout 1	**0.44**
Gypsum board 1596 shell elements Layout 1, E_g=1.0 GPa	**1.82**
1596 shell element case: Layout 1, E_g=0.293 GPa	**1.00**

* 7.6 mm thick elements along the edges.

2.11 Lamarche

The study conducted by Lamarche (2005) consisted firstly of expanding the current database of dynamic properties of low-rise steel buildings and secondly of validating ambient vibration analysis as an adequate approximation of forced vibration behaviour through tests and modelling of a concrete structure built in a test laboratory. The study on steel buildings is most relevant to the research on diaphragms presented in this thesis.

Twelve buildings were reviewed by Lamarche, all of which had frequencies between 2 and 5 Hz, meaning periods of 0.2 to 0.5 seconds. Using the experimental data, the influence of the height h, the length L, the diaphragm length perpendicular to the direction of the seismic loading L_d and the width l on the period of vibration of the building was studied. Ten linear regressions were computed for approximations of the period of vibration of the buildings. Lamarche recommended that the following equations

could be used to estimate the period of a single-storey building with a concentrically braced frame and a steel roof deck diaphragm.

$$T = \frac{\sqrt{5.75L^2 + 1.25L_d hl}}{1000} \qquad (2\text{-}3)$$

$$T = 0.003L_d^{0.75}h^{0.675} \qquad (2\text{-}4)$$

$$T = 0.003(L_d h)^{0.725} \qquad (2\text{-}5)$$

L_d, L, l and h are in metres. These three equations have R^2 values of 0.85, 0.94 and 0.94 respectively when compared with all the results from the in-situ testing that were conducted. The period of vibration estimates obtained using the 2005 NBCC equation for CBFs did not correspond with the values obtained from the in-situ testing that was conducted for this research project (R^2 = 0.29). The results presented by Lamarche indicate that a more accurate prediction of the period of vibration than that prescribed in the 2005 NBCC is needed for single-storey steel buildings with flexible roof diaphragms.

2.12 Turek

Turek co-published a paper with Ventura entitled *"Ambient Vibration of Low-Rise Buildings with Flexible Diaphragms"* (2005). Upon conducting ambient vibration studies of five low-rise buildings in western Canada, results have shown that there is a considerable difference between the periods computed from current design and modelling practice and real structures. The studies also indicate that the flexibility in the building can be attributed to a large extent to the in-plane flexibility of the roof diaphragm.

The five buildings studied all had periods of less than one second for the first fundamental mode of vibration. The computed design periods for these types of structures, according to the NBCC-95, did not compare with either the finite-element analyses or with the data acquired during testing. Turek and Ventura came to two important conclusions.

For the three steel buildings that were tested, the periods of vibration ranged from 0.25 to 0.9 seconds, although they were all of similar height. This suggests that computing the period of vibration based on height alone is not adequate for low-rise steel structures. Furthermore, the mode shapes that were obtained showed that there is a significant amount of flexibility in the roof diaphragm. These two conclusions suggest that the current design methods for low-rise steel buildings are not adequate, as they do not reproduce the actual dynamic behaviour of these structures.

2.13 2005 NBCC

The 2005 National Building Code of Canada (NBCC) (NRCC, 2005) is the model code that will be used throughout Canada, in part, to estimate the loads that act on structures. The seismic provisions in this document declare that:

"Structures shall be designed with a clearly defined load path, or paths, to transfer the inertia forces generated in an earthquake to the supporting ground. The structures shall have a clearly defined Seismic Force Resisting System(s) (SFRS). The SFRS shall be designed to resist 100% of the earthquake loads and their effects, other structural framing elements not considered to be part of the SFRS must keep elastic, or have sufficient nonlinear capacity to support both gravity loads and earthquake effects."

The NBCC presents two methods for seismic analysis: equivalent static and dynamic. Four equations are recommended to estimate the fundamental period of vibration of the building:

$T_a = 0.085(h_n)^{3/4}$, for steel moment frames *(2-6)*

$T_a = 0.1N$, for other moment frames *(2-7)*

$T_a = 0.075(h_n)^{3/4}$, for concrete moment frames *(2-8)*

$T_a = 0.025(h_n)$, for steel braced frames *(2-9)*

$T_a = 0.05(h_n)^{3/4}$, for shear walls and other structures *(2-10)*

In the above equations, h_n is the height in metres of the building above ground level and N in Eq. 2-7 is the total number of storeys. Equation 2.9 is used for single-storey concentrically braced frame (CBF) steel buildings. If dynamic analyses or other means are used to determine the value of T_a for a particular building, then the value must not be greater than two times the result of Eq. 2-9 for the CBF seismic force resisting system.

These equations were developed for multi-storey buildings. It has been shown that they do not adequately recreate single-storey steel building dynamic behaviour, mainly due to the fact that the diaphragm flexibility is not accounted for (Tremblay, 2005). If Eq. 2-9 is used to compute the period of vibration of CBF buildings, the values obtained do not correspond to those measured by in-situ testing that was completed at the University of British Columbia (Ventura and Turek, 2005) and at the Université de Sherbrooke (Lamarche, 2005).

2.14 CSA S16

Clause 27 of the CSA S16 Standard (2001) provides for the seismic design of steel buildings, which is based on a capacity design concept. No specific design information with regards to roof deck diaphragms is prescribed; rather the S16 Standard addresses mainly the design of beams, columns, braces and common frames subjected to seismic loads. However, it is stated that all members in the seismic force resisting system except the weak link element must be capable of resisting the full seismic load. Only the chosen element, typically the brace in CBFs, is allowed to reach the inelastic range. It also states that the diaphragm and "*collector elements are capable of transmitting the loads developed at each level to the vertical lateral-load-resisting system.*" This obviously also applies to roof deck diaphragms.

However, there is some flexibility in the requirements of the S16 Standard. Clause 27.11 states that *"Other framing systems and frames that incorporate [...] other energy-dissipating devices shall be designed on the basis of published research results or design guides, observed performance in past earthquakes, or special investigation."* Therefore,

the use of the roof deck diaphragm as the weak element, although not discussed in S16, is possible if justified through appropriate research and testing.

2.15 Summary

The behaviour of bare sheet steel roof deck diaphragms has been extensively studied. In contrast, tests of only two diaphragms with non-structural components have been conducted (Yang, 2003). It has been shown that these additional roofing components result in a significant increase in both strength and stiffness of the diaphragm. In addition, recent studies by Medhekar, Tremblay & Steimer, Lamarche as well as Ventura and Turek have shown that the flexibility of the clad diaphragm affects the overall building period. Hence there is a need to identify the impact of non-structural roof diaphragm components on building behaviour, such that more accurate, and perhaps economic, seismic designs can be obtained. The FEM study by Yang can be used as a starting point for the development of a more detailed and larger scale linear elastic diaphragm model. The connection data presented in this Chapter will also be useful in developing finite element models. Moreover, the results of the large-scale diaphragm tests by Essa *et al.*, Martin and Yang will be of significant importance in the calibration of any finite element model that is developed.

CHAPTER 3
MATERIAL AND CONNECTION EXPERIMENTS

3.1 General

The objective of the experimental phase of this research project was to determine the material properties of the non-structural roofing components and their connections. These properties are not readily available in the literature, and hence, physical testing was necessary. The resulting material properties were needed for the development of the finite element models described in Chapter 4. A total of four different test setups were used for this research. The first is a simple two-sided shear test in which the shear stiffness of the gypsum and fibreboard can be measured on a local scale (Section 3.2). The second test setup is a centre point load flexural test, which was necessary to determine the flexural stiffness of the gypsum and fibreboard (Section 3.3). The third test is a four-sided shear test, for which the shear stiffness of the gypsum, fibreboard and combinations of other roofing components were measured (Section 3.4). It was the most complex of all setups, but was necessary because of the type and size of roofing components. The final test setup was of the screw connection between the gypsum and underlying steel deck, as well as the screw sidelap connections and nailed deck-to-frame connections. In Section 3.5 a discussion of how the stiffness values were determined for this connection type, and their values, is presented. Each of the test setups will be described in detail; the size and shape of tested specimens, test frame geometry and construction, testing protocol, material combinations and results will be provided. In addition, the preliminary conclusions for all of the experimental results are provided in Section 3.6.

The non-structural components remain constant throughout this chapter: the fibreboard is Cascade *Securpan* 1" and the gypsum board is *CGC* Type X ½".

3.2 Two-Sided Shear Test

3.2.1 *Setup and Test Procedure*

The two-sided shear test was conducted in order to obtain shear stiffness values for the roofing materials on a local scale. It was carried out in accordance with ASTM D1037 (1999). A similar setup was used by Boudreault (2005) for the testing / evaluation of

shear stiffness properties of plywood and oriented strand board (OSB) sheathing. Figure 3.1 shows a photograph of the test setup with a gypsum board specimen, as well as a schematic drawing. The inner surface of the steel loading rails was serrated such that no slippage would occur under loading when the bolts on each side of the specimen were tightened. Slippage would compromise the accuracy of the test; in addition it would cause bearing failure of the specimen against the bolts. This failure mode would result in a much lower strength and stiffness than if shear failure were to occur along the length of the specimen. The shear deformation of the specimen was directly measured by an LVDT placed in line with the loading plates, as shown in Figure 3.1. The steel loading rails are precisely 25.4 mm (1") apart.

The machine used for this setup was an *MTS Sintech 30/G* with a 150kN load cell. The load was applied through a uniform rate of motion of the crosshead of the testing machine. The rate of loading is taken as 0.2% of the length of the specimen per minute, that is 0.508 mm/min (0.02 in/min). The LVDT and load cell were connected to a Vishay Model 5100B scanner, which was used to record the data using the Vishay System 5000 StrainSmart software.

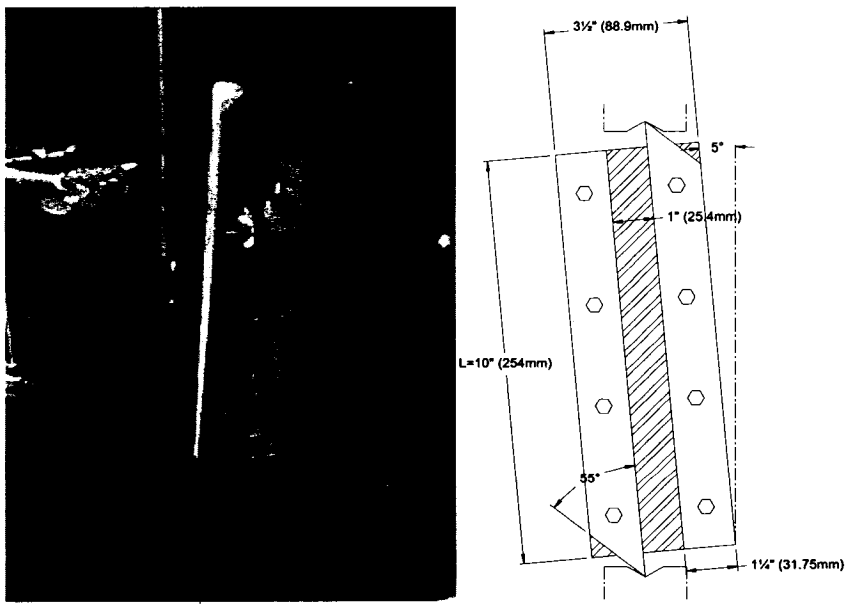

Figure 3.1: Two-sided shear setup *(Boudreault, 2005)*

3.2.2 *Test Specimens*

Test specimens were cut in rectangular sections of 254 mm by 88.9 mm (10" by 3.5") as per the ASTM D1037 Standard. 12.7 mm (½") holes were drilled in order to secure the specimen properly to the test setup. The specimens were also the full thickness of the gypsum board (12.7 mm nominal) and the fibreboard (25.5 mm nominal). Furthermore, according to the ASTM standard, all specimens were cut at least four inches from the panel edges.

Special care was taken when cutting the gypsum board, as it is very brittle and the corners tend to break. Therefore the gypsum board was cut by knife to slightly larger than specified, and then the specimen was scraped along its edges with a knife blade until the size of the specimen was acceptable. Furthermore, the same brittleness caused problems when the holes were drilled: the paper on the back of the gypsum board tended to rip and damage the board next to the hole. Therefore, the gypsum board had to be drilled with a support underneath it, such as a piece of plywood.

The fibreboard was cut on the table saw and with the radial saw. When drilling the fibreboard, the same problem of ripping occurred as with the gypsum board, although this time, it was caused by the low density of the material. The same method was used to limit ripping at the back of the specimen.

The thickness of each specimen was measured prior to testing at six different locations on the specimen. Afterwards, the arithmetic average and the standard deviation were calculated. The average values were then used to calculate both stiffness and strength values (Tables 3.1 & 3.2).

A total of six fibreboard specimens and four gypsum board specimens were tested. However, only five test results are compiled for the fibreboard because the data obtained from Test 1 was corrupted. A typical gypsum specimen after testing is shown in Figure 3.2.

Figure 3.2: Gypsum shear test specimen

3.2.3 *Specimen Behaviour*

3.2.3.1 *Fibreboard*

The fibreboard shear specimens behaved linearly up to approximately 40% of the ultimate load. After this load level a non-linear region existed, that included a significant decrease in strength once the peak shear load had been attained. Figure 3.3 shows the shear load versus deformation curve of the fibreboard. In the post-elastic range, Test 2 did not behave in the same manner as the remaining specimens. However, the linear elastic range of the data was relatively similar for all tests. Since only these linear elastic properties were used in the finite element analyses (Chapter 4) the unusual result obtained for Test 2 after the elastic range did not play a substantial role. However, Test 2 was not used to compute the average shear strength of the fibreboard.

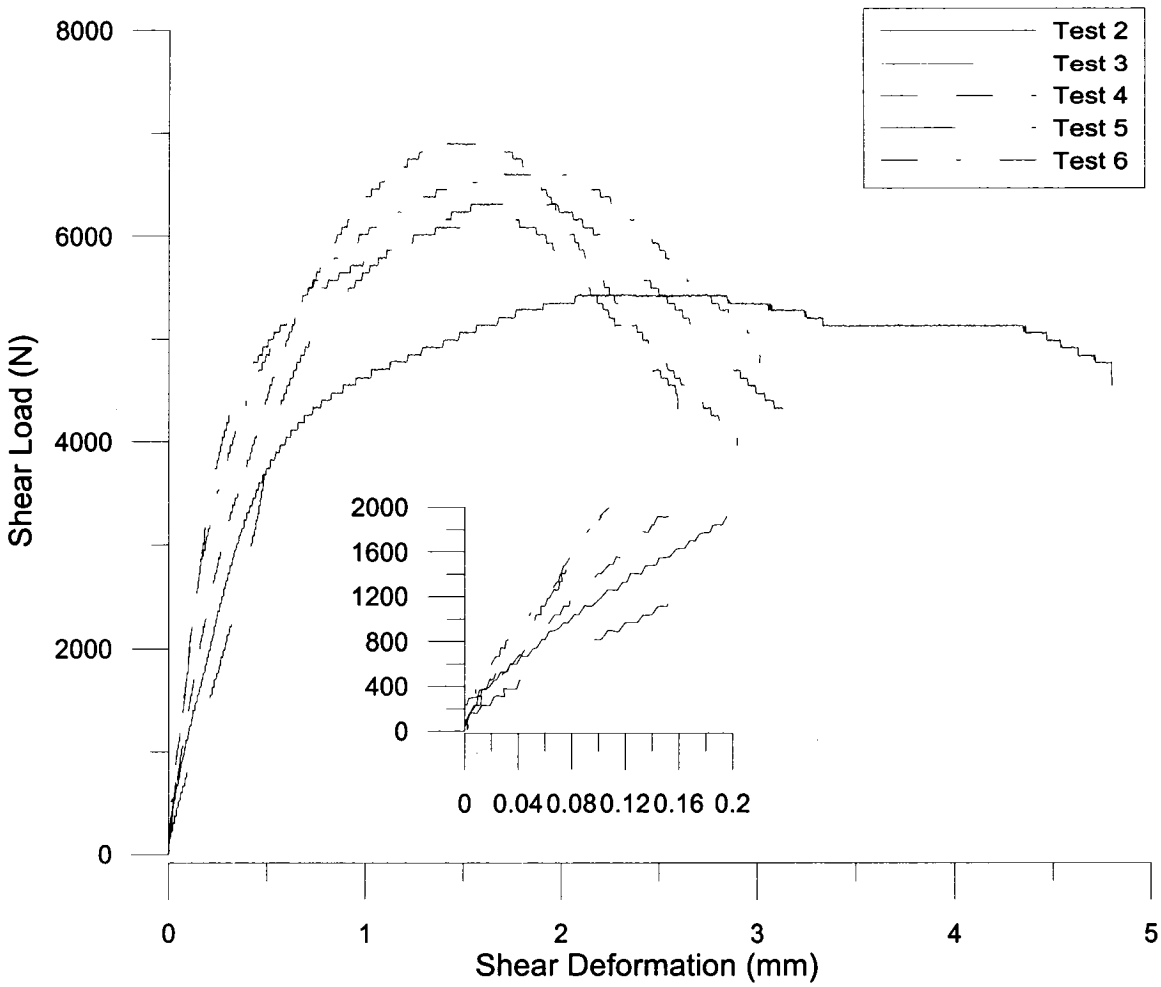

Figure 3.3: Fibreboard specimens – shear load vs. shear deformation

3.2.3.2 *Gypsum Board*

The gypsum board behaved linearly up to approximately 50% of its ultimate load. As with the fibreboard, it was followed by a non-linear region, however the decrease in capacity was much more drastic and the overall behaviour of the gypsum board much more brittle than that of the fibreboard. Figure 3.4 shows the shear load vs. shear deformation for the gypsum board specimens.

The result of Test 4 was not used for the compilation of the average ultimate shear strength. This specimen had a defect near the connector, thus causing a significant decrease in strength. Failure occurred next to the connector, instead of in the shear plane, thus reducing the capacity considerably. However, the load vs. deformation behaviour in

the linear range did not seem to be affected by this defect. Therefore, the data acquired from Test 4 was used to compute gypsum board shear stiffness.

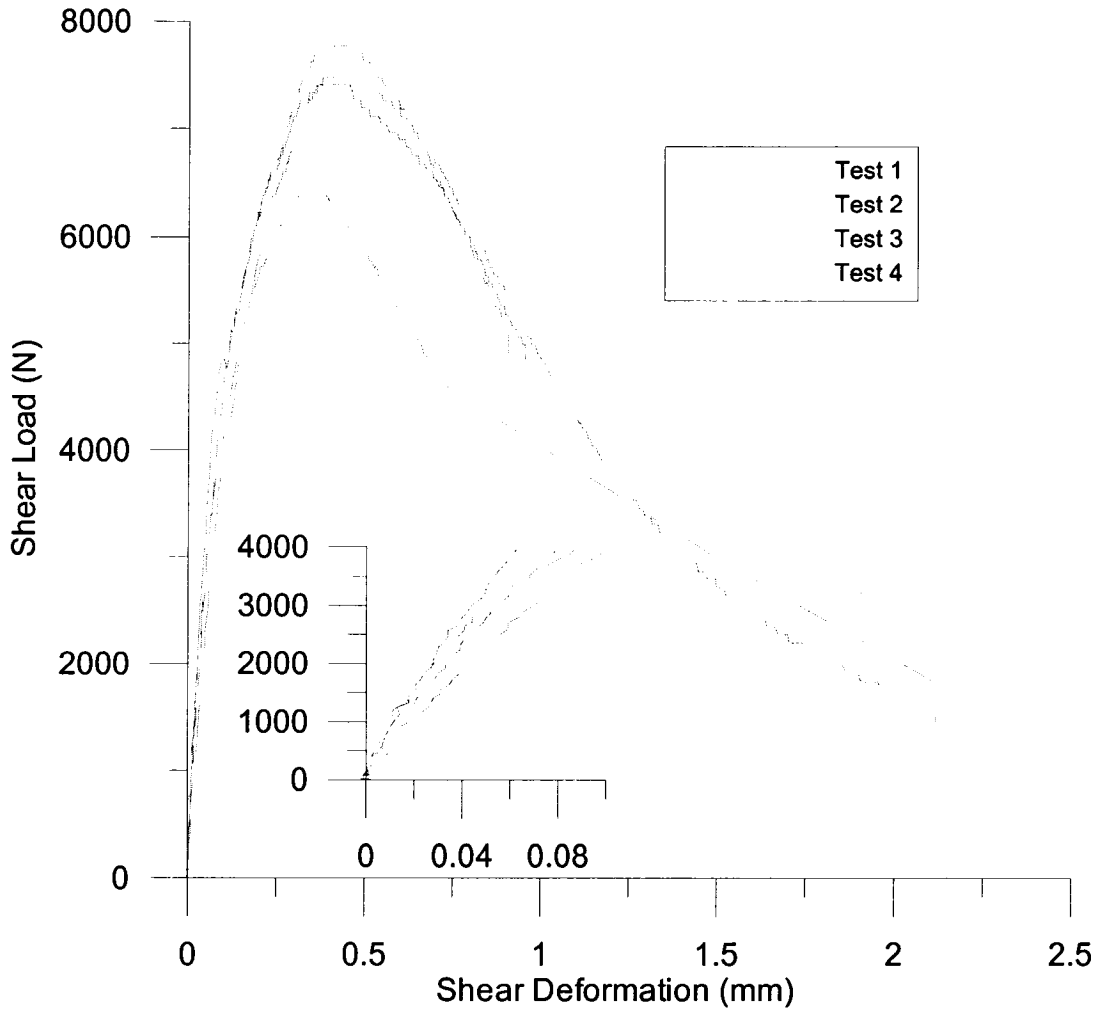

Figure 3.4: Gypsum board specimens – shear load vs. shear deformation

3.2.4 *Data Analysis*

In terms of shear strength calculations the following equation was taken from the ASTM D1037 Standard:

$$f_s = P/Ld \qquad (3\text{-}1)$$

where:

d = Thickness of specimen (mm),

f_s = Edgewise shear strength (MPa),

L = Length of specimen (mm),

P = Maximum compressive load (N).

However, there is no recommended equation given in the ASTM standard to calculate the stiffness of the specimen for this specific test setup. Two equations were used and the results from both equations are shown. The two equations are presented below. The first one is taken from the ASTM D1037, for shear stiffness (D1037a for this Thesis). This equation was developed for a shear through the thickness of a plywood panel, therefore the full width *(b)* of the specimen is used as opposed to the width between the rails.

$$G = P_l d/Lbr \qquad (3\text{-}2)$$

where:

b = width of specimen (mm), taken as 88.9 mm (3.5"),

d = thickness of specimen (mm),

G = shear modulus (MPa),

L = length of specimen (mm),

P = load at proportional limit, taken as 40% ultimate (N),

r = displacement of LVDT (mm).

The second stiffness equation, shown below is also taken from the ASTM D1037 (D1037b for this Thesis). This equation was developed by Boudreault (2005).

$$G = \frac{P \times b}{L \times t \times r} \times F^{*} \qquad (3\text{-}3)$$

Where:

v_p = Edgewise shear strength (MPa);

P_{max} = Maximum compressive load (N);

G = Shear modulus (modulus of rigidity) (MPa);

P = Compressive load (N);

b = Width of portion of the specimen in shear (mm) (b = 25.4 mm in this case);

L = Length of specimen (mm);

t = Average thickness of shear area (mm);

r = In-line displacement at load P (mm);

F = Multiplication factor to compensate nonuniform stress distribution in small specimens. F = 1.19 (ASTM D2719, 1994)

The above equations were used to compute the values of the shear strength and stiffness for all the specimens. The results for stiffness and strength of the fibreboard and gypsum board panels are shown in Tables 3.1 and 3.2, respectively.

Table 3.1: Two-sided shear test – fibreboard results

	Test 2	Test 3	Test 4	Test 5	Test 6
Thickness (mm)	24.2	24.0	24.5	23.8	24.0
%CoV	0.77%	2.49%	1.66%	1.97%	1.38%
f_s (MPa)	0.88	1.05	1.11	1.02	1.09
Avg. f_s (MPa)	**1.07***				
%CoV of f_s	**8.73%**				
ASTM D1037a - G (MPa)	134.6	105.4	152.4	253.7	232.7
Avg. G (MPa)	**175**				
%CoV of G	**36.7%**				
ASTM D1037b - G (MPa)	45.8	35.8	51.8	86.3	79.1
Avg. G (MPa)	**59.8**				
%CoV of G	**36.7%**				

*Note: the average f_s was determined without the result of Test 2.

Table 3.2: Two-sided shear test – gypsum results

	Test 1	Test 2	Test 3	Test 4
Thickness (mm)	15.4	15.2	15.2	15.4
%CoV	1.29%	0.83%	0.86%	3.11%
f_s (MPa)	1.89	1.94	2.02	1.64
Avg. f_s (MPa)	**1.95***			
%CoV of f_s	**3.07%**			
ASTM D1037a - G (MPa)	1460	1000	1240	1440
Avg. G (MPa)	**1290**			
%CoV of G	**16.6%**			
ASTM D1037b - G (MPa	497	340	423	488
Avg. G (MPa)	**437**			
%CoV of G	**16.6%**			

*Note: the average f_s was determined without the result of Test 4.

3.2.5 Discussion

It was found that on average the shear strength of the gypsum was approximately twice that of the fibreboard. The average ultimate strength of the gypsum board, for this data

set, was 1.95 MPa, while the average strength for fibreboard was 1.07 MPa. This shows that the gypsum has the potential to provide much more shear strength to the steel deck roof diaphragm than the fibreboard if adequately connected to the roof panels. Furthermore, in the cross-section of the roof shown by Yang (2003) (Fig. 3.5) visual inspection of the failed diaphragm test specimen revealed that the gypsum board was able to carry more load than the fibreboard, i.e. the gypsum showed extensive damage due to loading, because it was fastened directly to the steel deck, while the fibreboard was not.

Figure 3.5: Deformation of steel deck and non-structural components under shear load - Test 45 *(Yang, 2003)*

More importantly, in terms of this research project, the shear stiffness of the gypsum board was significantly greater than that of the fibreboard (Fig. 3.6). The average initial modulus of shear rigidity for the gypsum board was 1290 MPa, whereas only 175 MPa (ASTM D1037a) was measured on average for the fibreboard, an increase of over eight times. However, the results for both the fibreboard and the gypsum stiffness were scattered, as can be seen in the coefficient of variation of 36.7% and 16.6%, for the two materials, respectively. Shear stiffness is not a codified requirement in the manufacture of these construction materials, and hence it is not surprising that the measured f_s value varies from specimen to specimen. One possible cause of the scatter of results may be the grain direction for gypsum board (paper backing) and the fibreboard. Depending on the direction of the specimen with respect to the grain, as well as the small scale and localized loading of the test setup, the experimental results may vary. This theory will be further investigated with the results of the flexural tests (Section 3.3). Furthermore, the test setup was originally not developed to determine stiffness, but rather the shear strength properties of a material. Both stiffness equations (3-2, 3-3) were obtained for the same test standard (ASTM D1037) for slightly different test setups. The four-sided shear

test setup results (Section 3.4) will later be relied on to provide additional information on the shear stiffness of the non-structural components.

The two equations give very different results for local shear rigidity although they are both taken from the ASTM D1037 standard. The interlaminar shear equation (D1037a) gives a rigidity almost three times higher than the shear though the thickness equation (D1037b). The results of the four-sided shear tests can be used to confirm which of these two equations, if any, is adequate to calculate shear rigidity.

For comparison purposes the load vs. deformation curves for both the gypsum and fibreboard are plotted in Figure 3.6. When comparing the gypsum board and the fibreboard specimens, it is clear that the gypsum board has much higher local shear rigidity than the fibreboard.

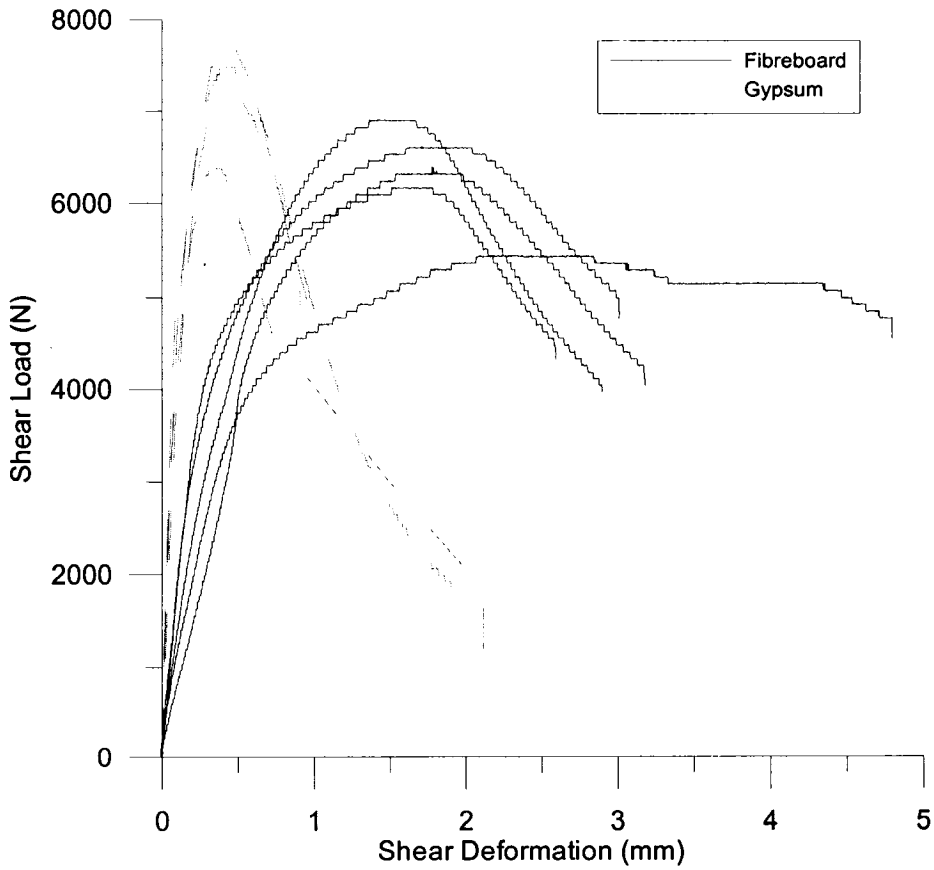

Figure 3.6: Comparison of gypsum board and fibreboard specimens – shear load vs. shear deformation

3.3 Flexural Test

3.3.1 *Setup and Test Procedure*

The flexural tests were conducted in order to obtain the flexural rigidity and strength of the fibreboard and gypsum board panels. Even though the roof diaphragm structure is assumed to be subjected to in-plane shear forces during lateral loading, due to the warping deformation of the steel roof deck panels (Fig. 3.5), the flexural strength and stiffness of the non-structural roofing components are of relevance (Yang, 2003). The flexural test setup is a simple centre-point flexure test, which is based on ASTM Standard C473 (1997). The loading plate and all bearing supports, which are rounded to a radius of 3.2 mm (⅛"), are the full width of the specimen. Figure 3.7 shows the test setup during loading of a gypsum board specimen. The two bearing supports were placed at a distance of 355.6 mm (14").

The machine used for this setup was an *MTS Sintech 30/G* with a 150 kN load cell. Each test was conducted in displacement control at a crosshead speed of 6.35 mm/sec (0.25 in/sec) until failure of the specimen. The load and the displacement of the crosshead were used in the calculation of flexural properties.

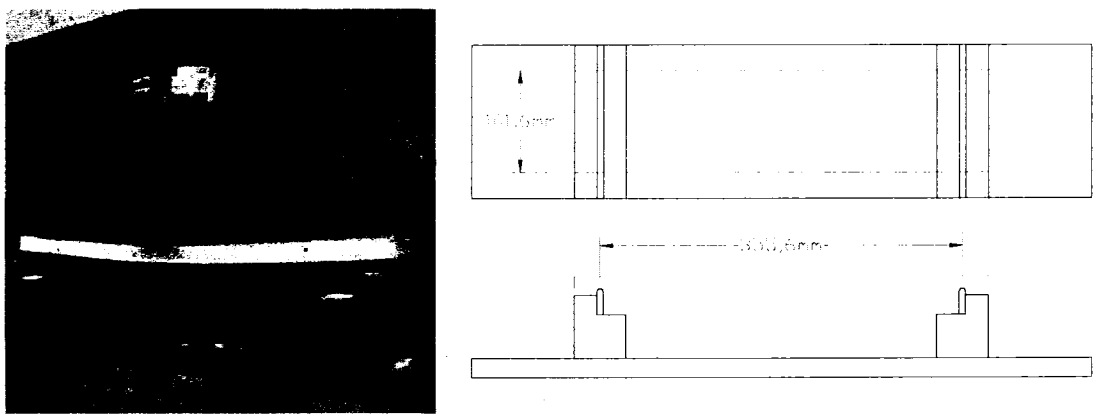

Figure 3.7: Flexural test setup

3.3.2 *Test Specimens*

All test specimens were cut with a table and radial saw to 406.4 millimetres (16") long by 101.6 millimetres (4") wide, as per ASTM C473. The specimen dimensions were then

measured precisely using a micrometer and callipers. Three measurements were taken for the width of each specimen and six were taken for the thickness. The arithmetic average of the thickness and width for each specimen were used to compute the flexural stiffness and strength. As required for the two-sided shear tests, test specimens were cut at least four inches from the panel edges: all fibreboard specimens met this requirement. However, specimens G-PL1, G-PL11, G-PL13, G-PL22, G-PP1, G-PP2, G-PP12 and G-PP13 were cut at less than 4 inches from the sides.

In all, 24 fibreboard specimens were tested. This included specimens F1 to F16, which were cut from a single panel but without a specific orientation with respect to the grain. Eight additional specimens were cut from the same panel: Four were cut in one direction and the other four were cut perpendicular to the previous specimens. These specimens were labelled FDA and FDB, FDA meaning "Fibreboard Direction A" and FDB meaning "Fibreboard Direction B." This approach was used to investigate the hypothesis that any existing directionality of the wood fibres would affect the flexural properties. Directions A and B have no precise meaning other than they are perpendicular to one another.

A total of 44 flexural gypsum board tests, consisting of two series of specimens, were performed. The first series consisted of specimens parallel to the long side of the panel (PL), while the second series was oriented perpendicular to the long side (PP). In the identification of each test flexural specimen, the PL or PP designation is preceded by G, identifying them as gypsum board specimens.

Gypsum board is typically fabricated with a finishing layer of paper on one side of the panel. The fabrication direction of gypsum board panels is parallel to the long side of the board. It was felt that this fabrication method may have an effect on the flexural stiffness and strength of the panel depending on whether the paper was placed in tension or compression during testing. Specimens G-PL1 and G-PP1 through G-PL11 and G-PP11 were tested with the white finishing paper in compression. Specimens G-PL12 and G-PP12 through G-PL22 and G-PP22 were tested with the finishing paper in tension. These specimens were cut from the same panel as the first specimens.

3.3.3 *Specimen Behaviour*

3.3.3.1 *Fibreboard*

Specimens F1 through F16 all behaved, in terms of flexural strength vs. stiffness, in a similar fashion. First, there existed a linear elastic range, which was then followed by a decrease in stiffness (Fig. 3.8). The test specimen then reached its maximum load, followed by a sudden brittle failure of the tensile fibres.

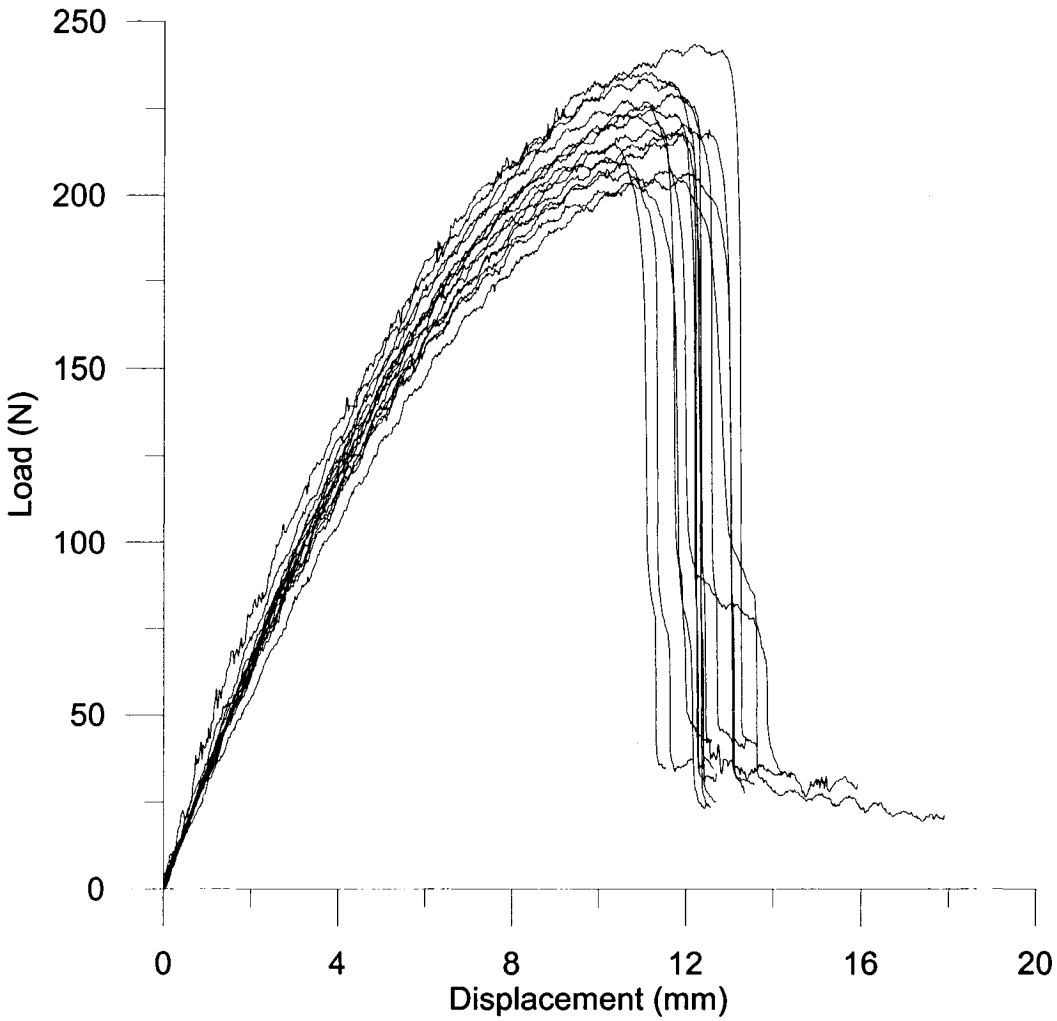

Figure 3.8: Flexural test results – F1 to F16

However, specimens FDA and FDB, which were cut perpendicular to one other, provided test results which indicated that the behaviour of the fibreboard is direction dependent. Figure 3.9 shows the load versus displacement curves for specimens FDA and FDB.

There are clearly two separate sets of curves, of which the FDA samples have higher strength and slightly higher stiffness properties.

Upon inspection of the tested specimens, there seems to be very little difference between the FDA and FDB specimens. The only visible difference is the fracture area: it is more compact for the FDA specimens, but still the fracture looks similar. A good assumption would be that the wood fibres are oriented along the FDA direction, which would give slightly better performance.

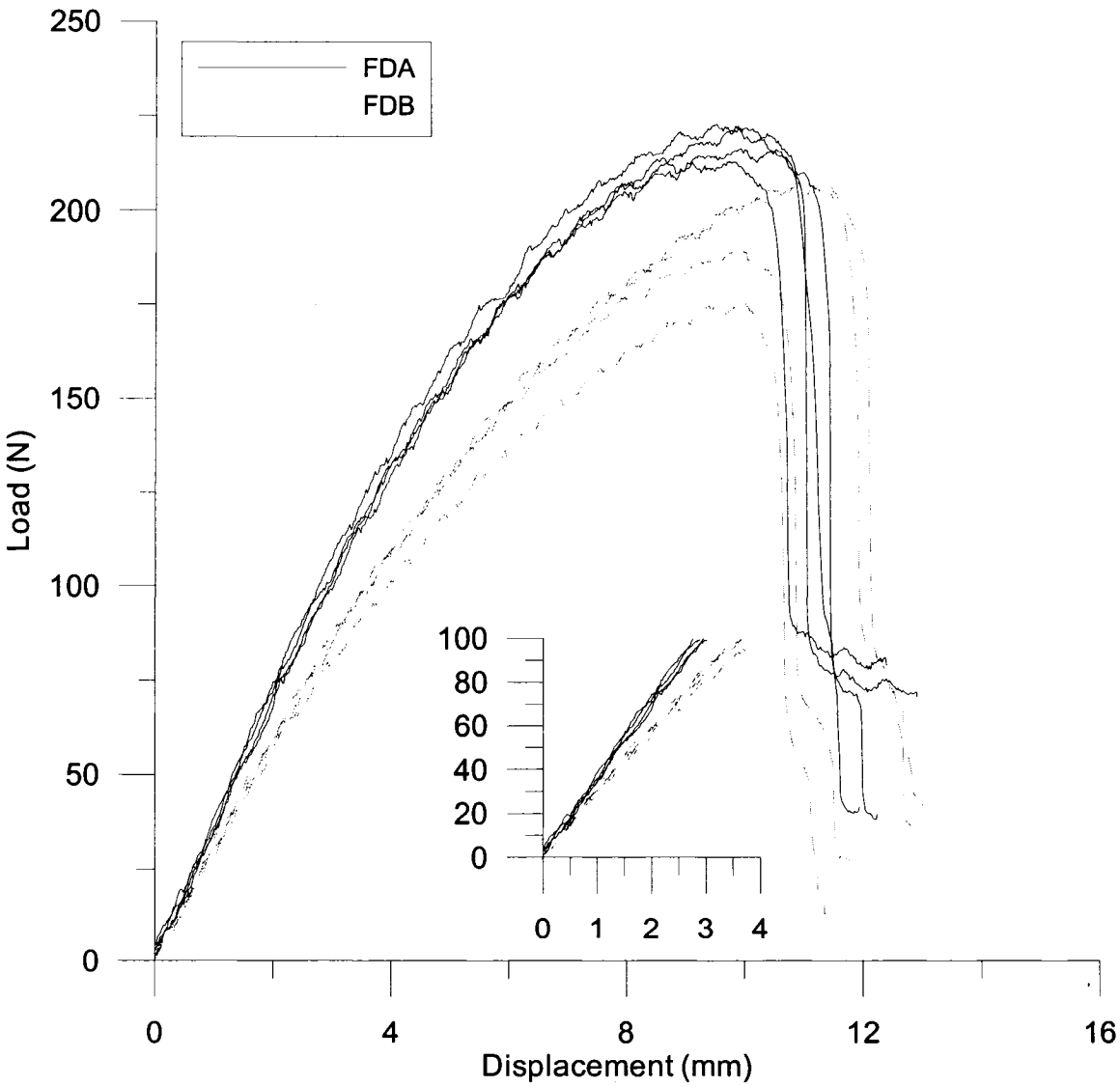

Figure 3.9: Flexural test results – FDA and FDB

3.3.3.2 *Gypsum Board*

The gypsum board behaved quite differently from fibreboard for the flexural test. Figure 3.10 shows the behaviour of gypsum board with PP specimens where the finishing paper was in compression. There clearly exist two sections to the curve: first a linear elastic range that extends to approximately 80-100 kN; second a yield plateau is developed until a final brittle fracture of the specimen. Failure occurred on the tension side of the specimen. The paper fails first, but at a low enough load that the gypsum itself still has enough strength to resist the load applied. Cracks slowly propagate through the thickness of the gypsum until the complete cross-section fractures.

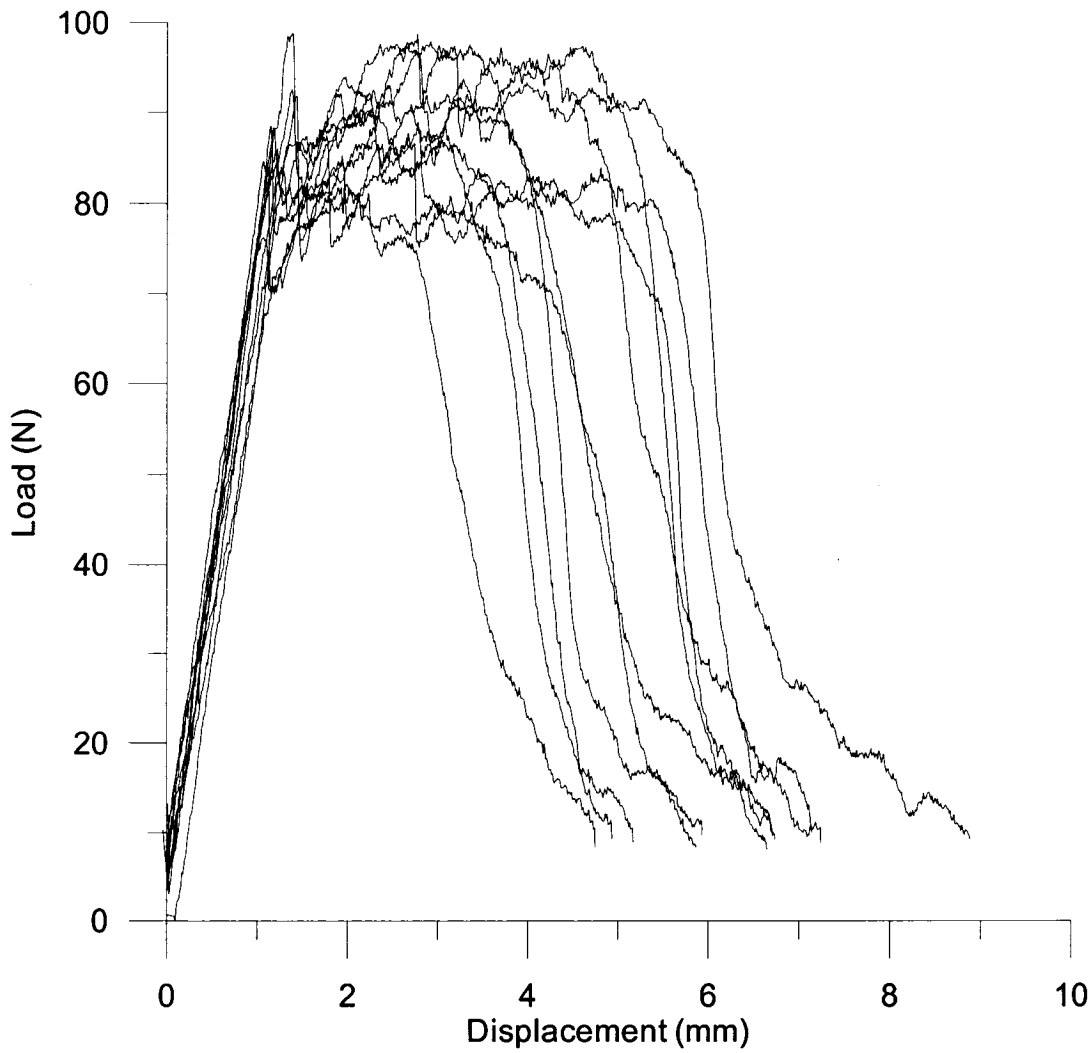

Figure 3.10: Flexural test results – G-PP1 to G-PP11

Specimens G-PP12 through G-PP22, for which the finishing paper is in tension, behave in roughly the same manner as specimens 1 through 11. The capacity of the specimen is slightly higher, probably due to the higher capacity of the paper. When the paper breaks, it goes down to roughly the same capacity as the previous specimens, which shows that the gypsum itself seems isotropic (Fig. 3.11). The non-isotropic is probably due to paper fibre orientation.

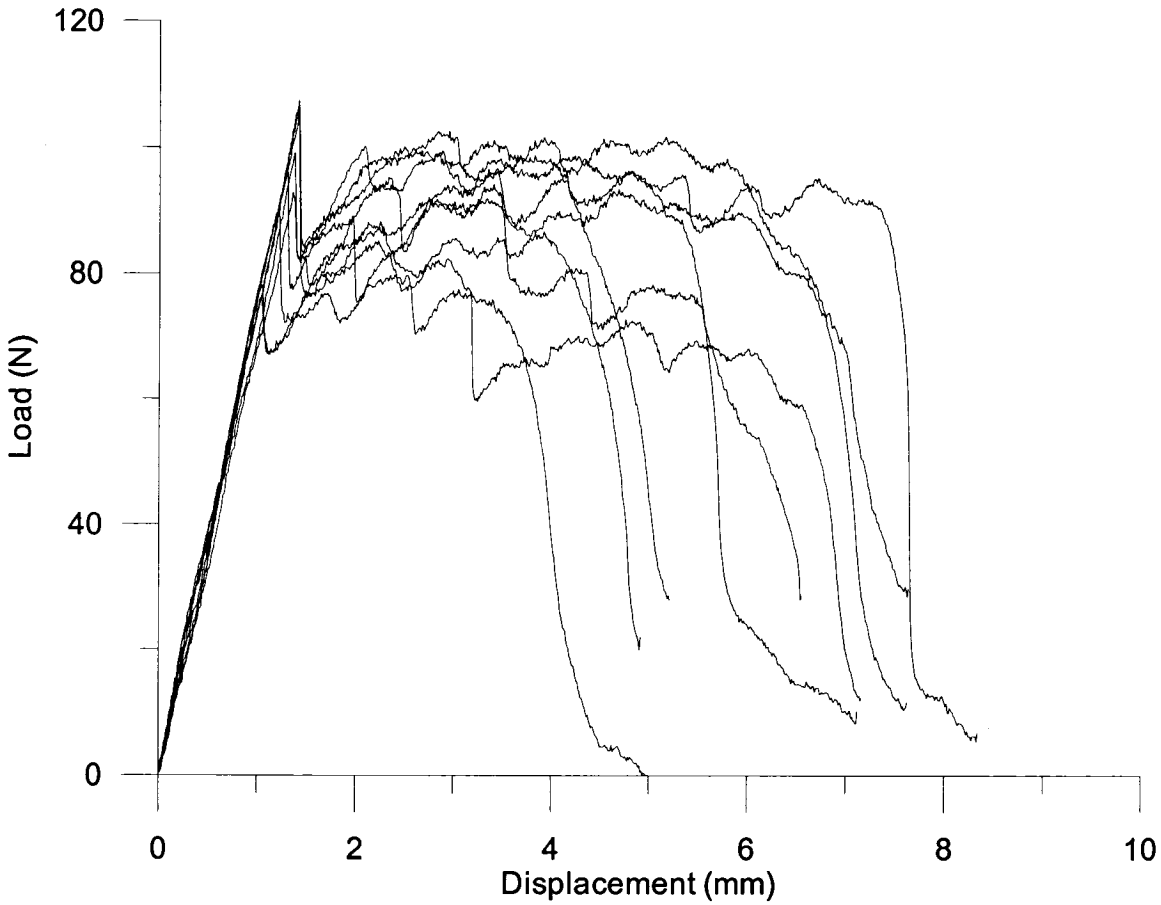

Figure 3.11: Flexural Test Results – G-PP12 to G-PP22

Figure 3.12 shows the behaviour of gypsum board with PL specimens. The behaviour is much different from that of the PP specimens. The load versus displacement curve is bilinear: at first a steep linear elastic curve up to approximately 150 N exists, which is followed by a less steep linear zone that reaches approximately 300 N. This is followed by a very brittle failure at a crosshead displacement between 8 and 10 millimetres. The

failure occurred on the tension side, as with the PP specimens. However, since this is the fabrication direction, the paper had a much higher capacity, thus reaching 300 N. Once the paper had broken, the tensile capacity of the gypsum was too little to carry the load, therefore the specimen fractured almost instantaneously. The behaviour is very to that of a reinforced concrete beam: the gypsum itself acts at the concrete and the paper acts as the reinforcing steel bars. Cracking in the gypsum at around 140 N creates a softening of the cross section, thus a reduction a stiffness which is shown in Figure 3.12 as the less steep slope. From that point, the paper carries the load and the crack remains relatively stable in size until fracture of the paper, at which point the specimen fails abruptly.

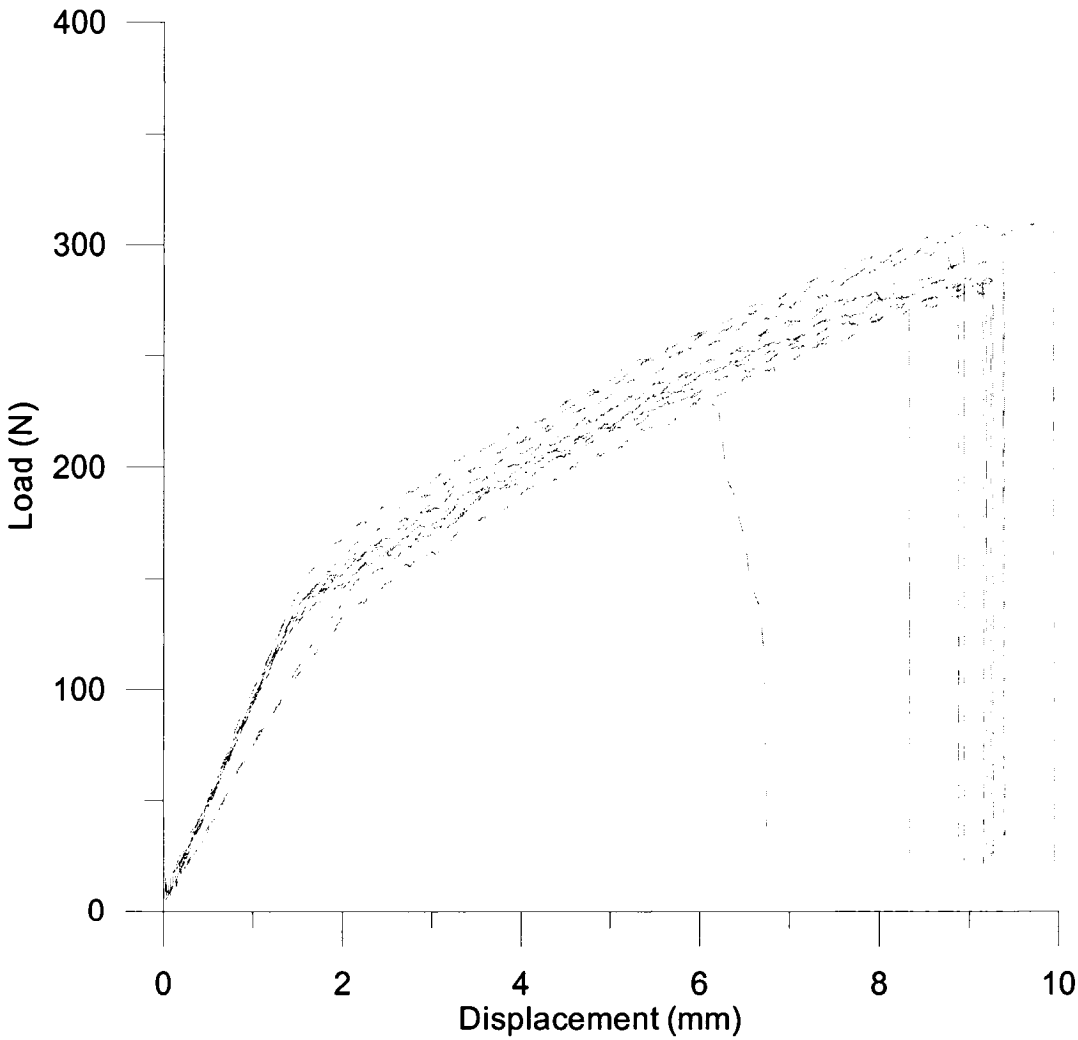

Figure 3.12: Flexural test results – G-PL1 to G-PL11

Specimens PL-12 through PL-22 behaved in the same manner, although their ultimate capacity was slightly lower. Still similar to a reinforced concrete beam, there are two sections to the slope: the uncracked stiffness and the cracked stiffness. From that point the paper takes the load until it breaks. At that point, the load drops abruptly to zero.

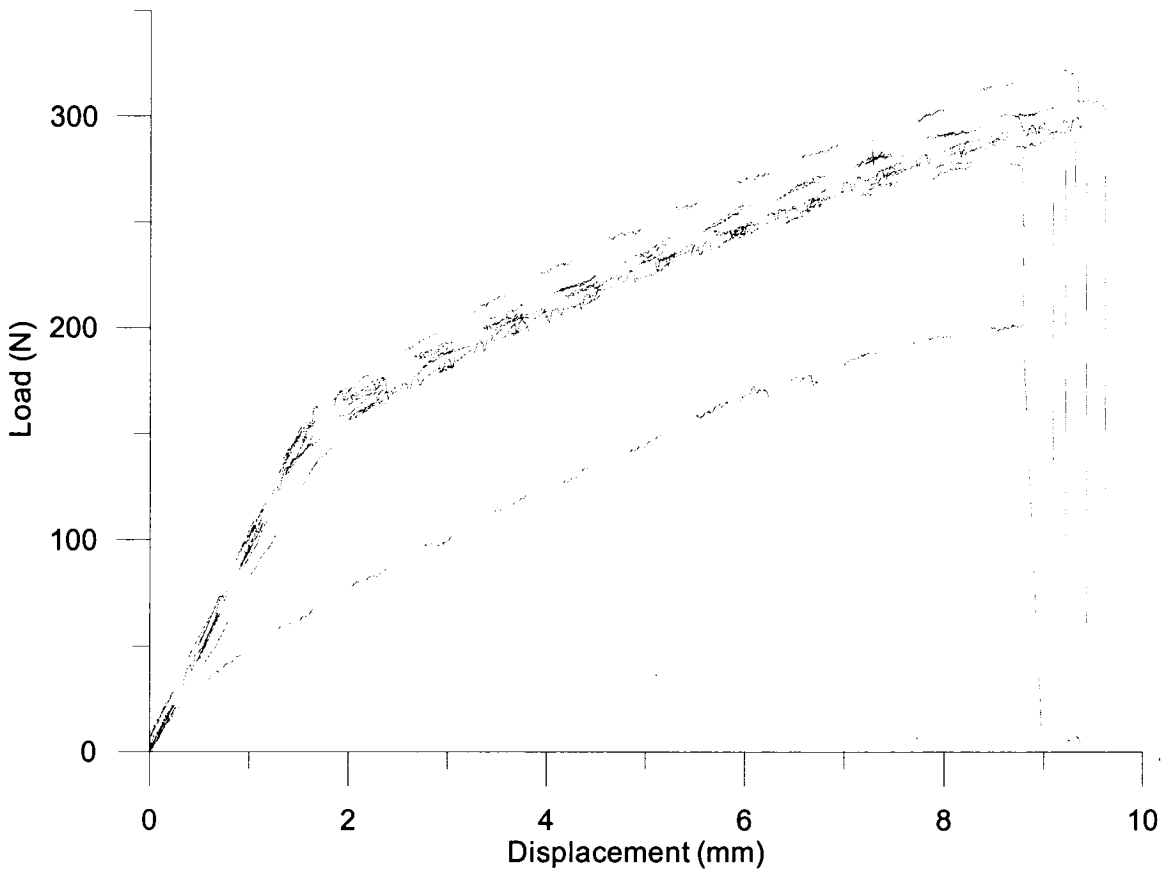

Figure 3.13: Flexural test results – G-PL12 to G-PL22

3.3.4 *Data Analysis*

The two desired properties were the flexural strength and rigidity of the fibreboard and gypsum board. In order to determine the flexural rigidity, *EI*, the following ASTM D3043 (1995) equation was used:

$$EI = (L^3/48)*(P/\Delta) \qquad (3\text{-}4)$$

where:

E = Young's modulus in flexure (MPa),

I = moment of inertia (mm^4) taken as $\frac{bh^3}{12}$,

L = span (mm),

P = load (N),

P/Δ = slope in the initial linear range of the load vs. deflection curve (N/mm).

Young's modulus in flexure, E, could then be calculated given that all other variables were known. EI is the flexural rigidity.

Furthermore, the strength of the fibreboard and gypsum board is calculated using the following equation, which is also taken from ASTM D3043:

$$S_b * I/c = PL/4 \qquad (3\text{-}5)$$

where:

S_b = modulus of rupture or maximum fibre stress, (MPa),

I = moment of inertia (mm^4) taken as $\frac{bh^3}{12}$,

c = distance from neutral axis to extreme fibre (mm),

L = span (mm),

P = maximum load (N)

The value c was taken as half the thickness of each board. The modulus of rupture, S_b, could then be calculated given that all other variables were known.

3.3.4.1 *Fibreboard Specimens*

Specimens F1 through F16 were cut out from the panel and tested, with no regard for possible strand orientation of the fibreboard. In contrast the FDA and FDB specimens were oriented with the fibres as was explained in Section 3.3.2. There were no edge specimens in this data set. The individual moduli of elasticity and fibre strengths for all of the fibreboard test specimens are provided in Table 3.3. The average flexural rigidity and

strength of the combined FDA, FDB and the F1 to F16 specimens are 255 MPa and 1.95 MPa, respectively.

Table 3.3: Flexural test – fibreboard results

Specimen	*E (MPa)*	S_b *(MPa)*	Specimen	*E (MPa)*	S_b *(MPa)*
F1	306	2.14	FDA-1	299	2.02
F2	251	2.09	FDA-2	310	2.13
F3	246	1.97	FDA-3	291	2.07
F4	259	1.91	FDA-4	290	2.11
F5	247	2.01	**Avg. FDA**	**298**	**2.08**
F6	256	2.00	**%C.o.V.**	**3.07%**	**2.31%**
F7	240	1.97	FDB-1	232	1.68
F8	233	1.95	FDB-2	245	1.80
F9	250	1.92	FDB-3	238	1.98
F10	257	2.01	FDB-4	249	1.96
F11	283	2.13	**Avg. FDB**	**241**	**1.85**
F12	237	1.81	**%C.o.V.**	**3.09%**	**7.74%**
F13	243	2.01			
F14	227	1.90			
F15	253	2.16			
F16	239	1.96			
Avg. F1-F16	**248**	**1.99**			
%C.o.V.	**5.36%**	**4.56%**			

3.3.4.2 *Gypsum Board Specimens*

The modulus of elasticity and strength values for the gypsum board test specimens are shown in Table 3.4. Flexural test specimens G-PL1 and GPP1 through G-PL11 and G-PP11 were oriented such that the finishing paper was in compression, whereas specimens G-PL12 and G-PP12 through GPL22 and G-PP22 were tested with the finishing paper in tension. In addition, test specimens G-PL1, G-PL11, G-PP1, G-PP2, G-PL13, G-PL22, G-PP12 and G-PP13 were cut from the edge of the gypsum panels. Although these specimens were tested, and their values for flexural strength and stiffness determined, these calculated values were not included in the statistical information provided, as the ASTM recommends not taking these specimens into consideration.

Table 3.4: Flexural test – gypsum results

Specimen	*E (MPa)*	S_b *(MPa)*	Specimen	*E (MPa)*	S_b *(MPa)*
G-PL1*	2113	6.28	G-PP1*	2079	1.78
G-PL2	2651	4.90	G-PP2*	2742	3.82
G-PL3	2780	6.58	G-PP3	1711	1.98
G-PL4	2748	6.45	G-PP4	2459	1.92
G-PL5	2169	6.06	G-PP5	2494	1.85
G-PL6	2880	6.21	G-PP6	2400	1.93
G-PL7	2897	6.41	G-PP7	2668	2.25
G-PL8	3011	6.42	G-PP8	2595	2.24
G-PL9	2883	6.41	G-PP9	2434	2.18
G-PL10	2767	6.42	G-PP10	2120	2.12
G-PL11*	2779	6.59	G-PP11	2416	2.14
Av. G-PL 1-11	**2750**	**6.21**	**Avg. G-PP 1-11**	**2560**	**2.07**
%C.o.V.	**8.83%**	**8.26%**	**%C.o.V.**	**12.2%**	**7.27%**
G-PL12	2800	6.36	G-PP12*	2434	2.45
G-PL13*	1083	4.31	G-PP13*	1686	2.10
G-PL14	2901	6.93	G-PP14	2190	2.26
G-PL15	3025	6.53	G-PP15	2276	2.16
G-PL16	3064	6.75	G-PP16	2277	1.98
G-PL17	2898	6.81	G-PP17	2320	2.33
G-PL18	2973	6.53	G-PP18	2289	1.86
G-PL19	3211	6.53	G-PP19	2150	2.35
G-PL20	2776	6.20	G-PP20	2260	2.39
G-PL21	2873	6.42	G-PP21	2020	2.09
G-PL22*	2529	6.23	G-PP22	2263	1.75
Av. G-PL 12-22	**2950**	**6.56**	**Av. G-PP 12-22**	**2250**	**2.13**
%C.o.V.	**4.66%**	**3.50%**	**%C.o.V.**	**4.89%**	**10.6%**
Average G-PL	***2850***	***6.39***	***Average G-PP***	***2410***	***2.10***
%C.o.V.	***15.7%***	***9.21%***	***%C.o.V.***	***10.9%***	***19.9%***

* Specimens cut from the edge of the gypsum panel. Results not included in calculation of statistical parameters.

3.3.5 *Discussion*

The average ultimate flexural strength, S_b, of the fibreboard for this data set was 1.95 MPa, for both directions combined (Table 3.3). Looking at both directions separately, the FDA data set has an average of 2.08 MPa and the data set FDB has an average of 1.85 MPa. The difference is not very significant; however, it does show that some directionality exists with respect to the flexural strength properties. The gypsum board, on the other hand, exhibited two very different flexural strength values depending on the direction that the specimen was cut from. The G-PL specimens had an average

ultimate flexural strength of 6.39 MPa, whereas the G-PP specimens had an ultimate flexural strength of 2.10 MPa (Table 3.4). Therefore, in terms of strength, the gypsum board is highly anisotropic, due mainly to the orientation of the surface paper, while the flexural strength of the fibreboard is much less direction dependent comparatively. In effect, the gypsum board specimens cut perpendicular to the direction of the paper grain and the fibreboard specimens possessed very similar flexural strength; while the parallel gypsum board flexural specimens were of approximately three times greater strength.

Regarding the modulus of elasticity, the average of fibreboard specimens F1 to F16 was 248 MPa (Table 3.3). However, when the data from the FDA and FDB data sets were compared, there were two different values: 298 MPa for FDA and 241 MPa for FDB. This represents a difference of approximately 20%, which is much larger than the calculated coefficient of variation of the data set. Nonetheless, the general shape of the load vs. deformation curve is the same for the two sets of data (Fig.s 3.7 & 3.8). The fibreboard material is anisotropic with respect to modulus of elasticity to a similar extent as noted for the flexural strength. The modulus of elasticity of the gypsum panel was much higher than that of the fibreboard panel, Values of E = 2850 MPa in the PL direction and 2410 MPa in the PP direction were determined (Table 3.4). The material rigidity is still somewhat direction dependent, however not to the extent observed for the flexural strength properties. Furthermore the gypsum board was found to be roughly 10 times stiffer in flexure than the fibreboard.

Finally, the flexural strength and rigidity results were similar for the gypsum board specimens for which the finishing paper was in tension (specimens 12 to 22) and compression (specimens 1 to 11). A more profound change in behaviour existed between the specimens that were cut from different directions, compared with those that were tested with the finishing paper on top or bottom.

Figure 3.14 shows the results of the PL and PP gypsum flexural tests on the same graph. It is clear that the PL specimens have a much greater strength than the PP specimens. Furthermore, there is a slight difference between the initial stiffness of the PL and PP

specimens: the slope of PL specimens is steeper than that of the PP specimens in the linear range.

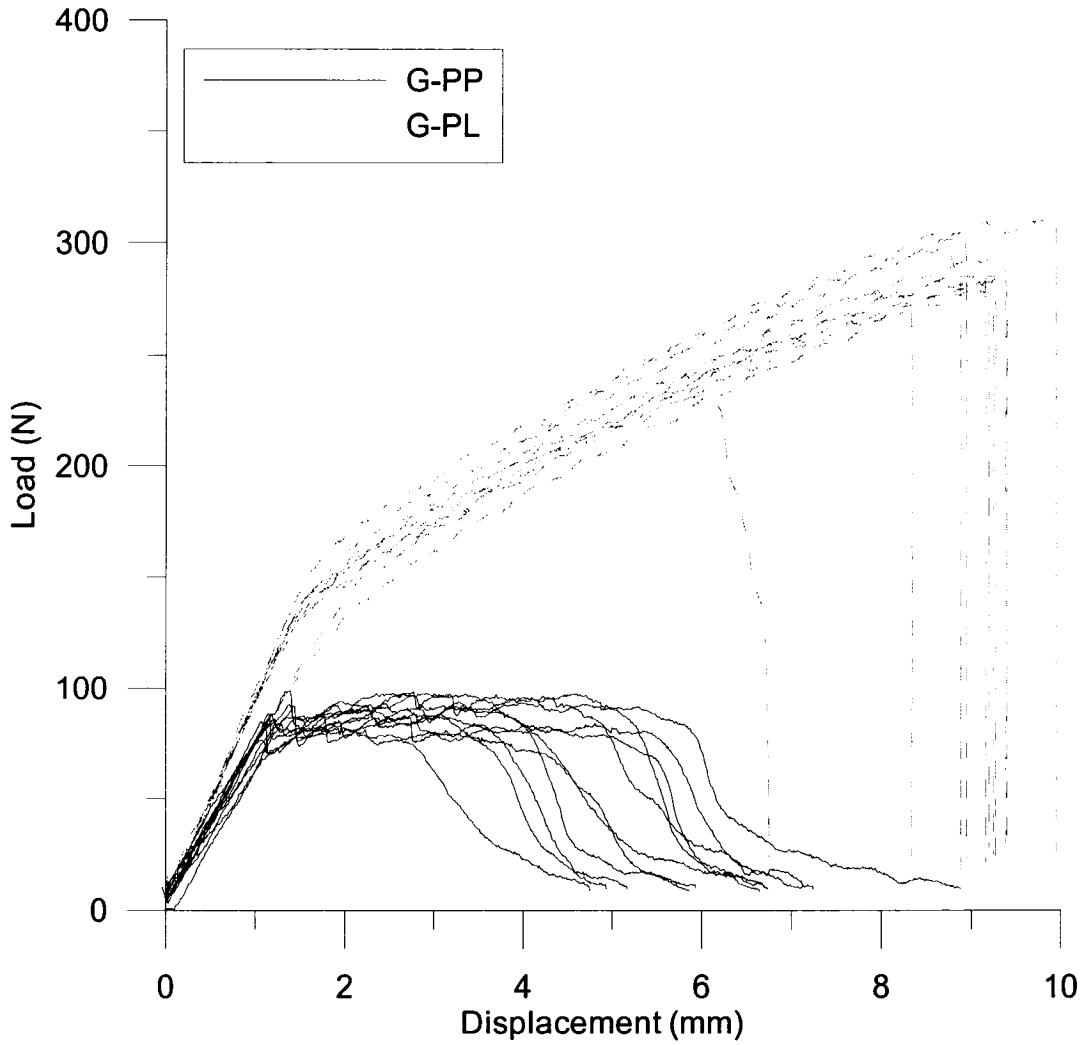

Figure 3.14: Flexural test results – G-PP vs. G-PL

Figure 3.15 shows the curves of the GPL, GPP and Fibreboard test specimens. It is clear that the slope of the fibreboard specimens is lower than that of both the G-PL and G-PP specimens. It is important to note that Figure 3.15 is a load versus displacement curve. No conclusions can be drawn directly from these graphs as the different materials have different thicknesses.

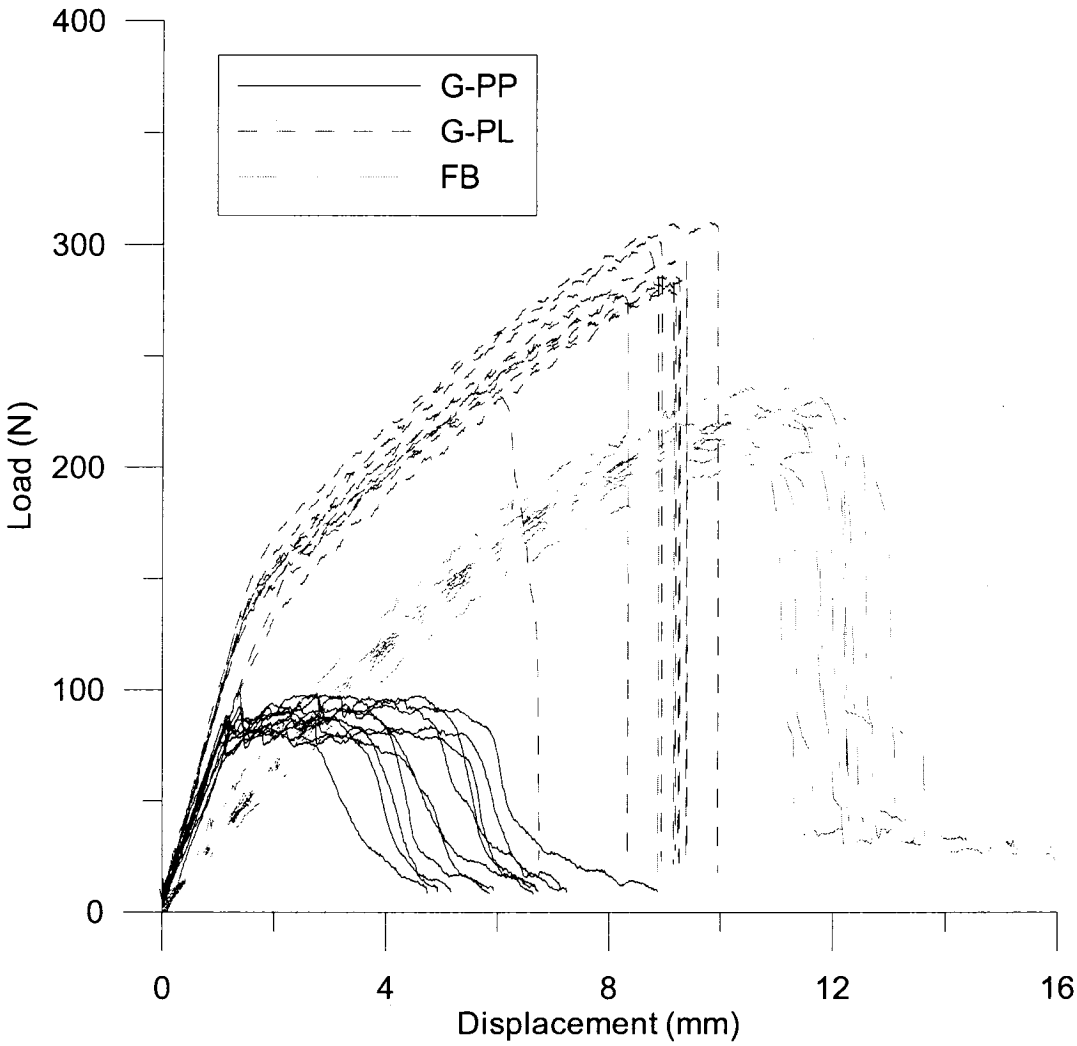

Figure 3.15: Flexural test results – FB vs. G-PP vs. G-PL

3.4 Four-Sided Shear Test

3.4.1 *Setup and Test Procedure*

The four-sided shear test was conducted in order to obtain the shear stiffness of the gypsum, fibreboard and combinations of other roofing components. This test setup, which was based on ASTM D2719 (1994), was necessary because of the type and size of the non-structural roofing elements. A specimen having a square shear area was loaded along all four edges by a system of hinges and rails (Fig. 3.16). As the cross head of the loading machine moved vertically upwards, bearing forces were applied at the corners of the panel, resulting in shear forces along the four sides of the panel. The diagonal elongation of the specimen was measured with LVDTs placed on both sides of the panel.

With the acquired data, the shear load versus shear deformation curves were plotted, from which the stiffness of the material was calculated. The panels were not tested to failure because the objective of these tests was to measure the shear stiffness parameters and not the ultimate strength.

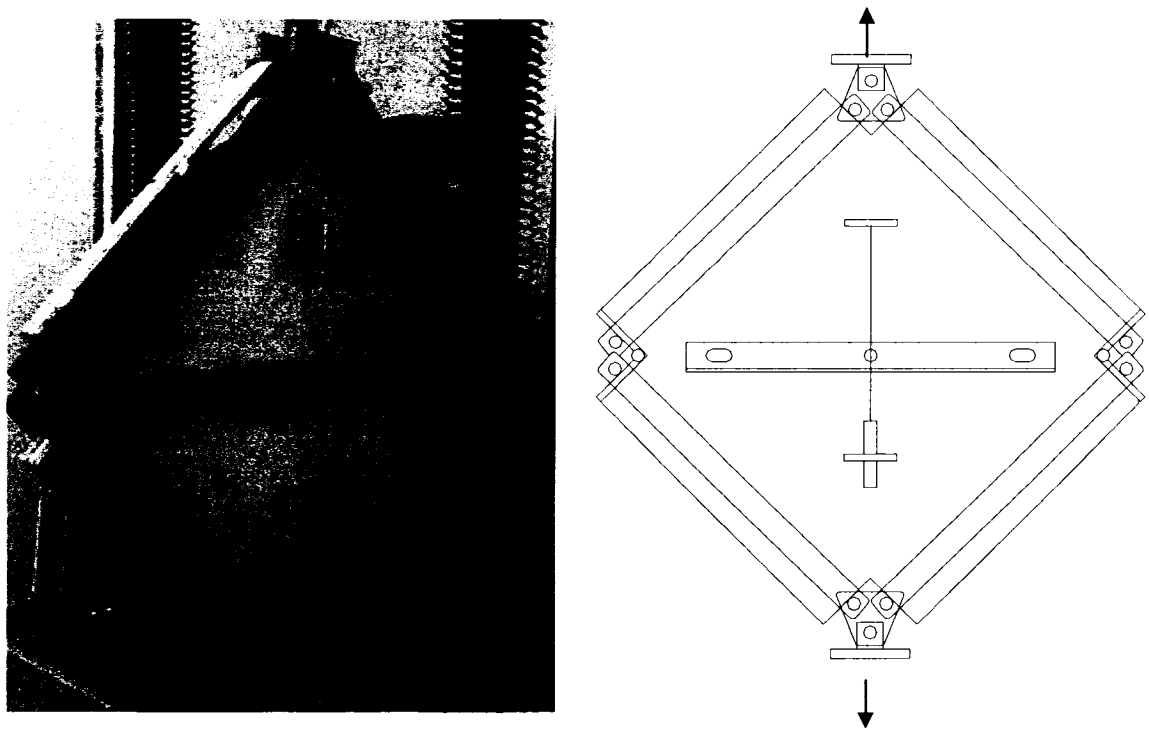

Figure 3.16: Four-sided shear test frame

To avoid bearing at the ends of the panel and to provide a more uniform transfer of shear, two 19 mm (3/4") thick plywood rails were screw fastened to the panel along each edge. Figure 3.17 shows a close-up of the hinge area, with the plywood rails fastened to a gypsum board test specimen. Thus the bearing load was applied to the ends of the plywood rails, not directly to the panel. The rails, which were secured with 10 to 12 drywall screws, then transferred the applied loads in a uniform fashion to the test specimen. To secure the rails to the gypsum board, 6x1" gypsum screws were used whereas the fibreboard required 6x2" screws because of the higher thickness.

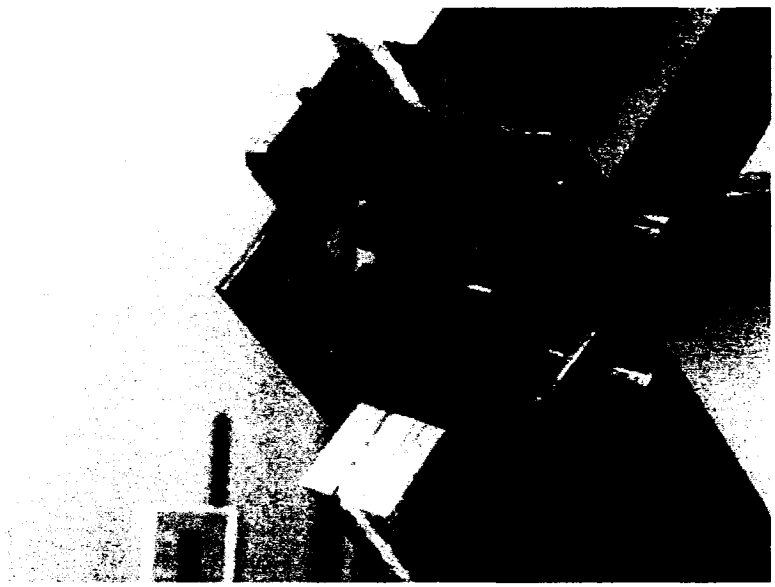

Figure 3.17: Hinge area close-up

The most important aspect of the test setup was the alignment of the test specimen. It was necessary to ensure that the specimen was directly in line with the centre of the load cell and bottom support. The impact of any eccentricity in the installation of the test specimen is further discussed in Section 3.4.3.

The machine used for this setup was an *MTS Sintech 30/G* with a 150 kN load cell. Each test was conducted in displacement control at a crosshead speed of 2.1 mm/min (0.083 in/min). The LVDTs and load cell were connected to a Vishay Model 5100B scanner, which was used to record the data using the Vishay System 5000 StrainSmart software.

The loading rate was determined using the recommendations of ASTM D2719, as follows:

$$n = ZL / \sqrt{2} \qquad (3\text{-}6)$$

where:

n = speed of crosshead (mm/min),

L = length of side of shear area (mm),

Z = shear strain rate, taken as 0.005 (mm/mm/min).

3.4.2 *Test Specimens*

In all, 22 specimens were tested, the shape and dimensions of which are shown in Figure 3.18. As per ASTM D2719 the sides measured 620 mm (24-½"). To avoid stress concentrations at the re-entrant corners of the panel 25.4 mm (1") holes were drilled as shown. All cuts were made with a table saw to ensure that the specimen was square in shape. Figure 3.19 shows a tested fibreboard specimen as well as a tested gypsum board specimen. For most of the test specimens, stiffeners were installed to ensure that flexural deformations of the panel were minimized.

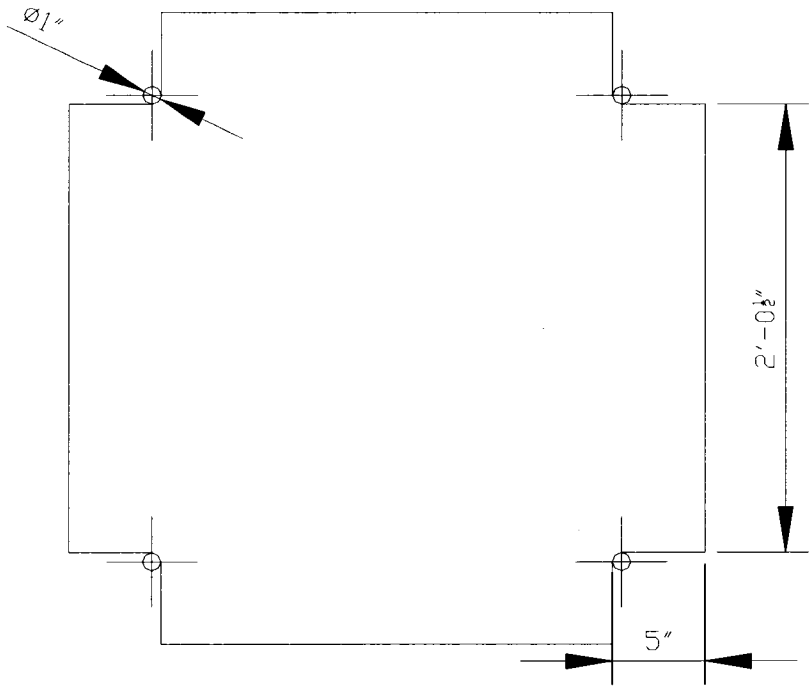

Figure 3.18: Test specimen dimensions

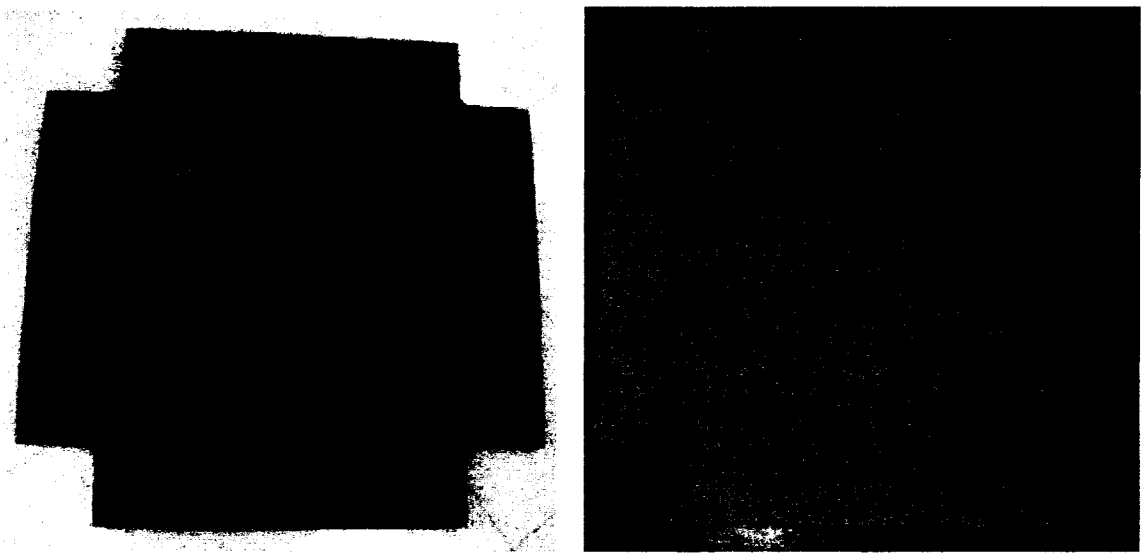

Figure 3.19: Fibreboard specimen (left); Gypsum specimen (right)

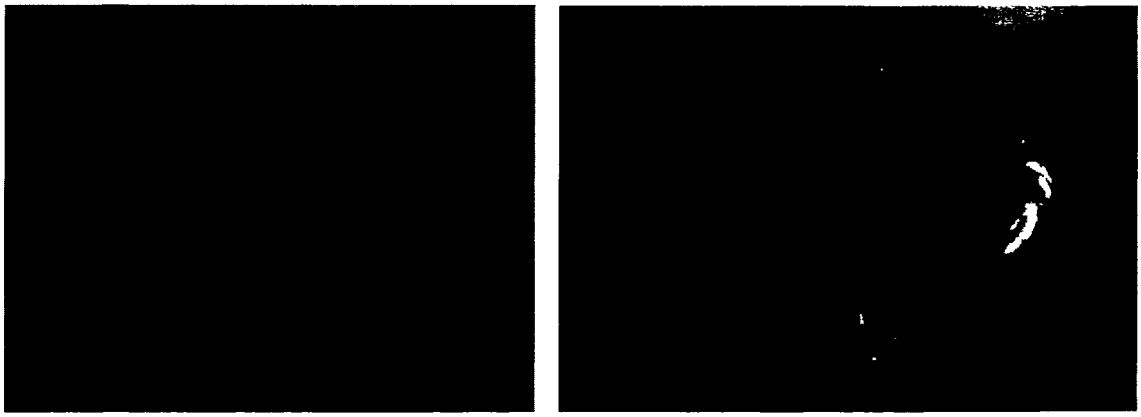

Figure 3.20: Fibreboard specimen (left); Hot bitumen application (right)

Of the 22 specimens, eight fibreboard panels and seven gypsum panels were tested in the setup described above. These specimens are referred to by the name FB for fibreboard and FB-STIFF for fibreboard with a stiffener, as well as GYP-STIFF for gypsum with a stiffener. In addition to these single panel specimens, it was necessary to fabricate specimens that consisted of combinations of fibreboard, ISO insulation, felt vapour retarder and gypsum. These test specimens were similar to the diaphragm specimens with non-structural components tested by Yang (2003). For three tests a 25.4 mm (1") by 609mm by 609mm (24"x24") insulation board was hot bitumen adhered to a fibreboard

panel, as shown in Figure 3.20. These specimens were called FB+ISO. Figure 3.21 shows the finished product once the insulation board had been added on top of the fibreboard.

Figure 3.21: FB+ISO specimen plan view (left);
FB+ISO specimen cross-section view (right)

A total of four FULL SECTION specimens were fabricated in an attempt to represent the non-structural components of a roof. A 609mm by 609mm (24"x24") sheet of felt vapour retarder was first hot bitumen adhered to the FB+ISO section. As a second step in the fabrication a 609mm by 609mm (24"x24") gypsum layer was then hot bitumen adhered to the vapour retarder. Figure 3.22 shows a plan view and an elevation view of a finished specimen.

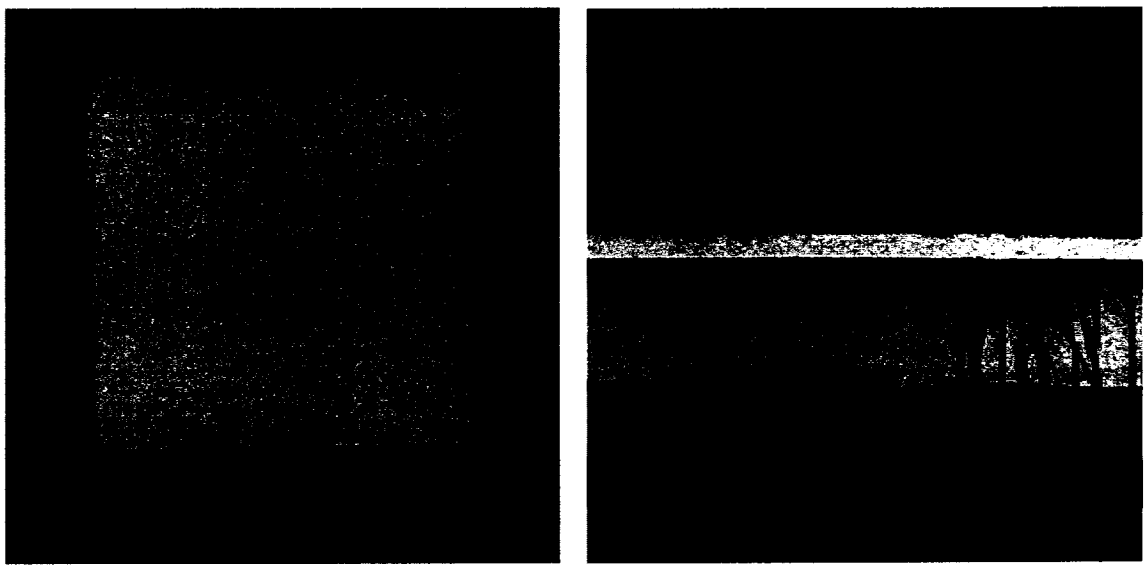

Figure 3.22: FULL SECTION specimen plan view (left); FULL SECTION specimen cross-section view (right)

The fibreboard was used as the base material in all the "sandwich" constructions specimens because it has a lower stiffness than the gypsum board. This facilitated the measurement of any change in stiffness as the additional non-structural layers were added. If gypsum had been used as the base material, the relative increase in stiffness due to the added layers would have been much lower than the stiffness of the gypsum itself, perhaps even negligible. Also, note that only the fibreboard was sandwiched between the two plywood rails; the other non-structural layers were located within the central portion of the test specimen, as can be seen in Figure 3.18. These specimens were tested in the same test setup as the plain gypsum board and fibreboard specimens (Fig. 3.23).

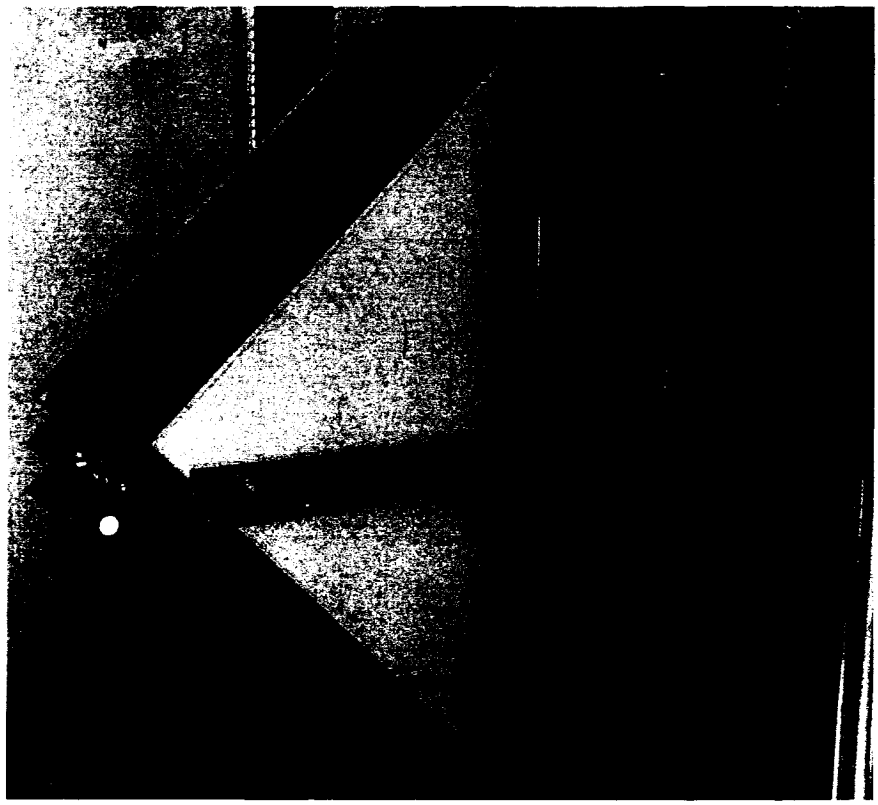

Figure 3.23: FULL SECTION specimen in test frame before loading

The ISO insulation board could not be tested by itself because of its relative shear flexibility and its thickness. The testing frame as fabricated could not accommodate for this thickness and type of material.

The thickness and length were precisely measured for each specimen before it was tested. For the FB+ISO and the FULL SECTION specimens, only the thickness and length of the fibreboard base was taken into account. The reasons behind this will be further explained in Section 3.4.4.

3.4.3 *Specimen Behaviour*

3.4.3.1 *Unstiffened Specimens*

In all, four unstiffened fibreboard panels and one unstiffened gypsum panel were tested. Although the ASTM D2719 test setup was respected, the failure mechanism was not what was expected: a shear buckling failure of the panel in the vertical plane due to horizontal

compression forces occurred rather than a shear failure. Figure 3.24 shows the load paths that exist in this type of test specimen. Because of this failure mode the results from these specimens were not considered to represent the in-plane shear stiffness of the fibreboard and gypsum panels, and hence were not used.

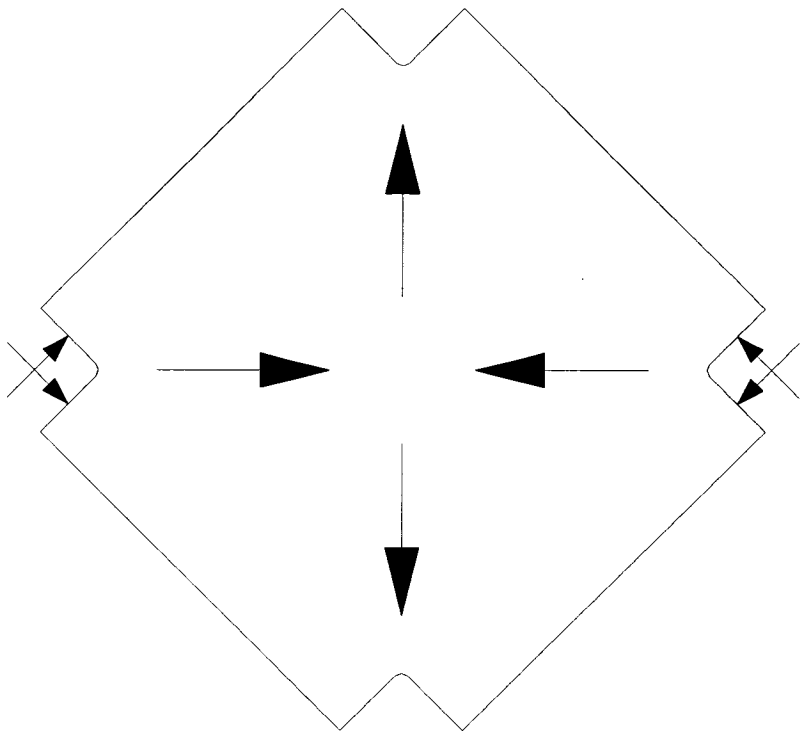

Figure 3.24: Panel load forces

3.4.3.1.1 *Addition of Stiffeners*

Flexural deformations were quite significant in the first test specimens. Stiffening the panels was attempted by testing two panels at once. The two panels were screwed together with 6x2" gypsum screws. This procedure did reduce the amount of buckling that occurred in the specimen, but not completely: failure still occurred by buckling. In light of these results, a second method was conceived.

To counter the problem of buckling, a horizontal stiffener angle (50mm x 50mm x 6.5mm) was attached to each side of the test panel to increase its flexural rigidity and strength (Fig. 3.25). The angles were attached at three locations with 12.7 mm (1/2") threaded rods. The centre threaded rod hole was circular, while the two end holes were

slotted to allow for any axial deformations of the panel and to ensure that the angles did not carry any axial force. The nuts on the end threaded rods were hand-tightened to minimize any friction forces between the panel and the angles. This stiffener setup was used for all of the remaining tests.

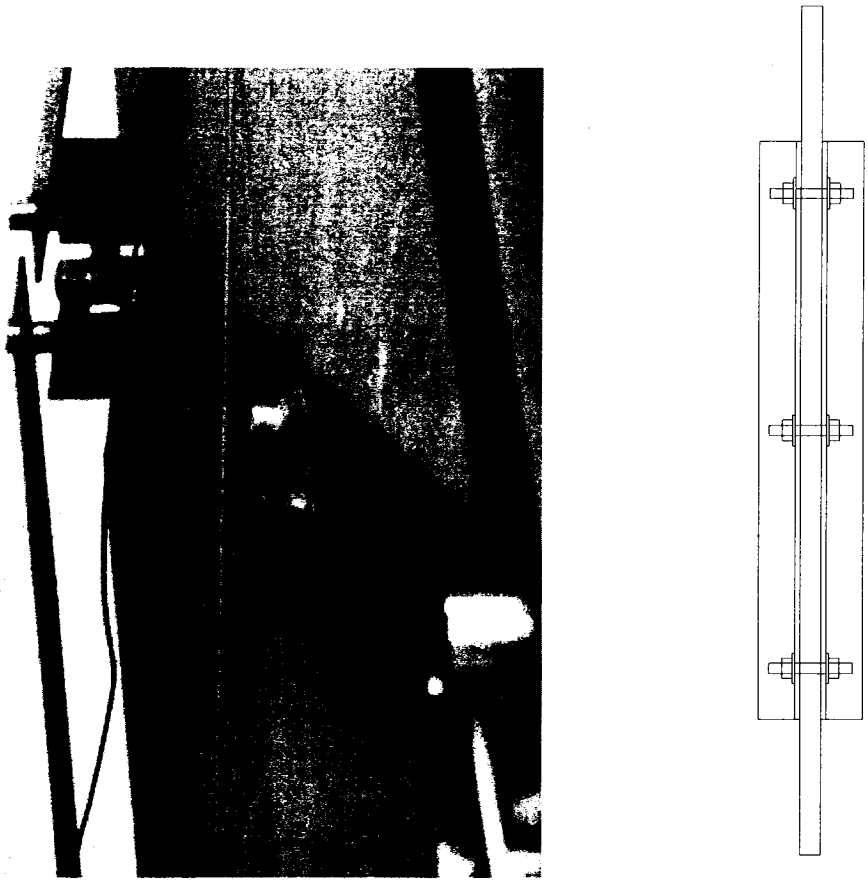

Figure 3.25: Stiffener installed on gypsum board panel

3.4.3.2 *FB-STIFF (Stiffened Fibreboard)*

A typical load versus elongation curve for a fibreboard shear specimen is provided in Figure 3.26. The two plots provide the readings for the two LVDTs that were installed on each specimen. The load versus elongation curves for fibreboard panels were very consistent in shape. The first part of the graph, where the two curves are moving in different directions represents the straightening of the panel. There typically exists a

residual curvature in the panels due to the manufacturing process and possibly the storage conditions. As a shear load is applied one side of the panel elongates, while the other shortens. This behaviour will take place until the panel becomes straight. At this point the two load versus elongation curves become parallel to one another. The average slope of these parallel sections of the curves was used in the calculation of the shear stiffness of the panel.

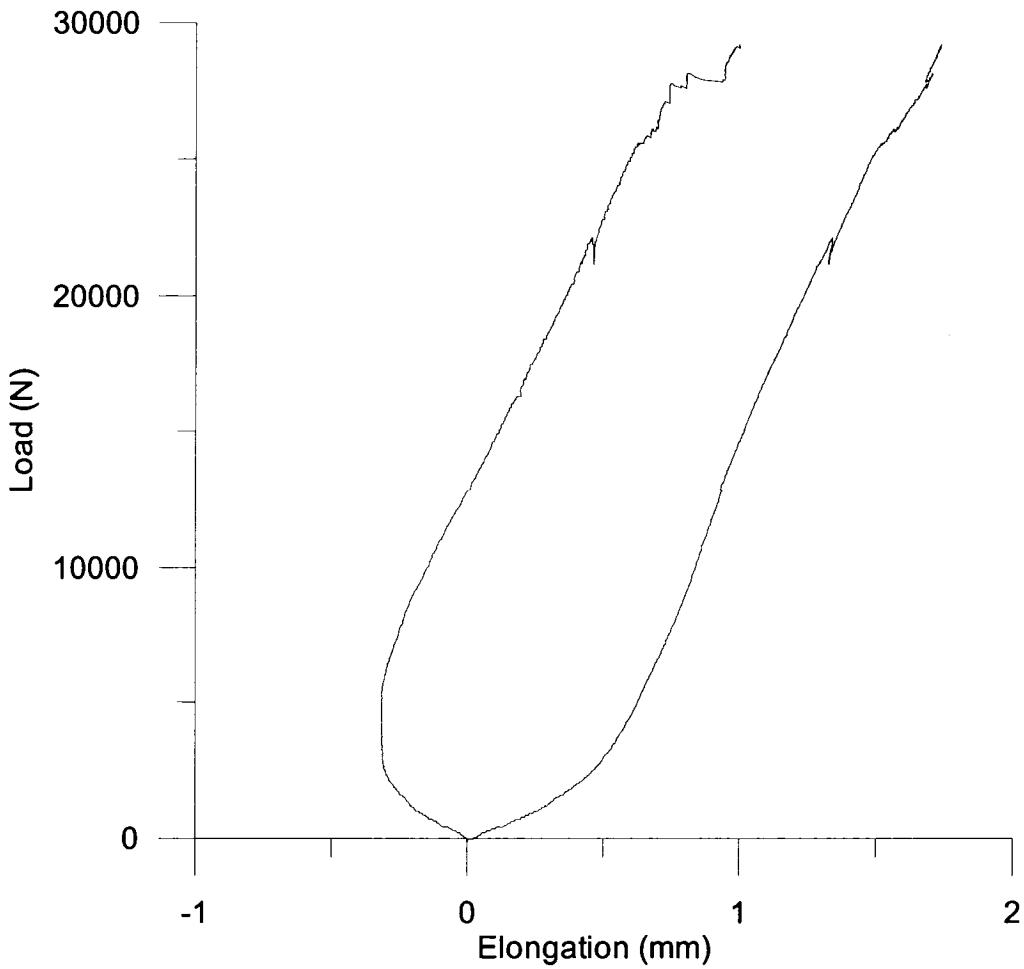

Figure 3.26: Stiffened fibreboard – load vs. elongation

3.4.3.3 *GYP-STIFF (Stiffened Gypsum Board)*

The load vs. deformation behaviour of the stiffened gypsum board specimens was very similar to that of the fibreboard panels (Fig. 3.27). The panel would first straighten, then the two curves would continue parallel to one another. The two parallel sections of the

curves were once again used to determine the shear stiffness of the test panel. The results for the gypsum board tests were also consistent in shape.

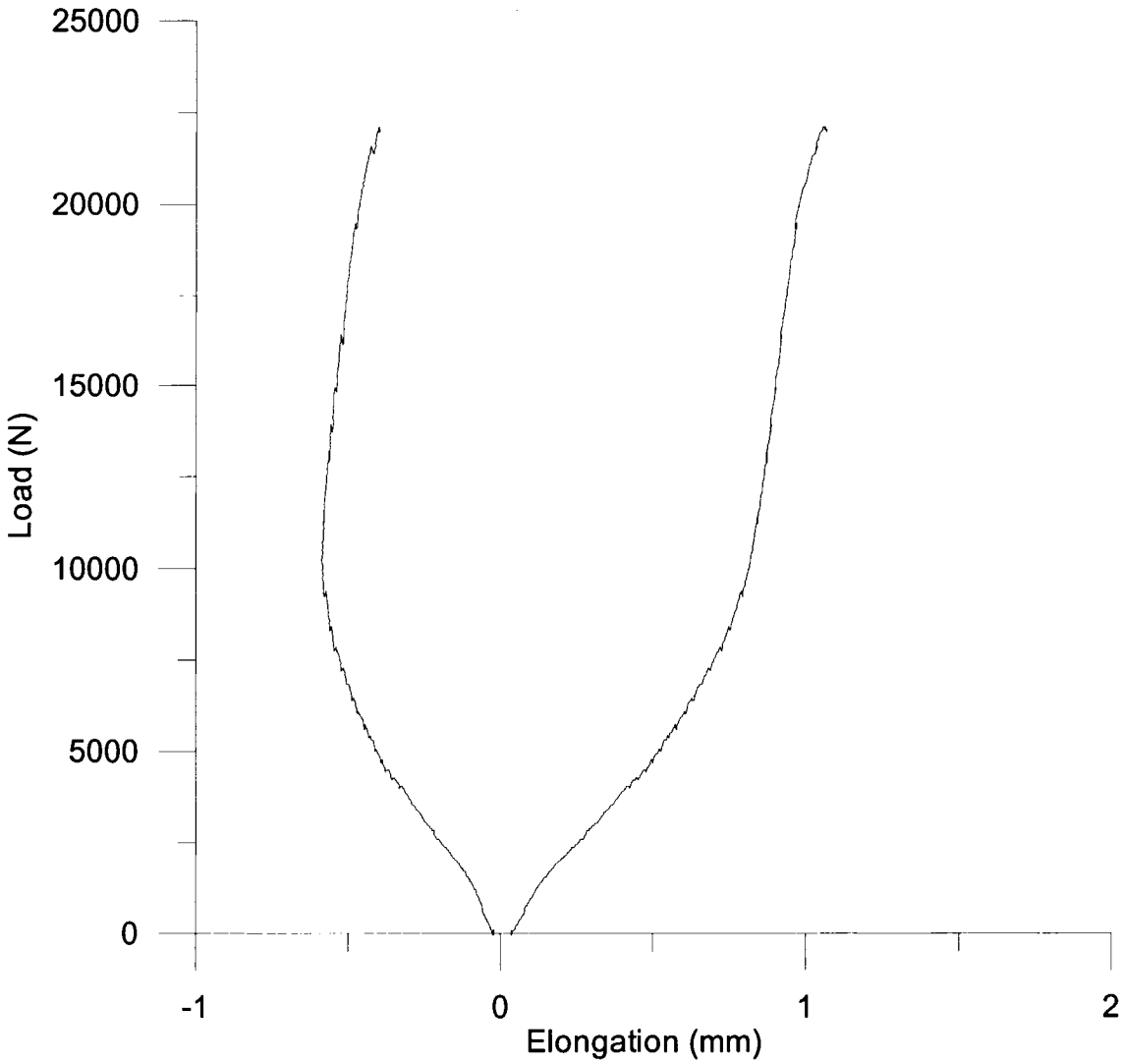

Figure 3.27: Stiffened gypsum board – load vs. elongation

3.4.3.4 *FB+ISO*

The load versus displacement curve of the FB+ISO specimens, shown in Figure 3.28, were similar in shape to the curves obtained for the fibreboard panels alone. However, upon closer inspection it can be seen that the two curves, once the specimen had straightened, did not run parallel to one another. For these tests an LVDT was attached

directly to the fibreboard panel on one side of the specimen, while the other LVDT was attached to the ISO insulation. The two curves did not attain the same slope because the ISO layer was not directly loaded by the test frame. Rather, the shear deformations were applied to the fibreboard layer, which then caused the ISO layer to deform from one side. Since the elongation measurements were obtained from the side of the ISO layer away from the fibreboard there was some variation between the two LVDT readings. The data set obtained from the LVDT that was attached directly to the fibreboard panel was selected for use in the calculation of the stiffness of the panel. For these tests the shape of the curves varied quite a bit from specimen to specimen. All the four-sided shear test curves are included in Appendix C.

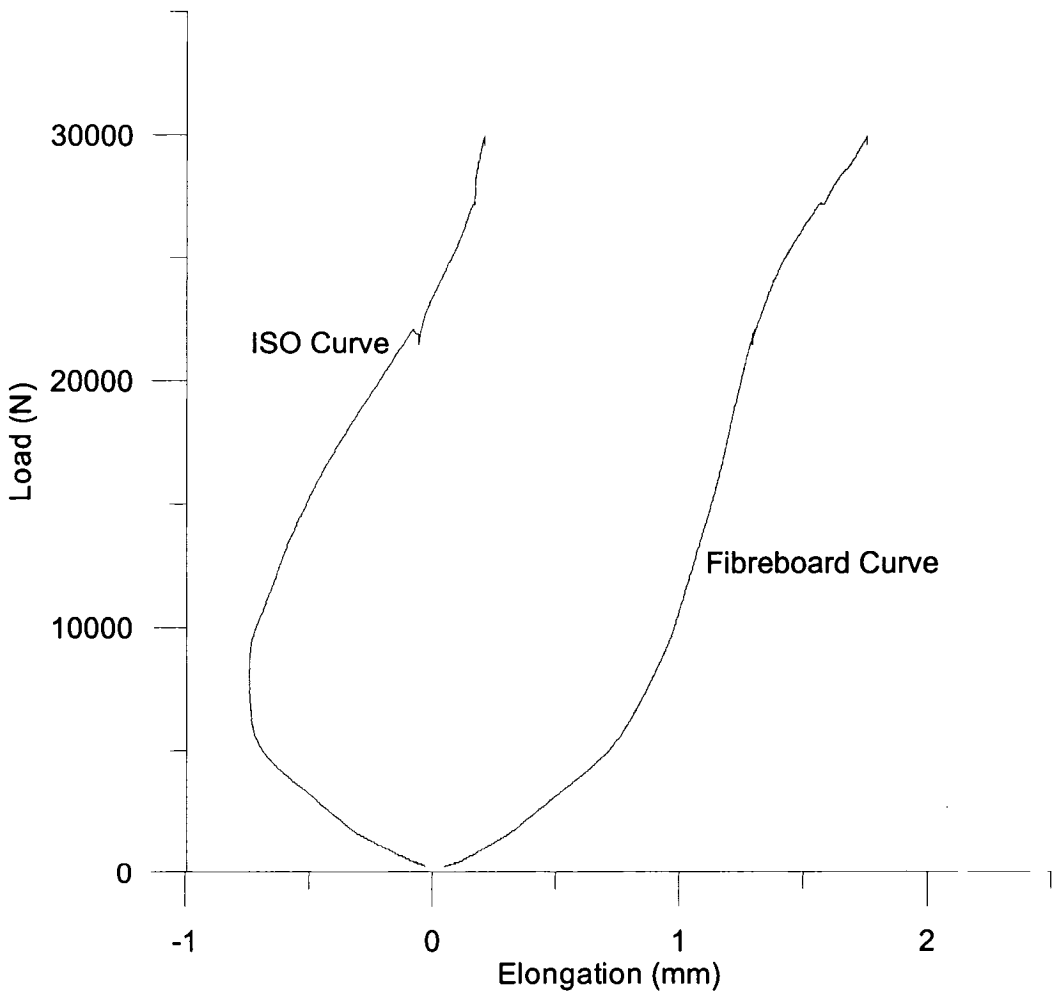

Figure 3.28: FB+ISO – load vs. elongation

3.4.3.5 *FULL SECTION*

FULL SECTION specimens were instrumented and tested in the same manner as the FB+ISO specimens. For this reason the LVDT measurements on the fibreboard side of the specimen did not match those obtained on the gypsum side. It was decided that the data set obtained from the LVDT on the fibreboard panel was to be used to compute the shear stiffness. For these specimens also, the shape of the curves varies greatly from one specimen to another. Figure 3.29 shows a typical load versus elongation curve for a FULL SECTION specimen.

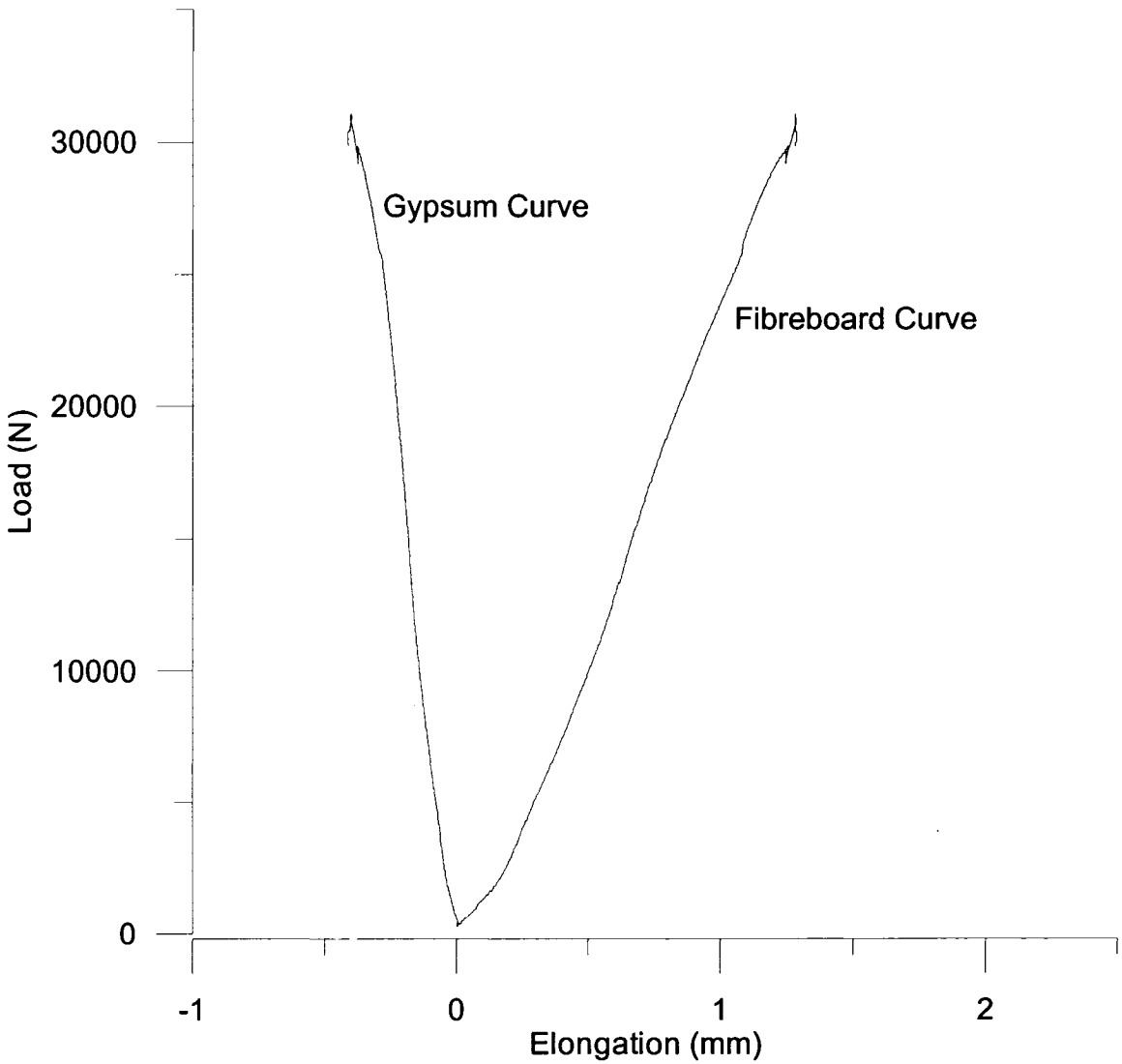

Figure 3.29: FULL SECTION – load vs. elongation

All the curves had similar behaviours and slopes from approximately 6000 N to 10000-12000 N. Therefore the slope for all FULL SECTION specimens was taken at that load level. All load versus elongation curves can be found in Appendix C.

For the FULL SECTION specimens, the gypsum curve had a negative slope, hence that side of the specimen is in compression. Drawing the free-body diagram of the specimen, it is clear that bending occurs in the section because of the eccentricity of the load with respect to the centre of rigidity (Fig 3.30). In the same figure is included the distribution of stresses, both shear and bending.

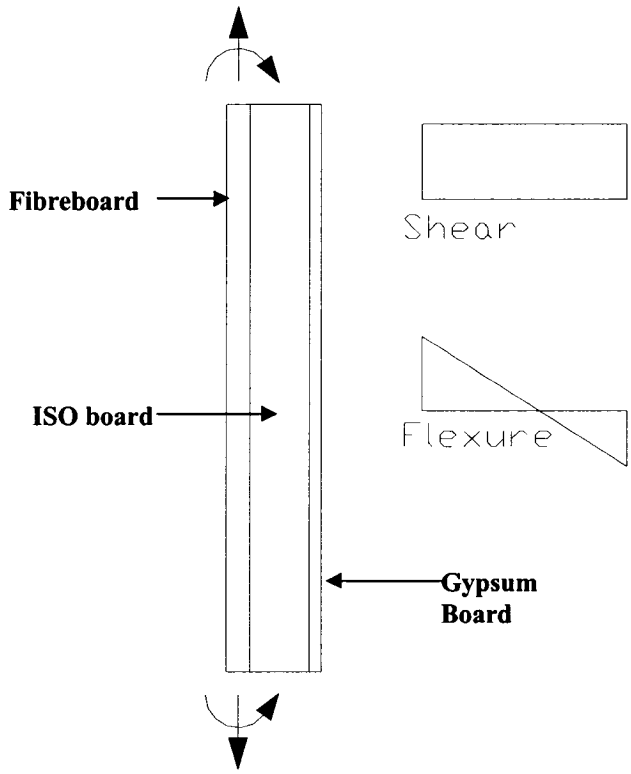

Figure 3.30: Specimen free body diagram

Two methods were used to estimate the shear modulus of the built-up section. For the first method, the eccentricity was ignored, and the load was assumed to be concentric. Therefore, the bending of the specimen during testing was ignored and only the slope of the fibreboard curve was taken into account. This assumption resulted in a slightly inaccurate estimate of the shear stiffness of the FULL SECTION specimen. The second

method consisted of building a finite element model of the built-up section and obtaining the shear modulus of the FULL SECTION specimen from the analyses. Both methods will be further discussed in Section 3.4.5. This investigation was needed to interpret the results of the FB-ISO and FULL SECTION tests due to eccentricity present in the specimens.

3.4.4 *Data Analysis*

3.4.4.1 *Concentrically loaded specimen*

The stiffness of each test panel was obtained from the load vs. elongation graphs described previously and Equation 3.6 from ASTM D2073 (1994). This equation has been formulated for use with the four-sided shear test.

$$G = 0.3536(P/\Delta)*[L_1 / (L*t)] \qquad (3\text{-}6)$$

where:

G = modulus of rigidity (MPa),

P/Δ = slope of force/deformation curve (N/mm)

L_1 = gauge length (mm),

L = length of side of shear areas (mm),

t = thickness of shear specimen (mm).

It is possible to derive this equation from the following:

$$G = \tau / \gamma \qquad (3\text{-}7)$$

where:

τ = shear stress defined as $P / (2\sin 45) * 2\sin 45 / (L * t) = P / (L * t)$,

γ = shear strain defined as $(2\Delta\cos 45) / (L_1 / 2\cos 45) = \Delta / (0.3536 * L_1)$.

The thickness of the shear specimen, t, was defined simply as the thickness of the fibreboard or gypsum panels when either of these two materials were tested alone. However, for the FB+ISO and FULL SECTION specimens, the thickness was taken as

that of the fibreboard panel. With this assumption, it was possible to determine the contribution provided by the insulation board and the gypsum board in terms of an increased stiffness for the fibreboard. That is, the other non-structural layers were simply thought of as reinforcement for the fibreboard test specimen. As noted previously, the average slope of the two deformation curves once the test panel had straightened was taken as P/Δ for the gypsum and fibreboard specimens. In the case of the FB+ISO and FULL SECTION specimens, only the data acquired from the LVDT on the fibreboard panel was used to calculate the slope of the load vs. elongation graph. The results of the four-sided shear test have been provided in Table 3.5.

The test values for the unstiffened specimens are shown only for comparison with the stiffened specimens. FB1, FB2 and FB3 provided adequate results; it seems that buckling was not problematic for the fibreboard specimens. However it is clear that for the unstiffened gypsum specimen, buckling resulted in a severe reduction in stiffness (see Table 3.5). GYP-STIFF1 was installed incorrectly in the test frame which explains the very low stiffness value that was obtained even though the stiffener had been attached.

Table 3.5: Four-sided shear test results

Specimen	FB1	FB2	FB3	FB4+FB5	GYP1	
G (MPa)	234	241	263	388	259	
Average	**282**				N/A	
%C.o.V.	**25.6%**				N/A	
Specimen	FB2-STIFF	FB3-STIFF	FB4-STIFF	FB5-STIFF		
G (MPa)	287	198	265	191		
Average	**235**					
%C.o.V.	**20.4%**					
Specimen	GYP1-STIFF	GYP2-STIFF	GYP3-STIFF	GYPS4-STIFF	GYP5-STIFF	GYP6-STIFF
G (MPa)	281*	1423	229*	997	1355	1363
Average	**1284**					
%C.o.V.	**15.11%**					
Specimen	FB+ISO1	FB+ISO2	FB+ISO3			
G (MPa)	265	352	302			
Average	**306**					
%C.o.V.	**14.13%**					
Specimen	FULL SECTION1	FULL SECTION2	FULL SECTION3	FULL SECTION4		
G (MPa)	401	280	310	492		
Average	**395**					
%C.o.V.	**18.89%**					

* Specimens were not used to calculate average values.

3.4.5 *Discussion*

Upon reviewing the various results obtained from the four-sided shear tests, it became clear that the gypsum board had the highest in-plane shear stiffness of all the materials tested. Its average shear stiffness of 1284 MPa was 5.5 times higher than that of the fibreboard (235 MPa) (Table 3.5). However, the most interesting information obtained from this experimental research is the data from the FB+ISO and FULL SECTION specimens. Firstly, the results using the concentric load method will be discussed, followed by the results of a finite element analysis.

3.4.5.1 *Concentric Load Analysis*

An increase in shear stiffness of 30 %, compared with the fibreboard alone, was measured (Table 3.5) when the ISO board was added to the fibreboard. A total shear stiffness increase of almost 70% compared to the fibreboard alone and an increase of almost 30% compared to FB+ISO were realised when the gypsum board and vapour retarder layers were added to the fibreboard and ISO board. However, it must be noted that these values may not be accurate because the concentric data analysis did not take into account the eccentric loading of the test specimen.

These results provide the stiffness of the roofing section with the load applied to the fibreboard. However, in the actual roof section, as shown in Figure 3.31, the shear load / deformation would first be applied to the gypsum board from the corrugated steel roof deck panels. Screw fasteners are typically used to connect the gypsum board to the deck panels. Hence, what needs to be addressed is the increase in stiffness to the gypsum board because of the addition of the vapour retarder, ISO and fibreboard panels.

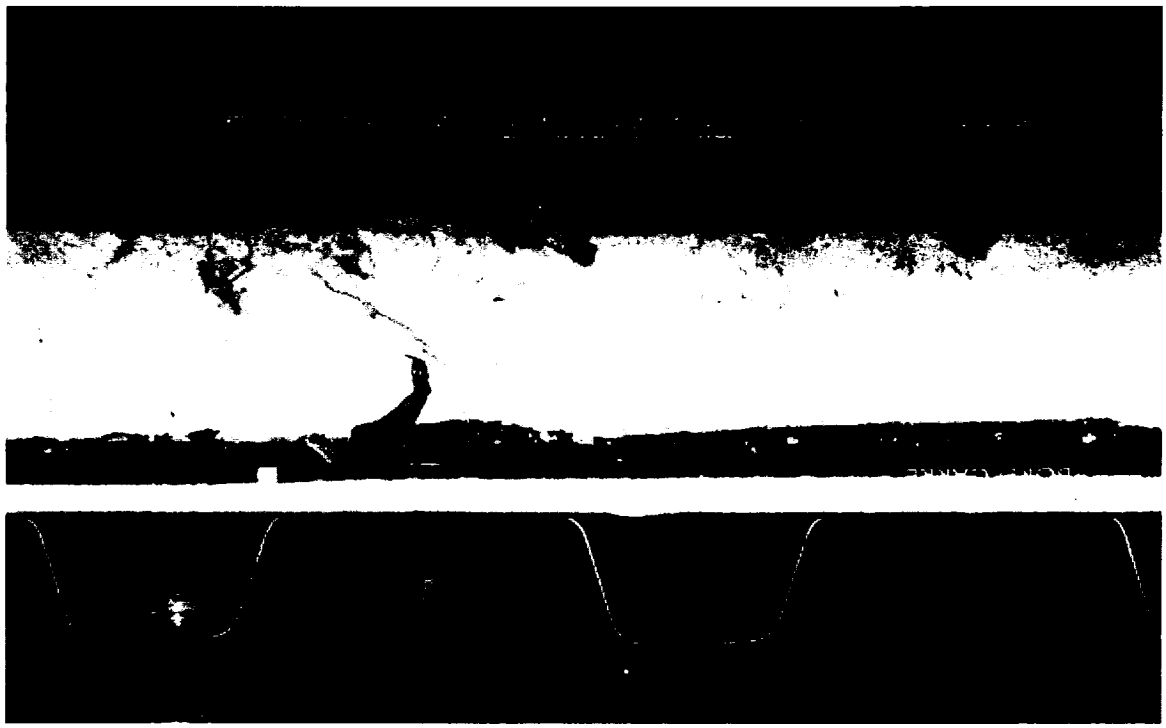

Figure 3.31: Roof Cross-Section *(Yang, 2003)*

The stiffness of the fibreboard and gypsum board panels is known, as well as the FULL SECTION and the FB+ISO section. The only individual non-structural component for which the shear stiffness is not known is the ISO board, excluding the vapour retarder which can be assumed to have negligible in-plane shear stiffness. For this reason an attempt was made to determine the stiffness of the ISO board given the test results listed in Table 3.5. Figure 3.32 shows the spring model that was used to represent the non-structural roofing cross section. The gypsum board was connected in parallel because it is directly attached to the steel deck, whereas the fibreboard and ISO board are attached in series. This approach was taken because the fibreboard and ISO layers, although they may stiffen the diaphragm, are not mechanically fastened to the steel deck.

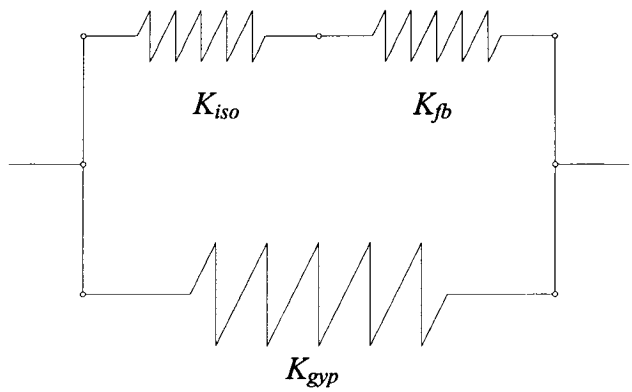

Figure 3.32: Spring-stiffness diagram of non-structural roofing components

This same correlation can be used for the FULL SECTION four-sided test specimens. Using the same concept and inversing the position of K_{fb} and $K_{gyp,}$ it was possible to compute the value of K_{iso}. The modified spring diagram used to compute the ISO board stiffness is shown in Figure 3.33.

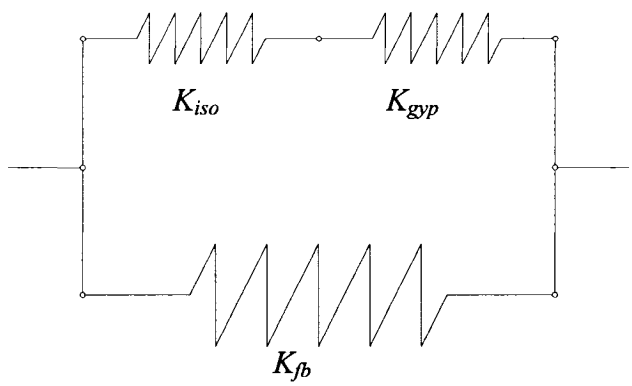

Figure 3.33: Modified spring-stiffness diagram of non-structural roofing components

Simply by using Ohm's law, Equation 3-7 can be derived as:

$$K_{full} = K_{fb} + \left(\frac{1}{K_{gyp}} + \frac{1}{K_{iso}} \right)^{-1}, \qquad (3\text{-}7)$$

Isolating K_{iso}:

$$K_{iso}^{-1} = \left(K_{full} - K_{fb}\right)^{-1} - \frac{1}{K_{gyp}} \qquad (3\text{-}8)$$

Using the average values listed in Table 3.5 and Equation 3-8, K_{iso} is calculated to be 184 MPa. With this value, the stiffness of the full section, K_{sys}, with the gypsum board as the base element can be computed. Using this approach the in-plane shear stiffness of the non-structural roofing components was found to be 1387 MPa.

3.4.5.2 *Finite Element Analysis*

In order to obtain a more realistic evaluation of the shear modulus of the built-up section, two linear elastic finite element models (FEM) were developed using the SAP2000 software. Firstly, a finite element model resembling the four-sided shear test specimen was built (Fig. 3.34). Loads were applied along the edges of the fibreboard panel in order to simulate the shear load applied by the test frame. As Figure 3.34 shows, bending occured in the built-up section due mainly to the eccentric loading. However, the values of E and G of the ISO board were unknown; therefore this model was used to obtain the value of the shear modulus and the modulus of elasticity of the polyisocyanurate panel. The deformation of the model was obtained at the same locations as were used to measure the deformation of the test specimens, followed by a comparison of the analysis results with the test results. A constant Poisson's ration, chosen as 0.3, was maintained throughout the parametric study. The values of E and G were systematically varied until the analytical deformations matched those measured during testing.

The models shown in Figures 3.34 and 3.35 were built using eight-node *Solid Elements*. These elements are direct extensions of rectangular plane element or shell elements (Cook *et al.*, 2001) and are produced by using the *Extrude* function. It is possible for strains and stresses to vary through the thickness of these elements. The model shown in Figure 3.34 has 1728 solid elements, 576 for each material. Continuity between the different solid elements is automatically recreated if adjacent solid elements are built using the same joints. If two faces of two distinct solid elements are bound by the same joints, the deformations of the two faces will be same for the whole surface of that face because their displacements are controlled by the same polynomial displacement field.

The elements are assigned the material properties of gypsum board and fibreboard that were obtained in Sections 3.3 and 3.4.

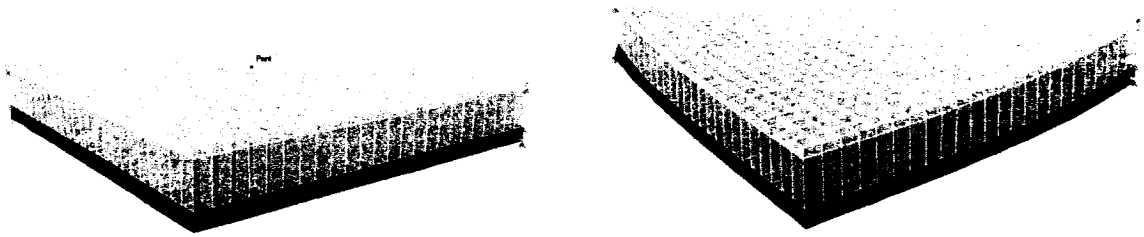

Figure 3.34: Undeformed (left) and deformed (right) FEM of FULL SECTION test specimen

It is mentioned in the literature that values for the shear modulus of elasticity of polyisocyanurate foams used in sandwich construction vary from 0 to 5 MPa (Vinson, 1999). Hence, the initial value of E, combined with a Poisson's ratio of 0.3, was assumed to be in this range. Upon successful correlation of the analysis and test results, the modulus of elasticity and the shear modulus of the polyisocyanurate board were determined to be 9.4 MPa and 4.0 MPa, respectively.

Once the material properties of the three non-structural components had been obtained, a second FEM was built (Fig. 3.35). A simple cantilever analysis model composed of only the gypsum, ISO and fibreboard layers was constructed. The model is 24" by 24", the same dimensions as the test specimen without the loading rails. The same eight-node element types were used in the model, although only three elements were required, one for each layer of material (Figure 3.35). The four sided shear test model was divided into thousands of elements primarily because it was necessary to obtain displacement readings at the specific locations that were used in the testing procedures. Furthermore, more accurate results for flexure will be obtained by using multiple elements, whereas shear deformation accuracy is not affected by the number of elements (Cook *et al.*, 2001). The cantilever model was supported at four locations; three of the supports were rollers and the fourth was pinned. A point load was applied to the gypsum board at one corner of the model which caused the shear deformation illustrated in Fig. 3.35. This deflection

allowed for an in-plane shear stiffness to be calculated. By comparing the stiffness of the model that contained the gypsum, ISO and fibreboard panels with that of a similar mode which consisted of gypsum board alone it was possible to determine the increase in shear stiffness of the system.

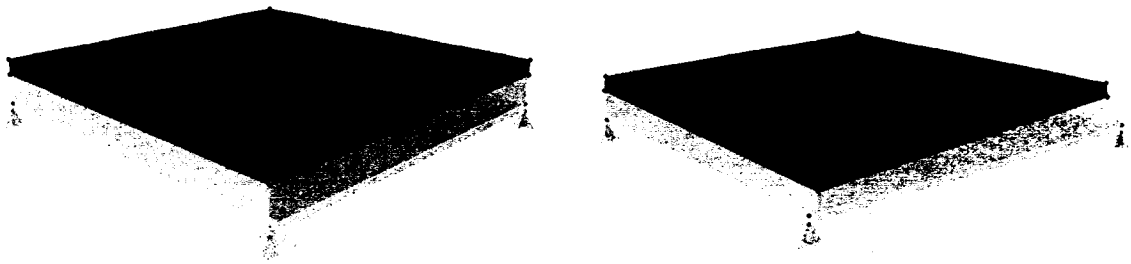

Figure 3.35: Undeformed (left) and deformed (right) shear model

Figure 3.35 shows that the ISO board and gypsum board deform under in-plane shear loading but the fibreboard panel does not undergo much deformation compared to the other two materials. This indicates that the load is not completely transferred to the fibreboard through the ISO board. While conducting the diaphragm analysis, it was clear that as the stiffness of the ISO board increased, the deformation in the fibreboard panel as well as its contribution to overall stiffness became higher. Using the values of the modulus of elasticity and shear modulus obtained from physical testing and finite element analyses, the effective shear modulus of all the combined non-structural components was 1353 MPa, an increase of 5.39% over the bare gypsum panel.

3.5 Connection Tests

3.5.1 *Setup and Test Procedure*

The objective of these tests was to determine the stiffness of the typical screw and nail (powder actuated fastener) connections that are present in roof deck diaphragms: gypsum board to steel deck, sidelap connections and frame-to-deck connections. A single overlap / single shear setup was used for the testing of all individual connections (Fig. 3.36). Each specimen was composed of two pieces (gypsum, steel deck or steel plates) that were connected by a single fastener. The free ends of the two pieces were then installed in a gripping device that was attached to the testing frame. In most cases four LVDTs were used to measure the elongation of a 101.6 mm gauge length in which the single fastener

was centred. This was done because the specimen was not necessarily straight at the start of loading and to eliminate the effect of possible slippage or distortion at the grip locations. The stiffness of the connector can then be found from the load-displacement curve. However, some frame-to-deck and sidelap tests were conducted using eight LVDTs rather than four. These displacement measuring devices were added to account for any out of plane rotation that may occur during testing.

The machine used for this setup was an *MTS Sintech 30/G* with a 150 kN load cell. Each test was conducted in displacement control at a crosshead speed of 1 mm/min (0.04 in/min). The LVDTs and load cell were connected to a Vishay Model 5100B scanner, which was used to record the data using the Vishay System 5000 StrainSmart software.

The deck-to-frame and sidelap connection tests were carried out in conjunction with Camelia Nedisan, a PhD student from École Polytechnique of Montreal. The discussion contained in this thesis covers the behaviour in terms of elastic stiffness of these two connection types. Information in the inelastic performance of the connections can be found in Nedisan *et al.* (2006).

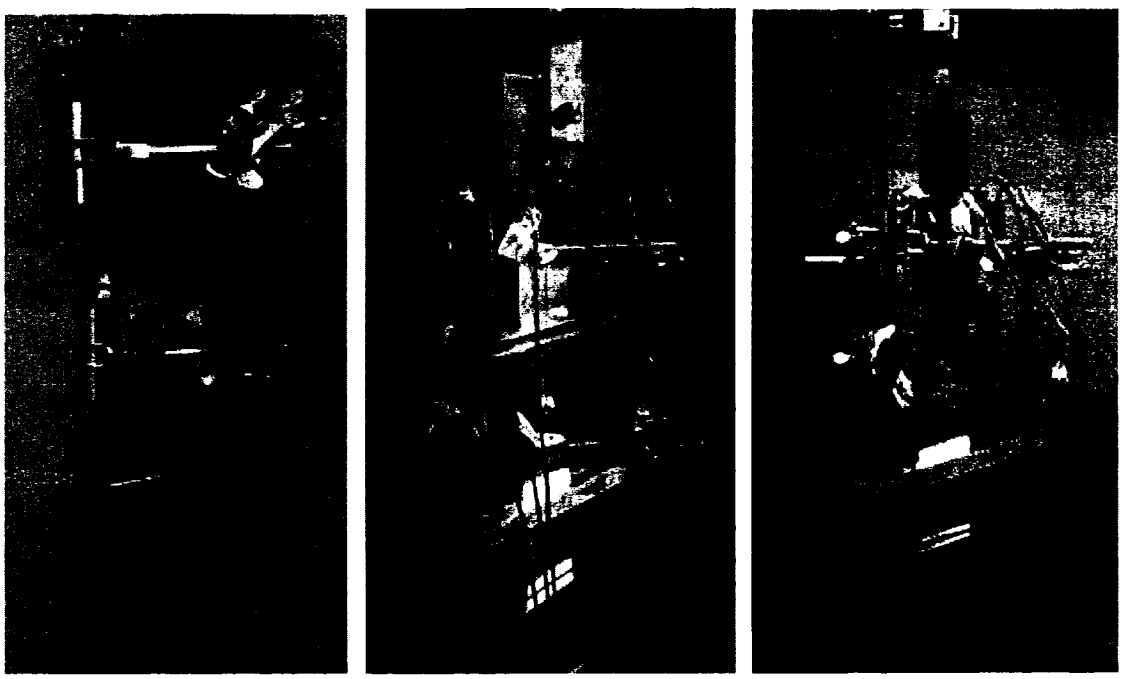

Figure 3.36: 4 LVDT connection test setup gypsum test (left);
8 LVDT connection test setup side lap (middle) and deck-to-frame (right)

3.5.2 *Test Specimens*

Three types of connections were tested, deck-to-frame, sidelap, and gypsum board-to-deck. A short description of each specimen type is presented in the following sections. As noted previously each test specimen was constructed of two pieces and a single fastener. All steel test pieces were between 254 mm (10") and 406.4 mm (16") in length. It was assumed that the length of the piece did not influence the results, because of the LVDT arrangement which was used to measure the localized deformation around the connector. The gypsum board pieces were approximately 254 mm (10") in length. In all cases the connector was installed 50 mm (2") from the end of the overlapped segment of the test piece.

The sheet steel pieces were fabricated with two 25.4 mm flanges at one end. This was done because prior testing had shown that without these flanges the end portion of the test piece would often deform due to the compression loading caused by the test setup. In a real deck system this buckling is not observed under loading due to the stiffening effect of the web elements. Hence, these flanges can, in effect, be assumed to represent the webs of a typical roof deck panel. The gypsum and steel plate pieces were simply fabricated from either flat panels or bar stock, respectively.

Test specimens were constructed of 0.76 mm, 0.91 mm, 1.22 mm and 1.51 mm ASTM A653 (2002) Grade 230 MPa sheet steel. The gypsum board was 12.7 mm (1/2") *CGC* Type X, and the steel plates were 4.8 mm (3/16") grade 300W CSAG40.20/G40.21 (1998) material.

3.5.2.1 *Deck-to-Frame*

Hilti X-ENDK22-TH12 powder actuated (nail) fasteners (Hilti, 2001) were used to connect the deck elements to the frame (Fig. 3.37). These nails were installed with a HILTI DX A41 SM tool and the 6.8/11M HILTI #5 short red cartridge. The tool setting was at the maximum, which allowed for the nail standoff height limits to be met.

Figure 3.37: Typical deck-to-frame connection test specimen

3.5.2.2 *Sidelap*

Sidelap connections exist between two deck panels. In order to evaluate the stiffness of the connection alone two sheet steel pieces (with flanges) of the same thickness were instead connected back-to-back with a single screw fastener (Fig. 3.38). Hilti S-MD 12-14 X 1 HWH #1 screws were used in all cases.

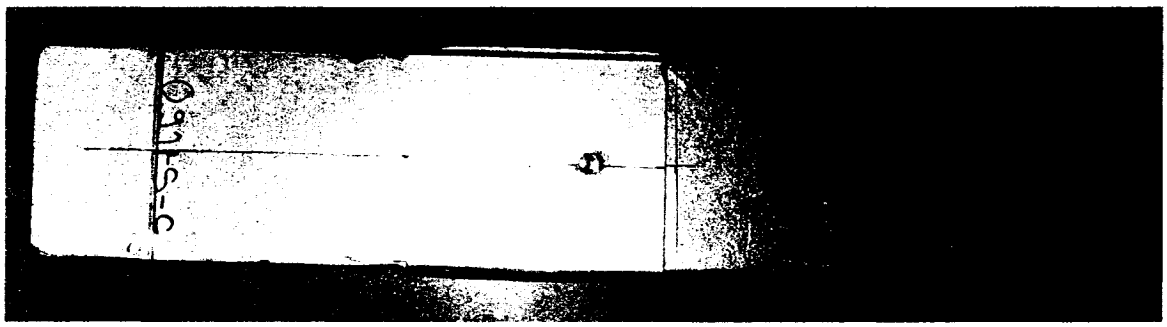

Figure 3.38: Typical sidelap connection test specimen

3.5.2.3 *Gypsum-to-Deck*

The gypsum-to-deck connectors are used to fasten the gypsum board to the steel deck diaphragm. A typical test specimen is shown in Figure 3.39. The connectors are #12 Hex with Round Galvalume Plate Dekfast™ products, made by SFS intec (Fig. 3.40).

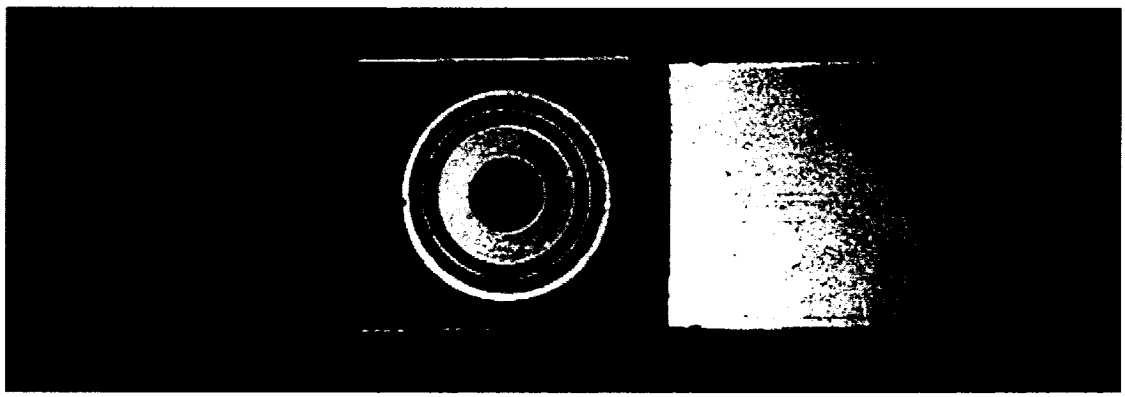

Figure 3.39: Typical gypsum-to-deck connection test specimen

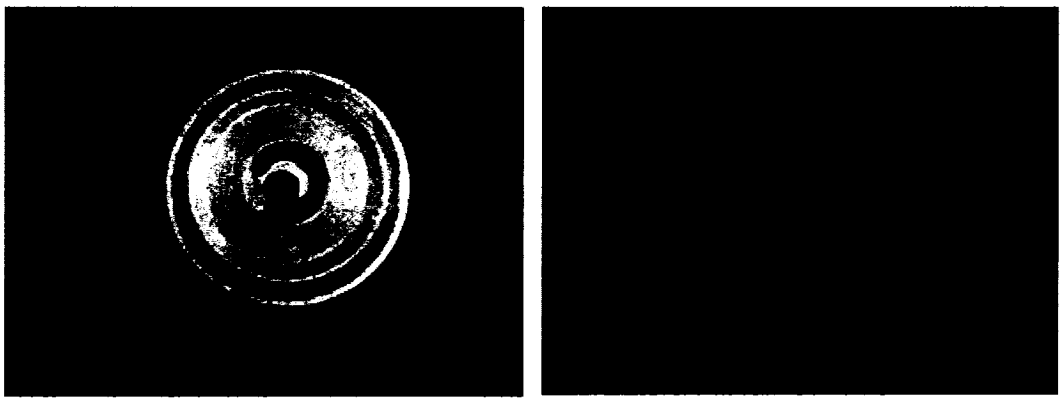

Figure 3.40 Screw and washer assembly used for gypsum-to-deck connections

3.5.3 *Specimen Behaviour*

3.5.3.1 *Deck-to-Frame*

Typical load vs. displacement curves for all four panel thicknesses of the deck-to-frame connections have been provided in Figure 3.41. The deck-to-frame connections behaved in a linear fashion under initial loading. Inelastic behaviour then commenced quite abruptly, however the load carrying capacity continued to increase until a displacement of approximately 4 mm. The 0.76 mm and 0.91 mm thick specimens were similar in behaviour, i.e. they reach approximately the same ultimate load and their stiffness seems similar. The 1.22 mm and 1.51 mm decks, however, exhibited much higher ultimate loads and stiffnesses than the two thinner sheet steels.

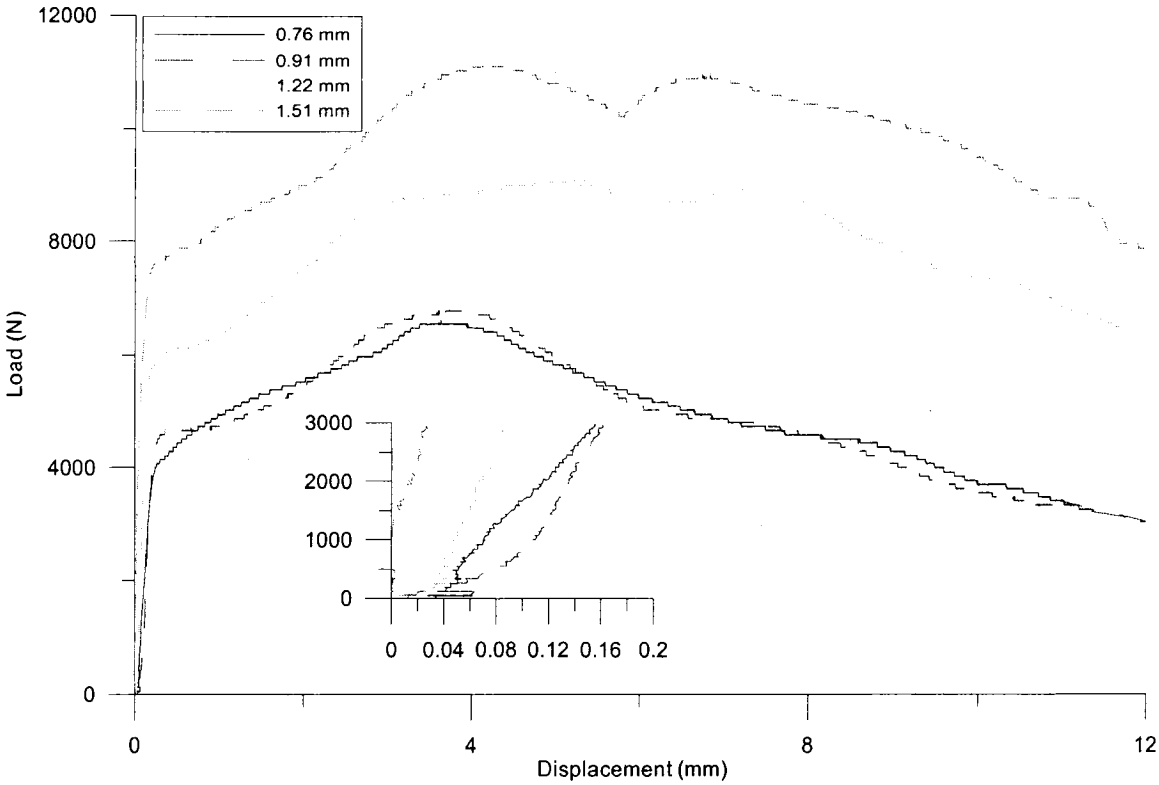

Figure 3.41 Deck-to-frame connection – load vs. displacement

3.5.3.2 *Sidelap*

Typical load vs. displacement curves for all four panel thicknesses of the sidelap connections have been provided in Figure 3.42. As with the deck-to-frame connections, the behaviour is linear at first and then followed by an inelastic zone. A substantial increase in capacity is obtained in this inelastic zone for the 1.22 and 1.51 mm thick specimens; however, this was not the case for the two thinner specimens. Similar to the deck-to-frame specimens, stiffness and strength increased with the deck thickness.

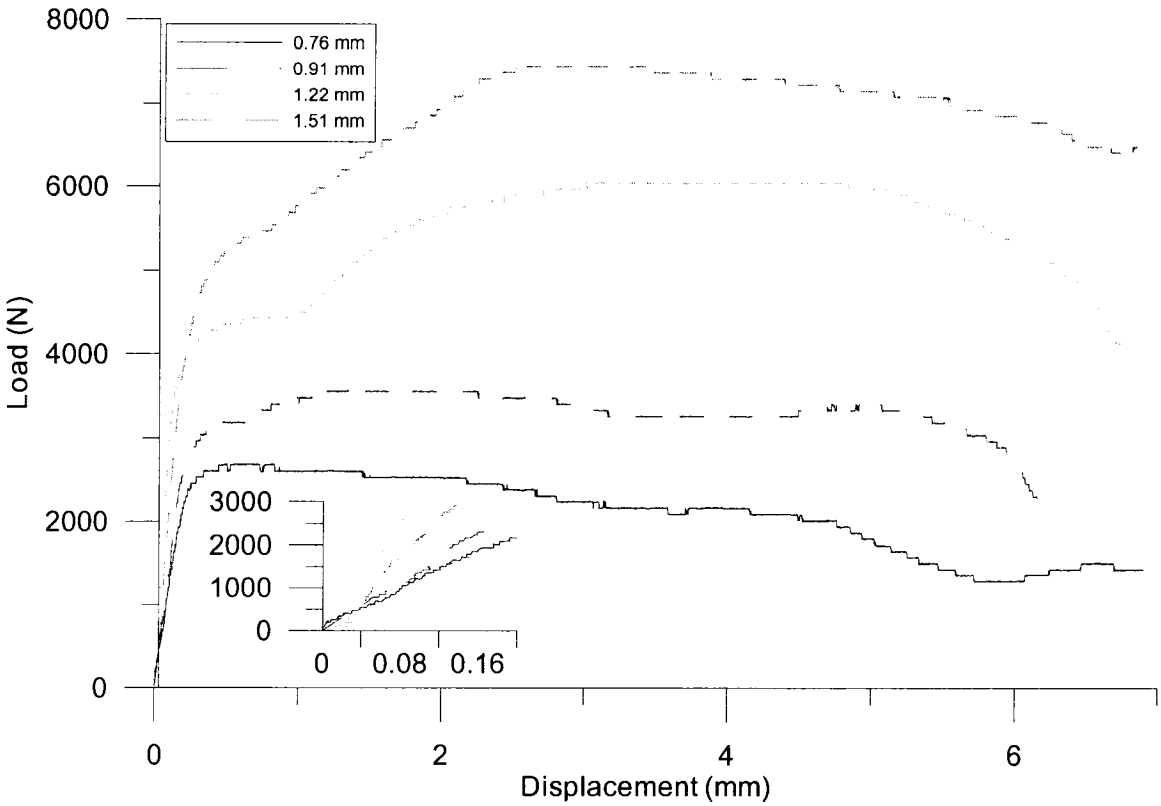

Figure 3.42: Sidelap connection – load vs. displacement

3.5.3.3 *Gypsum-to-Deck*

It was observed that for the gypsum-to-deck specimens the controlling factor that affects the load vs. displacement behaviour is the tightness of the connector. For example, if the screw does not tightly affix the gypsum to the sheet steel, then the connection stiffness will be drastically lower than that of a tightly connected specimen. A significant proportion of the connection rigidity is obtained by the bearing of the washer on the gypsum. The washers were not tight against the gypsum board and could move freely for tests 076-G-A, 076-G-C and 076-G-D, whereas they were very tight for tests 076-G-B and 076-G-E. This workmanship-related aspect reveals how the variability of screw installation may affect the connection performance, and eventually the overall shear stiffness of the roof deck diaphragm that is clad with non-structural components. Typical load versus deformation curves are shown in Figure 3.43. The 0.76 mm, 0.91 mm and 1.22 mm specimens all have similar behaviours as opposed to the 1.51 mm specimen.

This can be attributed somewhat to the thickness of the sheet steel; however the screw and washer tightness was more influential on the measured performance.

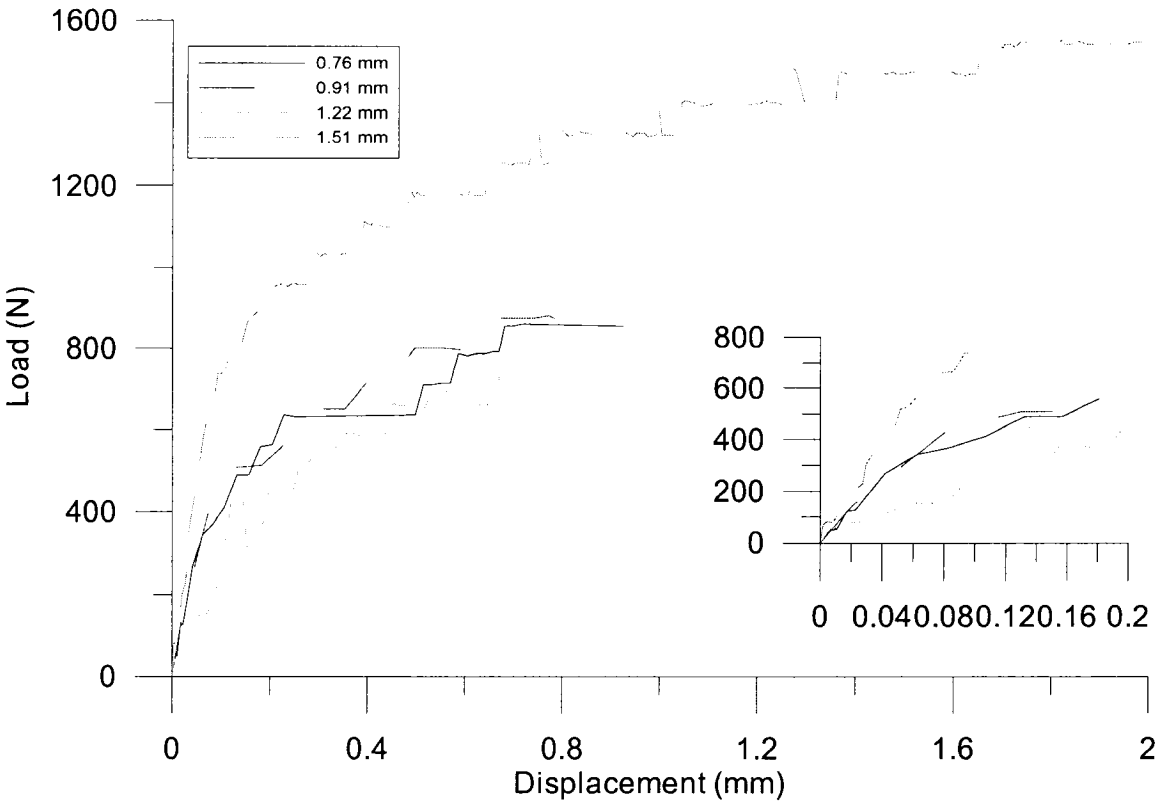

Figure 3.43: Gypsum-to-deck connection – load vs. displacement

3.5.4 *Data Analysis*

The connection stiffness for each of the test specimens was obtained from the slope of the load versus displacement curve. In most cases, the range between zero load and 40% of the ultimate load was used to evaluate the stiffness. However, in some instances the initial portion of the test curve was ignored because of slack and out-of-straightness of the connection test specimen. Test results for the deck-to-frame, sidelap and gypsum board-to-deck are listed in Tables 3.6, 3.7 and 3.8, respectively. Table 3.9 contains the average gypsum board-to-deck connection stiffness values for those specimens that were considered to have been adequately constructed, i.e. those which had a tightly installed screw and washer. The values that were not taken into account had failures modes that were different from the majority of the specimens.

Table 3.6: Deck-to-frame connection stiffness

0.76 mm	
Specimen	**Stiffness (kN/mm)**
076-N-A	36.8
076-N-B	11.6*
076-N-C	32.7
076-N-D	31.4
076-N-E	-49.8*
076-N-H	34.7
076-N-I	25.7
AVERAGE	**32.3**
%COV	**13.0%**

0.91 mm	
Specimen	**Stiffness (kN/mm)**
091-N-A	25.9
091-N-B	14.1*
091-N-C	32.1
091-N-D	16.25*
091-N-E	36.2
091-N-H	57.33*
091-N-I	32.8
AVERAGE	**31.7**
%COV	**13.6%**

1.22 mm	
Specimen	**Stiffness (kN/mm)**
122-N-A	47.9
122-N-B	49.0
122-N-C	32.0*
122-N-D	42.7
122-N-E	43.6
122-N-H	50.7
122-N-I	45.6
AVERAGE	**46.6**
%COV	**6.7%**

1.51 mm	
Specimen	**Stiffness (kN/mm)**
151-N-A	54.2
151-N-B	49.9
151-N-C	36.4*
151-N-D	43.7
151-N-E	45.9
151-N-H	57.6
151-N-I	40.0*
AVERAGE	**50.3**
%COV	**11.4%**

* Not used in the calculation of average values.

Table 3.7: Sidelap connection stiffness

0.76 mm	
Specimen	**Stiffness (kN/mm)**
076-S-A	11.6
076-S-B	10.6
076-S-C	5.6*
076-S-D	13.8
076-S-E	12.0
076-S-H	13.6
076-S-I	9.60
AVERAGE	**11.9**
%COV	**14.0%**

0.91 mm	
Specimen	**Stiffness (kN/mm)**
091-S-A	14.4
091-S-B	8.3*
091-S-C	5.6*
091-S-D	15.8
091-S-E	10.1
091S-H	10.6
091-S-I	22.5
AVERAGE	**14.7**
%COV	**34.0%**

1.22 mm	
Specimen	**Stiffness (kN/mm)**
122-S-A	10.2*
122-S-B	20.3
122-S-C	15.5
122-S-D	13.4
122-S-E	21.0
122-S-H	22.9
122-S-I	18.7
AVERAGE	**18.6**
%COV	**19.1%**

1.51 mm	
Specimen	**Stiffness (kN/mm)**
151-S-A	17.8
151-S-B	19.9
151-S-C	10.3*
151-S-E	24.0
151-S-F	22.1
151-S-H	22.3
AVERAGE	**21.2**
%COV	**11.5%**

* Not used in the calculation of average values.

Table 3.8: Gypsum-to-deck connection stiffness

0.76 mm	
Specimen	**Stiffness (kN/mm)**
076-G-A	0.21*
076-G-B	3.80
076-G-C	0.16*
076-G-D	0.40*
076-G-E	3.93
AVERAGE	**3.87**

0.91 mm	
Specimen	**Stiffness (kN/mm)**
091-G-A	3.93
091-G-B	3.13
091-G-C	2.93
091-G-D	0.52*
AVERAGE	**3.33**

1.21 mm	
Specimen	**Stiffness (kN/mm)**
122-G-A	2.67
122-G-B	1.69
122-G-C	0.33*
122-G-D	3.13
AVERAGE	**2.50**

1.51 mm	
Specimen	**Stiffness (kN/mm)**
151-G-A	6.98
151-G-B	5.34
151-G-C	6.28
151-G-D	6.62
AVERAGE	**6.30**

* Not used in the calculation of average values.

Table 3.9: Gypsum board to deck average connection stiffness

Deck Thickness	Stiffness (kN/mm)	%CoV
0.76mm 0.91mm 1.22mm	3.14	16.5%
1.51mm	6.30	11.1%

The results for the gypsum board connections are discussed in the following section.

3.5.5 *Discussion*

Only the gypsum-to-deck connection results will be discussed in this thesis: the results of the sidelap and frame-to-deck connections have been presented in general, however the results are discussed in detail by Nedisan *et al.* (2006).

The stiffness values for the first three steel thicknesses were all very similar, hence an average value was determined for these specimens as a group. The average stiffness value, ignoring tests 076-G-A, 076-G-C, 076-G-D, 091-G-D and 122-G-C, was 3.14 kN/mm. 076-G-A, 076-G-C, 076-G-D and 091-G-D all had very loose connections and 122-G-C had no washer, and for this reason were not included in the calculation of the average stiffness. It is clear that if the connector is not well installed, or if a washer is not used, the connection stiffness will be much lower than this average value. The thickness of the sheet steel did not seem to have an impact on the stiffness of the connection for these specimens.

However, the 1.51 mm thick sheet steel specimens possessed a much higher stiffness than the other specimens, with an average value of 6.30 kN/mm. It seems that the 1.51 mm deck prevented the screw from rotating, thus removing the dependence of the connection performance on the washer tightness. The connection stiffness can be assumed to be 3.14 kN/mm for the 0.76 mm, 0.91 mm and 1.22 mm decks and 6.30 kN/mm for the 1.51mm deck with 12.7 mm (1/2") gypsum board.

3.6 Conclusions

This section contains a review of the results obtained from the experimental material and connection testing. The stiffness properties that are presented will later be used for the elastic analyses of diaphragms which is described in Chapter 4. The following conclusions have been obtained:

1. Cascade 1" *Securpan* fibreboard: flexural Young's modulus is 250 MPa and in-plane shear modulus is 235 MPa.
2. Type X ½" *CGC* gypsum board: flexural Young's modulus is 2625 MPa and in-plane shear modulus is 1284 MPa.
3. ISO-board: In-plane shear modulus is 4.0 MPa, obtained from finite element analysis model.
4. Non-structural roofing section: In-plane shear modulus is 1353 MPa, obtained from finite element analysis model.
5. Gypsum board-to-steel deck: Connection stiffness for 0.76 mm, 0.91mm and 1.22 mm sheet steel is 3.14 kN/mm; for 1.51 mm sheet steel is 6.31 kN/mm.
6. Frame-to-deck: Connection stiffness for 0.76 mm, 0.91mm, 1.22 mm and 1.51 mm sheet steel are 32.3 kN/mm, 31.7 kN/mm, 46.6 kN/mm and 50.3 kN/mm, respectively.
7. Sidelap: Connection stiffness for 0.76 mm, 0.91 mm, 1.22 mm and 1.51 mm sheet steel are 11.9 kN/mm, 14.7 kN/mm, 18.6 kN/mm and 21.2 kN/mm, respectively
8. The four-sided shear tests have shown that the small scale shear tests are adequate to compute the shear stiffness of materials, using equation D-1037a. The test results in Tables 3.2 and 3.5 are similar for both the gypsum board and fibreboard.

CHAPTER 4
ELASTIC DIAPHRAGM ANALYSES

4.1 General

The objective of the analytical phase of this research project was to develop linear elastic finite element analysis models that would adequately reproduce the initial stages of the roof diaphragm in-plane shear behaviour for different steel panel thicknesses with or without the presence of non-structural roofing elements. The analytical models, based on the large-scale diaphragm tests conducted by Yang (2003) (Section 4.2), were built using the SAP2000 v.8.2.3 software (CSI, 2002). Two models were constructed, using the data acquired in the experimental stages of this project (Chapter 3), to try to reproduce the test results obtained by Yang of a bare steel diaphragm specimen, as well as a diaphragm that was constructed with non-structural roofing components. The first model, which was initially developed by Yang, was modified to suit the context of this research project (Section 4.3), whereas the second model was built specifically for this research project (Section 4.4). The data obtained from the analytical models is presented in Section 4.5 along with the computed results. A comparative study of the numerical results with the SDI calculated stiffness values for multiple connection properties is also provided. Section 4.6 is dedicated to the discussion of the analytical results.

4.2 Roof Diaphragm Tests by Yang

To understand the finite element models that are presented in this thesis, it is necessary to first provide an overview of the diaphragm tests conducted by Yang (2003). Yang carried out twelve large-scale roof diaphragm tests (3.658 m x 6.096 m, 12' x 20'), two of which were constructed with non-structural components. The following sub-sections present a description of the test frame and test configurations.

4.2.1 *Frame Setup*

The test frame used by Yang was identical to that used by Essa *et al.* (2001) and Martin (2002). It consisted of a system of pin connected beams and joists (Fig. 4.1), which represent the framing of a portion of a larger roof structure. The cantilever test frame

was constructed of perimeter beams along the edges of the specimen and three joists spanning the width of the diaphragm.

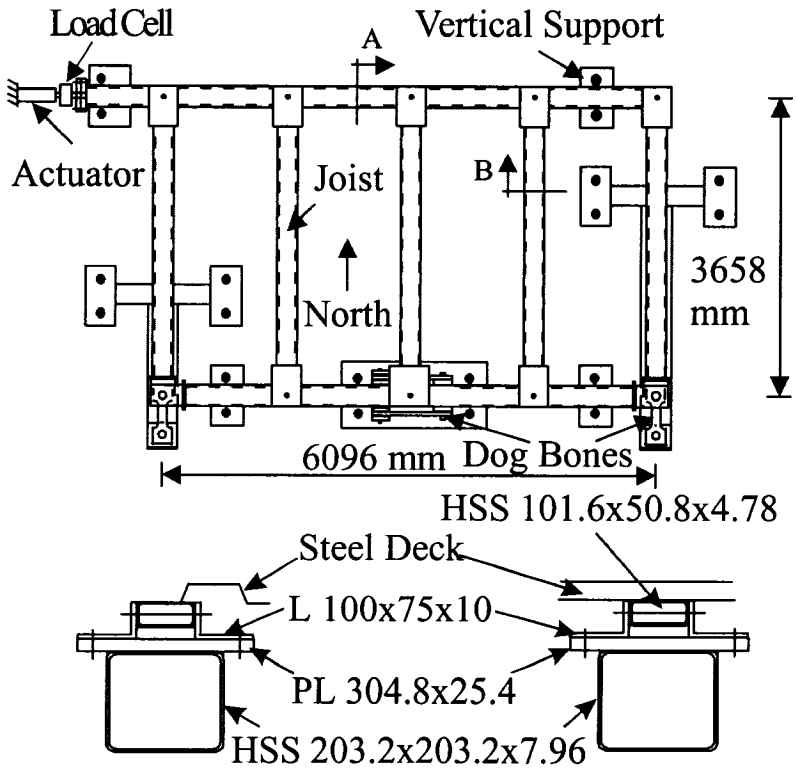

Figure 4.1: Plan view of frame setup *(Essa et al., 2001)*

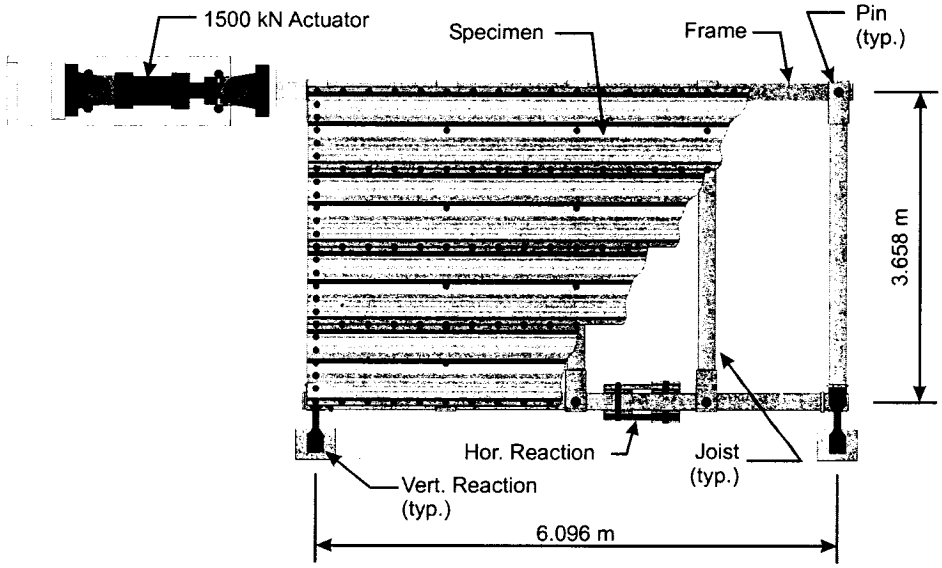

Figure 4.2: Diaphragm test setup (schematic plan view)

Roof deck panels were installed on top of the frame using standard sidelap and framing connections (Fig. 4.2). Monotonic and reversed cyclic displacements were applied by a high capacity dynamic actuator at the North West corner of the frame. The north side of the frame was free to move, while vertical and horizontal reaction points were located along the south side. Displacement and load readings were taken at multiple locations on the frame; from which the diaphragm stiffness could be computed.

4.2.2 *Specimen Configurations*

Although a number of configurations were tested by Yang, only the Group 3 tests, characterized by a 0.76 mm thick P3615 type steel deck, as well as nailed deck-to-frame and screwed sidelap connections, were used throughout the modelling process. This type of test diaphragm was constructed of three full steel panels and one half panel along the north and south edges of the frame. Deck-to-frame and sidelap connectors were placed at a spacing of 304.8 mm (12"). The deck-to-frame connectors were Hilti X-ENDK223-THQ12 powder actuated fasteners and the sidelap connectors were Hilti S-MD 12-14x1 HWH #1 F.P. screws (Fig. 4.3).

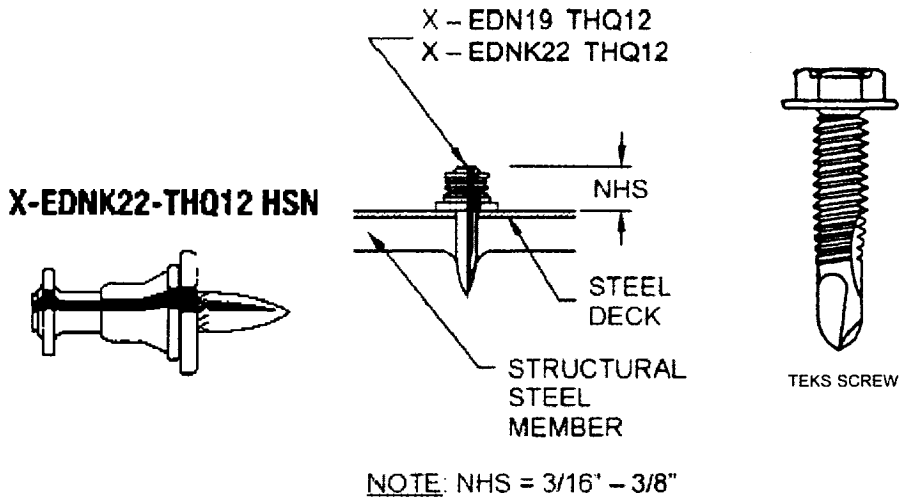

Figure 4.3: Hilti X-ENDK22-THQ12 nail and connection detail (left, middle); Hilti S-MD 12-14x1 HWH #1 F.P. screw (right), *(Yang, 2003)*.

Figure 4.4 shows a schematic plan view of a Group 3 specimen with panel and connection locations. Additional information regarding the detailed construction and

testing procedures, as well as test results, has been documented by Tremblay *et al.* (2004), Yang (2003), Martin (2002) and Essa *et al.* (2001, 2003).

Essa developed a nomenclature system which will be used throughout the following sections. An example of a name for a test specimen is 38-76-6-NS-M, which refers to a 38 mm deep deck, 0.76 mm thick deck, 6 m long specimen (actually 6.1 m, 20'), nailed deck-to-frame connectors and screwed sidelap connections and monotonic loading.

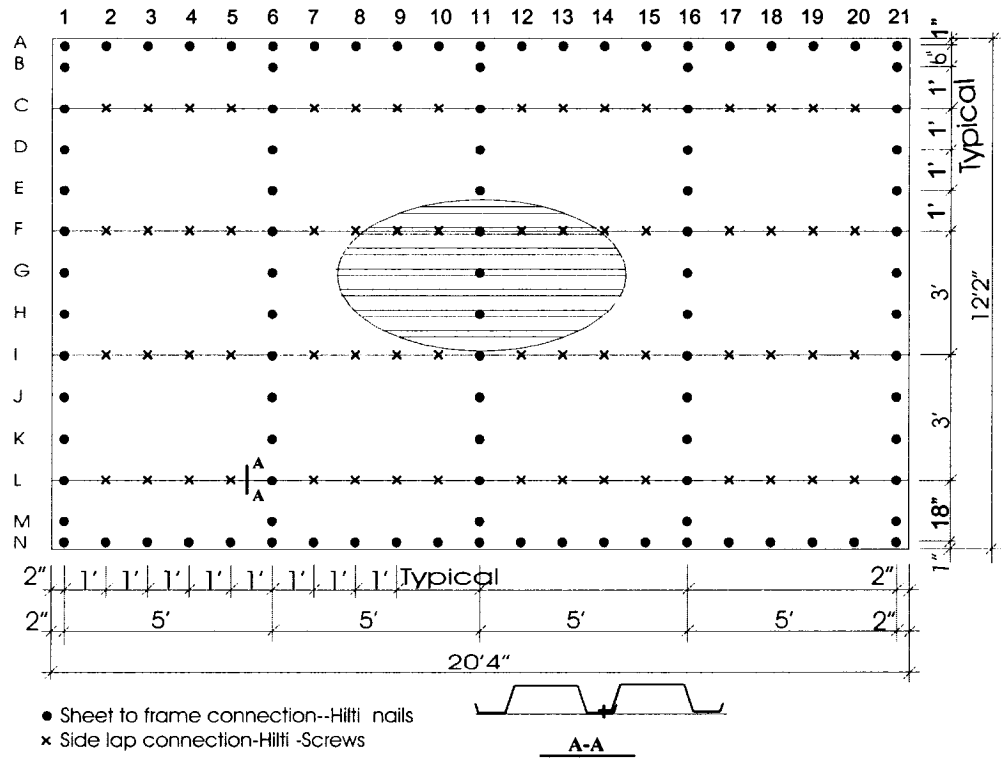

Figure 4.4: Plan of Group 3 test layout *(Yang, 2003)*

Although 49 diaphragms tests have been carried out since 1999, no tests were conducted with 1.22 and 1.51 mm thick deck. Furthermore, information on diaphragms with non-structural components is limited. Only two tests, both by Yang, included non-structural components and they had identical roofing assemblies. For the diaphragm tests conducted with the non-structural components, the roofing material composition was the AMCQ SBS-34. It is a common roof system composed of the following layers (Fig 4.5) (from top to bottom):

- Two layers (4 mm + 2.2 mm) of SBS waterproof membrane;
- One layer of 25.4 mm (1") thick non-flammable wood fibreboard, hot bitumen adhered;
- One layer of 63.5 mm (2.5") thick polyisocyanurate (ISO) insulation, hot bitumen adhered;
- Two layers of paper vapour retarder (No. 15 asphalted felts, hot bitumen adhered;
- One layer of 12.7 mm (1/2") thick gypsum board, 12 screws per panel;
- Steel deck.

Figure 4.5: Roofing cross-section *(Yang, 2003)*

Yang (2003) described the gypsum-to-deck fasteners as "*[...] special screws. Its washer is made of a 0.46 mm thick galvanized steel disc with a 76.2 mm (3 in.) diameter. The screw itself is 4.76 mm in diameter, 41 mm long, with 16 threads per inch long.*" Figure 4.6 shows the screws, which are produced by SFS Intec as an insulation assembly product under the name *#12* Hex *w/ Round Galvalume Plate.*

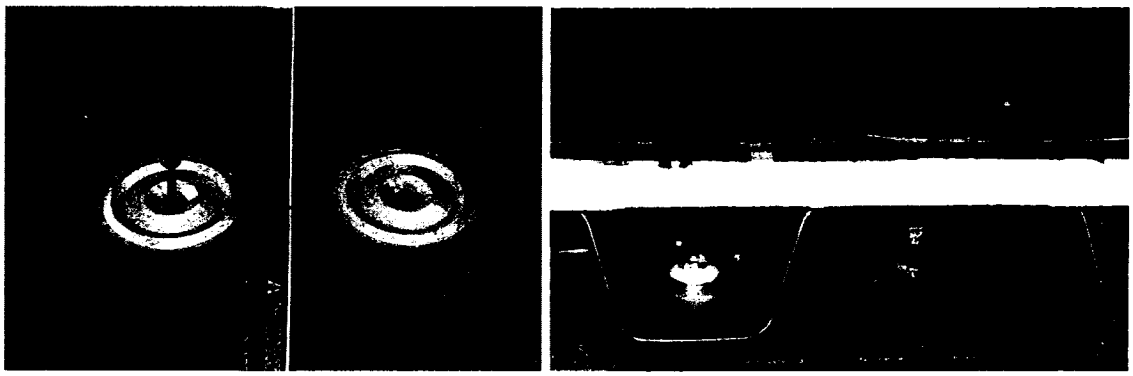

Figure 4.6: Gypsum-to-deck assemblies *(Yang, 2003)*

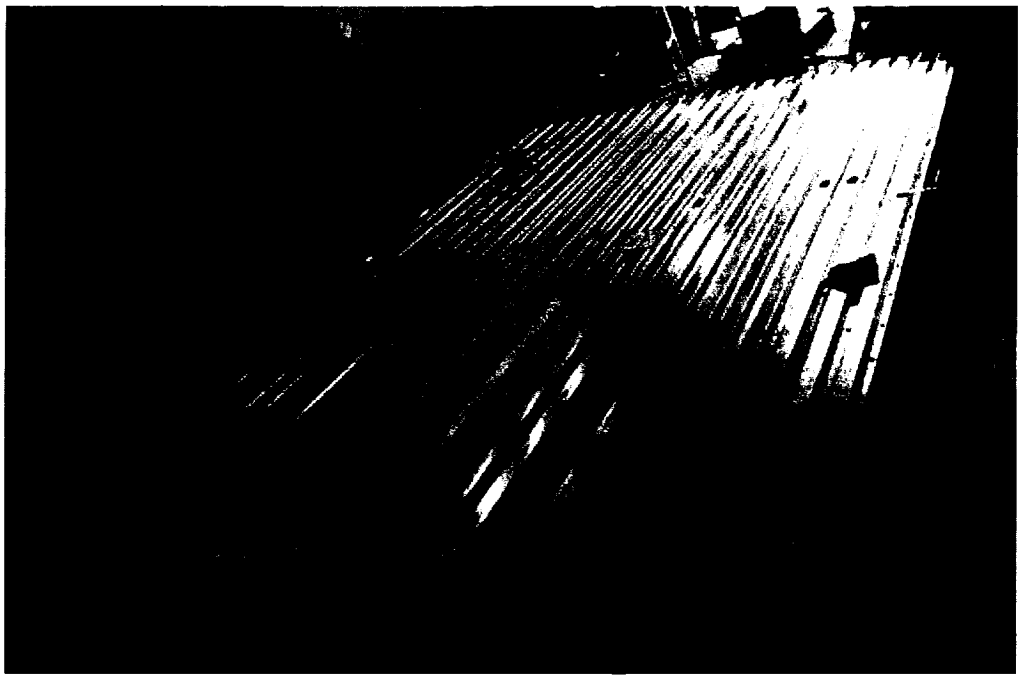

Figure 4.7: Steel deck installed on test frame *(Yang, 2003)*

Figure 4.8: Gypsum board layout *(Yang, 2003)*

Figure 4.7 shows the installed steel deck on the test frame. The gypsum-to-deck connector layout was obtained from Figure 4.8, as well as the gypsum board layout. There were six full gypsum boards and three half gypsum boards screwed directly to the top of the steel roof deck panels. A total of twelve screws per full panel and nine per half panel were installed.

The construction process is simple. Once the gypsum board is screwed to the deck (Fig. 4.8), bitumen is applied and the felt paper is rolled onto the gypsum board. Bitumen is applied again and the ISO board is adhered. Then the fibreboard is hot bitumen adhered to the ISO board. Finally, two layers of SBS water proof membrane are installed (Fig. 4.9).

Figure 4.9: Roof assembly procedure ***(Yang, 2003)***

4.2.3 *Diaphragm Test Results*

Group 3 monotonically loaded diaphragm tests 43 and 45 are the two that are of interest to this study. The first is composed of a bare sheet steel deck diaphragm (Fig. 4.7) and the second includes the non-structural components. Subsections 4.2.3.1 and 4.2.3.2 provide a review of the experimental results for the two deck diaphragms. Table 4.1 shows the results for all diaphragm specimens tested by Yang. Specimens 44 and 46 cannot be used for comparison purposes as the loading protocol was cyclic at a 0.5Hz frequency. Thus its results could only be compared to the SAP model if a similar loading protocol was used, which is not.

Table 4.1: Large-scale diaphragm test results *(Yang, 2003)*

GROUP	Description	Test number	Test result	
			S_u	G'
			kN/m	kN/mm
1	Buildex nail	38	15.25	3.52
2	Longitudinal overlapped	39	11.28	1.73
		40	12.68	1.58
		41	9.14	1.65
		42	10.29	1.55
3	**Bare sheet**	**43**	**13.40**	**2.58**
		44	10.47	2.85
	With roofing	**45**	**15.60**	**4.17**
		46	15.90	3.90
4	New profile	47	7.27	0.80
		48	7.02	0.72
		49	8.58	1.06

4.2.3.1 *Test 43*

As the load increased, the warping deformation of the panel profile became more and more extensive (Fig. 4.10). Warping is characterized by the elongation and shortening of the flutes. Figure 4.11 shows the normalized load versus rotation graph. At a load of 75.4 kN (S/S_u = 0.92), there was a sudden decrease in capacity due to failure of a deck-to-frame fastener. The load was then distributed to the other adjacent connectors. The ultimate capacity was 13.40 kN/m and the calculated initial stiffness was 2.58 kN/mm

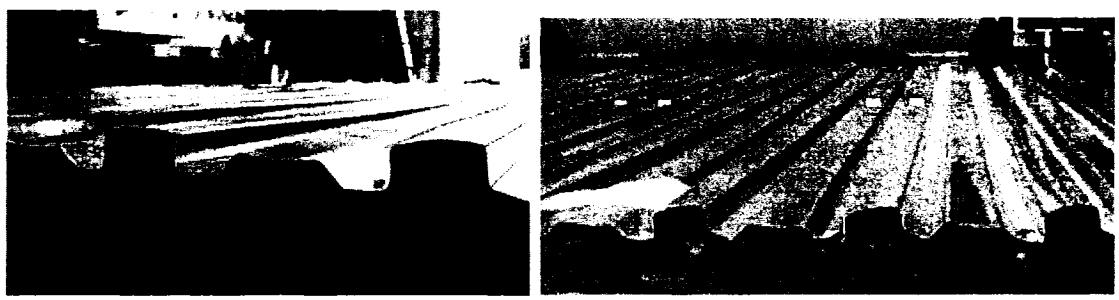

Figure 4.10: Warping deformation of steel deck profile *(Yang, 2003)*

Test No.43
P3615B - 0.76 mm
Sidelap fasteners : screwed @ 305
Frame fasteners : Hilti nailed @ 305
*Su , SDI * = 10.83 kN/m*
Su , MON Test 44 = 10.47 kN/m
Su , MON Test 43 = 13.40 kN/m

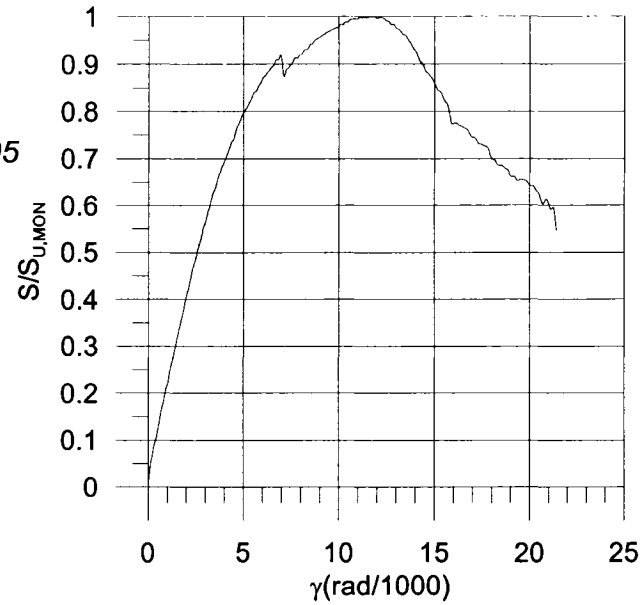

Figure 4.11: Normalized shear vs. rotation curve of Test 43 ***(Yang, 2003)***

Figure 4.12 shows the sheet buckling that occurred around the sidelap connectors after loading. There is also significant rotation of the connector. All sidelap screws tilted to some degree under loading. Furthermore, at two locations screws were pulled out of the bottom sheet while remaining in the top sheet.

Figure 4.13 shows the deformation that occurred around the deck-to-frame connector that failed first. The failure consisted of a combination of slip between the connector and the sheet steel, as well as tearing and bearing of the sheet steel. This is the typical failure mode of the deck-to-frame connectors. Only one connector failed through shear fracture.

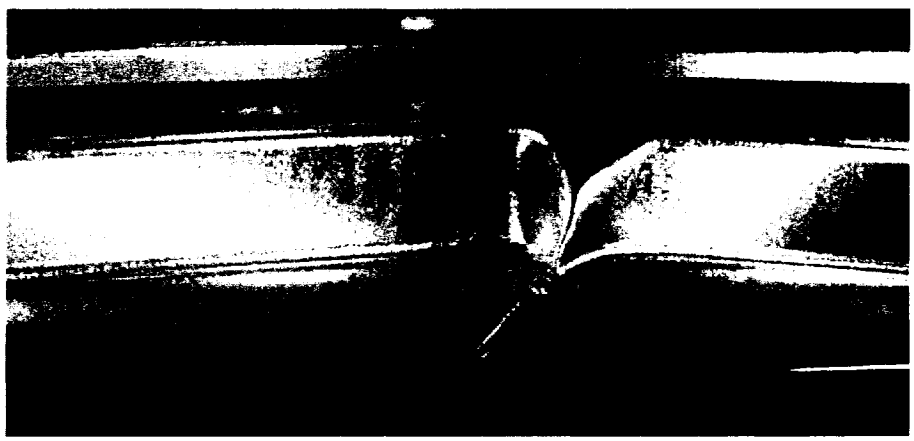

Figure 4.12: Sheet buckling, screw tilt and pull out at C20 ***(Yang, 2003)***

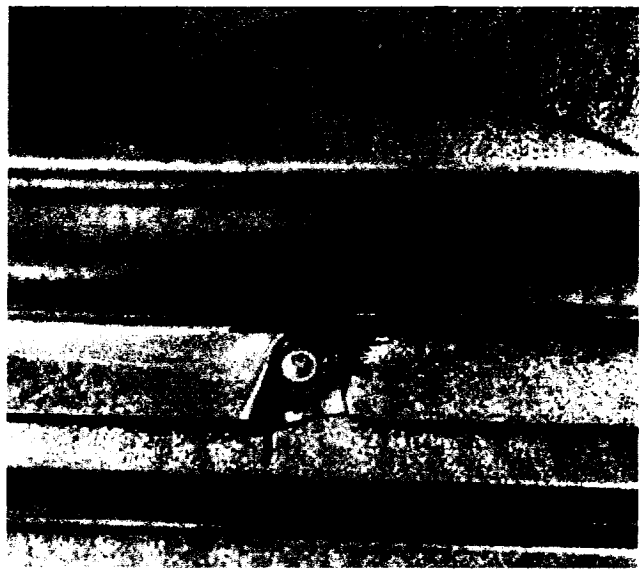

Figure 4.13: Deck-to-frame slip and bearing, tearing damage of steel sheet at I11, *(Yang, 2003)*

4.2.3.2 *Test 45*

The general failure modes for this test were deformation of the steel sheet, the cracking of the gypsum board, as well as the buckling and tearing of the steel sheet around the nails. Significant warping deformations occurred in the sheet steel, as shown in Figure 4.14, although this was not as extensive as observed for Test 43. Gypsum-to-deck fasteners caused the gypsum board to crack (Fig. 4.15). The steel deck pulled the gypsum down, causing a flexural failure of the gypsum board. No significant deformation was visibly apparent in the non-structural components other than the gypsum board. Figure 4.16 shows the overall warping and cracking of the gypsum board along its width. No connector shear failures occurred during the testing of this specimen.

Figure 4.17 shows the normalized load versus rotation graph for test 45. The ultimate capacity was 15.60 kN/m and the calculated initial stiffness was 4.17 kN/mm.

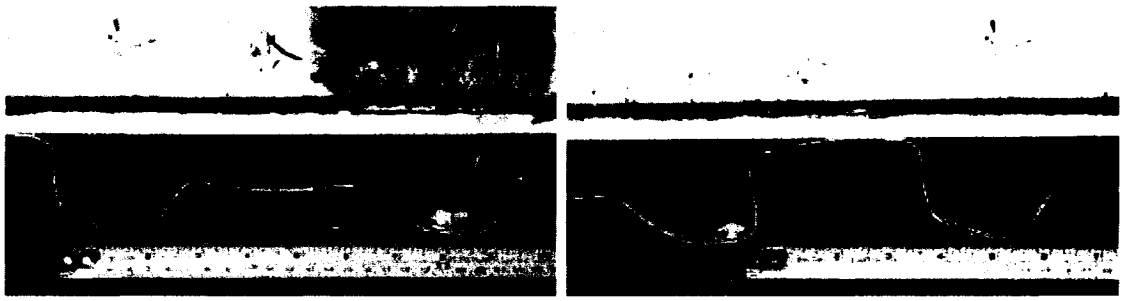

Figure 4.14: Steel sheet deformation during loading, flute width enlarged (left), Steel sheet deformation during loading, flute width reduced (right) ***(Yang, 2003)***

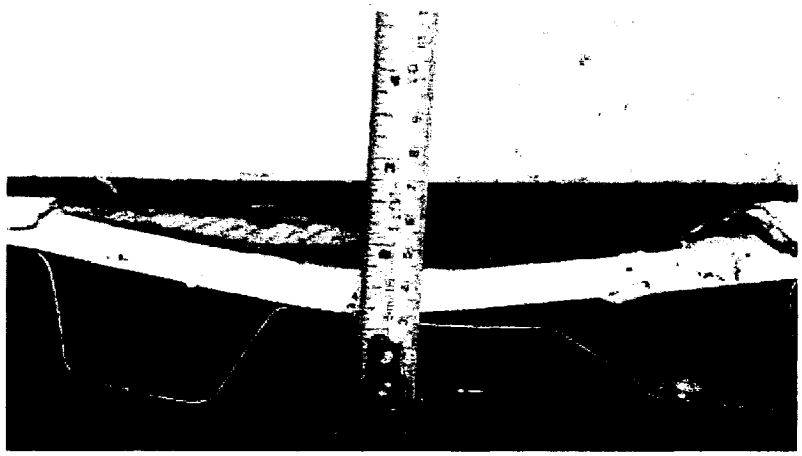

Figure 4.15: Steel deck flute height diminished, gypsum board cracked ***(Yang, 2003)***

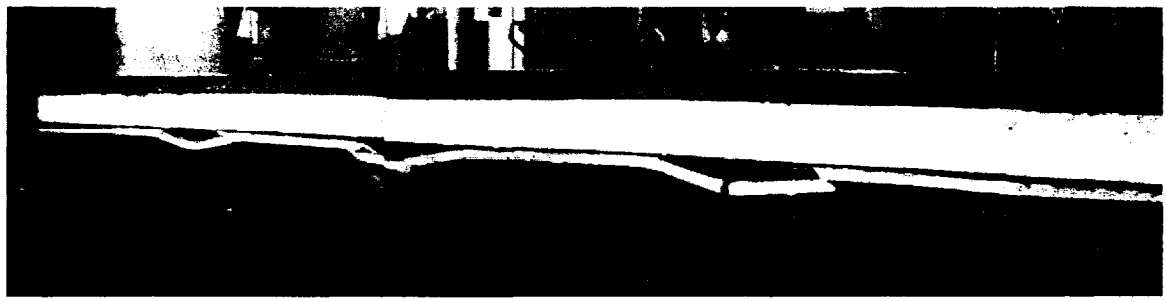

Figure 4.16: Warping deformation of steel deck and cracking of gypsum board – Test 45 ***(Yang, 2003)***

Test No.45-With roofing, monotonic
P3615B - 0.76 mm
Sidelap fasteners : screwed @ 305
Frame fasteners : Hilti nailed @ 305
*S_u , SDI * = 10.83 kN/m*
S_u , MON Test 46 = 15.90 kN/m
S_u , MON Test 45= 15.60 kN/m

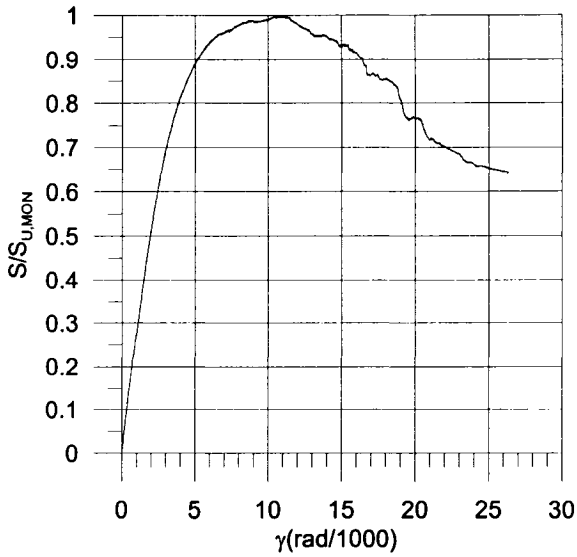

Figure 4.17: Normalized shear vs. rotation curve of Test 45

4.3 SAP2000 Models by Yang

Yang developed two linear elastic finite element models in SAP2000. These models were the basis of the full-scale FEM model that was built for this research project. A review of the models is provided in this Section. Only the essential information required for the understanding of the large-scale model will be discussed. A more thorough discussion of the model parameters has been provided by Yang (2003).

4.3.1 *General Information*

Both models were treated as cantilever analysis models, as shown in Figure 4.18. A 1 kN load was applied on the frame corner, and transferred to the deck by link elements, that emulated the screwed and nailed connections. Once the analysis was run, the computed displacement of the joint at which the load was applied was used to calculate the shear stiffness of the diaphragm.

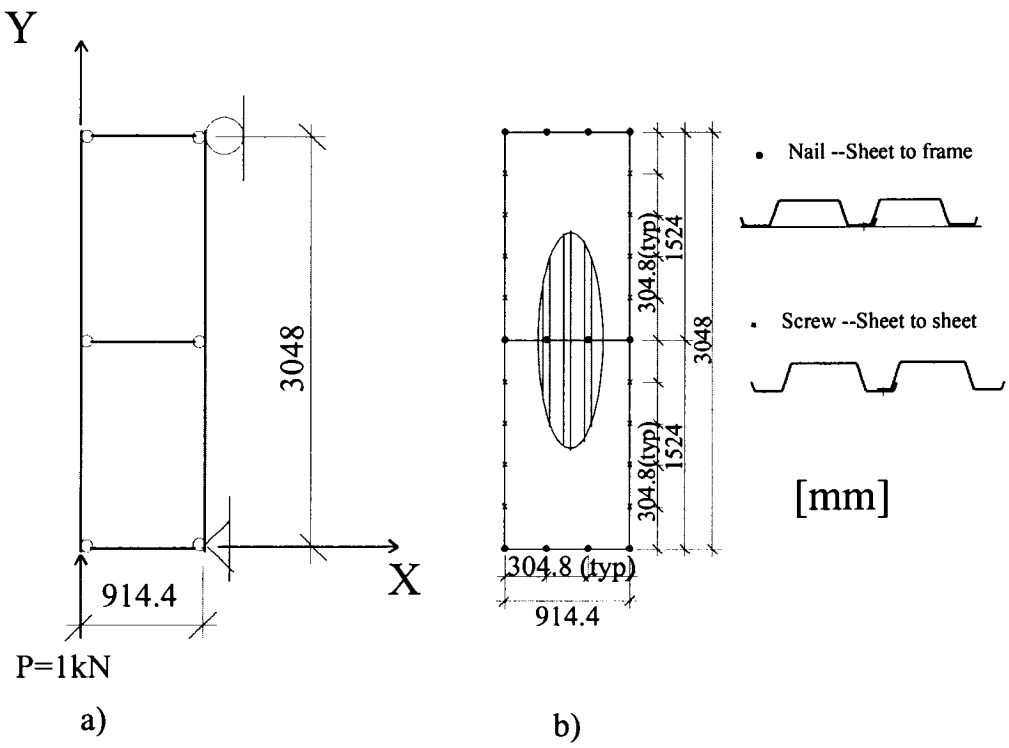

Figure 4.18: Cantilever analysis model; Frame & joists (left); Sheet layout (right) (*Yang, 2003*)

The first model was a reduced version of the bare sheet steel large-scale diaphragm tests. It contained one 3028.8 mm (10 ft) sheet of steel deck rather than four 6057.6 mm (20 ft) sheets, as is shown in Figure 4.19.

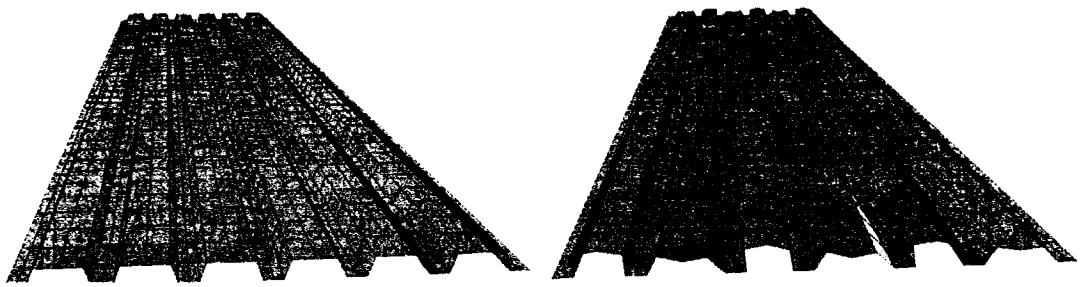

Figure 4.19: Undeformed (left) and deformed (right) shape of small-scale steel deck model *(Yang, 2003)*

The second model was the same reduced version of the large-scale diaphragm tests, although this time elements were added to represent the non-structural roofing components. Again, it contained only half of a sheet of steel deck; however one and a

quarter gypsum boards were added to the previous model rather than the six full boards and three half boards (Fig. 4.20). The steel deck sheet was 3048 mm (10') long, whereas the gypsum boards were only 2438.4 mm (8') long. Therefore a full sheet and a 609.6 mm (2') section were modelled. A gap of 2 mm was placed between the two boards to avoid contact between the sheets.

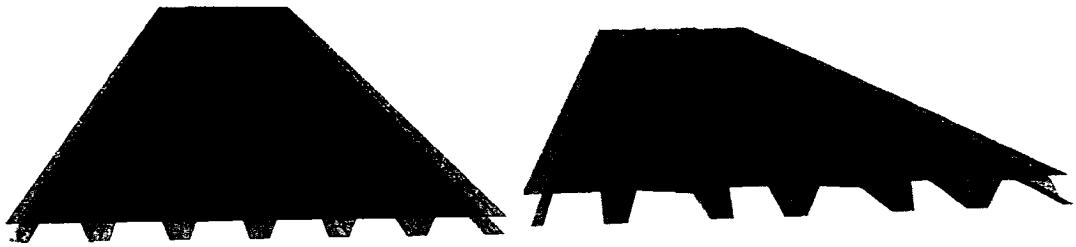

Figure 4.20: Undeformed (left) and deformed (right) shape of small-scale steel deck model with roofing elements *(Yang, 2003)*

4.3.2 *Yang Elements*

The steel deck and gypsum board were modelled using shell elements. The shell element properties were determined from experimental data acquired through testing and a literature review done by Yang. The gypsum board thickness was taken as 12.7 mm (1/2") and its flexural modulus of elasticity and Poisson's ratio were assumed for this model, because no data on shear or flexural stiffness was available in the literature.

The screws and nails were modeled using link elements called *rubber isolators*. The link properties were determined through testing. These link elements simply act as springs when a linear static analysis is run. For this analysis, axial and shear stiffness of the connections were assigned, however a rotational or bending stiffness were not input.

Finally, link elements called *gap* elements were inserted in order to prevent the movement of the gypsum board into the steel deck or of the steel deck into the frame below. These link elements were present at each joint where there could be contact between two elements. Figure 4.21 shows a typical gap link element location: joint "i"

would be the top of the steel deck and joint "j" would be the bottom of gypsum board, for example.

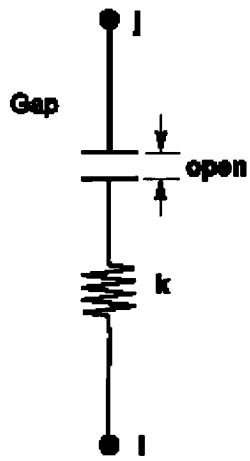

Figure 4.21: Gap property types, shown for axial deformations *(CSI, 2002)*

The intent is for gap elements to act as "compression only" springs; however, gap elements are actually linear springs that work both in compression and tension when simple static linear analyses are run. This was not taken into account when Yang (2003) carried out his analyses; therefore the gap elements acted as linear springs, not as non-linear link elements. Instead of simply preventing the two elements to coincide, these elements caused a stiffening of the axial component of the screw connections, which resulted in a higher stiffness than expected because of added warping rigidity. Proper use of the gap elements is addressed in the construction of the large-scale model in Section 4.4. Table 4.2 shows all the properties that were used in Yang's two finite element models.

Table 4.2: Properties used by Yang in SAP models

		0.76	0.76 + roofing
ST1	E (GPa)	195.2	195.2
	ν	0.3	0.3
	G (GPa)	75.1	75.1
	t (mm)	0.72	0.72
GP1	E (GPa)	N/A	1.0
	ν	N/A	0.3
	G (GPa)	N/A	0.38
	t (mm)	N/A	12.7
LINK (kN/mm)	NL1	24.04	24.04
	NL2	10.1	1.35
	NL4	N/A	1.0

4.4 SAP2000 Models of Full Size Test Diaphragms

The objective of this phase of the research project was to create linear elastic finite element models with SAP2000, which could be used to accurately replicate the initial in-plane shear behaviour of diaphragm Tests 43 and 45 by Yang (2003). The models were built according to the dimensions and specifications of the specimens described in Section 4.2. In addition, the information on non-structural material properties and connections, as described in Chapter 3, was incorporated into the models to improve upon the efforts of Yang. Once the first models were properly calibrated, a parametric study of the influence of deck thickness, connection pattern and non-structural components on overall diaphragm stiffness was conducted.

4.4.1 *General Information*

The FE study was carried out to develop a numerical analysis tool which would accurately recreate roof diaphragm behaviour of the tested specimens and from which roof diaphragm stiffness could be computed. The test data acquired by Yang represents the benchmark on which the model was calibrated, specifically Tests 43 and 45. Once the model was considered adequate, it was possible to extrapolate results for diaphragm configurations and thicknesses that had not been physically tested.

Cantilever models were built according to the specifications of Group 3 test specimens, as cited in Yang (2003) and described in Section 4.2. Figure 4.22 shows the general

geometry of the model and the steel deck orientation. A total of eight models were created for this research project: four bare sheet steel roof deck diaphragms with deck thickness of 0.76 mm, 0.91 mm, 1.22 mm and 1.51 mm, and four roof deck diaphragms clad with non-structural components. Additional analyses were carried out while varying the deck-to-frame and sidelap connector steel deck diaphragms with and without gypsum board. Initially, the connectors were spaced 305mm (12") apart for both sidelap and deck-to-frame connectors for all four deck thicknesses. Subsequently the spacing was reduced to 152mm (6"): firstly for the sidelap connectors, then for deck-to-frame connectors only, and finally both connector spacings were reduced to 152mm (6"). In all, 40 SAP2000 analyses were performed.

The nomenclature used to identify these models was similar to that specified by Essa (2001). There is one slight difference: a monotonic loading in this case implies a 1 kN load applied at the corner of the model, not a monotonically increasing load as with a pushover analysis.

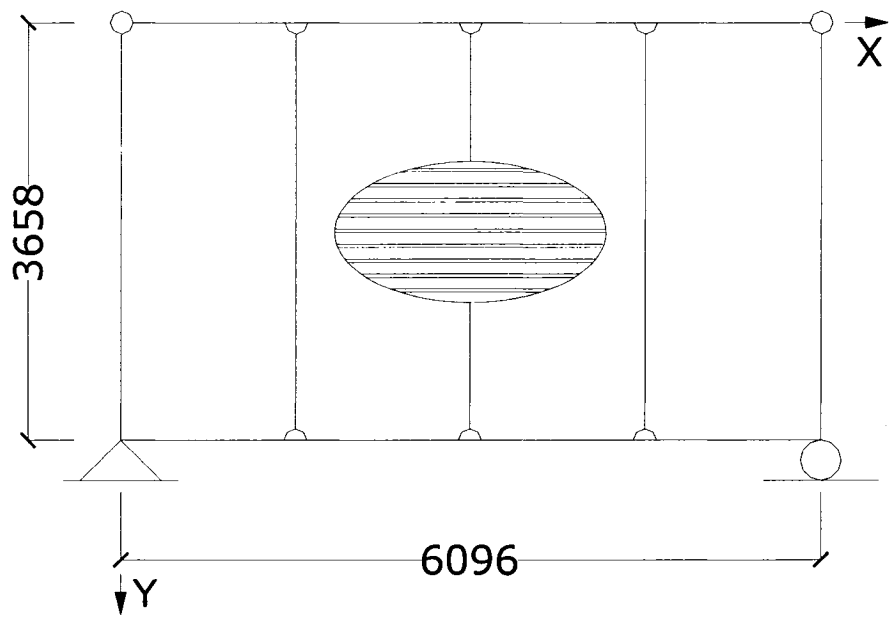

Figure 4.22: Cantilever analysis model

The bare sheet steel model had three full 6.096 m (20') long sheets and two half width sheets, similar to the tests that were conducted by Yang (2003). The deck-to-frame, sidelap and gypsum board to steel deck layout is shown in Figures 4.4 and 4.8. The deck-to-frame and sidelap connector spacing was 304.8mm (12"). The model contained 600 frame elements, 17812 shell elements, 1999 link elements and 20456 nodes. Mesh density was established by Yang (2003). His convergence study showed that his 1592 shell element model was sufficient, therefore the same mesh density was used for this model. The frame elements were restrained in terms of the z-direction translation and for rotations about x and y. The boundary conditions were continuous for the interior elements and pinned-fixed for the outer elements. With these boundary conditions, the frame elements acted as continuous members that were pin connected to one another. The middle purlins had pinned end connections at the outer elements and continuous at the inner elements. The frame setup is explained in Section 4.4.2.4 and Figure 4.27 shows the member end conditions, loading points and supports.

The non-structural roofing component model consisted of the same number of frame elements, 600, as well as 35092 shell elements, 1870 link elements and 37264 nodes. There were less link elements than with the bare sheet steel model in order for a converged solution to be reached and to reduce computation times. A model was first built with approximately 9000 link elements. Regardless of what parameters were used, the computations would not converge, even after 1000 steps, with very high convergence criteria. Therefore "gap" links were inserted at every 152 mm (6") instead of 50.8 mm (2"), which gave a decent approximation of the real behaviour. A single layer of material that represented the complete non-structural section was used, not the gypsum board alone. This is fully explained in Section 4.4.2.

The end conditions of all the shell elements were continuous. However, each sheet was modelled separately such that link elements, which represent the sidelap or deck-to-frame connections, were needed to connect the various panels and framing members.

The frame members were inserted 0.5 mm below the bottom of the steel deck. If this had not been done, it would have been necessary to insert *duplicate nodes*, which would have greatly increased the complexity of the model. *Duplicate nodes* are two or more joints that are in the same physical location but are free to move with respect to each other. This is problematic for a model of this size, because it would be difficult to determine node connectivity without accessing the properties at that specific joint.

Figure 4.23 and Figure 4.24 show the undeformed shapes of the bare steel deck and of the steel deck with the roofing components both at full scale, and also a magnified view of a corner.

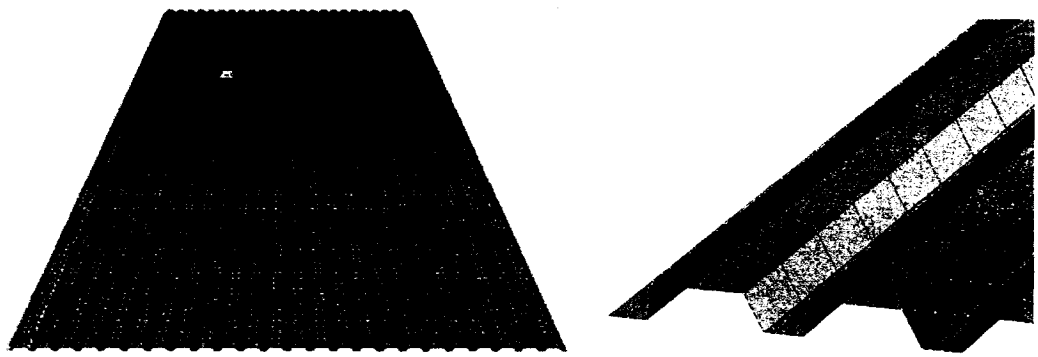

Figure 4.23: Undeformed shape of full-scale steel deck model

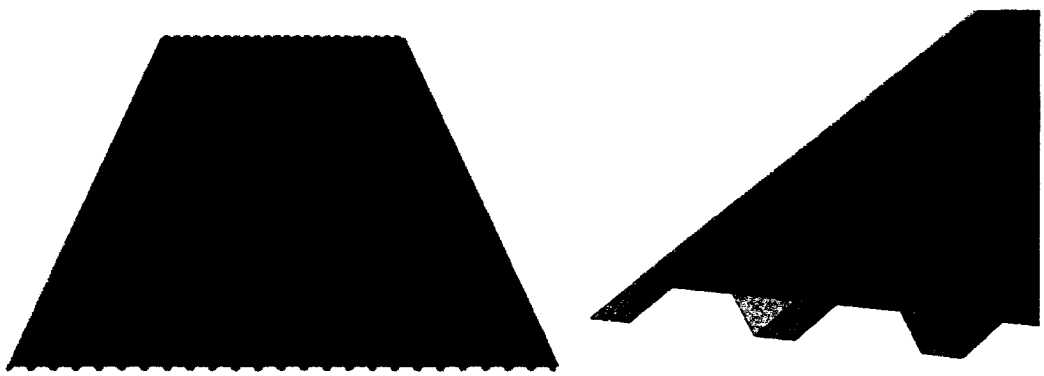

Figure 4.24: Undeformed shape of full-scale steel deck model with roofing elements

4.4.2 *Elements*

Each element in the model is thoroughly discussed in this section. Firstly, the material properties are presented, followed by shell elements, link elements and finally frame elements.

4.4.2.1 *Material Properties*

It was necessary to assign material properties to the frame and shell elements. Two different material properties were used throughout the analyses: the properties of the steel were called ST1 and the non-structural component properties were called GP1.

The ST1 material properties were taken from the test data compiled in Yang (2003) for the 0.76 and 0.91 mm thick deck. Since testing of the two thicker deck types has not been carried out the material properties were defined as prescribed by the CSA S136 Standard (2001) for the design of cold-formed steel members. The properties of the non-structural components (GP1) were taken from the results of the tests presented in Chapter 3. However, the values that were required for input in SAP2000 were the modulus of elasticity and Poisson's ratio, not the shear stiffness. The modulus of elasticity (E) in flexure was known for the gypsum board, as well as the shear modulus (G). The relationship between the flexural modulus of elasticity and shear modulus is described as for a Hookean material:

$$E = \frac{G}{2(1+\nu)} \qquad (4\text{-}1)$$

where:

E = Flexural modulus of elasticity (MPa),

G = Shear modulus (MPa),

ν = Poisson's ratio.

Isolating ν in equation (4-1):

$$\nu = \frac{G}{2E} - 1 \qquad (4\text{-}2)$$

Using the data acquired in Chapter 3, a value for Poisson's ratio of 0.11 was found for the gypsum. This value was used to determine the equivalent flexural modulus of elasticity of the roof deck configuration with non-structural components.

This is not the real modulus of elasticity of the built-up section. This value is only computed because the SAP2000 software requires the input of the modulus of elasticity and a Poisson's ration to compute the shear modulus of the material.

Using the shear stiffness measured for the FULL SECTION test specimens and a Poisson's ratio of 0.11, a value of E = 3.07 GPa was determined. The values of the material properties used for all models can be found in Table 4.3. The value of F_y is not included in the material properties because the intent was to model the initial linear elastic stiffness of the diaphragm, not the yielding behaviour.

All shell elements and frame elements are assigned material properties, as shown in Table 4.3. Link elements, however, cannot be assigned material properties, rather it is necessary to define stiffness parameters for these elements.

Table 4.3: SAP2000 – material properties

		0.76	0.91	1.22	1.51
ST1	E (GPa)	195.2	197	203	
	ν	0.3			
	G (GPa)	75.1	75.8	78.1	
GP1	E (GPa)	3.07			
	ν	0.11			
	G (GPa)	1.38			

4.4.2.2 *Shell elements*

As with Yang's model, the gypsum board and sheet steel were modeled as shell elements each containing four nodes. In finite element analysis, two types of shell behaviour are possible: membrane behaviour, also known as Kirchhoff theory, and plate behaviour

which is referred to as Mindlin-Reissner theory (Cook *et al.*, 2001). When defining a planar element in the SAP2000 software, three choices are possible: pure membrane, pure plate or full shell behaviour, which is a combination of the previous two. Obviously, pure plate behaviour, which could be used for flat slabs for instance, is inadequate for this model. Therefore, membrane behaviour or full shell behaviour would be possible choices for this model. However, the CSI manual recommends that full shell behaviour be implemented unless the entire structure is planar and is adequately restrained, which it is not. Furthermore, the use of full membrane behaviour prohibits out-of-plane translations and in-plane rotations, which would not adequately serve this model. Therefore four-node flat shell elements capable of developing bending and membrane behaviour (full shell) were used throughout the diaphragm and non-structural portions of the models.

Each model contained two types of this four-node flat shell element: the first called SH1 was used to model the steel deck, and the second, called SH2, was needed to model the gypsum board, which was further stiffened to account for the other non-structural components. When defining shell elements, a thickness must be chosen for bending and membrane behaviour (Table 4.4). For all specimens, the bending and membrane behaviour thickness is equal. The measured thickness of the 0.72 and 0.905 mm steel deck (Yang, 2003) was utilized, whereas the nominal thickness was incorporated in the models with the 1.22 and 1.51 mm deck. The thickness of the non-structural shell elements was set as the thickness of the gypsum board even when the other non-structural components were to be modeled.

Table 4.4: SAP2000 – shell element thickness (mm)

	SH1		SH2	
	Bending	Membrane	Bending	Membrane
0.76	0.72		12.7	
0.91	0.905		12.7	
1.22	1.22		12.7	
1.51	1.51		12.7	

The ST1 material property is assigned to the SH1 shell elements and the GP1 material property is assigned to the SH2 element.

4.4.2.3 *Link Elements*

According to the CSI manual, "*The **Link** element is used to model local structural nonlinearities. Nonlinear behavior is only exhibited during nonlinear analyses. For all other analyses, the Link element behaves linearly" (CSI, 2002).* This section provides a review of the link elements that were used for this project.

As mentioned previously, link elements act as deformation independent linear springs for all six degrees of freedom (axial, shear, torsion and pure bending) if linear stiffness properties are input or if linear analyses are used. Four link elements were used throughout the modeling process: NL1, NL2, NL4 and GAP. NL1 acts as the deck-to-frame connectors; NL2 reproduces the sidelap connectors; the third, NL4, represents the gypsum-to-deck fasteners; the fourth is called GAP and acts as the "gap" elements between the steel deck and frame and also between the gypsum board and the steel deck such that the upper layer of material does not penetrate into the lower or vice versa.

NL1 and NL2 and NL4 were chosen as *Rubber Isolator* link elements. However, since these links were considered to act as simple linear springs, there was no need to define the non-linear properties of the *rubber isolator*. Stiffness properties were input in the axial direction as well as in both shear directions. No bending stiffness was assigned to any of the link elements.

The connection stiffness properties for the NL1, NL2 and NL4 links are shown in Table 4.5. It is important to note that for link elements, each direction must have its own defined stiffness. For this model, it was assumed that u1 = u2 = u3, meaning that the stiffness value shown in Table 4.5 is assigned to all translation directions.

Table 4.5: SAP2000 – link properties (kN/mm)

		0.76	**0.91**	**1.22**	**1.51**
LINK (kN/mm)	NL1	32.0	32.0	46.6	50.3
	NL2	11.6	14.7	18.6	21.2
	NL4	3.14	3.14	3.14	6.30

For both the 0.76 mm and 0.91 mm decks, the value of 32.0 kN/mm was used for the NL1 link elements. This was done because the experimental connection data that was gathered gave very similar stiffness values for the 0.91 mm and the 0.76 mm deck, the 0.91 mm deck value being the lower of the two (Table 3.30). It was decided that both connection types most probably have the same stiffness values, therefore the average of the two values for stiffness was taken. The connection properties for the two thicker decks were taken directly from the test results (Table 3.30).

The GAP elements were initially defined as *gap* (compression-only) elements, as in Yang's model. However, preliminary analyses were conducted using a non-linear static analysis rather than a linear elastic static analysis in order for the gap elements to act as "compression-only" springs. While conducting these analyses, significant computational problems arose. It was decided to change the gap link elements to *multi-linear* link elements to facilitate modeling of the diaphragm test specimens. It is possible to define different stiffness levels dependent on the displacement of the Multi-linear link elements. It was established that the computing problems were due to the size of the model and to the high number of gap elements. Each gap element in tension returns a zero value into the stiffness matrix and complicates the computations. When using multi-linear springs, a very low tension stiffness is defined along with a very high compression stiffness. Although it is not a perfect "compression-only" spring, its behaviour was considered to be similar enough to be used for the analyses. By defining multi-linear link elements rather than *gap* elements, computation times were reduced tenfold and it was possible for a converged solution to be obtained.

Although non-linear analyses were conducted because of the multi-linear link elements, the results of the analysis still remain as those of an elastic analysis. The non-linear analysis was run simply to obtain the actual behaviour of the contact between the gypsum board and the deck, as well as the behaviour of the contact between the deck and the frame elements below. The frame and shell elements were all linear elastic in nature.

The properties of the GAP link elements were as defined in Figure 4.25.

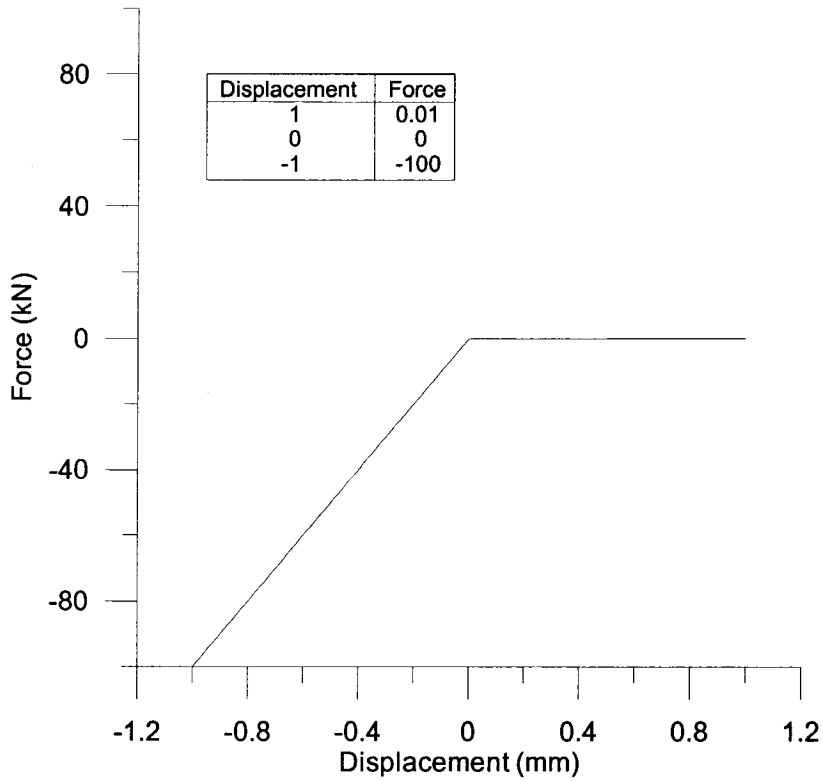

Figure 4.25: Multi-linear spring stiffness of GAP element

4.4.2.4 *Frame Elements*

Frame elements are small beam elements with specific cross-sectional properties and boundary conditions with a node at each end. The element has all 6 degrees of freedom, as it recreates all three translations and rotations. The frame elements were used to recreate the frame setup shown in Figures 4.1 and 4.22. This setup by itself has no in-plane shear stiffness as the members are pin-ended as it is shown in Figure 4.22. Two frame elements were used throughout: FM1 and FM2. They have the same cross-sectional properties (Table 4.6), and both are assigned ST1 material properties. Two elements were used to differentiate the elements in the X-direction from the elements in the Y-direction (Figure 4.22). The properties were chosen so that no deformation would take place in the frame. A test run was conducted without any steel deck panels to check for any shear stiffness of the frame setup. It was concluded that the frame setup had no shear stiffness and very low stresses were present throughout the frame elements.

Table 4.6: SAP2000 – frame element properties

FM1 and FM2	
Cross-section (axial) area	10000000
Torsional Constant	0
Moment of Inertia about 3 axis	1.00E+10
Moment of Inertia about 2 axis	1.00E+10
Shear area in 2 direction	0
Shear area in 3 direction	0
Section Modulus about 3 axis	0
Section Modulus about 2 axis	0
Plastic Modulus about 3 axis	0
Plastic Modulus about 2 axis	0
Radius of Gyration about 3 axis	0
Radius of Gyration about 2 axis	0

Figure 4.26 shows a corner of the frame as well as the whole frame outline. As mentioned previously, the FM2 elements have continuous end connection between each other, but are pinned when connected to the FM1, and vice versa for the FM1 elements.

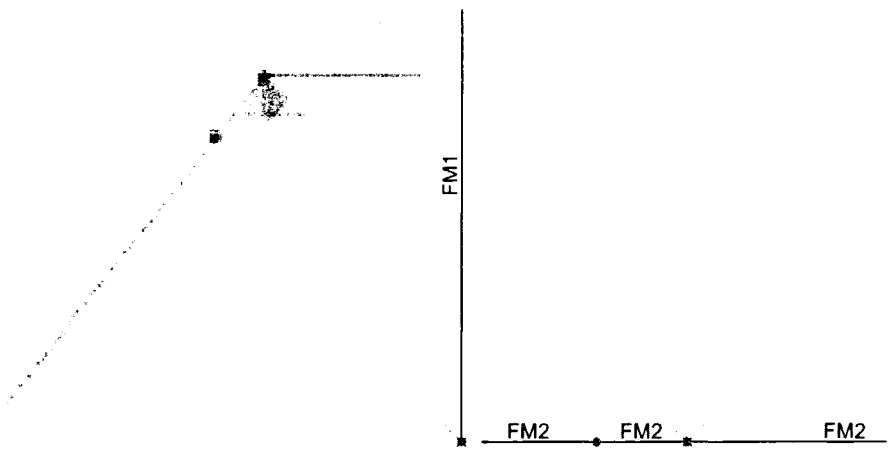

Figure 4.26: Support (lower left); Frame elements and end releases (lower right)

4.4.3 *Analysis Parameters*

As mentioned above, the analyses were run as non-linear static analyses even though a linear elastic analysis was actually sought. When running these types of analyses, many parameters must be defined, including: the number of steps and iterations, convergence criteria – called lumping tolerances in the SAP2000 software – and the load redistribution method (hinge unloading method). The maximum number of steps, null steps, iterations

per step and the unloading method are the default setting. The incremental displacement convergence criteria and the load imbalance convergence criteria – called iteration loading tolerance and event loading tolerance in the SAP2000 software – have been defined differently than the default values (Table 4.7).

The convergence criteria values were found by trial and error. These values define the level of precision of the calculation for the incremental displacement as well as for the load imbalance. As the values for these two parameters increase, the computation time decreases; as the number of steps needed to arrive to an answer decreases, the results obtained from the analysis becomes less and less precise. These values must be chosen with care or the results obtained may be rendered unacceptable. Through a convergence study, by comparing the calculated results with the physical diaphragm test results for these models, it was determined that a twelve to fifteen step procedure was necessary to ensure that the finite element analysis was acceptable.

The hinge unloading option is primarily intended for pushover analysis using frame hinge properties that exhibit sharp drops in their load-carrying capacity. The "Apply Local Distribution" setting attempts to imitate how local inertia forces stabilize a rapidly unloading frame hinge element. However, we are not conducting a SAP2000 pushover analysis or using frame hinge elements, therefore this option has little effect the model results but does affect computation times. The "Apply Local Distribution" setting, which is considered to be the most effective of all the methods *(CSI, 2002)*, was chosen for its lower computation times for the model used in this research.

Table 4.7: Non-linear analysis parameter values

	Bare Sheet Steel Model				Roofing Model			
	0.76	**0.91**	**1.22**	**1.51**	**0.76**	**0.91**	**1.22**	**1.51**
Max. Steps	200	200	200	200	200	200	200	200
Max. Null Steps	50	50	50	50	50	50	50	50
Max. Iterations per Step	10	10	10	10	10	10	10	10
Iteration Convergence Tolerance	0.04	0.04	0.05	0.04	0.01	0.01	0.01	0.01
Event Lumping Tolerance	0.08	0.08	0.10	0.08	0.02	0.01	0.01	0.01

4.4.4 *Model Specific Properties*

This section will review some of the geometric properties that are specific to the full-scale model. The use of multi-linear link elements and joint constraints will also be discussed.

4.4.4.1 *Multi-Linear Link Elements*

Multi-linear (M-L) link elements were used to prevent the movement of the gypsum board into the steel deck or the movement of the steel deck into the test frame. In addition, they were also used to prevent two sheet steel decks from moving into each other at the sidelap (NL2) locations and at the deck-to-frame (NL1) locations at panel edges. Figure 4.27 shows the typical locations of M-L (GAP) links.

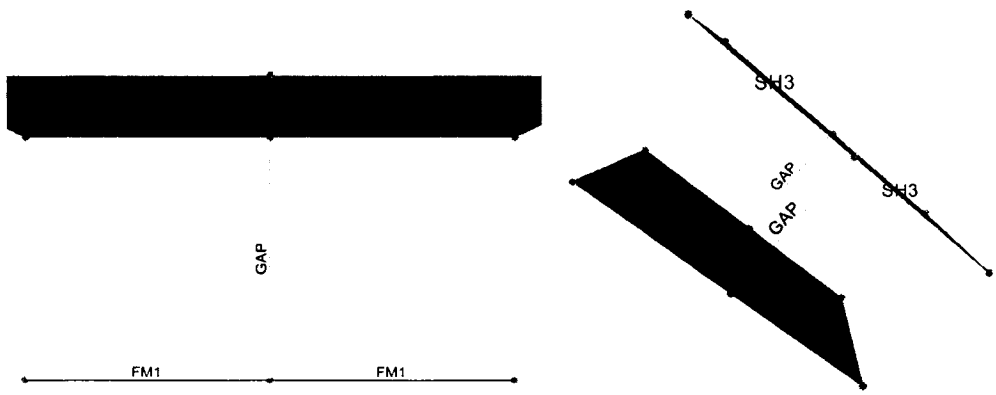

Figure 4.27: M-L (GAP) link typical locations

4.4.4.2 *Joint Constraints*

The CSI manual states that "*constraints are used to enforce certain types of rigid-body behaviour, to connect together different parts of the model, and to impose certain types of symmetry conditions" (CSI, 2002).* Constraints were only used on 60 joints in the whole model, but nonetheless play an important part in the overall deck behaviour.

At the edges of the panels, where two steel deck panels lapped, there were three joints aligned along the Z-axis. Only one NL1 link element was used to model the nail that connected both steel deck panels to the frame elements. Using 2 NL1 elements would not

have been adequate, because the stiffness would have been double that which existed in a real roof. Furthermore by using two link elements, unrealistic displacement could occur. Therefore, a line joint constraint was used to model the behaviour of the nail.

A line constraint is modeled as equal displacement behaviour for the constrained joints. Therefore, all three joints behave as if they were connected by a straight line, i.e. the two edge joints move freely while the middle joint movement is controlled by the constraint conditions. Furthermore, they are also free to move independently in the axial direction of the constraint. It is adequate to assume this, because deck-to-frame tests have shown that, except for the 1.51 mm deck, the connection behaviour was controlled by rotation of the nail and not bending of the nail. Figure 4.28 shows the link element configuration, where the three joints were assigned with a line constraint. The top and middle nodes were separated by an M-L link element to prevent movement of the joints into each other. Only the top and bottom joints were connected with the NL1 link element, which was used to model the deck-to-frame connections.

Only the top and bottom joints are connected by the link. All three joints along the NL1 link are assigned the LINE joint constraint, and therefore the displacement of the middle joint is governed by the constraint and the displacement of the top and bottom joints.

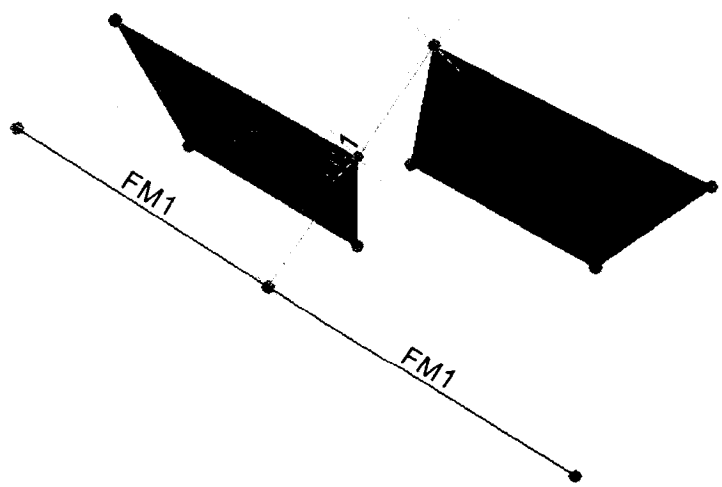

Figure 4.28: NL1 link element with joint constraint

4.5 Data Analysis, Results and Discussion

Once each finite element analysis had been run, the following parameters were used to obtain the final equation for stiffness of the diaphragm:

- L, the model length, L = 6096 mm = 20 ft;
- A, the model width, A = 3657.6 mm = 12 ft;
- P, the Y-direction unit force of 1 kN;
- S, the unit shear force, S = P/L;
- Δ, the Y-direction deflection due to P, mm;
- γ, the shear distortion, $\gamma = \Delta/A$
- G', the shear stiffness, $G' = S / \gamma$.

From these parameters, a simple equation to compute the shear stiffness was determined. Since:

$S = P / L = 1\ kN / 6096\ mm = 1.64E\text{-}04\ kN / mm$, and (4-3)

$\gamma = \Delta / A = \Delta\ (mm)\ / 3657.6\ mm = 2.73E\text{-}04 * \Delta\ (mm)\ / mm$ (4-4)

therefore,

$G' = S / \gamma = 164E\text{-}04\ kN/mm / 2.73E\text{-}04 * \Delta\ (mm)\ / mm$ (4-5a)

$G' = 0.6 / \Delta\ kN / mm$ (4-5)

With equation *(4-5)*, the shear stiffness of the diaphragm was computed by using the Y-direction displacement of the joint at which the load was applied. Table 4.8 shows the displacements obtained from the finite element analyses, as well as the computed stiffness of the model. In addition, the stiffness values of three diaphragm specimens have been listed for comparison purposes. The test-to-predicted ratio varies from 0.94 to 0.96 for these specimens. Given these ratios, the model can be considered as relatively accurate, and hence it was used to evaluate the stiffness of the remaining configurations for which test data was not available. As expected, the overall stiffness of the bare sheet diaphragm increased as the thickness of the panels increased. The stiffness of the diaphragm with 1.51 mm thick panels is 4.5 times that obtained for the diaphragm with 0.76 mm panels. A significant increase in the elastic stiffness of the steel sheets was determined when the non-structural components were added to the model. This result was

most evident for the diaphragm with the thinnest steel deck panels. The effect of the non-structural components diminished as the sheet steel thickness increased, i.e. a 58.6% increase in stiffness was calculated for the 0.76 mm steel, whereas only a 16.9% increase was obtained for the 1.51 mm panels. Nonetheless, even with the thickest roof deck panel commonly available on the market, the non-structural components still caused a substantial increase to the initial elastic stiffness of the diaphragm.

Table 4.8: Analytical model displacements and stiffnesses

Specimen	Displacement (mm)	Stiffness (kN/mm)	Test Value (kN/mm)	% Inc Vs. Prev.	% Inc vs. Bare	Test/SAP
38-76-6-NS-M	0.219	2.74	2.58	N/A	N/A	0.94
38-91-6-NS-M	0.134	4.49	4.22	63.5%	N/A	0.94
38-122-6-NS-M	0.072	8.30	N/A	85.0%	N/A	N/A
38-151-6-NS-M	0.046	13.04	N/A	57.1%	N/A	N/A
38-76-6-NS-R-M	0.138	4.35	4.17	N/A	58.6%	0.96
38-91-6-NS-R-M	0.093	6.42	N/A	47.7%	43.2%	N/A
38-122-6-NS-R-M	0.055	10.85	N/A	68.9%	30.8%	N/A
38-151-6-NS-R-M	0.039	15.24	N/A	40.4%	16.9%	N/A

Figures 4.29 through 4.32 show the deformed bare steel deck diaphragm and the deformed shape of the deck with the gypsum board, respectively. The displacement values listed in Table 4.8 were taken at the bottom left corner of the model at coordinates (X,Y,Z) = (25.4, 50.8, -0.5).

Figure 4.29: Deformed shape of bare steel deck

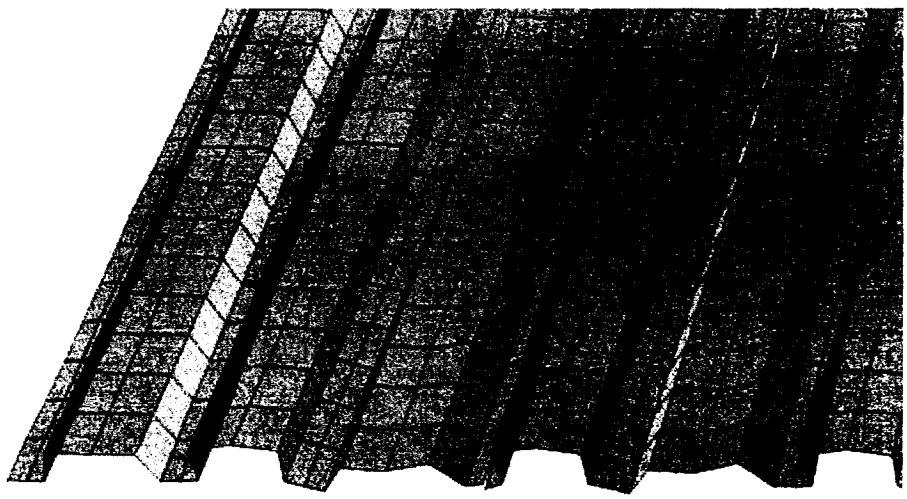

Figure 4.30 Close-up of warping for bare steel deck

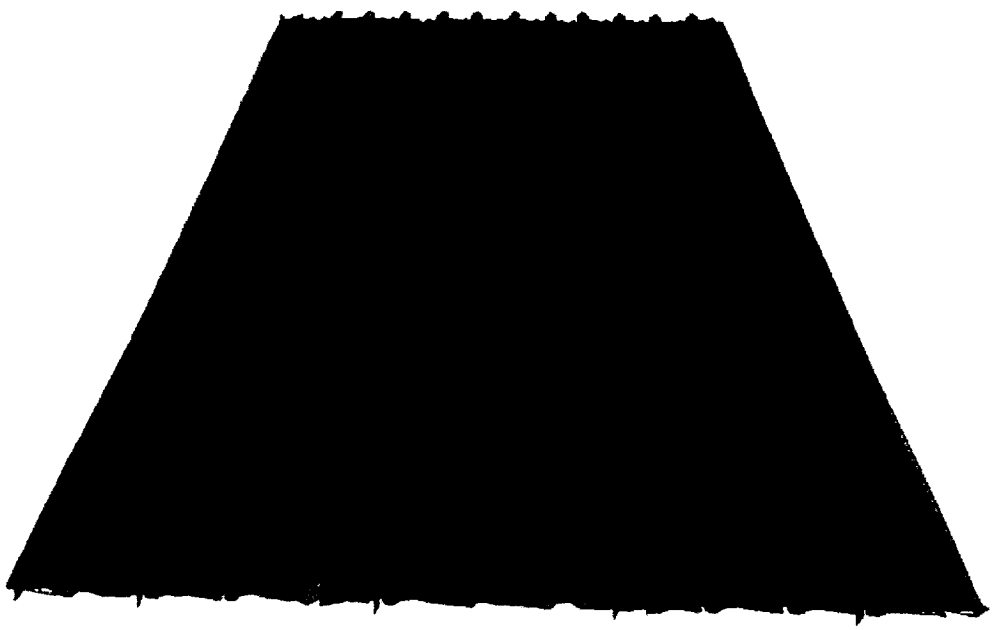

Figure 4.31: Deformed shape of steel deck with roofing components

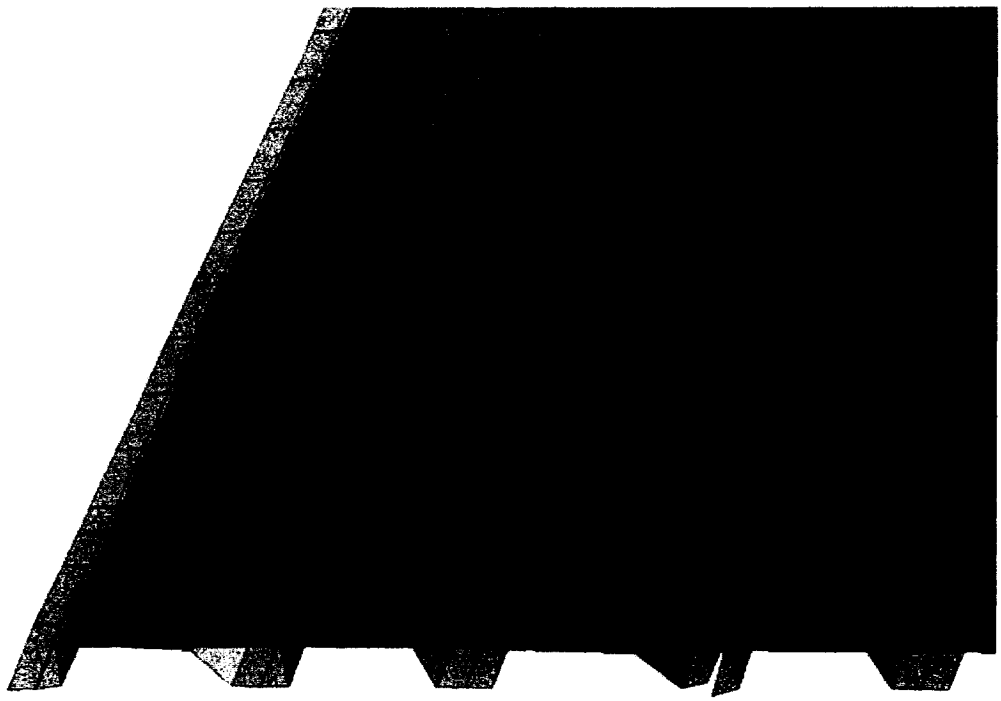

Figure 4.32: Close-up of warping for steel deck with roofing components

As it is shown in Figures 4.29 and 4.30, there is warping in the steel deck, which corresponds to that observed during testing of the bare steel specimens. The warping distortion is much less apparent in the model with the non-structural components (Figs. 4.31 & 4.32). Based on observations and the reduced displacement values it can be said that the non-structural roofing elements limit the extent of deck warping. Figures 4.30 and 4.32 were taken with the same scale factor to amplify the deformations, so a visual comparison between the two figures is possible. Figure 4.33 shows the flexural deformation in the non-structural components, as was observed in the diaphragm specimens tested by Yang (Fig. 4.16). The gypsum board is pulled down at both ends where NL4 link elements are present. Furthermore, there is no flexural deformation in the non-structural components over the middle flute because there is no link element.

Figure 4.33: Deformation of non-structural components

The SAP model reproduced the behaviour of the tests with precision. Flexure of the non-structural components in the test specimen (Fig. 4.16) is accurately reproduced in the SAP model (Fig. 4.33). The non-structural components are pulled down where NL4 links are present and do not undergo any flexure where there are no link elements, as with the test specimen. Furthermore, the warping of the deck is accurately reproduced for both the bare sheet steel deck and for the specimens with the roofing components; the presence of the non-structural components on the steel deck reduced the warping of the panels.

The stiffness values obtained with the FEM models were slightly higher than the values measured during testing, for both the bare sheet steel model and the model that included the roofing materials. The difference in elastic stiffness between the test specimen and the analytical model is approximately 5%. This could be due to material non-uniformity or irregularities that occurred during the construction of the test specimen.

The overall stiffness of a steel roof deck diaphragm is highly dependent on the individual frame and side-lap connections. It is possible that in the diaphragms tested by Yang (2003) the quality of installation of the fasteners was not consistent, and hence in some locations the connection stiffness may have been lower than used in the FE models. This would have led to a decrease in the measured shear stiffness of the test diaphragm. To verify whether the 5% discrepancy between the test and FE derived stiffness was due to poor connector quality an additional model was created in which 10% of the connectors had their stiffness reduced by 10% for the 38-76-6-NS-M configuration. Note, this 10% decrease was arbitrarily selected to examine the possibility that less stiff connections may have reduced the measured diaphragm stiffness. The same incremental displacement and load imbalance convergence criteria, as well as the same hinge load redistribution method were used for the additional finite element model. The results of the analysis gave a displacement of 0.228 mm, which corresponds to a shear stiffness of 2.63 kN/mm. A test-to-predicted result of 0.98 indicates that only a slight change in the connection stiffness, perhaps due to a lack of quality control during construction, for a small number of fasteners can change the overall diaphragm stiffness. Based on the stiffness obtained for this model it is conceivable that the connections for Yang's diaphragm test specimen had

less stiffness than assumed for the finite element model, which resulted in the 5% difference listed in Table 4.8.

4.6 SDI Results and Discussion

Luttrell (1995) published a document in collaboration with the Steel Deck Institute (SDI) which presents stiffness and strength equations for the design of bare sheet steel diaphragms. The SDI design method for diaphragms is directly dependent on the fastener contribution to overall diaphragm in-plane shear stiffness. Individual stiffness values for welds, screws and powder actuated fasteners form the basis of the overall shear stiffness equation, presented below:

$$G' = \frac{Et}{\Delta_S + \Delta_D + \Delta_C} \qquad (4\text{-}7),$$

where:

Δ_S, Δ_D, Δ_C are shear displacements, diaphragm warping displacements and connection displacements. When replacing the three displacement values by their respective equations, the following is obtained:

$$G' = \frac{Et}{2.6\left(\frac{s}{d}\right) + \phi D_n + C} \qquad (4\text{-}8),$$

where:

E = modulus of elasticity,
D_n = warping constant of the deck assembly,
C = connector slip parameter,
s = girth of corrugation per rib, in.,
d = corrugation pitch, in.,

t = base metal thickness, in.,

ϕ = reduction factor based on number of equal spans.

The equations for the parameters C and D_n are also presented in the SDI Design Manual. C is dependant on the connection stiffness and strength properties, whereas D_n is dependant on the faster arrangement at panel ends and the warping constant of the deck panel itself. Both sidelap and deck-to-frame fastener stiffness and strength equations are presented for typical types of connectors: arc-spot welds, sidelap welds, welds with washers, screw connections, powder driven fastener connections and button punched sidelaps. The ϕ values reduce the effect of the D_n values as the number of equal spans increase for one sheet length. As the number of spans increase, the ϕ value decreases.

Although the models with the 0.76 and 0.91 mm deck seem to indicate good correlation between the analytical and test results by Yang (2003), there is no diaphragm test data available in the literature with which to compare the results of the 1.22 mm and 1.51 mm deck models. Therefore it is difficult to confirm the accuracy of the model for the thicker two roof deck panels. However, SDI diaphragm stiffness values were calculated, using three different series of connector stiffnesses, to compare with the finite element results to identify whether the results of the FEM analyses were in the expected range.

Using the SDI equations presented above, three different diaphragm stiffness values were computed and compared with the results of the SAP 2000 analyses. The first SDI based stiffness was determined using the individual connection stiffness values as documented in the SDI Design Manual (1991). The second stiffness, SDI*, was calculated using the connection stiffness values obtained from Rogers and Tremblay (2003a,b). There were no test values for deck-to-frame and sidelap connections for the 1.22 mm and 1.51 mm decks, thus a connection stiffness could not be provided. The SDI** stiffness values were based on the connection properties presented in Chapter 3 of this Thesis. Table 4.9 shows the connection properties used for each SDI computation. The results of the SDI computations are shown in Table 4.10 and compared to the stiffness values obtained from

the SAP 2000 finite element analyses. The calculation sheets for the SDI method are provided in Appendix F.

Table 4.9: Connection stiffness used for SDI calculation (kN/mm)

		0.76	0.91	1.22	1.51
SDI	Deck-to-frame	23.9	25.5	24.6	27.4
	Sidelap	9.90	10.6	12.8	14.2
SDI*	Deck-to-frame	23.2	23.9	N/A	N/A
	Sidelap	1.35	2.26	N/A	N/A
SDI**	Deck-to-frame	32.0	32.0	46.6	50.3
	Sidelap	11.6	14.7	18.7	21.2

Table 4.10: SAP vs. SDI predictions of bare steel diaphragms stiffness (kN/mm)

Specimen	SAP Stiff. (kN/mm)	SDI (kN/mm)	SAP/SDI	SDI* (kN/mm)	SAP/SDI*	SDI** (kN/mm)	SAP/SDI**
38-76-6-NS-M	2.74	3.21	0.853	2.86	0.957	3.28	0.835
38-91-6-NS-M	4.46	5.25	0.850	4.52	0.987	5.46	0.817
38-122-6-NS-M	7.87	9.65	0.816	N/A	N/A	10.51	0.749
38-151-6-NS-M	12.36	14.04	0.880	N/A	N/A	15.75	0.785

Using the SDI values for connector stiffness resulted in poor agreement between the SAP and SDI values. The SDI values were larger than the values obtained by numerical analyses, although the ratio of the two is relatively consistent. The ratio of SAP/SDI was approximately 0.85 for the 0.76 mm, 0.91 mm. 1.22mm decks had a slightly lower ratio of approximately 0.82. However, the results were slightly better for the 1.51 mm panels, with a ratio of 0.88.

For the SDI* results, the correlation between the SAP results and the SDI gave much better results. The ratio of the SAP values over the SDI values was between 0.96 and 0.99 for the 0.76 mm and 0.91 mm decks.

The SDI** results were calculated using the connection stiffness values presented in Chapter 3 of this thesis. The much higher deck-to-frame and sidelap connector stiffness values that were used caused the SAP/SDI values to respond accordingly. The SDI predicted diaphragm stiffness values are the highest of those calculated. Furthermore, the SAP/SDI** ratios do not correspond to the values obtained with the FEM model. For the

lighter panels, the ratio is approximately 0.82, but for the two thicker panels, the ratios are 0.749 and 0.785 for the 1.22 mm and 1.51 mm decks respectively.

The results presented above show that the SDI results consistently overestimate the stiffness values of the deck diaphragms. Regardless of the combination of stiffness values used, the model results were much lower than the SDI values obtained. Because the SDI* values are the closest to the SAP analysis values and the values obtained by Yang (2003), it seems clear that the connection properties calculated by Rogers and Tremblay (2003a,b) are more accurate than the values predicted by the SDI equations.

In light of these results, it is safe to assume the finite element model adequately estimates diaphragm behaviour of thicker decks. The consistency with which the model overestimates the SDI values points to a realistic estimation of deformations of the steel deck diaphragms for thicker steel panels.

However, the analysis was run with a 1 kN point load only. The behaviour of this model is most likely non-linear. The interaction between the gypsum board and the steel deck is likely to change as deformations in the steel deck increase due to higher loads. As the load increases, the shear stiffness of the diaphragm may decrease because of this interaction. Further analyses should be run, using higher loading values.

4.7 Influence of Non-Structural Components on Diaphragm Stiffness: Parametric Study

The goal of this parametric study was to determine the contribution of the non-structural components to overall roof diaphragm in-plane shear stiffness for different sheet steel thicknesses and, more importantly, connection configurations using SDI values of deck-to-frame and sidelap connector stiffness. Designers commonly rely on SDI connection stiffness values to calculate steel deck diaphragm stiffness and capacity, therefore this series of analyses was conducted to identify the possible impact that non-structural components may have on SDI calculated G' values.

The findings in the previous Section seem to point to a significant contribution to shear stiffness by the non-structural components, although the effect of structural connector spacing is unknown. The purpose of this study was to explore the effects of deck-to-frame and sidelap connector layouts on non-structural component contribution to overall in-plane diaphragm shear stiffness. In addition, it was previously found that the gypsum board provided for most of the increase in diaphragm shear stiffness, and that the remaining non-structural components were for the most part ineffective in changing G' of the overall roof system. For this reason the properties of the non-structural elements in the models used for the parametric study were defined based on the gypsum panels alone.

4.7.1 General Information

A total of 32 analyses were carried out for this study, comprising of four different steel deck thicknesses – 0.76, 0.91, 1.22 and 1.51 mm – and four structural connector configurations, with and without the gypsum board. Two spacings are typically used in construction for the deck-to-frame and sidelap connectors of a roof diaphragm: 305 mm and 152 mm. This study consisted of four connector spacing combinations: 305/305, 305/152, 152/305 and 152/152, where the first number is the deck-to-frame connector spacing and the second is the sidelap connector spacing, in millimetres. Although some minor changes were made to the FE models for these parametric study analyses, the elements and analysis settings were defined as for the previous models (Sections 4.4 & 4.5).

Given that the finite element analysis of the shear test model in Section 3.4.5.2 indicated that the actual contribution of the ISO board and fibreboard to the stiffness of the non-structural sandwich to be barely over 5%, it was decided that the material properties of the non-structural components for these analyses would be the shear modulus and modulus of elasticity of the gypsum board alone. Therefore, the SH2 shell element was defined to have values of 2625 MPa for the modulus of elasticity (E) and 1284 MPa for the shear modulus (G).

4.7.2 SDI Connector Stiffness

The SDI equations for deck-to-frame and sidelap connectors were used to calculate the values for the connector stiffnesses. These deck-to-frame and sidelap values were used in the SAP model for the NL1 and NL2 link elements respectively (Table 4.11). There are no equations or values provided for the gypsum-to-deck connector stiffness in the literature, therefore the data acquired in Chapter 3 was used for the NL4 elements, as was done for the previous models.

Table 4.11: SAP – link properties (kN/mm)

		0.76	0.91	1.22	1.51
LINK (kN/mm)	NL1	19.42	21.25	24.60	27.37
	NL2	10.10	11.05	12.79	14.23
	NL4	3.14	3.14	3.14	6.28

4.7.3 Results

Using the connector stiffness values shown in Table 4.11 in conjunction with the four nominal deck thicknesses and four connector configurations, diaphragm shear stiffness values were obtained for bare steel deck diaphragms and for diaphragms with a gypsum board layer (Table 4.12). The percentage increase in diaphragm stiffness due to the addition of the gypsum board is tabulated in Table 4.13 for all sixteen of the diaphragms that were modelled.

Table 4.12: SAP – diaphragm stiffness G' (kN/mm)

	Bare Steel				With Roofing			
	305/305	305/152	152/305	152/152	305/305	305/152	152/305	152/152
0.76	3.26	4.05	9.29	11.84	4.78	5.59	10.71	13.25
0.91	5.17	5.40	12.35	15.51	6.46	7.06	13.71	16.88
1.22	8.51	8.70	17.39	23.06	10.05	10.15	18.74	24.36
1.51	12.55	13.11	22.32	30.05	13.82	14.42	23.76	31.47

Table 4.13: Increase in G' stiffness with gypsum board

	305/305	305/152	152/305	152/152
0.76	46.4%	38.1%	15.3%	11.9%
0.91	25.0%	30.6%	11.0%	8.8%
1.22	18.1%	16.7%	7.8%	5.6%
1.51	10.1%	10.0%	6.5%	4.7%

The results clearly indicate a trend: as the steel diaphragm becomes stiffer due to either the use of a thicker deck or more closely spaced structural connections, the contribution of the gypsum board to overall diaphragm stiffness decreases on a percentage basis. For the 0.76 mm specimen with a 305/305 connector spacing, a significant increase in G' (46.4 %) was caused by the addition of the gypsum layer. Conversely, for the 1.51 mm specimen with a 152/152 spacing, the increase was less than 5%. However, when comparing G' values for bare diaphragms versus diaphragms with the gypsum board, the actual contribution of the non-structural layer is very similar in absolute terms for all of the configurations modeled. The increase in shear stiffness between the diaphragm with the gypsum board and the bare sheet steel diaphragm varied between 1.27 and 1.65 kN/mm, with an average value of 1.41 kN/mm and a CoV of 7.6%. These results indicate that the structural connector layout does not influence the non-structural component contribution to in-plane shear stiffness of a roof diaphragm.

In summary, it was possible to recreate the diaphragm test results in a realistic fashion through the use of a finite element model. The contribution to overall diaphragm shear stiffness of the non-structural components diminishes on a percentage basis as the overall stiffness of the bare sheet steel deck increases. Furthermore, the absolute contribution of the gypsum remains relatively constant, regardless of connector spacing or thickness of the roof deck panels.

CHAPTER 5
CONCLUSION AND RECOMMENDATIONS

5.1 Conclusions

The overall goal of this research was to provide a better understanding of the effect of non-structural roofing components on the performance of single-storey steel buildings subjected to seismic loading, specifically on roof diaphragm behaviour. This has been achieved by means of materials tests, finite element analyses and a comparative study of predicted diaphragm and stiffness values.

Firstly, series of experiments were conducted to evaluate the shear and flexural stiffness values of the non-structural components in a roof assembly, as well as the stiffness of the deck-to-frame, sidelap, and gypsum-to-deck connectors. In total, 171 tests were conducted: 9 small scale shear tests, 68 flexural tests, 22 large scale shear tests and 72 connection tests.

From these tests, the following data was acquired:

- Cascade *Securpan* fibreboard: Young's modulus in flexure is 250 MPa and in-plane shear stiffness is 235 MPa,
- Type X 12.7 mm (½") *CGC* gypsum board: Young's modulus in flexure is 2625 MPa and in-plane shear stiffness is 1284 MPa,
- ISO board: in-plane shear stiffness is calculated as 4.0 MPa, from the finite element analysis,
- AMCQ SBS-34 roofing system: In-plane shear stiffness is 1353 MPa, from the finite element analysis,
- Gypsum board to steel deck connection: connection stiffness for 0.76, 0.91 and 1.22 mm deck is 3.14 kN/mm; for 1.51 mm sheet steel is 6.30 kN/mm,
- Deck-to-frame: connection stiffness for 0.76, 0.91, 1.22 and 1.51 mm deck are 32.3, 31.7, 46.6 and 50.3 kN/mm, respectively,
- Sidelap: connection stiffness for 0.76, 0.91, 1.22 and 1.51 mm deck are 11.6, 14.7, 18.6 and 21.2 kN/mm, respectively,

- Small scale shear tests are adequate to compute the shear stiffness of materials with the ASTM D1073a equation, although non-isotropic materials could give multiple results.

It can be seen from the test data that the gypsum board is the stiffest element of the non-structural components, and because of this has the greatest influence on the in-plane force-deformation behaviour of the steel roof deck diaphragm. The other non-structural elements, either due to their low in-plane shear stiffness or lack of a direct connection to the steel deck, do not have as much of an effect.

A finite element model was developed using SAP2000 to analyse the linear elastic behaviour of bare sheet steel deck diaphragms and diaphragms constructed with non-structural roofing components. The material and connection test data was input into the finite element model, and a comparison of the measured stiffness of three diaphragm specimens tested by Yang (2003) and Essa *et al.* (2000) was carried out. The stiffness results of analyses 38-76-6-NS-M, 38-91-6-NS-M and 38-76-6-NS-R-M correlated well to the measured values, with test-to-predicted ratios in the range of 0.94 to 0.96. Given the close agreement of the test and analytical results it was concluded that the finite element model is adequate for the prediction of the linear elastic behaviour of roof deck diaphragms.

A study was then carried out in which the elastic stiffness of five additional roof diaphragms with varying configuration was evaluated with the finite element model. Test data for diaphragms of these configurations was not available. In general, the diaphragm stiffness increased as the thickness of the steel roof deck panels increased. Furthermore, the contribution of the non-structural components, in terms of an increase in in-plane shear stiffness, was apparent for all deck thicknesses. This increase in stiffness became less on a percentage basis as the deck thickness was increased. As an example, for the 0.76 mm deck, the increase in stiffness due to the non-structural roofing components was approximately 58.6% compared with a 16.9% increase for the 1.51 mm deck.

At this point, the stiffness results that were obtained by the finite element model were compared to three sets of SDI predicted values: SDI, SDI* and SDI**. SDI was calculated using the SDI values for connection stiffness, SDI** with the connection stiffness values obtained from Rogers and Tremblay (2003a,b) and SDI** with the connection property values presented in Chapter 3 of this Thesis. The SDI values gave consistently higher stiffnesses than the SAP models, for all three SDI results. However, the best convergence was obtained with SDI*.

To explain the 5% over-stiffness obtained using the SAP models, the 38-78-6-NS-M model was tested with 10% of its sidelap and deck-to-frame connectors at 90% of their original stiffness. The results of the analysis showed that the diaphragm shear stiffness decreased from 2.74 to 2.63 kN/mm. The Test/SAP ratio went from 0.94 to 0.98, which shows that an overestimate of the connection stiffness or a faulty installation of even a small percentage of connectors might be the cause of the higher stiffness in the SAP model than in the test diaphragms. However, as was discussed in Chapter 4, the event and iteration lumping tolerances play an important role with respect to the accuracy of the analysis results. Therefore, it is possible that the use of lower lumping tolerances would return more adequate results.

A parametric study was conducted in order to determine the contribution of gypsum board to overall in-plane shear stiffness of the steel deck diaphragm, with multiple deck thicknesses and connector layouts. For these FE models the stiffness of the sidelap and deck-to-frame connectors was based on the SDI predicted values, not test results. The study showed that the contribution of the gypsum board remained relatively constant regardless of deck thickness and connector spacing. On average, the diaphragm with the gypsum board was 1.41 kN/mm stiffer than the equivalent bare diaphragm. Moreover, the percentage increase in shear stiffness of the diaphragm became less as the deck thickness was increased and as the structural connectors were placed at a closer spacing.

As stated in Chapter 2, Medhekar (1997) and Tremblay et al. (1995, 2000) have shown that diaphragm stiffness influences the natural period of buildings to a large extent.

Therefore, non-structural roofing elements, when gypsum board is used, should be considered in the overall in-plane diaphragm stiffness when calculating the natural period of vibration.

5.2 Recommendations

This study has shown that the gypsum board has a much higher shear stiffness than the other non-structural components considered. From this finding, it can be assumed that the contribution of the non-structural components to the roof diaphragm stiffness would be significantly less if the gypsum board were not present.

One of this project's objectives was to accurately determine the in-plane shear stiffness properties of the non-structural components. The values obtained in Chapter 3 using the finite element analysis model of the four sided shear test specimen confirm that the shear stiffness of the AMCQ SBS-34 roof system is greater than that of the gypsum board alone. The SAP2000 analyses were run with the shear modulus determined with the simplifying equation of the concentric load. Although additional SAP2000 analyses could be carried out with the new shear stiffness values for the non-structural components, the change in predicted diaphragm deformations would be minor.

To better understand the contribution of non-structural components to overall structure behaviour, inelastic analyses of diaphragms including the non-structural components should be conducted.

Furthermore, a broader database of test information should be compiled for diaphragms constructed of 1.22 and 1.51 mm decks. Although the results of the SAP analyses of 0.76 and 0.91 mm decks showed good agreement with the diaphragm tests, the 1.22 and 1.51 mm decks have not been tested and their predicted behaviour cannot be confirmed.

Moreover, performing a finite element analysis to determine the diaphragm in-plane shear stiffness is tedious and time consuming. The development of empirical equations to

account of the contribution of the non-structural components to diaphragm in-plane shear stiffness or the addition of a term to the SDI equations should be carried out.

Lastly, the values obtained for diaphragm stiffness should be introduced into the equations developed by Medhekar (1997) and Tremblay (2005) to find new predictions for the natural periods of single storey steel buildings, which could be compared with the data acquired by Ventura and Turek (2005) and Lamarche (2005). This comparison should shed light on the actual influence of roof deck diaphragm stiffness on overall building period of vibration.

REFERENCES

AMERICAN SOCIETY FOR TESTING AND MATERIALS, A653 (2002), Standard Specifications for Steel Sheet, Zinc-Coated (galvanized) or Zinc-Iron Alloy-Coated (Galvannealed) by the Hot-Dip Process., Philadelphia, PA, USA.

AMERICAN SOCIETY FOR TESTING AND MATERIALS, C203 (1999), Standard Test Methods for Breaking Load and Flexural Properties of Block-Type Thermal Insulation. West Conshohocken, PA, USA.

AMERICAN SOCIETY FOR TESTING AND MATERIALS, C473 (1997), Standard Test Methods for Physical Testing of Gypsum Panels Products. West Conshohocken, PA, USA.

AMERICAN SOCIETY FOR TESTING AND MATERIALS, D1037 (1999). Evaluating the Properties of Wood-Base Fibre and Particle Panel Materials. West Conshohocken, PA, USA.

AMERICAN SOCIETY FOR TESTING AND MATERIALS, D2719 (1989, Reapproved 1994). Standard Test Methods for Structural Panels in Shear Through-the-Thickness. West Conshohocken, PA, USA.

AMERICAN SOCIETY FOR TESTING AND MATERIALS, D3043 (1995)., Standard Methods of Testing Structural Panels in Flexure. West Conshohocken, PA, USA.

AMERICAN SOCIETY FOR TESTING AND MATERIALS, E455 (2002), Test Method for Static Load Testing of Framed Floor or Roof Diaphragm Construction for Buildings., West Conshohocken, PA, USA.

BAKER, M.C., (1980), Roofs----Design, Application and Maintenance., Sponsored by the National Research Council of Canada, Montréal, Qc., Canada.

BÉRAIR, T., (1999), Étude expérimentale sur le comportement sismique de bâtiments d'un seul étage en acier avec diaphragme de toit flexible., École Polytechnique de Montréal, Montréal, Qc., Canada.

BOUDREAULT, F.A., (2005), Seismic Analysis of Steel Frame / Wood Panel Shear Walls., Masters Thesis, Department of Civil Engineering and Applied Mechanics, McGill University, Montréal, Qc., Canada.

CANADIAN SHEET STEEL BUILDING INSTITUTE, (1991), Design of Steel Deck Diaphragms., B13-91, Cambridge, Ont. Canada.

CANADIAN STANDARDS ASSOCIATION, CSA, (2004), A123.4, Asphalt for Construction of Built-Up Roof Coverings and Waterproofing Systems., Etobicoke, Ont., Canada.

CANADIAN STANDARDS ASSOCIATION, CSA, (1992), CAN/CSA-G40.20/G40.21-92, General Requirements for Rolled or Welded Structural Quality Steel/Structural Quality Steels., Etobicoke, Ont. Canada.

CANADIAN STANDARDS ASSOCIATION, CSA, (1994), CAN/CSA-S16. Limit States Design of Steel Structures. Etobicoke, Ont., Canada.

CANADIAN STANDARDS ASSOCIATION, CSA, (2001), CAN/CSA-S16. Limit States Design of Steel Structures. Etobicoke, Ont., Canada.

CANAM (1999). Steel deck. Canam Manac Gr., www.canammanac.com.

CARR, A.J., (2000), Ruaumoko - Inelastic Dynamic Analysis., Version March 15th 2000. Dept. Of Civil Eng., University of Canterbury, Christchurch, New Zealand.

COMPUTERS AND STRUCTURES, INC. (2002). SAP2000 Version 8.0, Integrated Finite Element Analysis and Design of Structures. Berkeley, CA, USA.

COOK, R.D., MALKUS, D.S., PLESHA, M.E., WITT, R.J., (2001), Concepts and Applications of Finite Element Analysis., Fourth Edition, Jon Wiley & Sons, Inc. New York, NY, USA.

ESSA, H.S., TREMBLAY, R., ROGERS, C.A., (2001), Inelastic Seismic Behaviour of Steel Deck Roof Diaphragms Under Qasui-static Cyclic Loading., Report no. EPM/CGS-2001-11. Department of Civil, Geologiccal and Mining Engineering, École Polytechnique de Montréal, Montréal, Qc., Canada.

ESSA, H.S., TREMBLAY, R., ROGERS, C.A., (2003), Behaviour of Roof Deck Diaphragms Under Quasi-Static Cyclic Loading., *Journal of Structural Engineering, ASCE, Vol. 129 No.12, 1658-1666.*

FEDERAL EMERGENCY MANAGEMENT AGENCY, FEMA, (1997), FEMA273/274, Guidelines for the Seismic Rehabilitation of Buildings., Washington, District of Columbia, USA.

HILTI, (2001), Hilti North America. Product Technical Guide-2001 Edition., Hilti Corporation, Schaan, Principality of Liechstenstein.

LAMARCHE, C.P., (2005), Étude Expérimentale du comprtement Dynamique des Bâtiments de Faible Hauteur en Acier., Masters Thesis, Dept. of Civil Engineering, Université de Sherbrooke, Sherbrooke, Qc., Canada.

LUTTRELL, L.D., (1995), Steel Deck Institute Design Manual., Second Edition, Department of Civil Engineering, West Virginia University, Morgantown, WV, USA.

MARTIN, E., (2002), Inelastic Response of Steel Roff Deck Diaphragms Under Simulated Dynamically Applied Seismic Loading., Masters Thesis, Dept. Of Civil, Geological and Mining Engineering, École Polytechnique de Montréal, Montréal, Qc., Canada.

MEDHEKAR, M.S., (1997), Seismic Evaluation of Steel Buildings with Concetrically Braced Frames., Ph.D. in Structural Engineering thesis, Department of Civil and Environmental Engineering, University of Alberta, Edmonton, Alberta, Fall, 1997.

MEDHEKAR, M.S., KENNEDY, D.J.L., (1999), Seismic Evaluation of Single-Storey Buildings., Canadian Journal of Civil Engineering, **26**, p.379-394.

NEDISAN, C.D., MASTROGIUSEPPE, S., TREMBLAY, R., ROGERS, C.A., (2006), Shear tests on HILTI nailed frame and screwed side-lap fasteners for 0.76 to 1.52 mm thick cold-formed sheet steel., Research Report No.EPM/CGS-2006-1, Department of Civil, Geological and Mining Engineering, École Polytechnique, Montréal, Canada.

NEDISAN, C., (2002), Comportement Sismique de Bâtiments d'un Seul Étage en Acier avec Diaphragme de Toit Flexible., Masters Thesis, Dept. of Civil, Geological and Mining Engineering, École Polytechnique de Montréal, Montréal, Qc., Canada.

NILSON, A.H., (1960), Shear Diaphragm of Light Gage Steel., Journal of the Structural Division, Proceedings of the American Society of Civil Engineers, Vol. 86, No. ST11, p.111-139.

NRCC, (1995), National Building Code of Canada 1995 (NBCC)., 11th ed.. Canadian Commission on Building and Fire Codes, National Research Council of Canada, Ottawa, Ontario, Canada.

NRCC, (2005), National Building Code of Canada 2005 (NBCC)., 12th ed.. Canadian Commission on Building and Fire Codes, National Research Council of Canada, Ottawa, Ontario, Canada.

ROGERS, C.A., TREMBLAY, R., (2000), Inelastic Seismic Response of Frame and Sidelap Fasteners of Steel Roof Decks., Research Report No. EPM/CGS-2000-09, Department of Civil, Geological and Mining Engineering, École Polytechnique de Montréal, Montréal, Qc., Canada.

ROGERS, C.A., TREMBLAY, R., (2003a), Inelastic Seismic Response of Sidelap Fasteners for Steel Roof Deck Diaphragms., *Journal of Structural Engineering, ASCE, Vol. 129 No12, p.1637-1646.*

ROGERS, C.A., TREMBLAY, R., (2003b), Inelastic Seismic Response of Frame Fasteners for Steel Roof Deck Diaphragms. *Journal of Structural Engineering, ASCE, Vol. 129 No.12, p.1647-1657*

ROGERS, C.A., TREMBLAY, R., YANG, W., MARTIN, E., (2004). Ductile design of steel roof deck diaphragms for earthquake resistance. Proceeding of the 13th World Conference on Earthquake Engineering, Paper No.1997.

STEEL DECK INSTITUTE, SDI, (1981), Diaphragm Design Manual., Canton, OH, USA.

STEEL DECK INSTITUTE, SDI, (1991), Diaphragm Design Manual., Second Edition, Canton, OH, USA.

TREMBLAY, R., BÉRAIR, T., (1999), Shake table testing of low-rise steel buildings with flexible roof diaphragms. Proceedings of the 8th Canadian Conference on Earthquake Engineering, Vancouver, Canada. 585-590.

TREMBLAY, R. AND STIEMER, S.F. (1996), Seismic behaviour of single-storey steel structures with flexible diaphragm. *Canadian Journal of Civil Engineering, Vol. 23: 49-62.*

TREMBLAY, R., (2005), Fundamental Period of Vibration of Braced Steel Frames for Seismic Design., *Earthquake Spectra 2005, August, Vol.21 No.3, p.831-861.*

TREMBLAY, R., et al., (2000), Experimental Behaviour of Low-Rise Steel Buildings with Flexible Roof Diaphragms., Proceeding of the 12th World Conference on Earthquake Engineering, Auckland, NZ. Paper No. 2567.

TREMBLAY, R., et al., (2004), Experimental investigation and dynamic simulation of low-rise steel buildings for efficient seismic design., 13th World Conference on Earthquake Engineering, Paper No.2919.

TREMBLAY, R., ROGERS, C.A., MARTIN, E., YANG, W., (2004). Analysis, Testing and Design of Steel Roof Deck Diaphragms for Ductile Earthquake Resistance., *Journal of Earthquake Engineering, Vol. 8 No. 5, 775-816.*

TREMBLAY, R., STIEMER, S.F., (1996), Use of Uniform Hazard Spectrum and Computed Period in the Seismic Design of Single-Storey Steel Structures., Proceedings of the 7th U.S. National Conference on Earthquake Engineering, Boston, MA, USA.

TUREK, M., VENTURA, C., (2005), Ambient Vibration of Low-Rise Buildings with Flexible Diaphragms., Proceedings of the 23rd International Modal Analysis Conference, Orlando, FL, USA, Februrary 2005, Paper 304.

VENTURA, C., (1995), Ambient Vibration test of the Safeway Store., report by the UBC Ambient Vibration Team, Dept. of Civil Engineering, University of British Columbia, Vancouver, BC, Canada.

VINSON, J.R., (1999), The Behaviour of Sandwich Structures of Isotropic and Composite Materials., Technomic Publishing Co., Lancaster, PA, USA.

YANG, W., (2003), Inelastic Seismic Response of Steel Roof Deck Diaphragms Including Effects of Non-Structural Components and End Laps., Masters Thesis, Dept. Of Civil, Geological and Mining Engineering, École Polytechnique de Montréal, Montréal, Qc., Canada.

APPENDIX A
TWO-SIDED SHEAR TEST DATA

The results of the two-sided shear tests are presented in Chapter 3, Section 3.2 and in this Appendix. The maximum loads and the thickness measurements of each specimen are presented in this Appendix. The shear load versus shear deformation curve is shown for each specimen as well.

Table A1: Fibreboard and gypsum board specimen thickness (mm)

Fibreboard						Gypsum Board			
Test 1	Test 2	Test 3	Test 4	Test 5	Test 6	Test 1	Test 2	Test 3	Test 4
23.96	24.48	25.22	24.50	24.52	23.85	15.77	15.27	15.17	15.84
22.96	24.14	23.81	24.44	24.00	24.20	15.64	15.25	15.13	15.54
	24.25	23.53	24.01	23.36	23.76	15.24	15.44	14.96	15.56
	24.26	23.51	24.47	23.36	24.06	15.36	15.24	15.12	15.56
	24.31	23.87	24.85	24.22	24.41	15.32	15.15	15.40	14.28
	24.39	23.97	25.32	23.60	24.48	15.25	15.10	15.16	15.59
	23.99	23.73	24.44	23.22	23.70	15.33	15.06	15.24	15.24
	23.94	24.66	24.15	24.00	23.60	15.58	15.09	15.29	15.21

Table A2: Fibreboard and gypsum board specimen width (mm)

	Fibreboard						Gypsum Board			
	Test 1	Test 2	Test 3	Test 4	Test 5	Test 6	Test 1	Test 2	Test 3	Test 4
Average	23.46	24.22	24.04	24.52	23.79	24.01	15.44	15.20	15.18	15.35
Std Dev.	0.71	0.19	0.60	0.41	0.47	0.33	0.20	0.13	0.13	0.48
%CoV	3.01%	0.77%	2.49%	1.66%	1.97%	1.38%	1.29%	0.83%	0.86%	3.11%

Table A3: Fibreboard and gypsum board maximum load (N)

Fibreboard						Gypsum Board			
Test 1	Test 2	Test 3	Test 4	Test 5	Test 6	Test 1	Test 2	Test 3	Test 4
N/A	5439	6396	6904	6171	6615	7417	7485	7774	6387

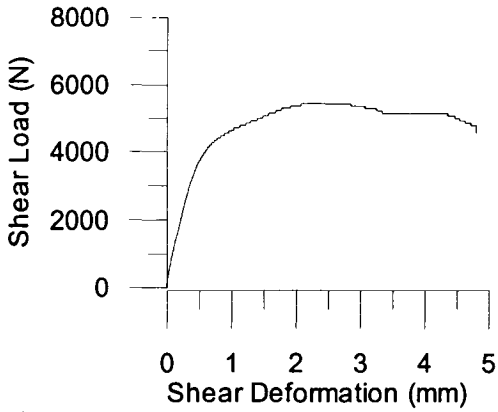

Figure A1: FB Test 2

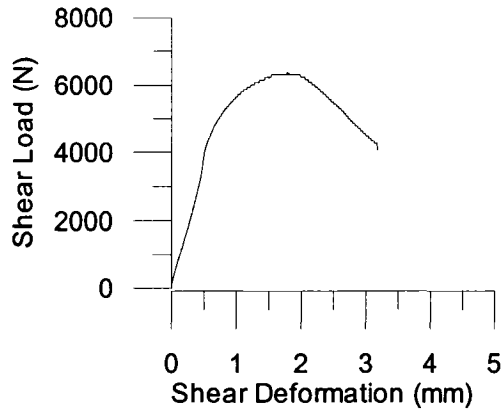

Figure A2: FB Test 3

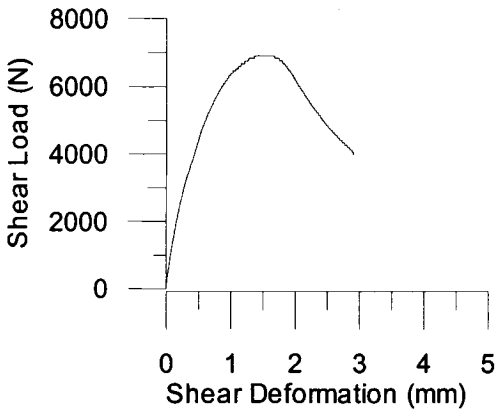

Figure A3: FB Test 4

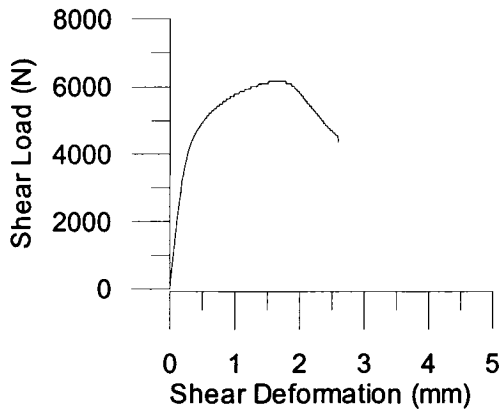

Figure A4: FB Test 5

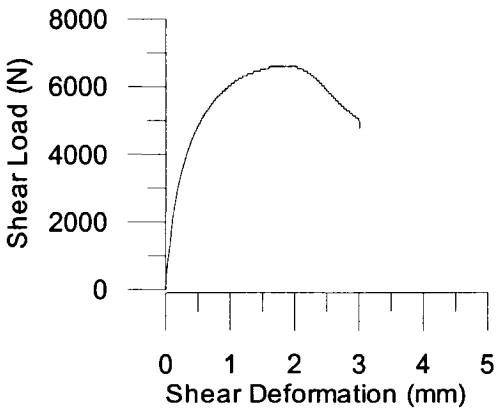

Figure A5: FB Test 6

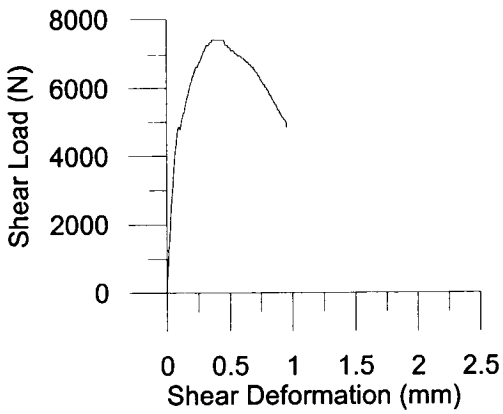

Figure A6: GYP Test 1

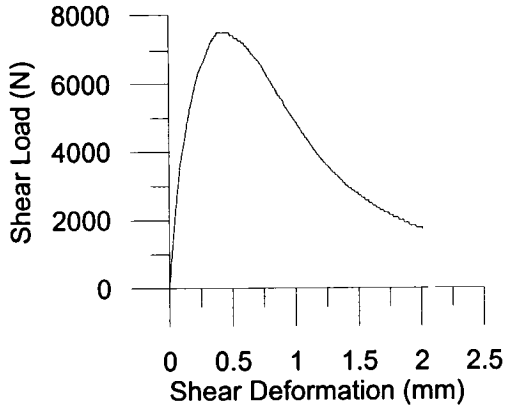

Figure A7: GYP Test 2

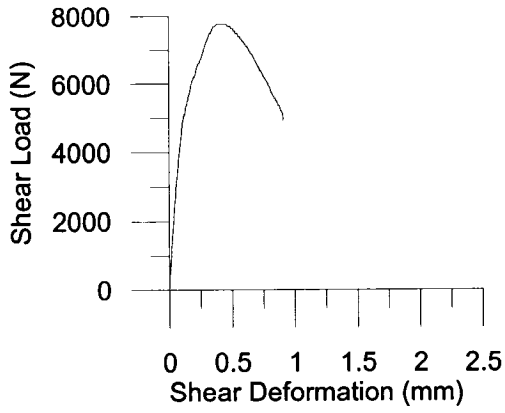

Figure A8: GYP Test 1

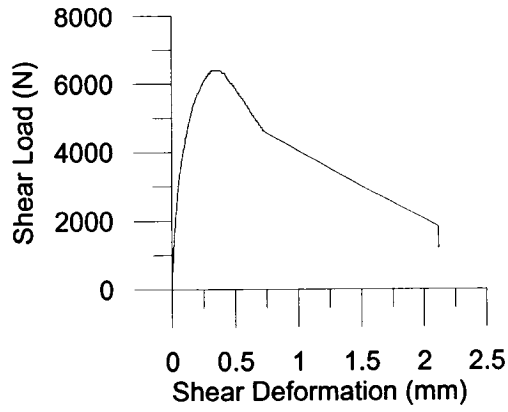

Figure A9: GYP Test 2

APPENDIX B
FLEXURAL TEST DATA

The results of the flexural tests are presented in Chapter 3, Section 3.3 and in this Appendix. The maximum loads as well as the thickness measurements of each specimen are presented in this Appendix. Furthermore, the load versus displacement curve of each specimen is also shown.

Table B1: Fibreboard specimen thickness (mm)

Specimen	Thickness						Average	%CoV
F1	23.80	23.74	23.71	23.77	23.70	23.75	23.75	0.16%
F2	23.63	23.62	23.81	23.73	23.77	23.80	23.73	0.35%
F3	24.08	24.20	24.04	24.01	24.36	23.90	24.10	0.67%
F4	24.10	23.76	24.13	24.10	24.09	23.80	24.00	0.70%
F5	24.00	23.75	24.15	23.91	24.22	24.07	24.02	0.71%
F6	23.93	23.61	23.82	23.91	24.26	23.33	23.81	1.32%
F7	24.74	24.28	24.40	24.44	24.12	24.10	24.35	0.98%
F8	23.91	23.94	23.53	23.99	23.90	23.51	23.80	0.91%
F9	23.87	23.84	23.97	24.07	23.76	24.12	23.94	0.58%
F10	24.09	24.20	24.01	23.86	24.05	24.29	24.08	0.62%
F11	23.61	23.77	24.02	23.88	23.72	24.15	23.86	0.84%
F12	24.06	23.99	24.57	23.87	23.96	23.94	24.07	1.06%
F13	23.79	23.90	23.78	23.94	23.96	23.86	23.87	0.32%
F14	24.15	24.12	24.18	24.06	24.14	24.63	24.21	0.86%
F15	24.05	24.36	23.42	24.35	24.20	23.79	24.03	1.52%
F16	23.66	24.76	24.13	23.61	24.14	23.99	24.05	1.73%
FDA -1	23.75	23.62	23.63	23.69	23.7	23.65	23.67	0.21%
FDA-2	23.63	23.62	23.62	23.63	23.65	23.49	23.61	0.25%
FDA-3	23.67	23.68	23.57	23.5	23.47	23.58	23.58	0.36%
FDA-4	23.73	23.61	23.63	23.71	23.71	23.68	23.68	0.20%
FDB-1	23.51	23.68	23.59	23.55	23.53	23.67	23.59	0.31%
FDB-2	23.66	23.71	23.74	23.66	23.61	23.71	23.68	0.20%
FDB-3	23.62	23.49	23.59	23.59	23.59	23.62	23.58	0.20%
FDB-4	23.76	23.66	23.56	23.64	23.66	23.68	23.66	0.27%

Table B2: Fibreboard specimen width (mm)

Specimen	Width			Average	%CoV
F1	104.21	104.32	104.17	104.23	0.07%
F2	103.94	103.74	104.17	103.95	0.21%
F3	104.42	104.19	104.06	104.22	0.17%
F4	104.24	104.46	103.80	104.17	0.32%
F5	103.50	103.70	103.87	103.69	0.18%
F6	100.44	100.43	100.13	100.33	0.18%
F7	99.83	100.02	100.64	100.16	0.42%
F8	100.39	100.22	99.89	100.17	0.25%
F9	100.84	100.70	99.31	100.28	0.84%
F10	104.49	104.30	104.18	104.32	0.15%
F11	102.29	102.92	103.50	102.90	0.59%
F12	104.82	103.98	103.64	104.15	0.58%
F13	102.70	102.82	103.60	103.04	0.48%
F14	104.48	104.25	103.75	104.16	0.36%
F15	104.22	103.95	104.37	104.18	0.20%
F16	103.76	104.43	103.73	103.97	0.38%
FDA-1	100.30	100.36	100.44	100.37	0.07%
FDA-2	100.09	100.25	100.12	100.15	0.08%
FDA-3	100.38	100.24	100.70	100.44	0.23%
FDA-4	100.25	100.25	99.99	100.16	0.15%
FDB-1	100.46	100.49	100.49	100.48	0.02%
FDB-2	100.14	100.23	100.47	100.28	0.17%
FDB-3	100.59	101.31	100.62	100.84	0.40%
FDB-4	100.49	100.61	100.57	100.56	0.06%

Table B3: Gypsum board specimen thickness (mm)

Specimen	Thickness						Average	%CoV
G-PL1	15.61	15.61	15.64	14.93	14.97	15.01	15.30	2.33%
G-PL2	15.59	15.61	15.65	15.58	15.61	15.57	15.60	0.18%
G-PL3	15.53	15.49	15.51	15.59	15.56	15.54	15.54	0.23%
G-PL4	15.40	15.39	15.40	15.61	15.65	15.59	15.51	0.79%
G-PL5	15.57	15.44	15.37	15.58	15.51	15.30	15.46	0.73%
G-PL6	15.25	15.40	15.49	15.53	15.26	15.30	15.37	0.78%
G-PL7	15.30	15.23	15.25	15.20	15.23	15.22	15.24	0.23%
G-PL8	15.52	15.25	15.26	15.21	15.24	15.41	15.32	0.80%
G-PL9	15.31	15.21	15.35	15.27	15.17	15.23	15.26	0.44%
G-PL10	15.68	15.51	15.60	15.60	15.36	15.34	15.52	0.89%
G-PL11	15.63	15.65	15.68	15.59	15.61	15.57	15.62	0.26%
G-PL12	15.85	15.67	15.32	15.21	15.92	15.77	15.62	1.87%
G-PL13	15.52	15.52	15.51	15.55	15.53	15.50	15.52	0.11%
G-PL14	15.52	15.52	15.51	15.45	15.45	15.44	15.48	0.25%
G-PL15	15.31	15.41	15.37	15.34	15.33	15.31	15.35	0.25%
G-PL16	15.32	15.32	15.29	15.22	15.22	15.22	15.27	0.33%
G-PL17	15.24	15.24	15.26	15.19	15.20	15.23	15.23	0.17%
G-PL18	15.25	15.22	15.22	15.19	15.23	15.23	15.22	0.13%
G-PL19	15.25	15.24	15.19	15.10	15.11	15.14	15.17	0.43%
G-PL20	15.43	15.44	15.42	15.57	15.60	15.58	15.51	0.55%
G-PL21	15.29	15.10	15.12	15.32	15.36	15.33	15.25	0.74%
G-PL22	15.60	15.66	15.67	14.68	14.60	14.50	15.12	3.83%
G-PP1	15.58	15.65	15.77	15.61	15.59	15.62	15.64	0.45%
G-PP2	15.58	15.59	15.57	15.51	15.57	15.53	15.56	0.20%
G-PP3	15.49	15.50	15.57	15.51	15.57	15.45	15.52	0.30%
G-PP4	15.49	15.52	15.50	15.47	15.57	15.60	15.53	0.32%
G-PP5	15.52	15.39	15.47	15.50	15.49	15.39	15.46	0.36%
G-PP6	15.49	15.51	15.39	15.48	15.45	15.35	15.45	0.40%
G-PP7	15.18	15.19	15.19	15.20	15.14	15.14	15.17	0.18%
G-PP8	15.17	15.20	15.15	15.16	15.14	15.19	15.17	0.15%
G-PP9	15.20	15.46	15.17	15.26	15.20	15.19	15.25	0.71%
G-PP10	15.17	15.17	15.18	15.19	15.19	15.12	15.17	0.17%
G-PP11	15.14	15.15	15.16	15.17	15.14	15.11	15.15	0.14%
G-PP12	15.85	15.67	15.32	15.21	15.92	15.77	15.62	1.87%
G-PP13	15.52	15.52	15.51	15.55	15.53	15.50	15.52	0.11%
G-PP14	15.52	15.52	15.51	15.45	15.45	15.44	15.48	0.25%
G-PP15	15.31	15.41	15.37	15.34	15.33	15.31	15.35	0.25%
G-PP16	15.32	15.32	15.29	15.22	15.22	15.22	15.27	0.33%
G-PP17	15.24	15.24	15.26	15.19	15.20	15.23	15.23	0.17%
G-PP18	15.25	15.22	15.22	15.19	15.23	15.23	15.22	0.13%
G-PP19	15.25	15.24	15.19	15.10	15.11	15.14	15.17	0.43%
G-PP20	15.43	15.44	15.42	15.57	15.60	15.58	15.51	0.55%
G-PP21	15.29	15.10	15.12	15.32	15.36	15.33	15.25	0.74%
G-PP22	15.60	15.66	15.67	14.68	14.60	14.50	15.12	3.83%

Table B4: Gypsum board specimen width (mm)

Specimen	Width			Average	%CoV
G-PL1	103.43	102.97	103.31	103.24	0.23%
G-PL2	104.21	104.35	103.99	104.18	0.17%
G-PL3	101.75	101.04	101.16	101.32	0.38%
G-PL4	101.00	101.58	101.45	101.34	0.30%
G-PL5	101.90	102.25	103.30	102.48	0.71%
G-PL6	102.35	102.03	101.38	101.92	0.48%
G-PL7	101.58	101.05	101.57	101.40	0.30%
G-PL8	100.88	101.36	101.46	101.23	0.31%
G-PL9	101.75	101.70	102.52	101.99	0.45%
G-PL10	102.07	102.74	103.03	102.61	0.48%
G-PL11	102.66	102.64	103.03	102.78	0.21%
G-PL12	103.73	104.02	103.21	103.65	0.40%
G-PL13	103.95	103.75	104.10	103.93	0.17%
G-PL14	103.78	103.90	103.86	103.85	0.06%
G-PL15	104.10	104.30	104.23	104.21	0.10%
G-PL16	104.12	103.88	104.16	104.05	0.15%
G-PL17	104.18	103.95	104.20	104.11	0.13%
G-PL18	104.30	103.98	104.21	104.16	0.16%
G-PL19	104.43	104.14	104.03	104.20	0.20%
G-PL20	103.82	104.43	104.61	104.29	0.40%
G-PL21	103.85	104.40	103.96	104.07	0.28%
G-PL22	104.29	104.27	104.42	104.33	0.08%
G-PP1	100.70	100.82	101.11	100.88	0.21%
G-PP2	102.10	102.00	102.15	102.08	0.07%
G-PP3	102.94	102.53	102.95	102.81	0.23%
G-PP4	100.92	101.14	100.97	101.01	0.11%
G-PP5	101.09	101.42	102.22	101.58	0.57%
G-PP6	102.60	102.70	103.31	102.87	0.37%
G-PP7	101.72	101.72	102.09	101.84	0.21%
G-PP8	101.03	101.98	101.05	101.35	0.54%
G-PP9	102.30	102.80	103.16	102.75	0.42%
G-PP10	101.91	101.91	101.95	101.92	0.02%
G-PP11	101.07	101.08	101.14	101.10	0.04%
G-PP12	104.31	104.54	104.42	104.42	0.11%
G-PP13	102.75	102.83	103.85	103.14	0.59%
G-PP14	104.11	103.86	103.79	103.92	0.16%
G-PP15	103.60	103.90	103.58	103.69	0.17%
G-PP16	104.15	103.85	103.75	103.92	0.20%
G-PP17	103.12	103.58	103.76	103.49	0.32%
G-PP18	104.24	104.30	104.19	104.24	0.05%
G-PP19	103.99	103.96	103.81	103.92	0.09%
G-PP20	103.85	103.77	103.82	103.81	0.04%
G-PP21	103.75	103.79	103.89	103.81	0.07%
G-PP22	104.20	104.63	104.25	104.36	0.23%

Table B5: Fibreboard specimen ultimate load (N)

Specimen	Ultimate Load
F1	235.66
F2	229.4
F3	223.23
F4	215.1
F5	225.26
F6	211.18
F7	219.16
F8	207.04
F9	206.96
F10	227.67
F11	233.62
F12	204.93
F13	220.82
F14	218.03
F15	243.49
F16	220.82
FDA-1	235.66
FDA-2	222.7
FDA-3	216.6
FDA-4	222.4
FDB-1	175.63
FDB-2	190.02
FDB-3	208.09
FDB-4	207.11

Table B6: Gypsum board specimen ultimate load (N)

Specimen	Ultimate Load	Specimen	Ultimate Load
G-PL1	284.19	**G-PP1**	82.21
G-PL2	232.92	**G-PP2**	90.11
G-PL3	301.65	**G-PP3**	91.77
G-PL4	294.5	**G-PP4**	87.7
G-PL5	278.35	**G-PP5**	84.09
G-PL6	280.35	**G-PP6**	88.61
G-PL7	282.91	**G-PP7**	98.84
G-PL8	285.77	**G-PP8**	97.94
G-PL9	285.39	**G-PP9**	97.49
G-PL10	297.44	**G-PP10**	93.35
G-PL11	310.09	**G-PP11**	93.12
G-PL12	301.71	**G-PP12**	113.35
G-PL13	202.14	**G-PP13**	99.56
G-PL14	323.28	**G-PP14**	101.75
G-PL15	300.5	**G-PP15**	97.15
G-PL16	306.68	**G-PP16**	91.13
G-PL17	308.18	**G-PP17**	105.74
G-PL18	295.53	**G-PP18**	85.1
G-PL19	293.72	**G-PP19**	106.87
G-PL20	291.54	**G-PP20**	107.62
G-PL21	291.46	**G-PP21**	94.14
G-PL22	278.58	**G-PP22**	79.68

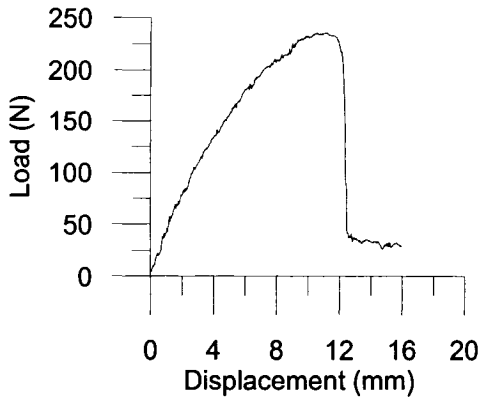

Figure B1: FB1

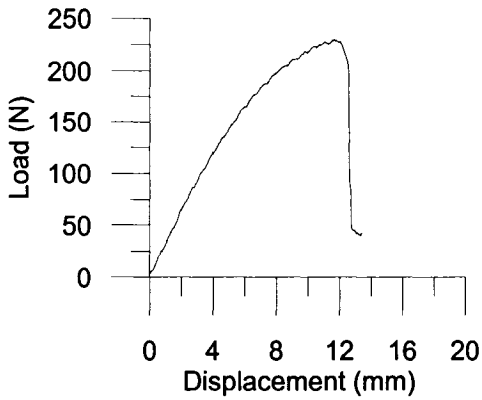

Figure B2: FB2

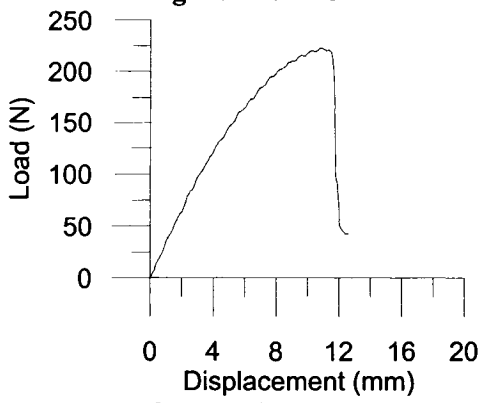

Figure B3: FB3

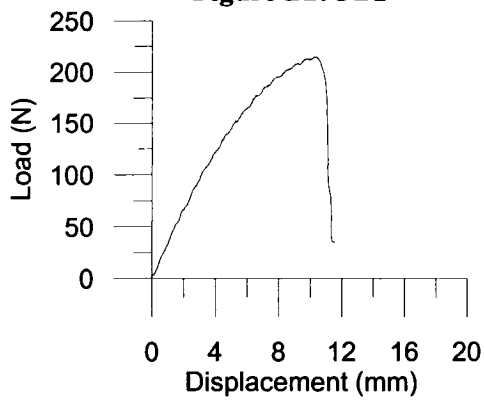

Figure B4: FB4

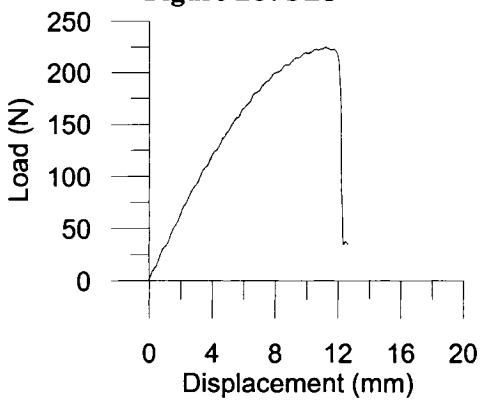

Figure B5: FB5

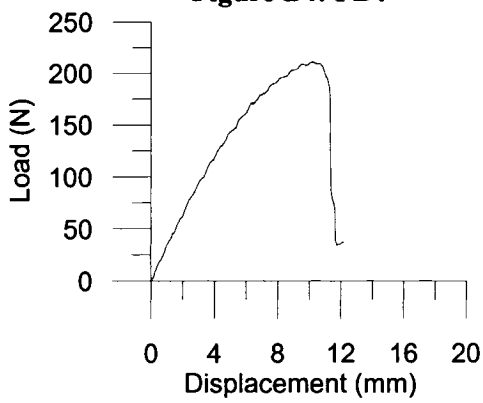

Figure B6: FB6

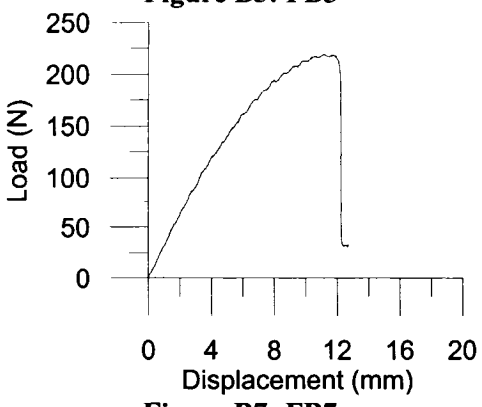

Figure B7: FB7

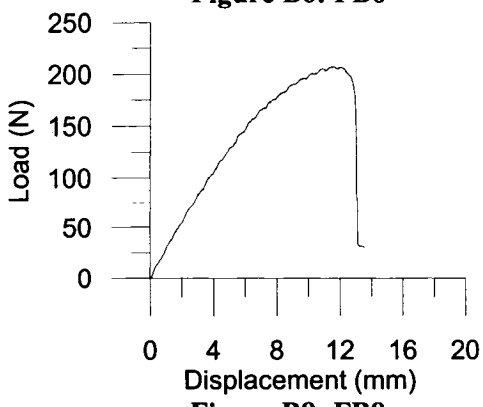

Figure B8: FB8

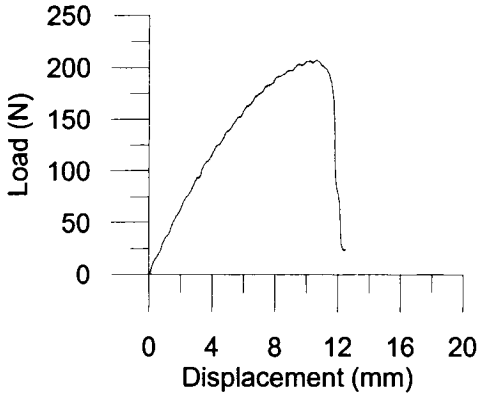

Figure B9: FB9

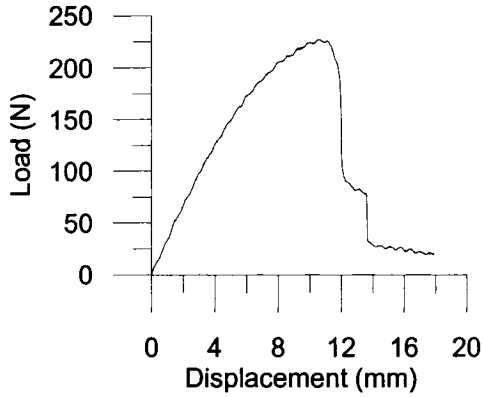

Figure B10: FB10

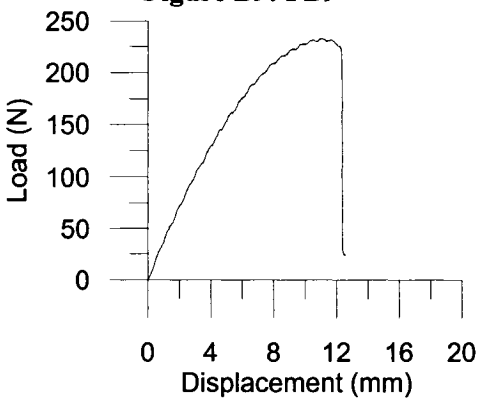

Figure B11: FB11

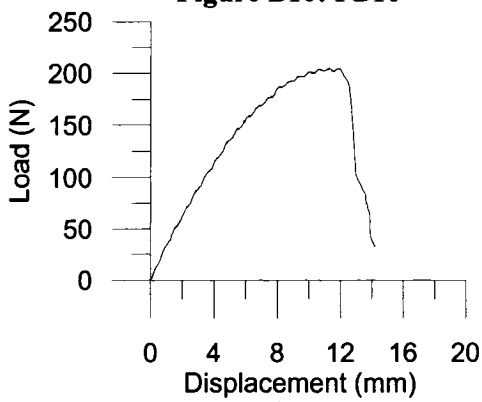

Figure B12: FB12

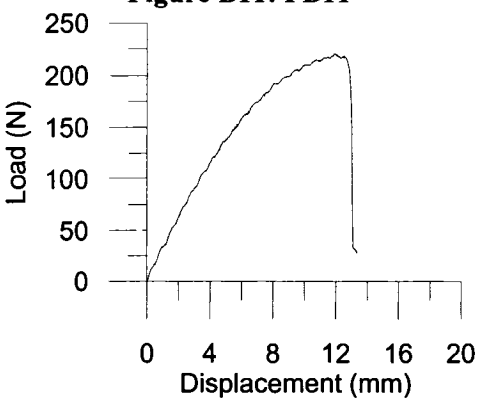

Figure B13: FB13

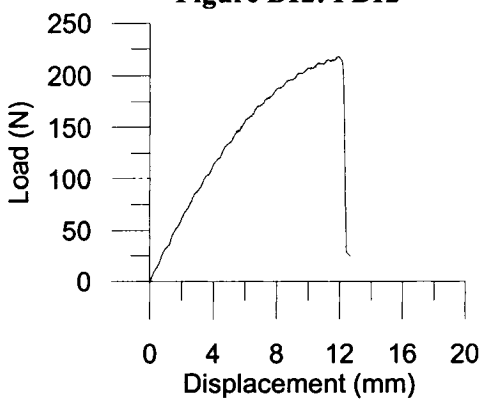

Figure B14: FB14

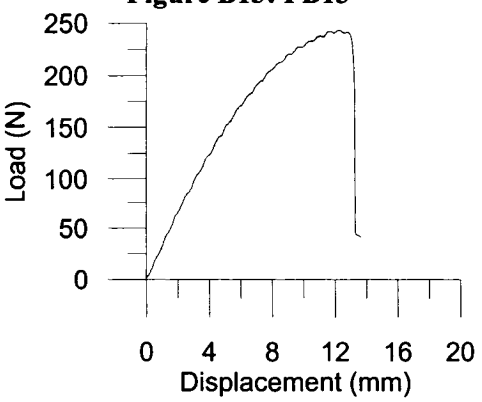

Figure B15: FB15

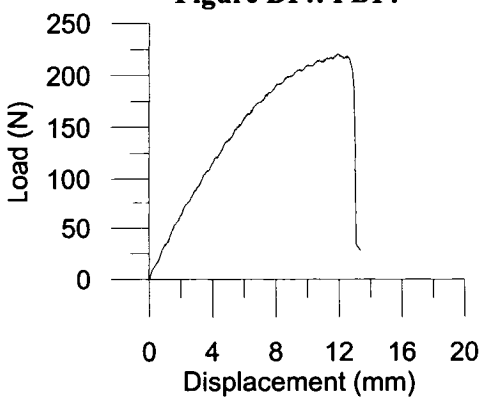

Figure B16: FB16

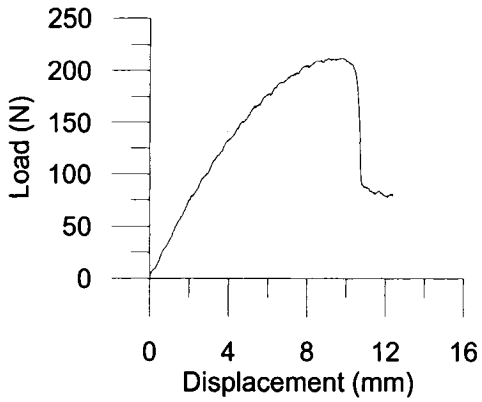

Figure B17: FDA-1

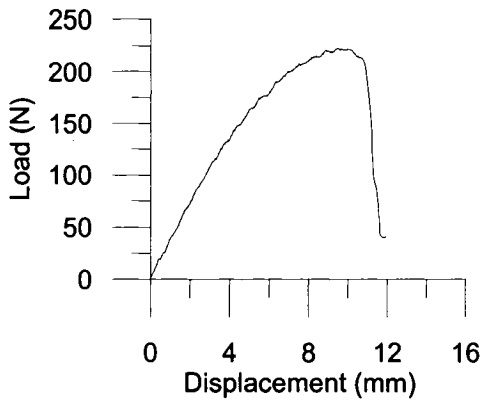

Figure B18: FDA-2

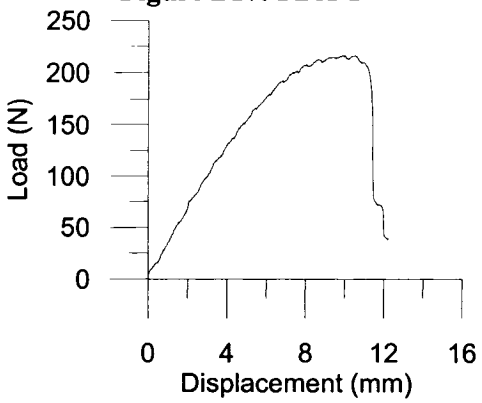

Figure B19: FDA-3

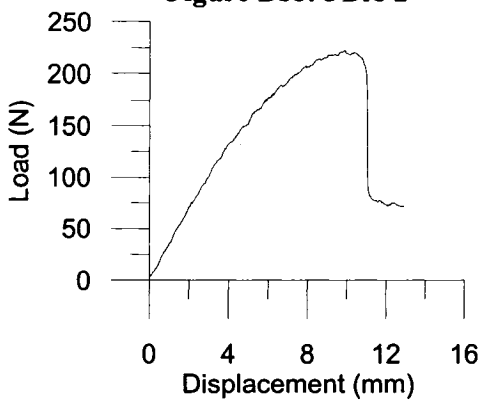

Figure B20: FDA-4

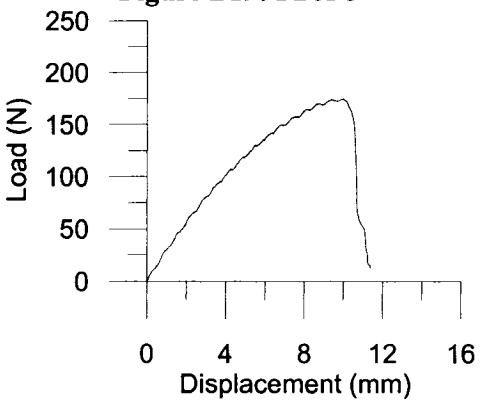

Figure B21: FDB-1

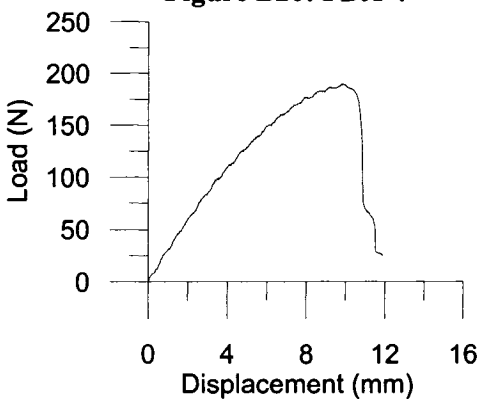

Figure B22: FDB-2

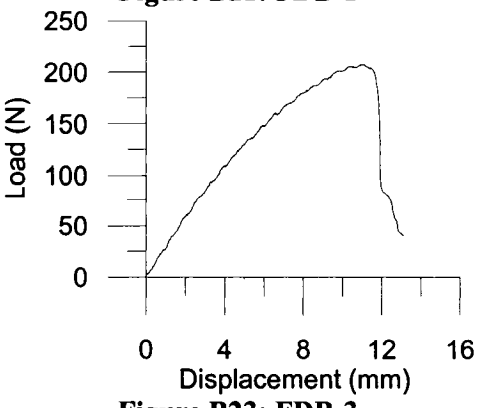

Figure B23: FDB-3

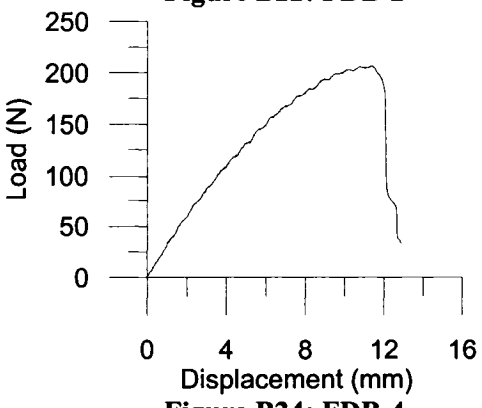

Figure B24: FDB-4

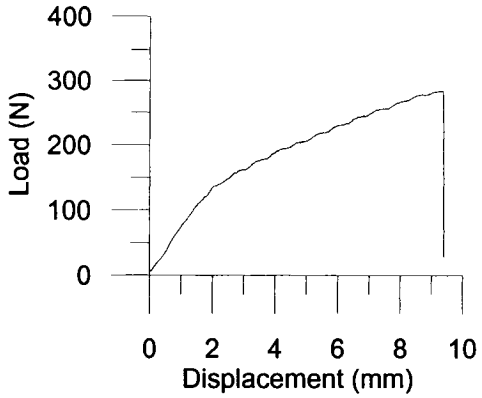

Figure B25: G-PL1

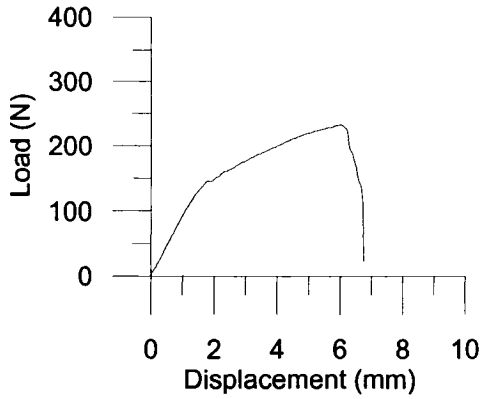

Figure B26: G-PL2

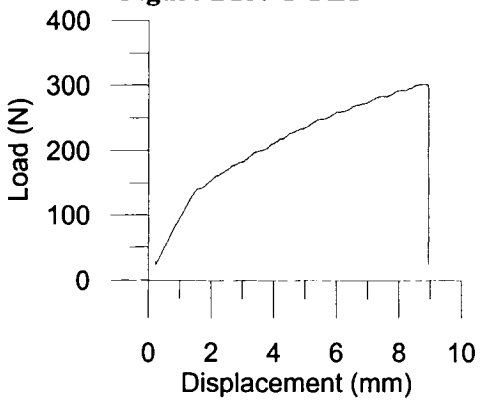

Figure B27: G-PL3

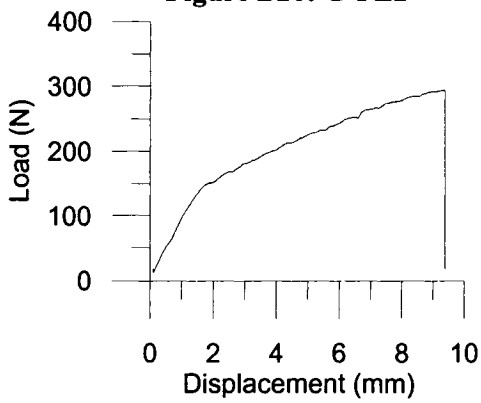

Figure B28: G-PL4

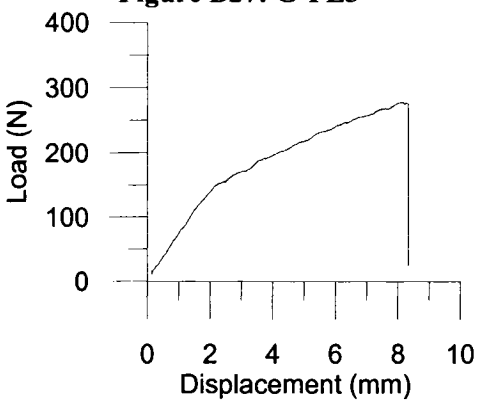

Figure B29: G-PL5

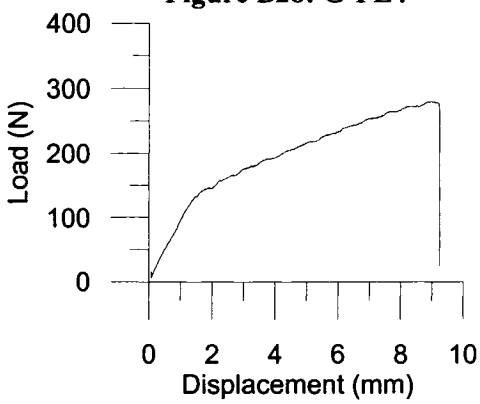

Figure B30: G-PL6

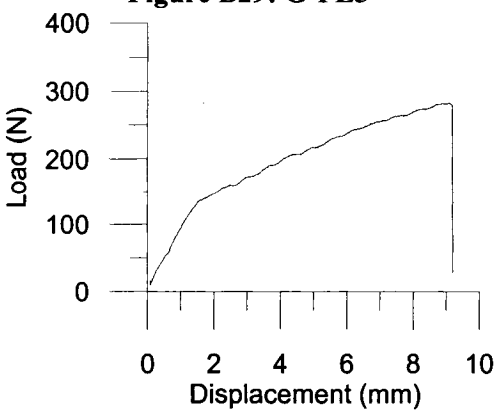

Figure B31: G-PL7

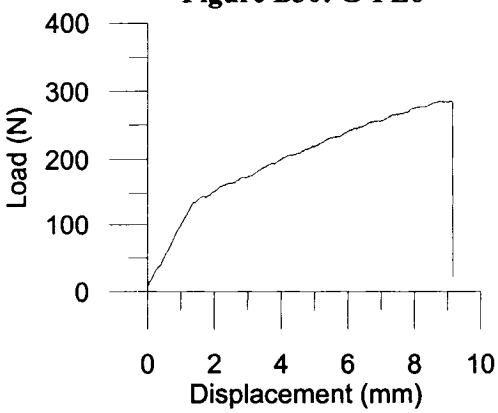

Figure B32: G-PL8

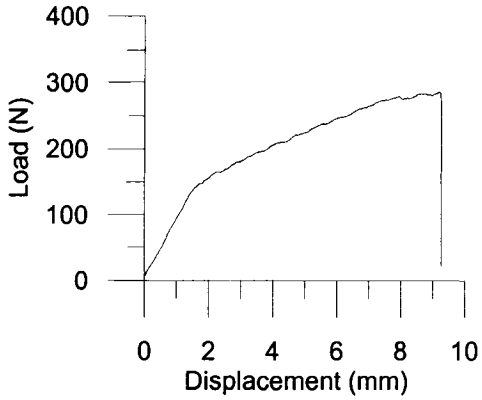

Figure B33: G-PL9

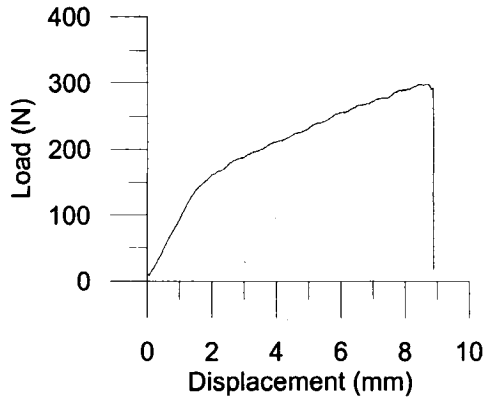

Figure B34: G-PL10

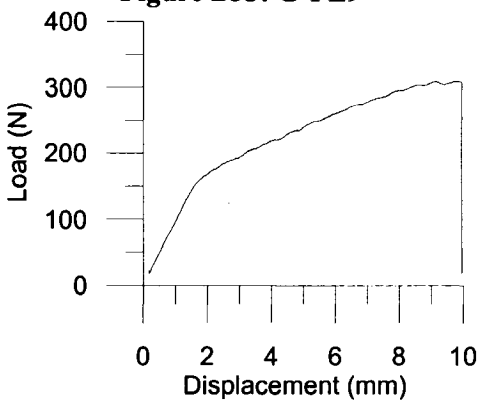

Figure B35: G-PL11

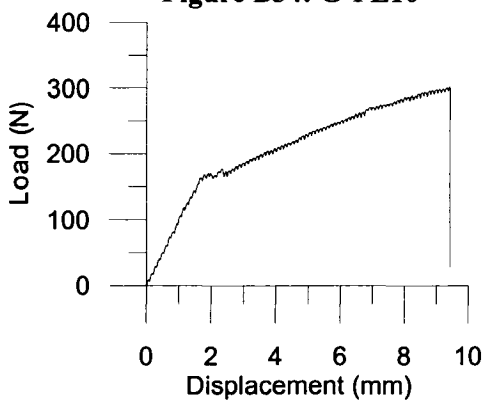

Figure B36: G-PL12

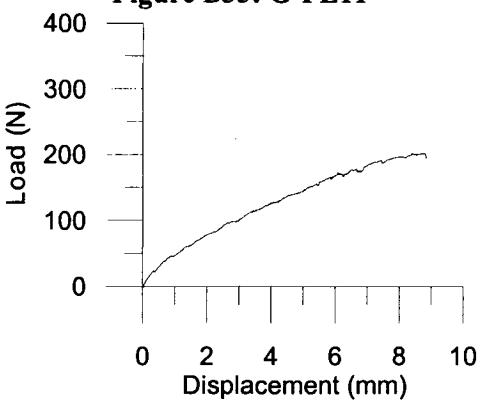

Figure B37: G-PL13

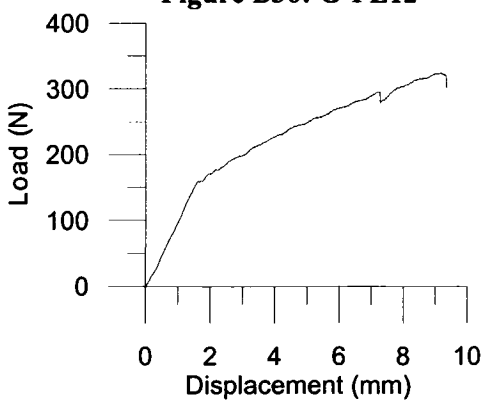

Figure B38: G-PL14

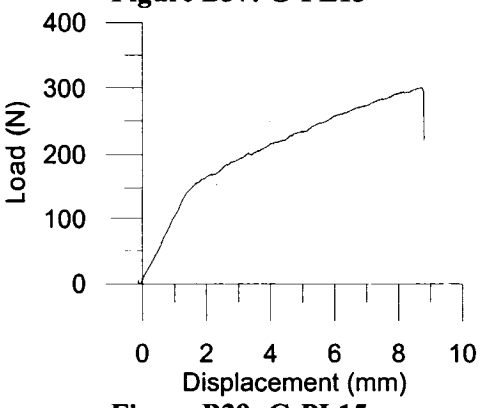

Figure B39: G-PL15

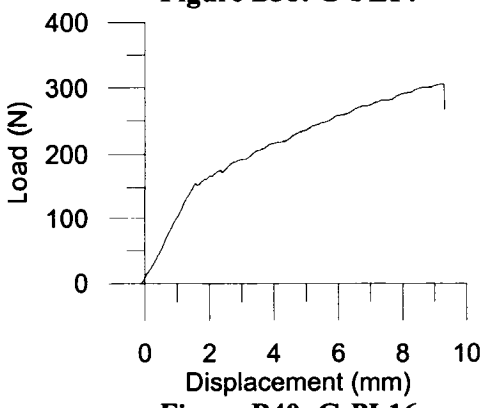

Figure B40: G-PL16

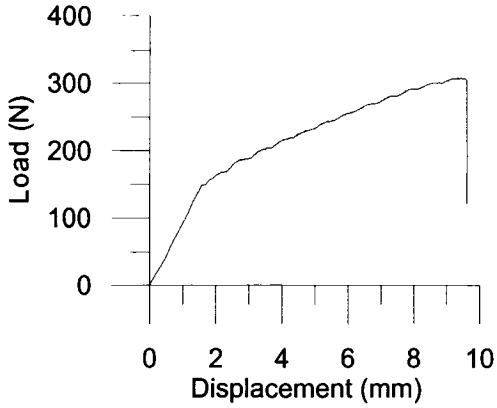

Figure B41: G-PL17

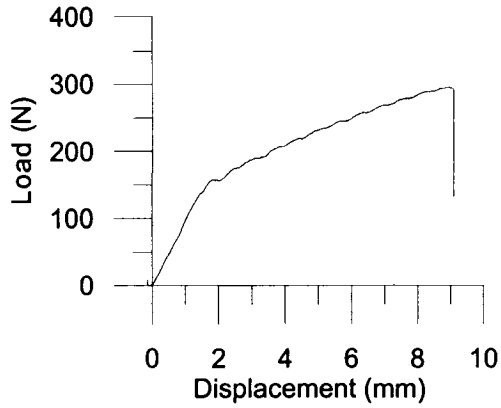

Figure B42: G-PL18

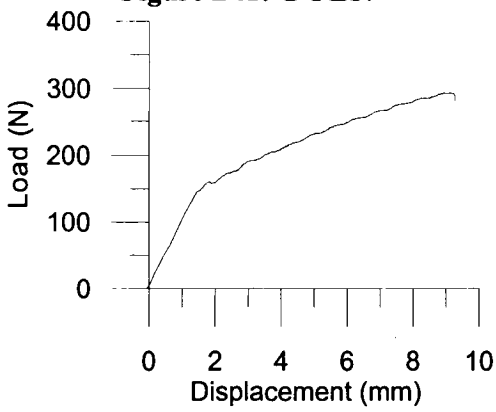

Figure B43: G-PL19

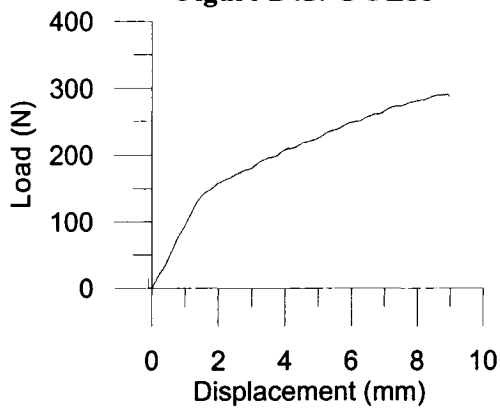

Figure B44: G-PL20

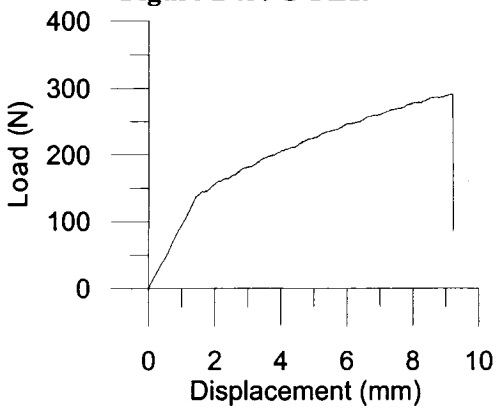

Figure B45: G-PL21

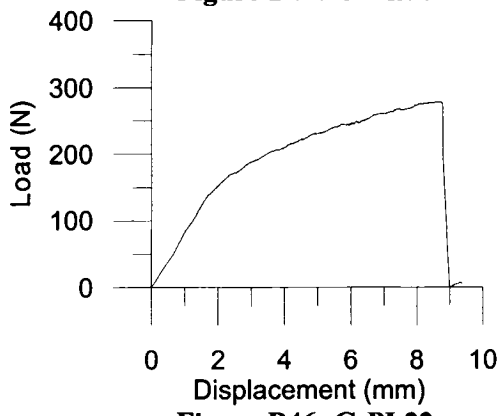

Figure B46: G-PL22

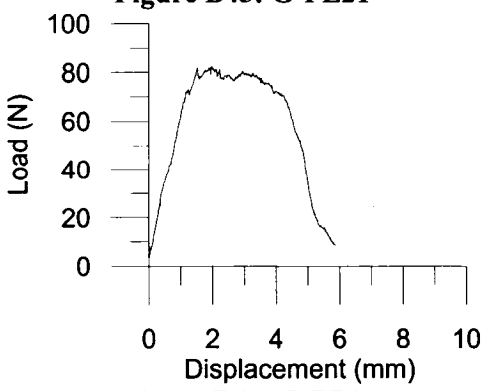

Figure B47: G-PP1

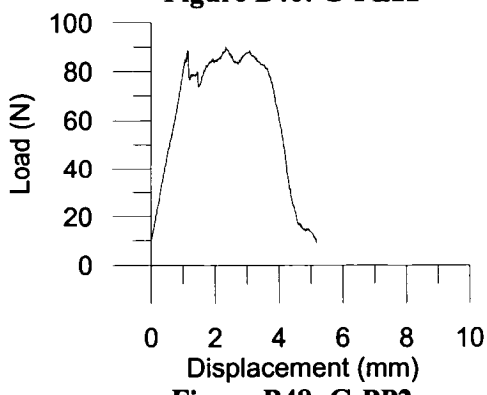

Figure B48: G-PP2

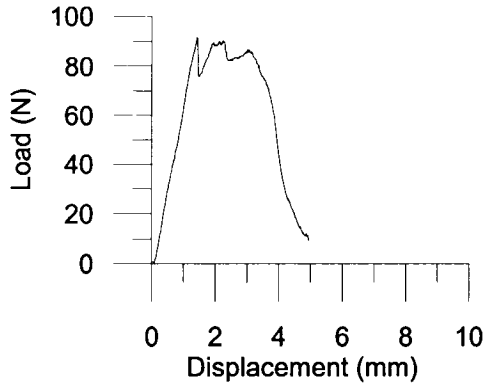

Figure B49: G-PP3

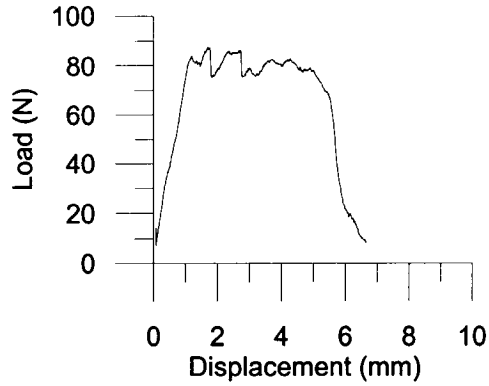

Figure B50: G-PP4

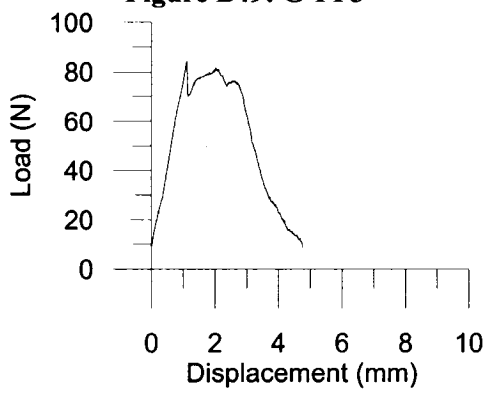

Figure B51: G-PP5

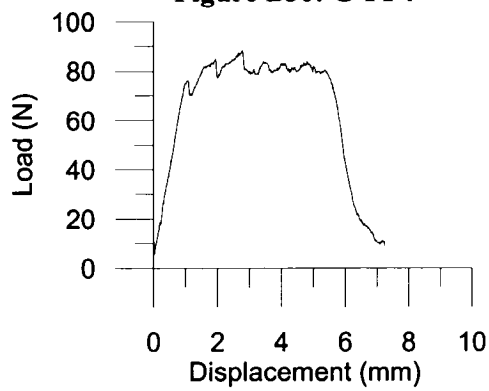

Figure B52: G-PP6

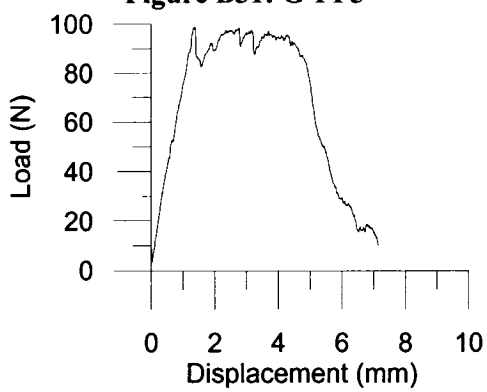

Figure B53: G-PP7

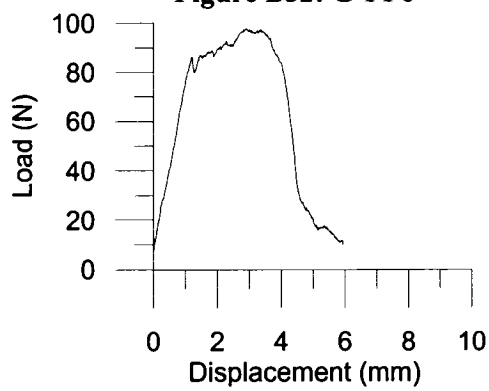

Figure B54: G-PP8

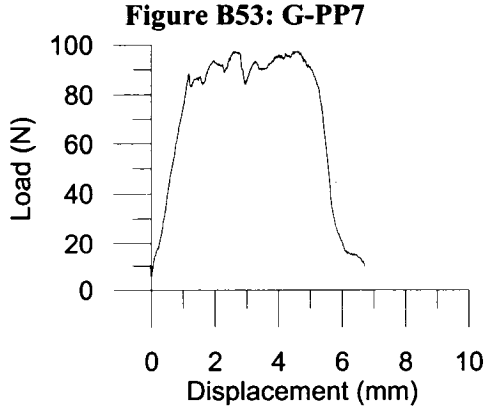

Figure B55: G-PP9

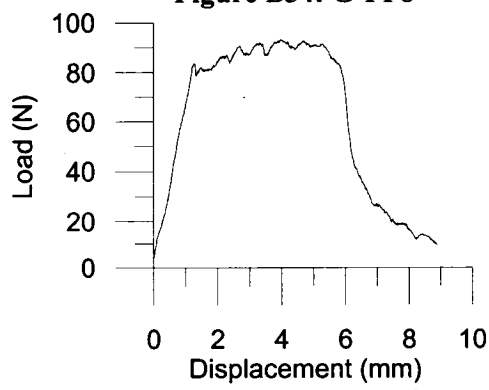

Figure B56: G-PP10

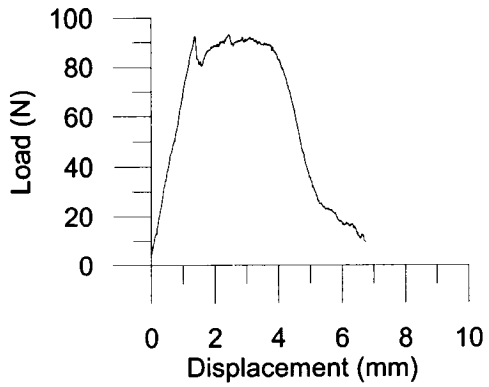

Figure B57: G-PP11

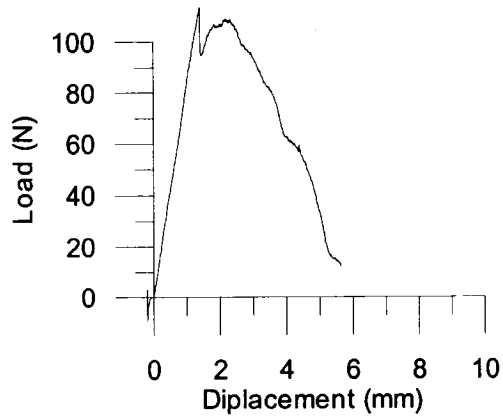

Figure B58: G-PP12

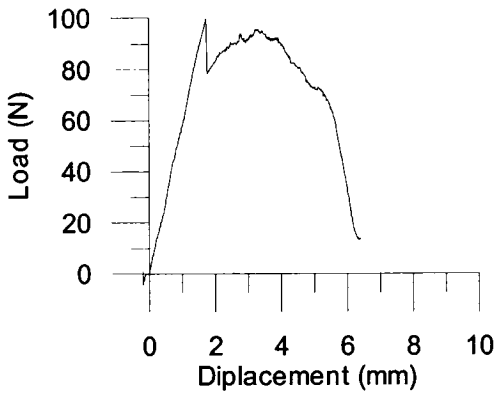

Figure B59: G-PP13

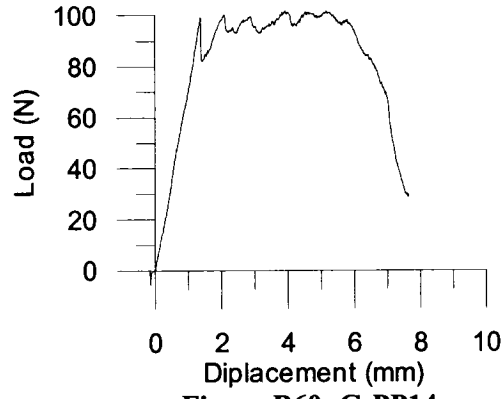

Figure B60: G-PP14

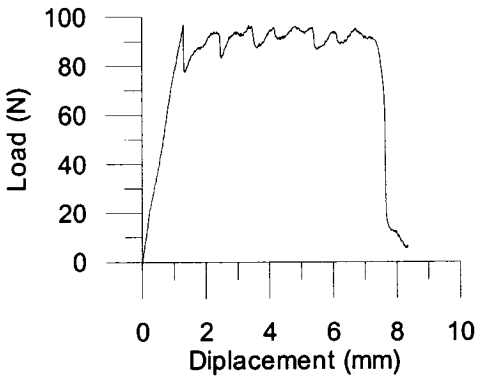

Figure B61: G-PP15

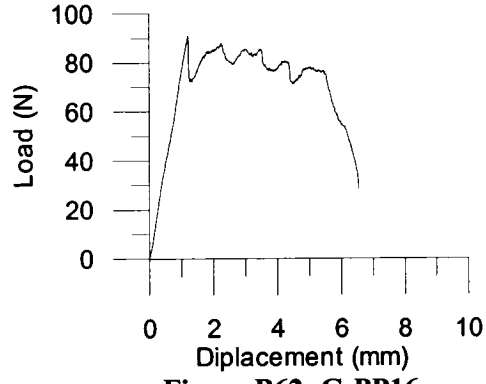

Figure B62: G-PP16

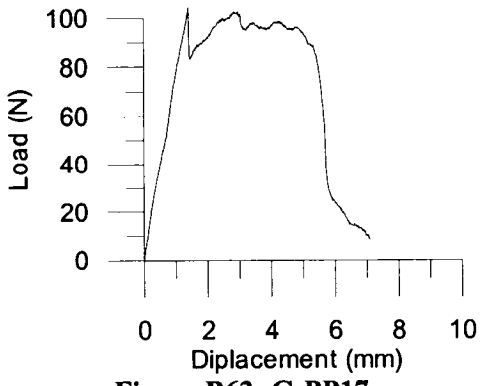

Figure B63: G-PP17

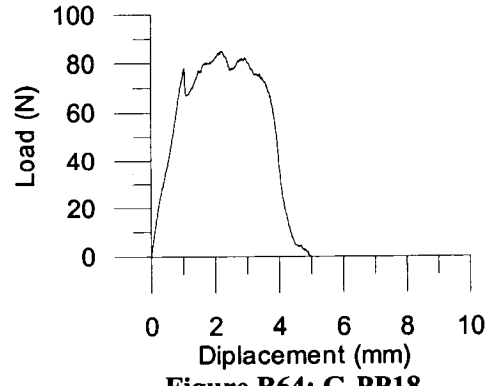

Figure B64: G-PP18

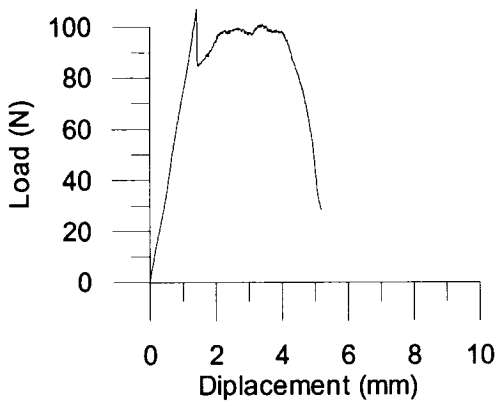

Figure B65: G-PP19

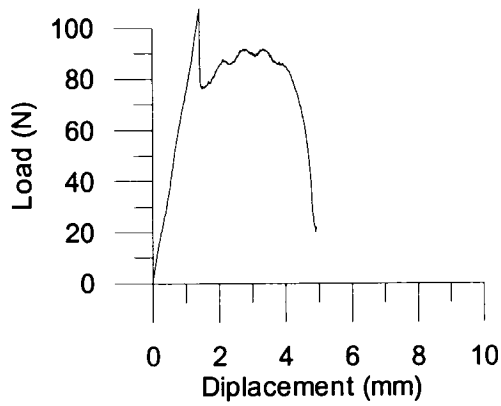

Figure B66: G-PP20

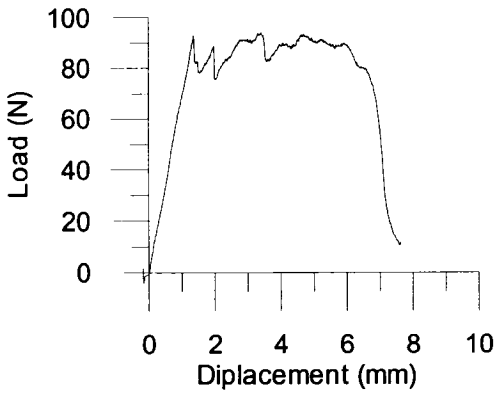

Figure B67: G-PP21

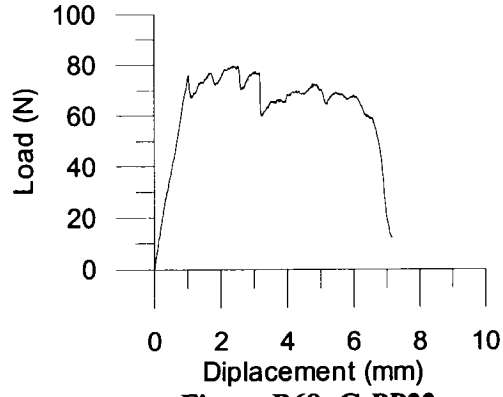

Figure B68: G-PP22

APPENDIX C
FOUR-SIDED SHEAR TEST DATA

The results of the four-sided shear tests are presented in Chapter 3, Section 3.4 and in this Appendix. The load versus elongation curve and a table summarizing the experimental data acquired for each specimen in presented in this Appendix.

Table C1: FB1 data

FB1					
Dimensions measured before testing				Stiffness	
Thickness at corners (mm)					
T1	T2	T3	T4	Slope 1	Slope 2
N/A	N/A	N/A	N/A	18938	N/A
Average Thickness (mm)				Average Slope	
23.52				18938	
Length of Sides (in)					
L1	L2	L3	L4	Stiffness	
24.25	24.31	24.25	24.25	234	MPa
Average Length (mm)		Gauge Length (mm)			
616.35		508			

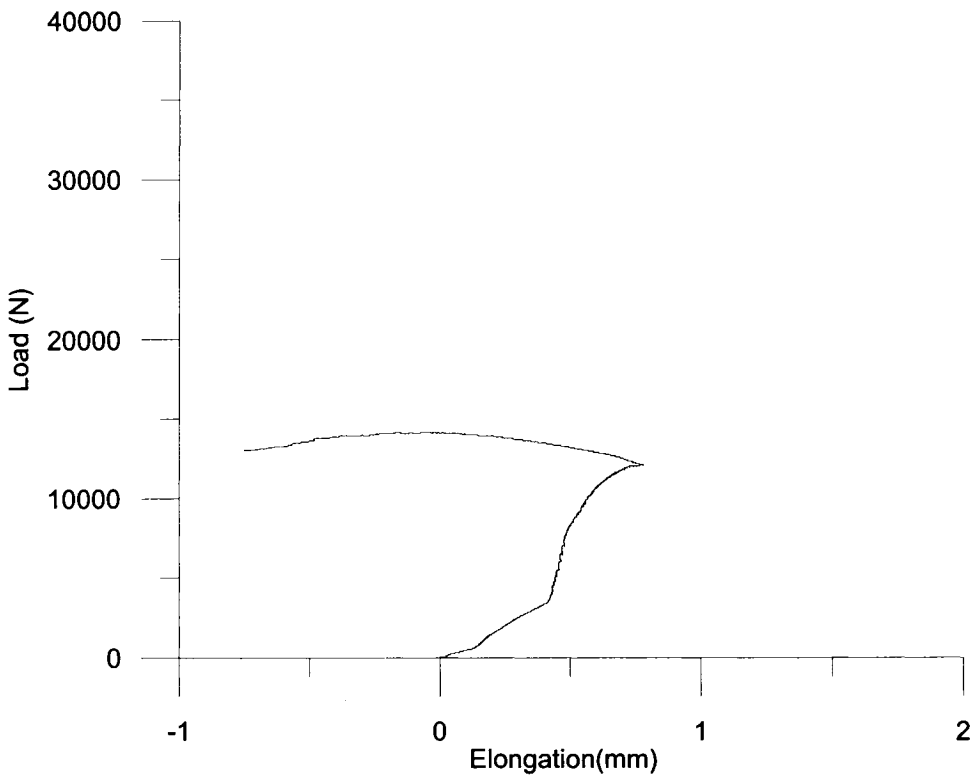

Figure C1: FB1 load vs. elongation

Table C2: FB2 data

FB2				
Dimensions measured before testing				Stiffness
Thickness at corners (mm)				
T1	T2	T3	T4	Slope 1 Slope 2
N/A	N/A	N/A	N/A	19334 N/A
Average Thickness (mm)				Average Slope
23.52				19334
Length of Sides (in)				Stiffness
L1	L2	L3	L4	
24.13	24.13	24.19	N/A	241 MPa
Average Length (mm)		Gauge Length (mm)		
613.30		508		

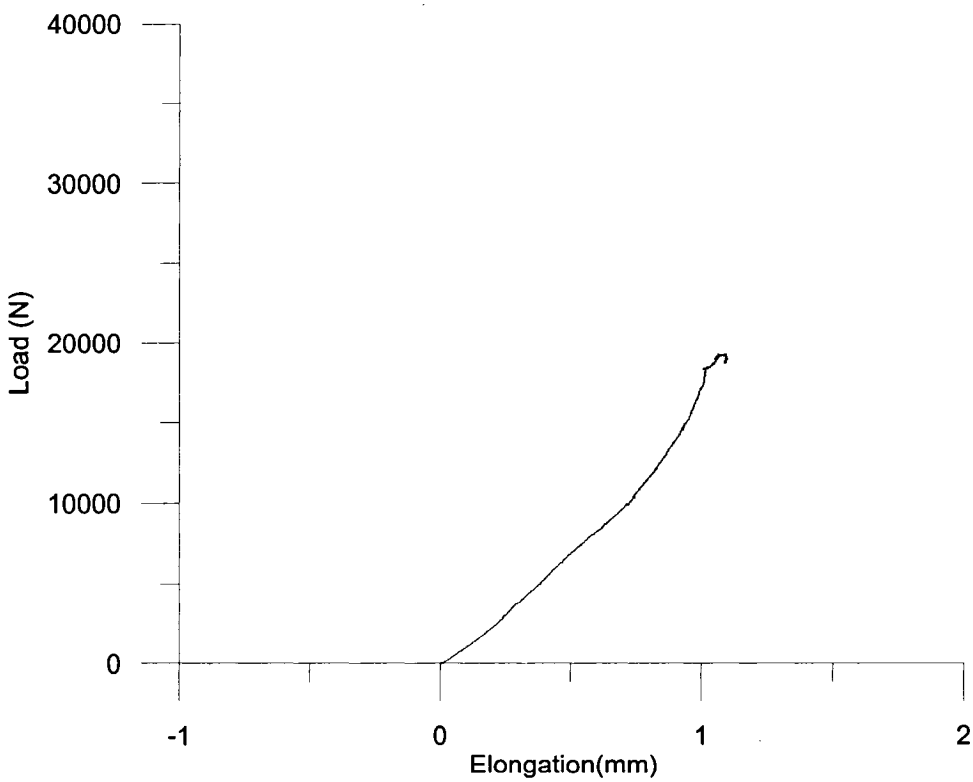

Figure C2: FB2 load vs. elongation

Table C3: FB3 data

FB3				
Dimensions measured before testing				Stiffness
Thickness at corners (mm)				
T1	T2	T3	T4	Slope 1 Slope 2
N/A	N/A	N/A	N/A	21209 N/A
Average Thickness (mm)				Average Slope
23.52				21209
Length of Sides (in)				Stiffness
L1	L2	L3	L4	
24.25	24.31	24.31	24.25	263 MPa
Average Length (mm)		Gauge Length (mm)		
616.74		508		

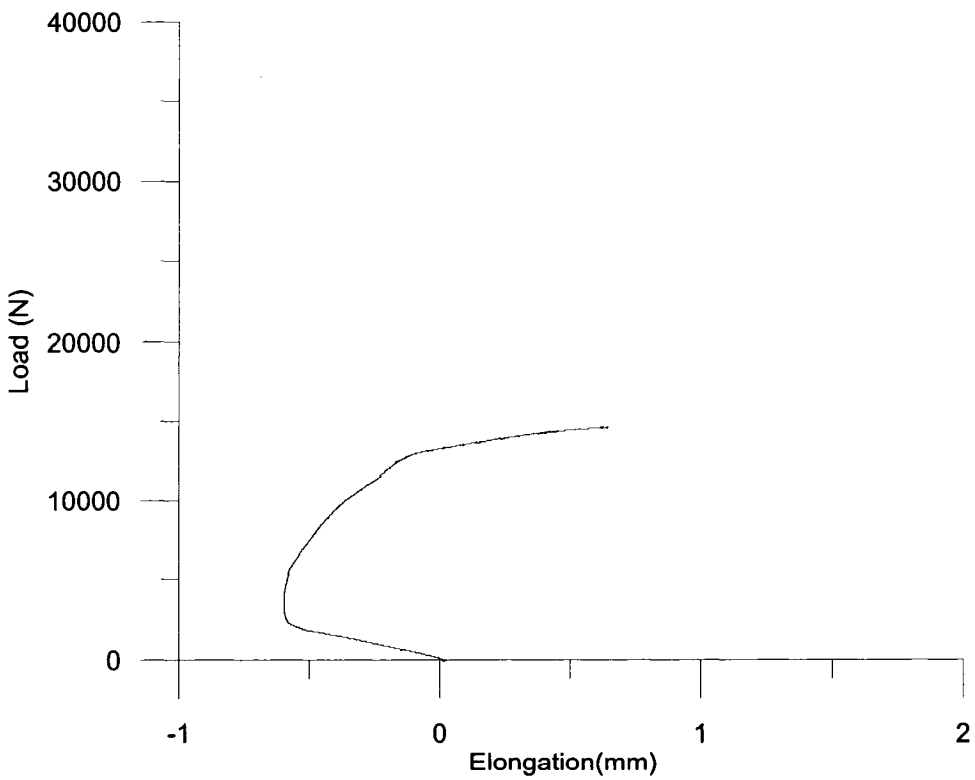

Figure C3: FB3 load vs. elongation

Table C4: FB4+FB5 data

FB4+FB5				
Dimensions measured before testing				Stiffness
Thickness at corners (mm)				
T1	T2	T3	T4	Slope 1 Slope 2
N/A	N/A	N/A	N/A	-21209 147000
Average Thickness (mm)				Average Slope
47.04				62896
Length of Sides (in)				
L1	L2	L3	L4	Stiffness
24.31	24.38	24.50	24.31	388 MPa
Average Length (mm)		Gauge Length (mm)		
619.13		508		

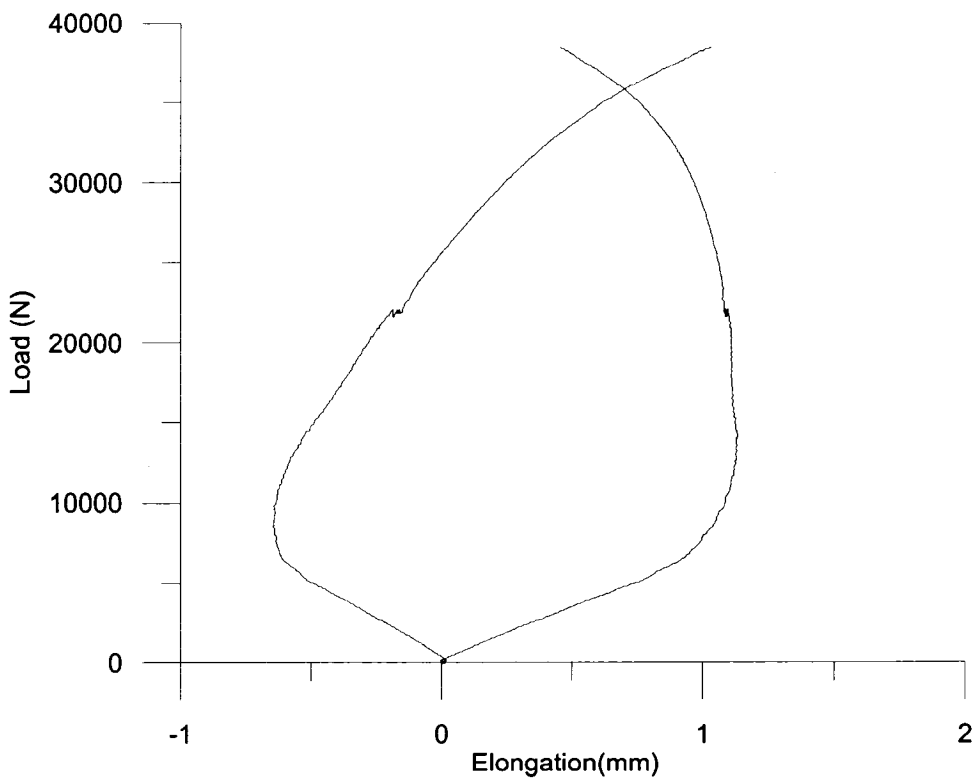

Figure C4: FB4+FB5 load vs. elongation

Table C5: GYP-1 data

GYP-1					
Dimensions measured before testing				Stiffness	
Thickness at corners (mm)					
T1	T2	T3	T4	Slope 1	Slope 2
N/A	N/A	N/A	N/A	13723	N/A
Average Thickness (mm)				Average Slope	
15.45				13723	
Length of Sides (in)					
L1	L2	L3	L4	Stiffness	
24.25	24.31	24.31	24.25	259	MPa
Average Length (mm)		Gauge Length (mm)			
616.74		508			

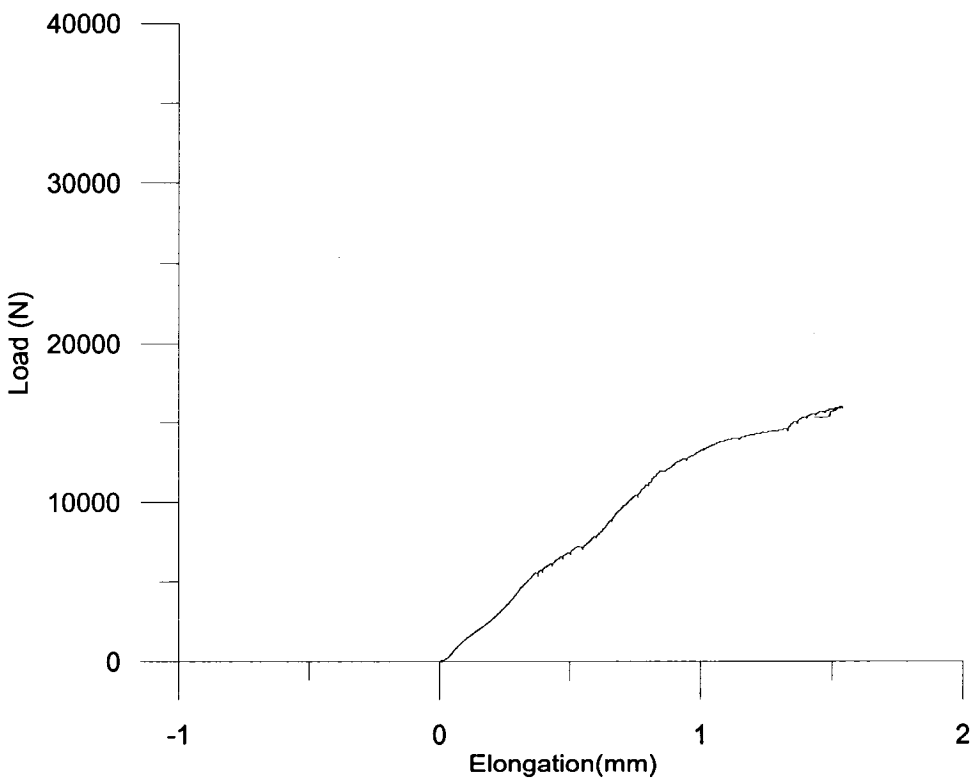

Figure C5: GYP-1 load vs. elongation

Table C6: FB-2 STIFF data

FB-2 STIFF				
Dimensions measured before testing				Stiffness
Thickness at corners (mm)				
T1	T2	T3	T4	Slope 1 Slope 2
23.26	23.06	23	22.88	19693 25743
Average Thickness (mm)				Average Slope
23.05				22718
Length of Sides (in)				
L1	L2	L3	L4	Stiffness
24.25	24.3125	24.25	24.25	287 MPa
Average Length (mm)		Gauge Length (mm)		
616.34		508		

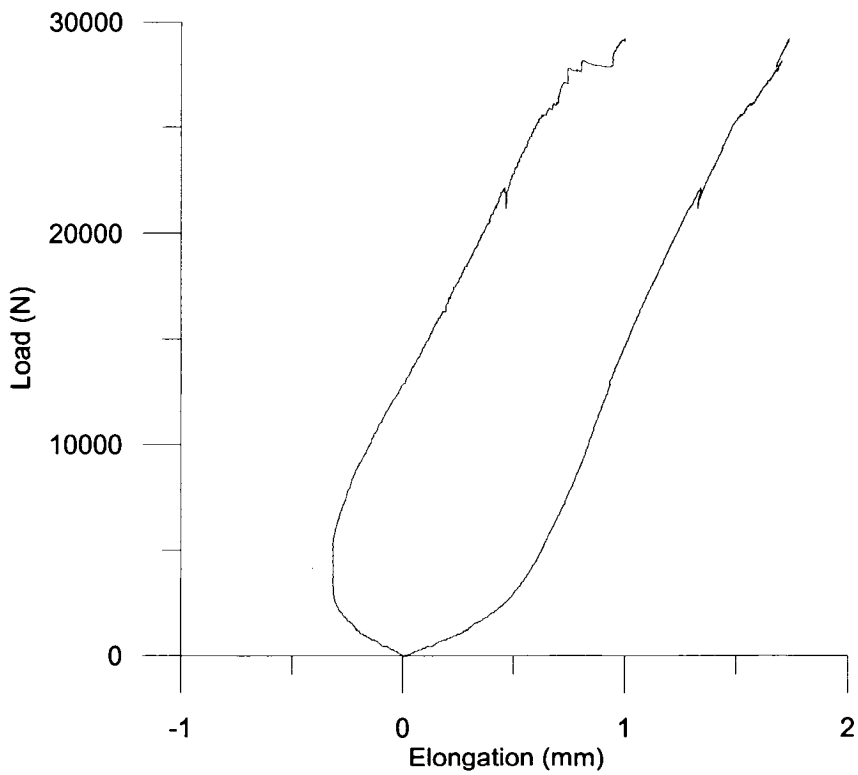

Figure C6: FB-2 STIFF load vs. elongation

Table C7: FB-3 STIFF data

FB-3 STIFF				
Dimensions measured before testing				Stiffness
Thickness at corners (mm)				
T1	T2	T3	T4	Slope 1 Slope 2
23.26	23.10	23.14	23.1	13869 17431
Average Thickness (mm)				Average Slope
23.15				15650
Length of Sides (in)				
L1	L2	L3	L4	Stiffness
24.13	24.13	24.19	N/A	198 MPa
Average Length (mm)		Gauge Length (mm)		
613.30		508		

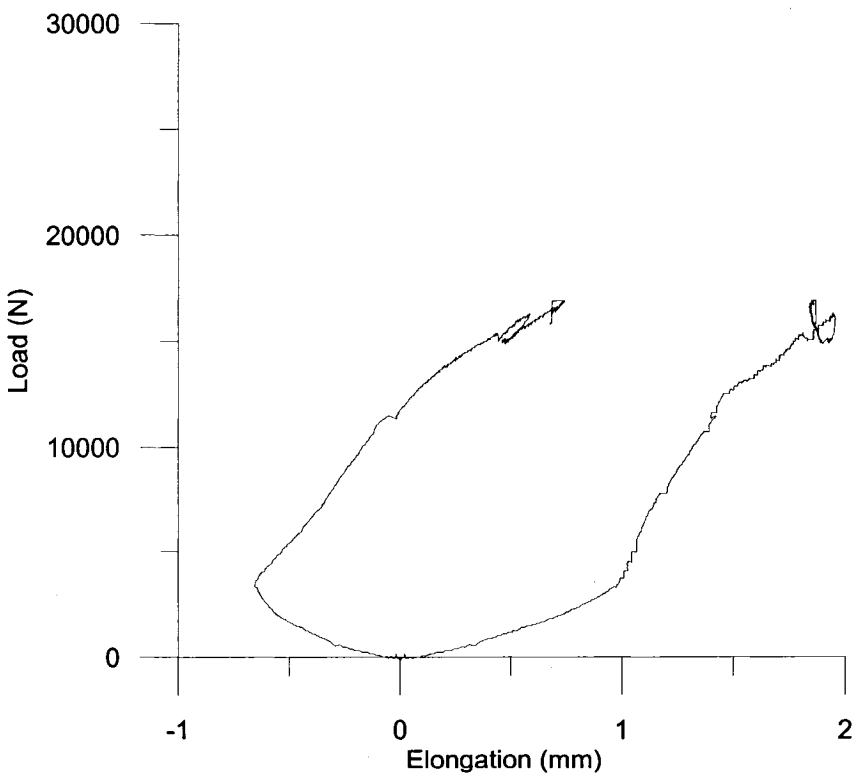

Figure C7: FB-3 STIFF load vs. elongation

Table C8: FB-4 STIFF data

FB-4 STIFF				
Dimensions measured before testing				Stiffness
Thickness at corners (mm)				
T1	T2	T3	T4	Slope 1 Slope 2
23.22	24.22	22.88	24.00	9039 33788
Average Thickness (mm)				Average Slope
23.58				21414
Length of Sides (in)				
L1	L2	L3	L4	Stiffness
24.25	24.31	24.31	24.25	264 MPa
Average Length (mm)		Gauge Length (mm)		
616.74		508		

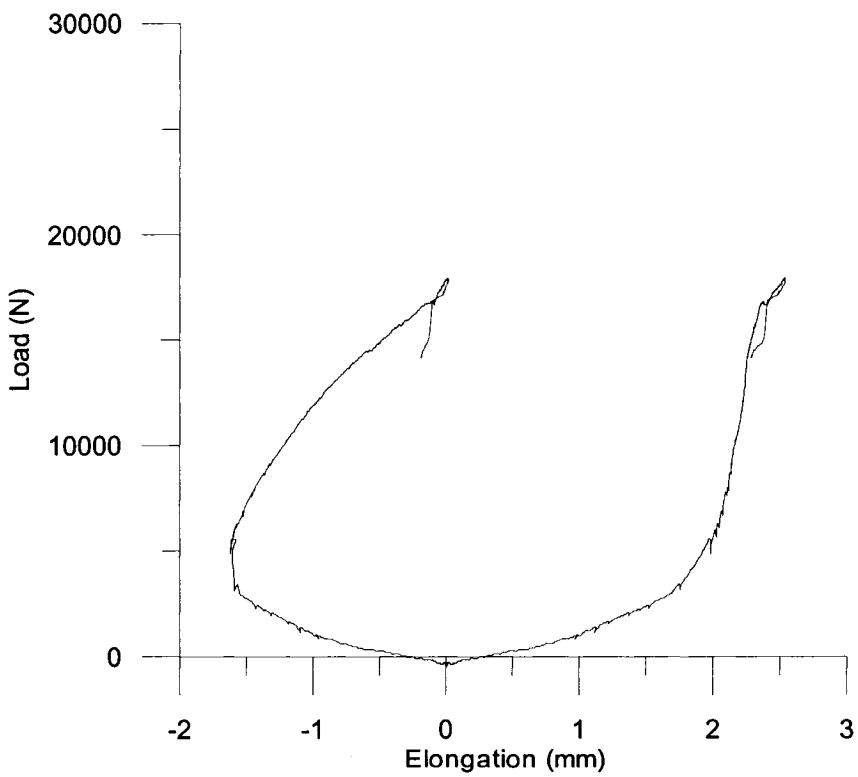

Figure C8: FB-4 STIFF load vs. elongation

Table C9: FB-5 STIFF data

FB-5 STIFF				
Dimensions measured before testing				Stiffness
Thickness at corners (mm)				
T1	T2	T3	T4	Slope 1 Slope 2
24.02	23.46	23.16	23.22	16413 14496
Average Thickness (mm)				Average Slope
23.47				15455
Length of Sides (in)				
L1	L2	L3	L4	Stiffness
24.31	24.38	24.50	24.31	191 MPa
Average Length (mm)		Gauge Length (mm)		
619.13		508		

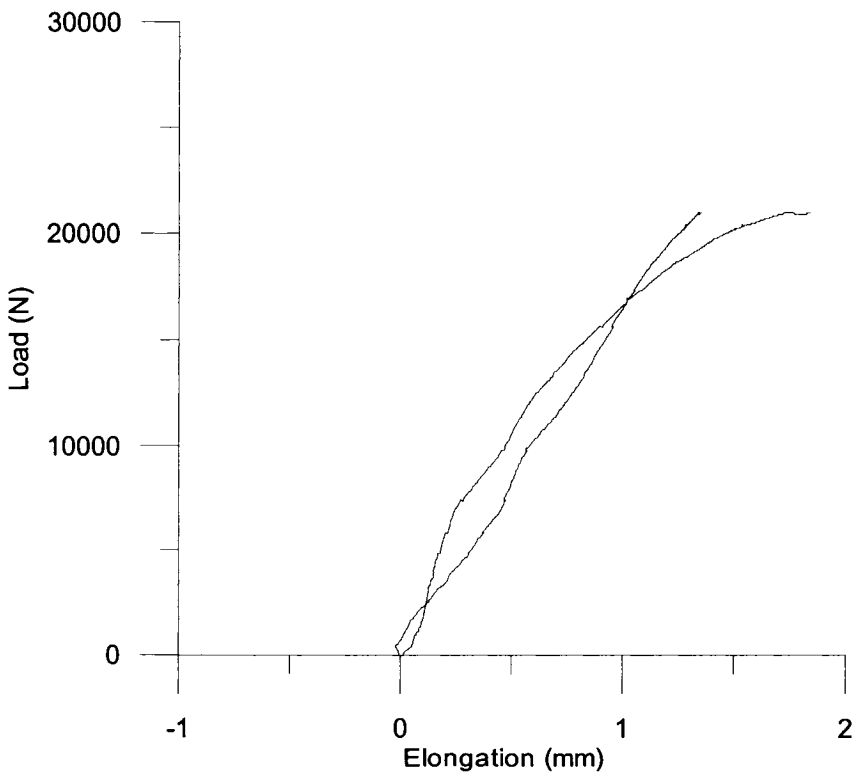

Figure C9: FB-5 STIFF load vs. elongation

Table C10: GYP-1 STIFF data

GYP-1 STIFF				
Dimensions measured before testing				Stiffness
Thickness at corners (mm)				
T1	T2	T3	T4	Slope 1 Slope 2
15.52	15.58	15.28	15.42	17456 12540
Average Thickness (mm)				Average Slope
15.45				14998
Length of Sides (in)				
L1	L2	L3	L4	Stiffness
24.50	24.50	24.38	N/A	281 MPa
Average Length (mm)		Gauge Length (mm)		
621.24		508		

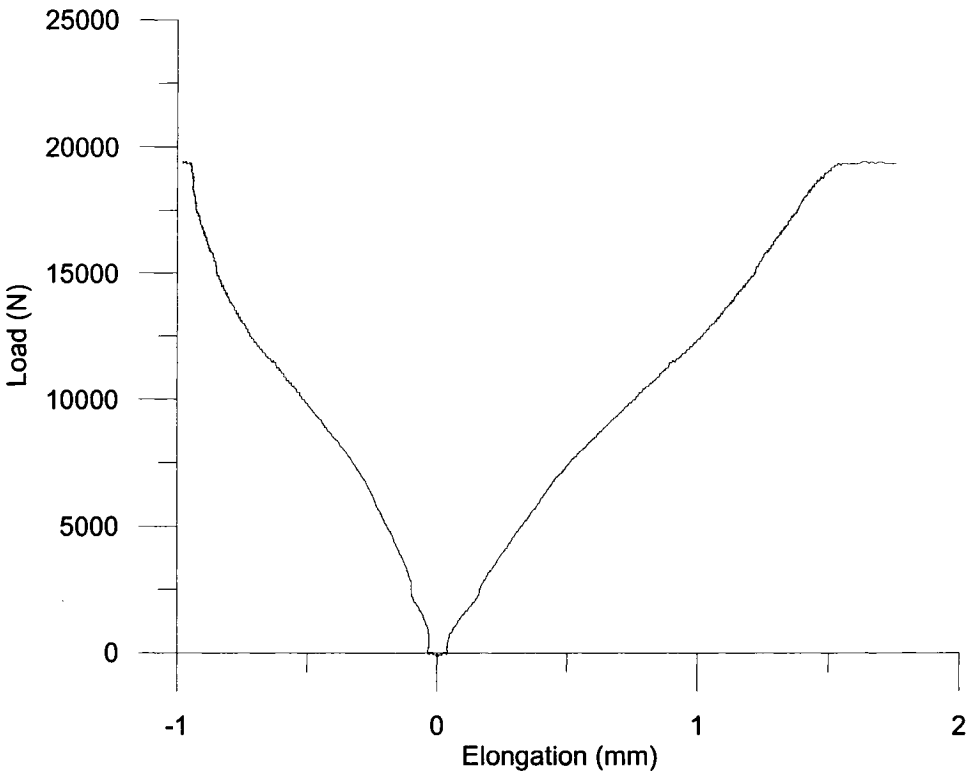

Figure C10: GYP-1 STIFF load vs. elongation

Table C11: GYP-2 STIFF data

GYP-2 STIFF				
Dimensions measured before testing				Stiffness
Thickness at corners (mm)				
T1	T2	T3	T4	Slope 1 Slope 2
15.28	15.70	15.50	15.72	60304 91898
Average Thickness (mm)				Average Slope
15.55				76101
Length of Sides (in)				Stiffness
L1	L2	L3	L4	
24.34	24.31	24.34	24.31	1423 MPa
Average Length (mm)		Gauge Length (mm)		
617.93		508		

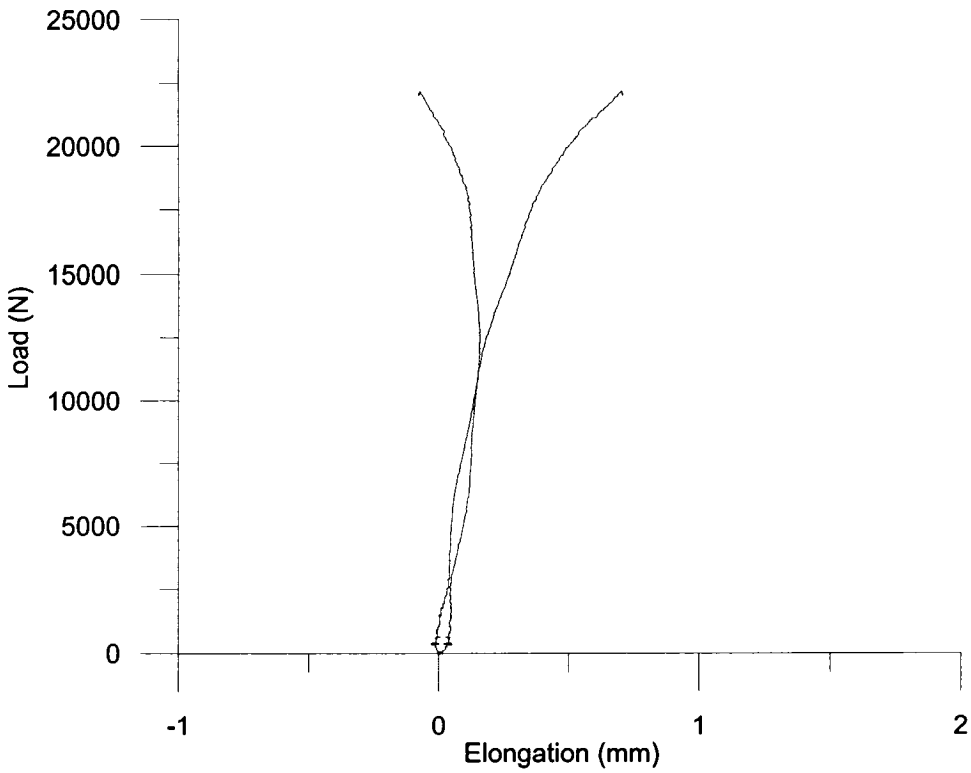

Figure C11: GYP-2 STIFF load vs. elongation

Table C12: GYP-3 STIFF data

GYP-3 STIFF					
Dimensions measured before testing				Stiffness	
Thickness at corners (mm)					
T1	T2	T3	T4	Slope 1	Slope 2
15.40	15.56	15.46	15.50	16335	8081
Average Thickness (mm)				Average Slope	
15.48				12208	
Length of Sides (in)					
L1	L2	L3	L4	Stiffness	
24.38	24.38	24.38	24.38	229	MPa
Average Length (mm)		Gauge Length (mm)			
619.13		508			

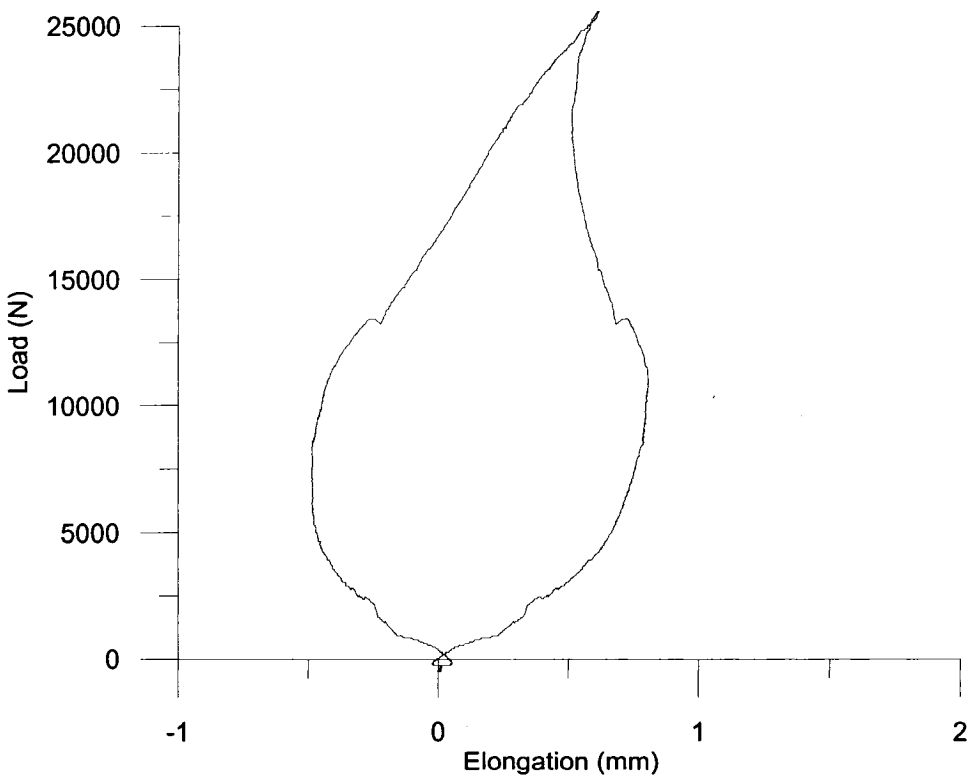

Figure C12: GYP-3 STIFF load vs. elongation

Table C13: GYP-4 STIFF data

GYP-4 STIFF				
Dimensions measured before testing				Stiffness
Thickness at corners (mm)				
T1	T2	T3	T4	Slope 1 Slope 2
15.38	15.74	15.34	15.32	71973 34008
Average Thickness (mm)				Average Slope
15.45				52990.5
Length of Sides (in)				
L1	L2	L3	L4	Stiffness
24.25	24.31	24.31	24.50	997 MPa
Average Length (mm)		Gauge Length (mm)		
618.33		508		

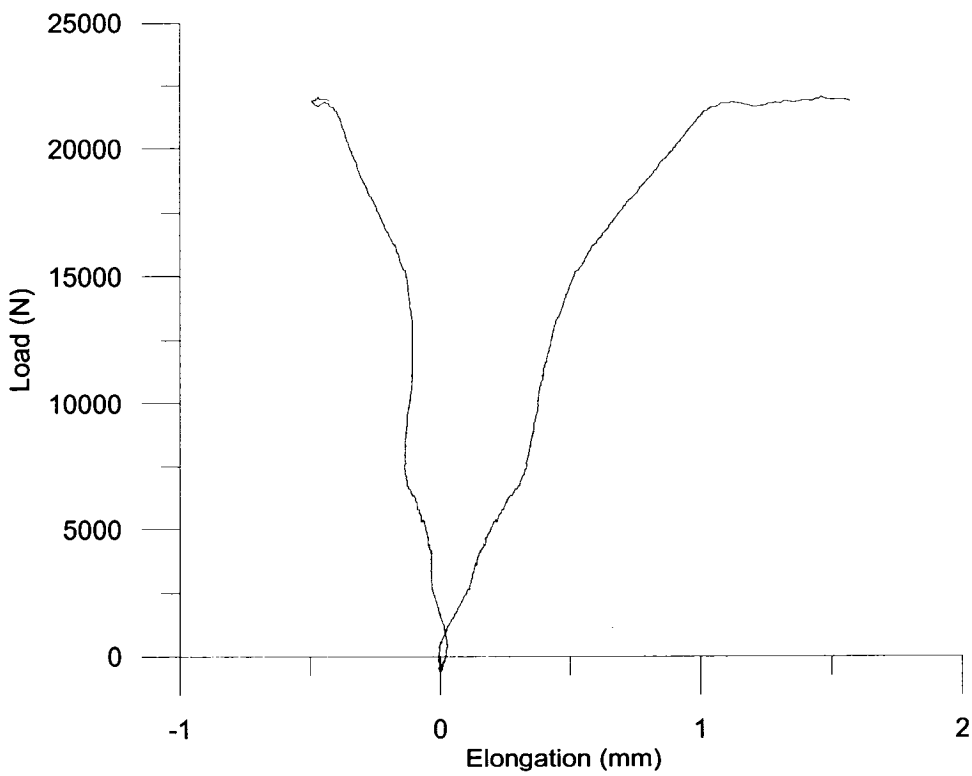

Figure C13: GYP-4 STIFF load vs. elongation

Table C14: GYP-5 STIFF data

GYP-5 STIFF				
Dimensions measured before testing				Stiffness
Thickness at corners (mm)				
T1	T2	T3	T4	Slope 1 Slope 2
15.60	15.60	15.50	15.12	79344 64660
Average Thickness (mm) 15.46				Average Slope 72002
Length of Sides (in)				
L1	L2	L3	L4	Stiffness
24.38	24.25	24.31	24.31	1355 MPa
Average Length (mm) 617.54		Gauge Length (mm) 508		

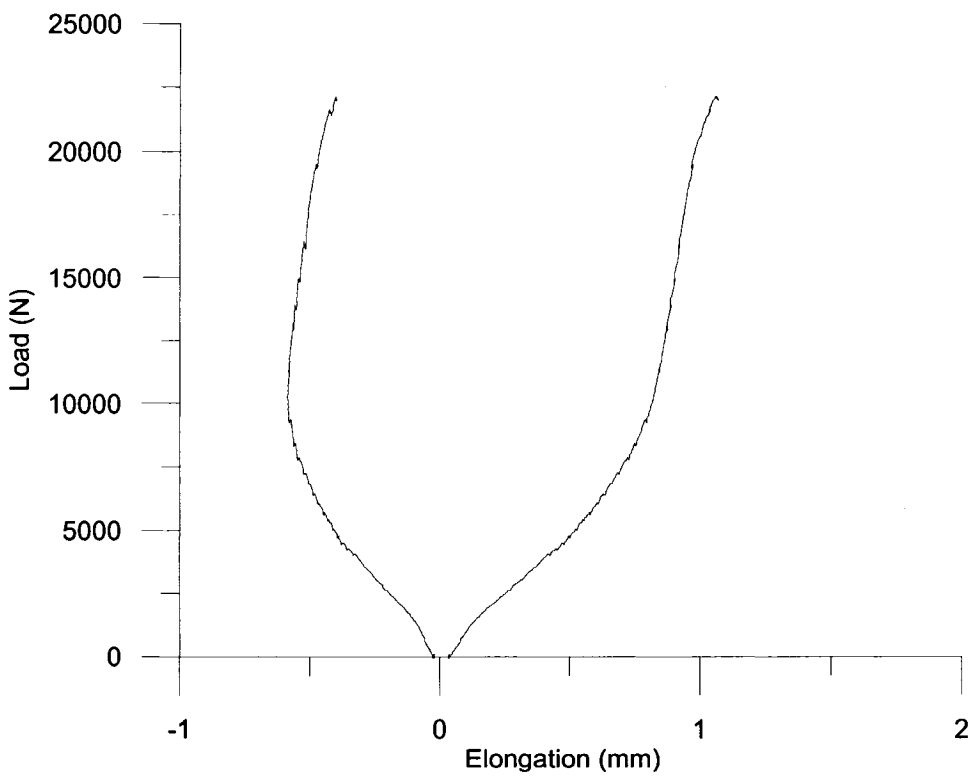

Figure C14: GYP-5 STIFF load vs. elongation

Table C15: GYP-6 STIFF data

GYP-6 STIFF					
Dimensions measured before testing				Stiffness	
Thickness at corners (mm)					
T1	T2	T3	T4	Slope 1	Slope 2
15.28	15.46	15.36	15.24	41241	102245
Average Thickness (mm)				Average Slope	
15.34				71743	
Length of Sides (in)					
L1	L2	L3	L4	Stiffness	
24.25	24.31	24.25	24.31	1363	MPa
Average Length (mm)		Gauge Length (mm)			
616.74		508			

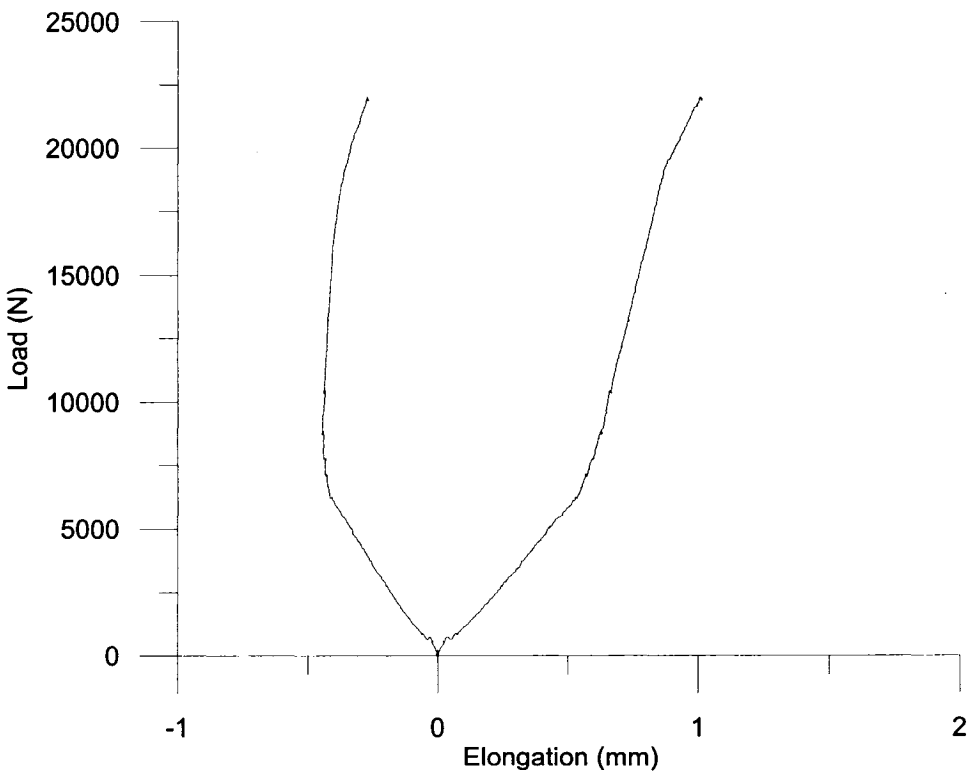

Figure C15: GYP-6 STIFF load vs. elongation

Table C16: FB+ISO 1 data

FB+ISO 1					
Dimensions measured before testing				Stiffness	
Thickness at corners (mm)					
T1	T2	T3	T4	Slope 1	Slope 2
23.44	24	24.06	24	21777	N/A
Average Thickness (mm)				Average Slope	
23.875				21777	
Length of Sides (in)					
L1	L2	L3	L4	Stiffness	
24.3125	24.3125	24.3125	24.25	265	MPa
Average Length (mm)		Gauge Length (mm)			
617.1406		508			

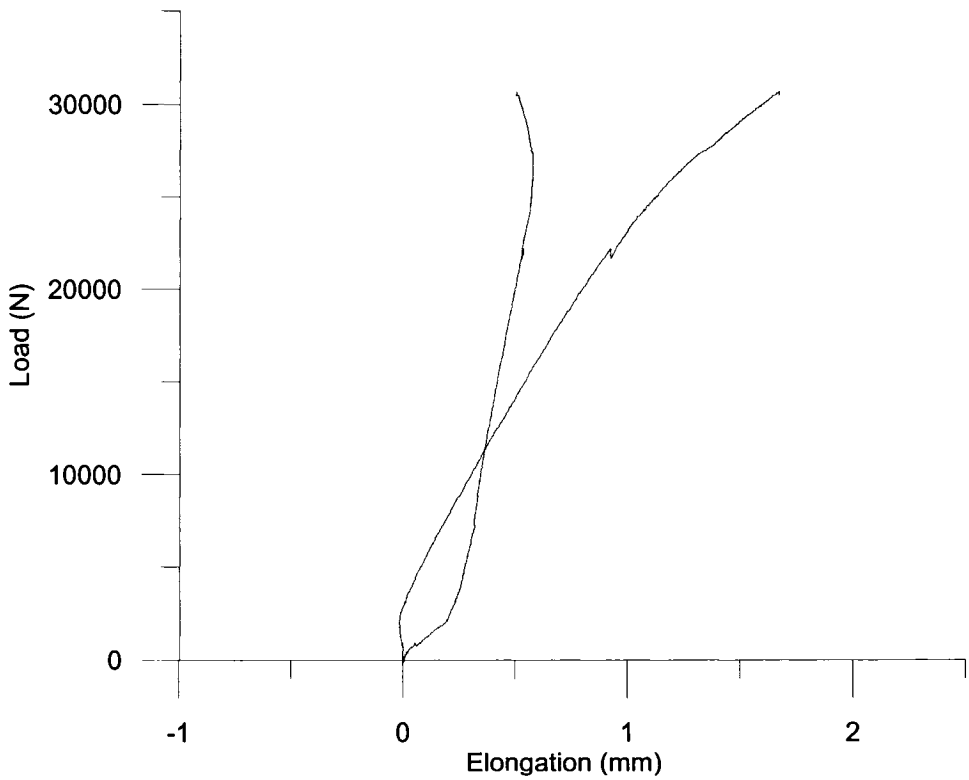

Figure C16: FB+ISO 1 load vs. elongation

Table C17: FB+ISO 2 data

FB+ISO 2					
Dimensions measured before testing				Stiffness	
Thickness at corners (mm)					
T1	T2	T3	T4	Slope 1	Slope 2
23.42	23.36	23.22	23.42	28261	N/A
Average Thickness (mm)				Average Slope	
23.36				28261	
Length of Sides (in)					
L1	L2	L3	L4	Stiffness	
24.31	24.25	24.31	24.44	352	MPa
Average Length (mm)		Gauge Length (mm)			
617.93		508			

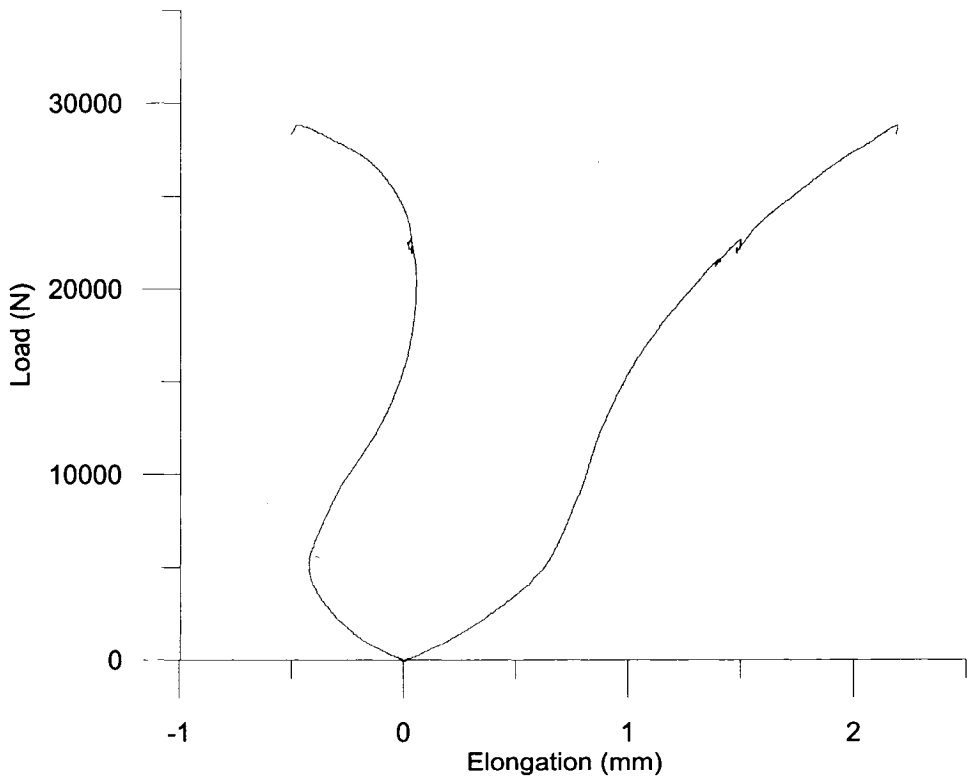

Figure C17: FB+ISO 2 load vs. elongation

Table C18: FB+ISO 3 data

FB+ISO3	
Dimensions measured before testing	Stiffness
Thickness at corners (mm) T1 T2 T3 T4 23.62 23.82 24.06 25.26	Slope 1 Slope 2 25075 N/A
Average Thickness (mm) 24.19	Average Slope 25075
Length of Sides (in) L1 L2 L3 L4 24.25 24.25 24.31 24.31	Stiffness 302 MPa
Average Length (mm) Gauge Length (mm) 616.74 508	

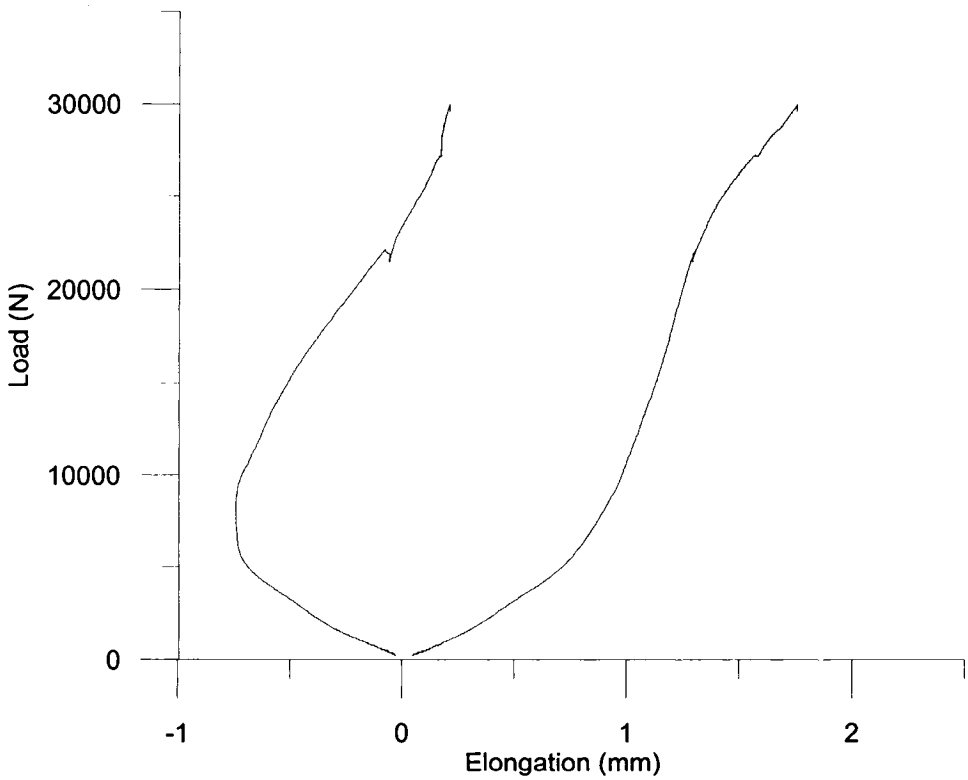

Figure C18: FB+ISO 3 load vs. elongation

Table C19: FULL SECTION 1 data

FULL SECTION 1					
Dimensions measured before testing				Stiffness	
Thickness at corners (mm)					
T1	T2	T3	T4	Slope 1	Slope 2
23.54	23.32	24.48	23.16	32535	N/A
Average Thickness (mm)				Average Slope	
23.63				32535	
Length of Sides (in)				Stiffness	
L1	L2	L3	L4		
24.25	24.31	24.13	24.38	401	MPa
Average Length (mm)		Gauge Length (mm)			
617.33		508			

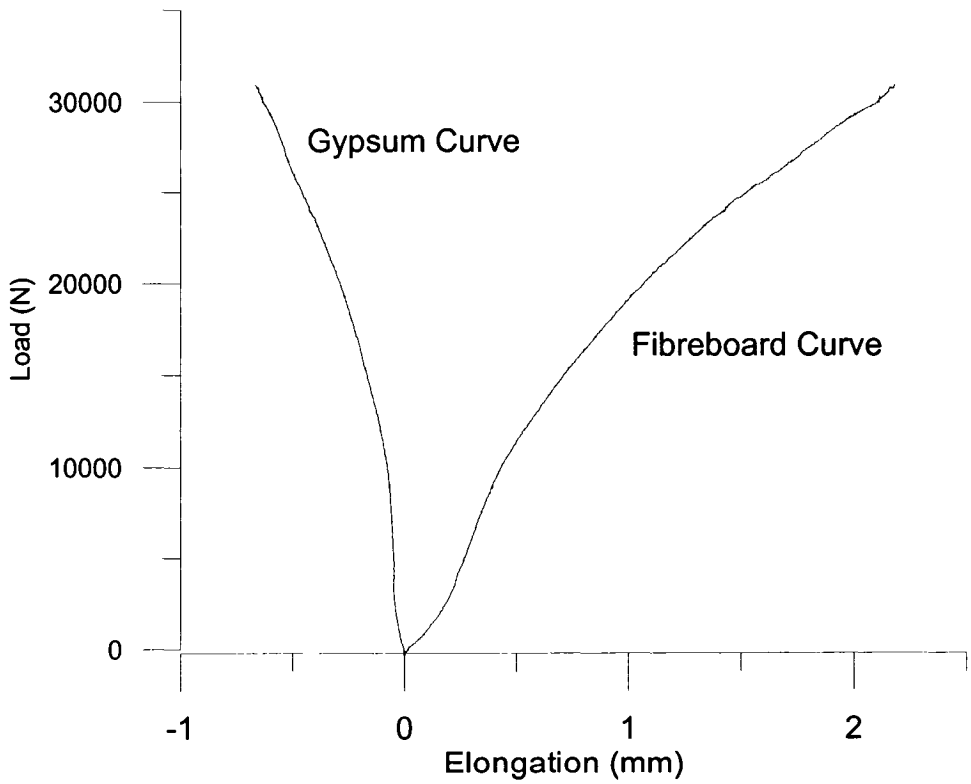

Figure C19: FULL SECTION 1 load vs. elongation

Table C20: FULL SECTION 2 data

FULL SECTION 2	
Dimensions measured before testing	Stiffness
Thickness at corners (mm) T1 T2 T3 T4 23.14 23.04 23.74 23.18	Slope 1 Slope 2 30346 N/A
Average Thickness (mm) 23.28	Average Slope 30346
Length of Sides (in) L1 L2 L3 L4 24.28 24.31 24.13 24.375	Stiffness 379 MPa
Average Length (mm) Gauge Length (mm) 617.33 508	

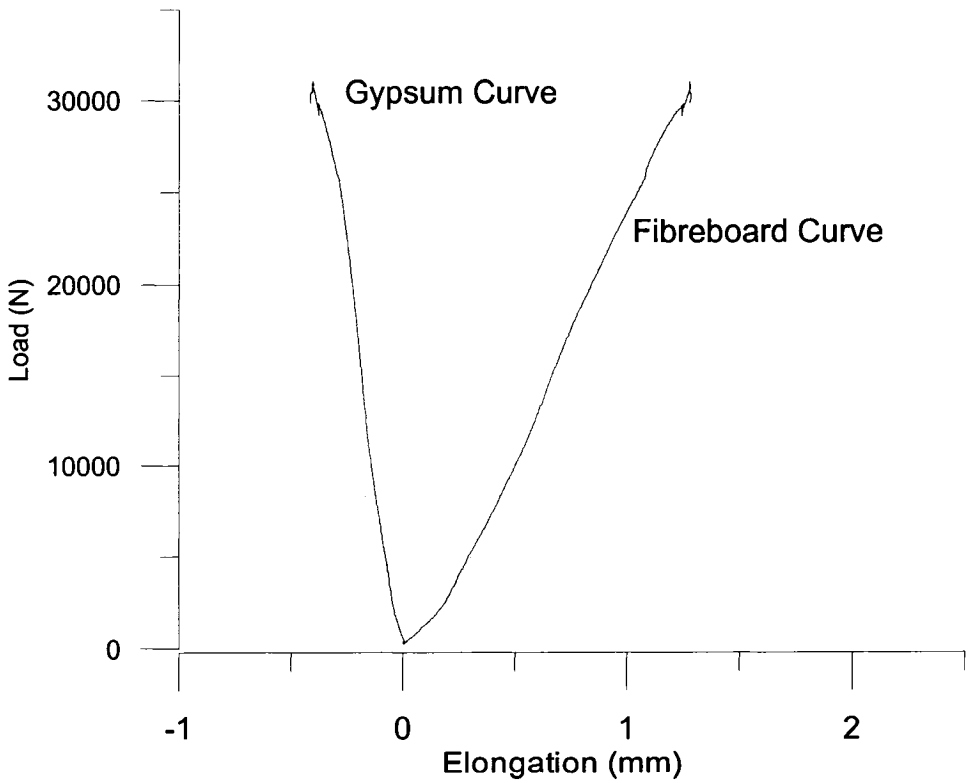

Figure C20: FULL SECTION 2 load vs. elongation

Table C21: FULL SEFCTION 3 data

FULL SECTION 3					
Dimensions measured before testing				Stiffness	
Thickness at corners (mm)					
T1	T2	T3	T4	Slope 1	Slope 2
24.12	24.02	N/A	N/A	25669	N/A
Average Thickness (mm)				Average Slope	
24.07				25669	
Length of Sides (in)					
L1	L2	L3	L4	Stiffness	
24.25	24.31	24.25	24.31	310	MPa
Average Length (mm)		Gauge Length (mm)			
617.33		508			

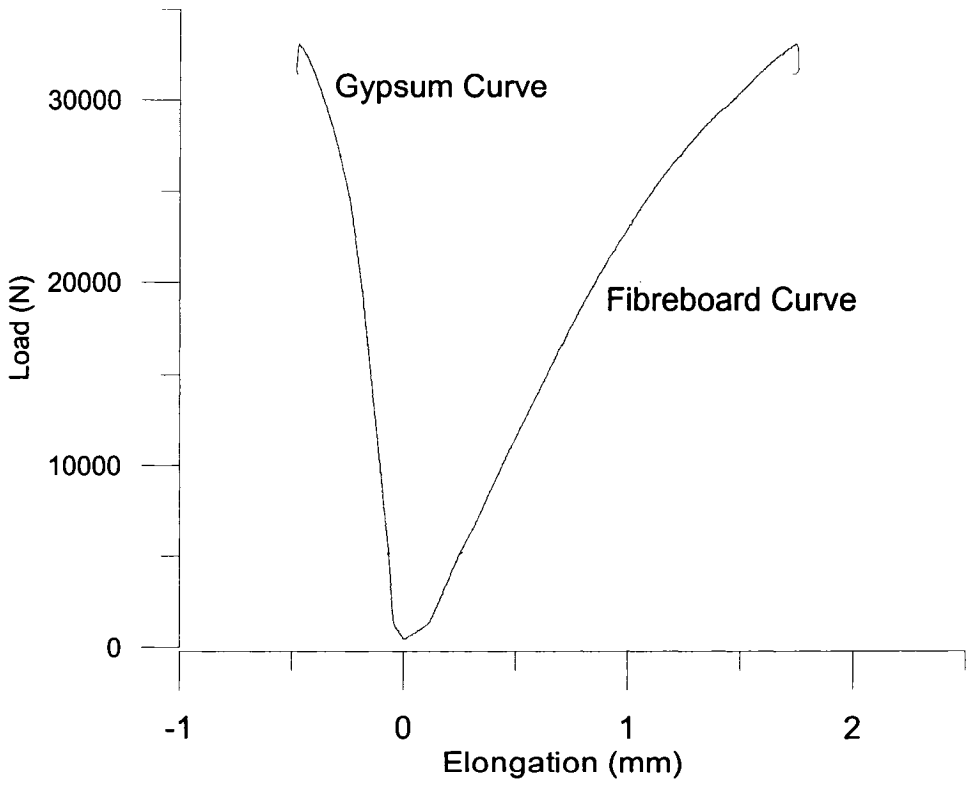

Figure C21: FULL SECTION 3 load vs. elongation

Table C22: FULL SECTION 4 data

FULL SECTION 4							
Dimensions measured before testing					Stiffness		
Thickness at corners (mm)							
T1	T2	T3	T4		Slope 1	Slope 2	
23.89	23.89	23.89	23.89		40342	N/A	
Average Thickness (mm)					Average Slope		
23.89					40342		
Length of Sides (in)							
L1	L2	L3	L4		Stiffness		
24.25	24.31	24.31	24.25		491	MPa	
Average Length (mm)		Gauge Length (mm)					
617.33		508					

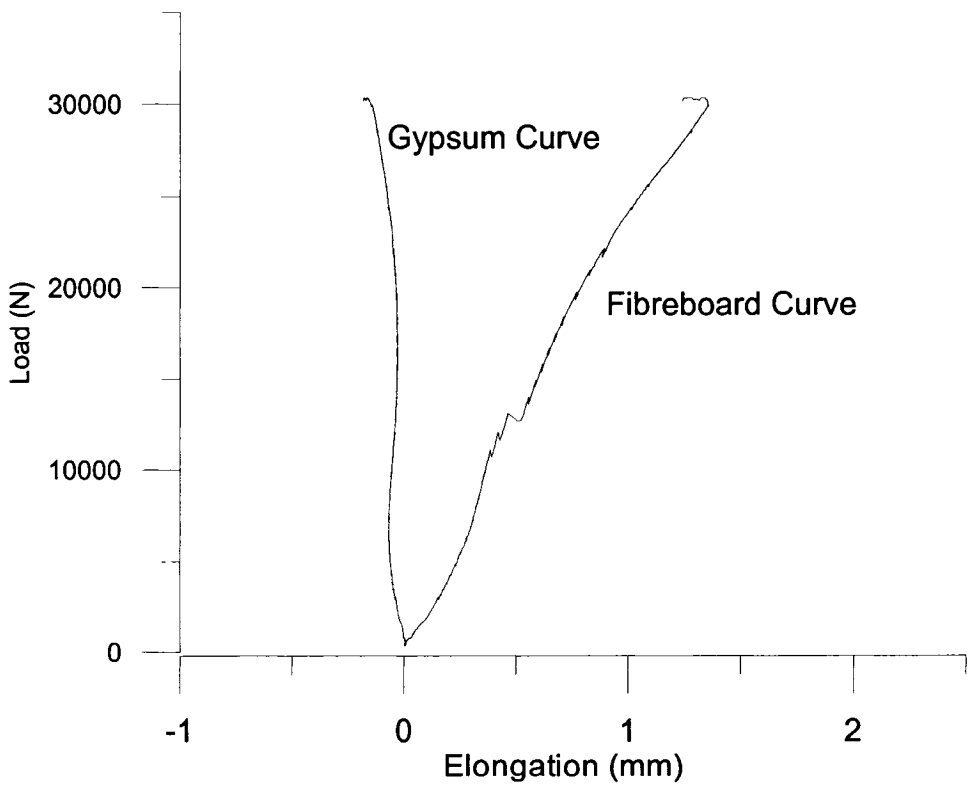

Figure C22: FULL SECTION 4 load vs. elongation

APPENDIX D

CONNECTION TEST DATA

The results of the connection tests were presented in Chapter 3, Section 3.5 and in this Appendix. The load versus elongation curve of each specimen is shown in this Appendix.

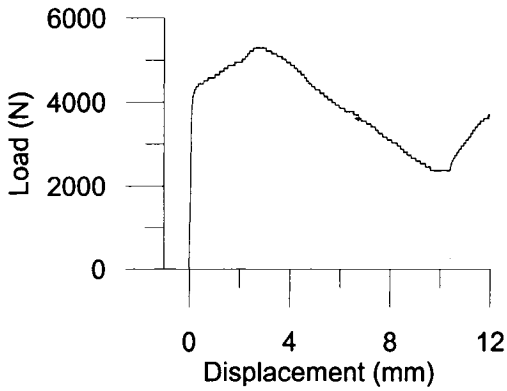

Figure D1: 076-N-A

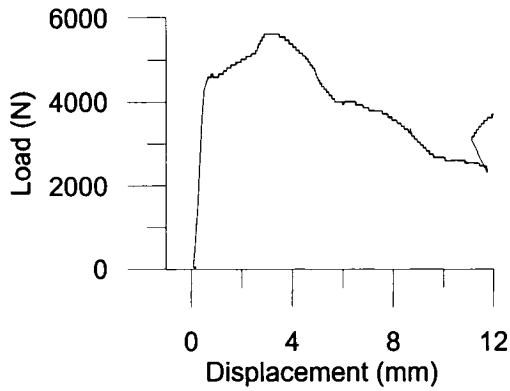

Figure D2: 076-N-B

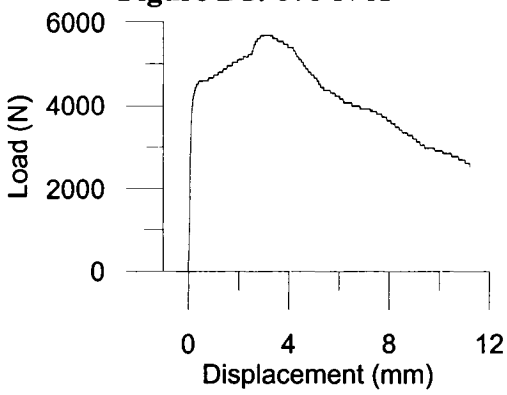

Figure D3: 076-N-C

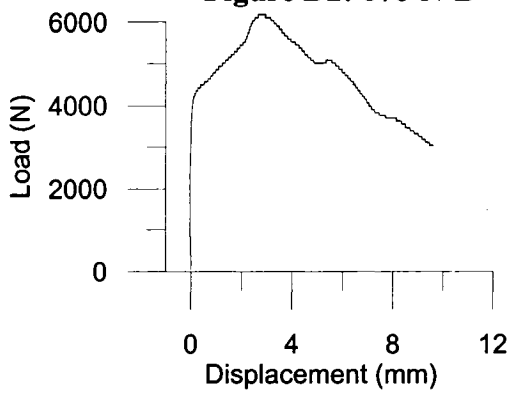

Figure D4: 076-N-D

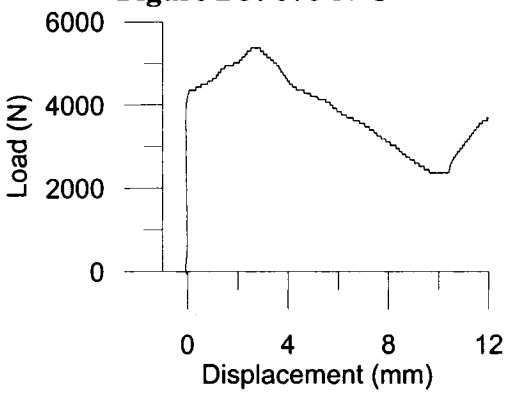

Figure D5: 076-N-E

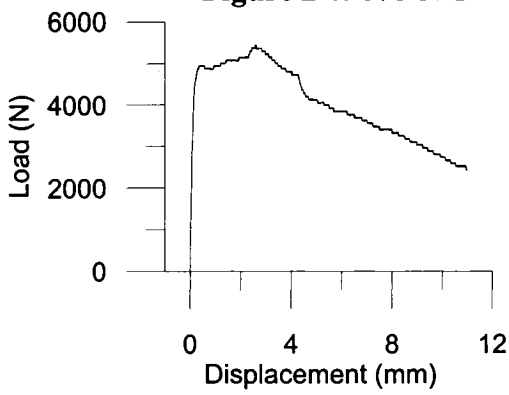

Figure D6: 076-N-H

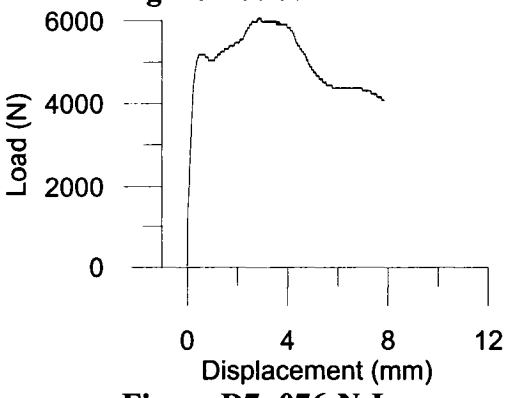

Figure D7: 076-N-I

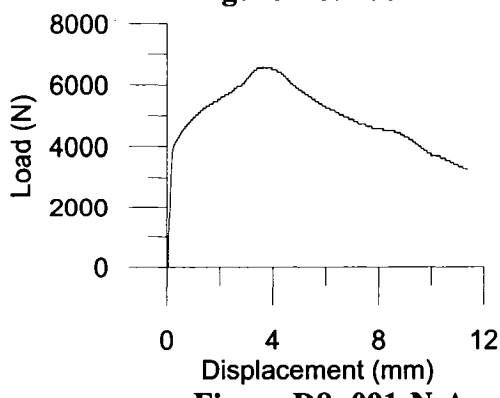

Figure D8: 091-N-A

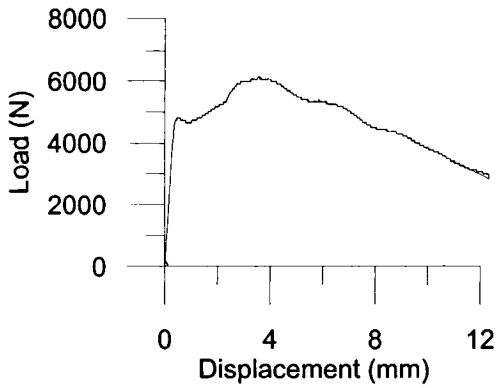

Figure D9: 091-N-B

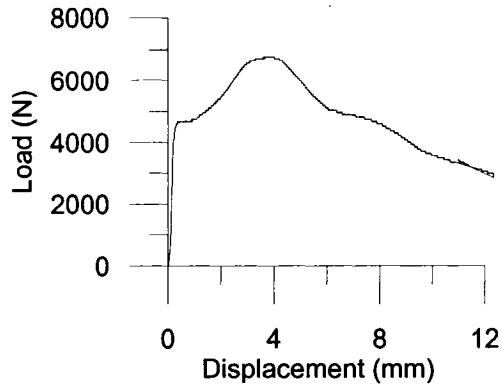

Figure D10: 091-N-C

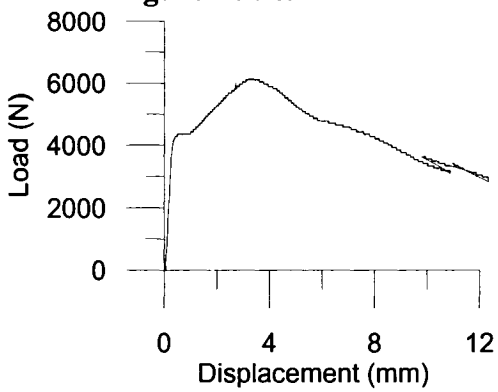

Figure D11: 091-N-D

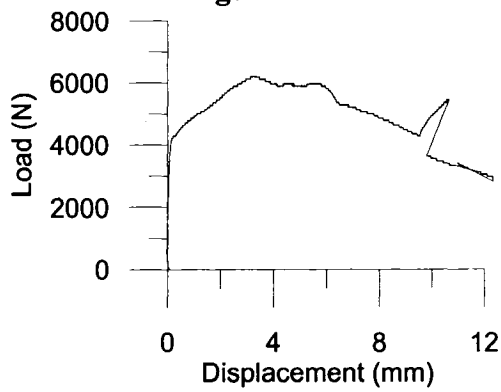

Figure D12: 091-N-E

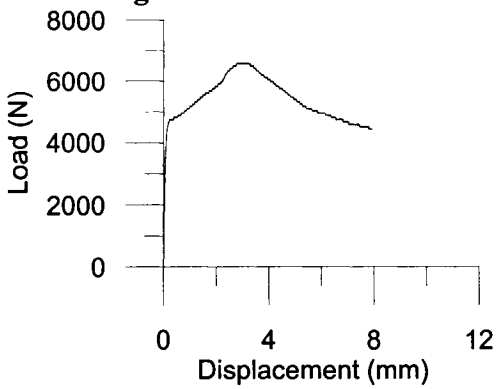

Figure D13: 091-N-H

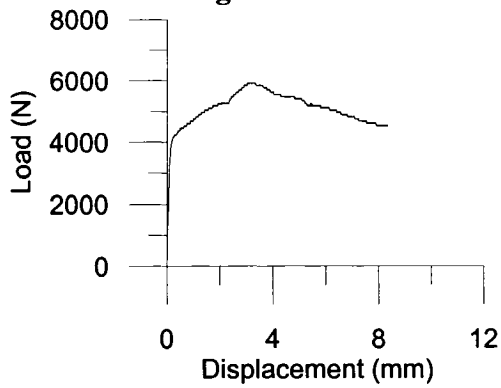

Figure D14: 091-N-I

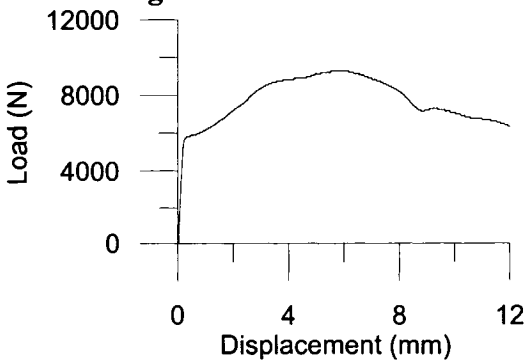

Figure D15: 122-N-A

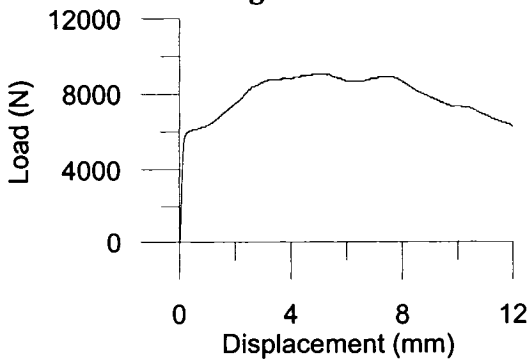

Figure D16: 122-N-B

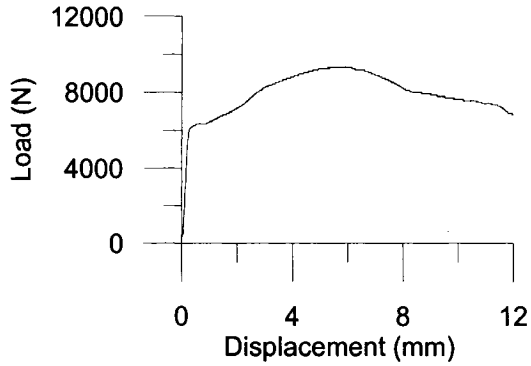

Figure D17: 122-N-C

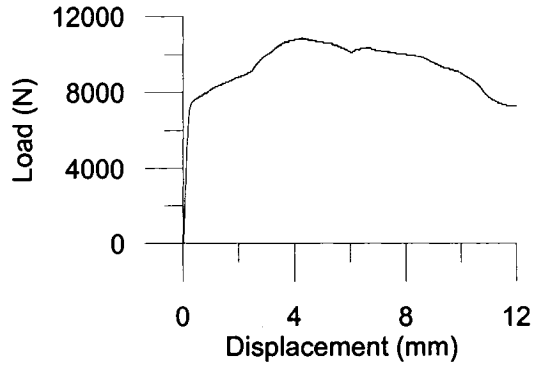

Figure D18: 122-N-D

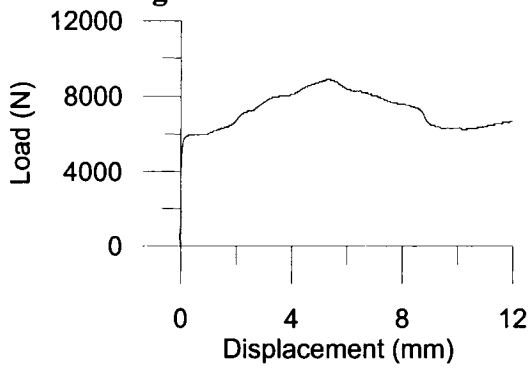

Figure D19: 122-N-E

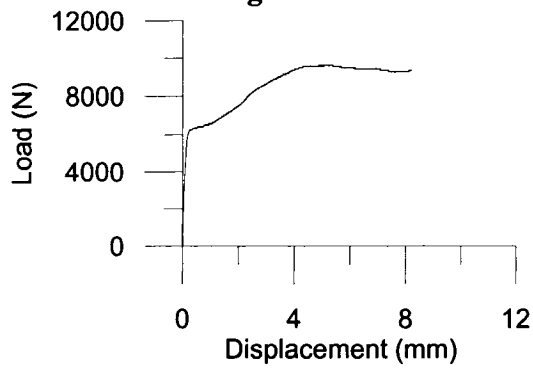

Figure D20: 122-N-H

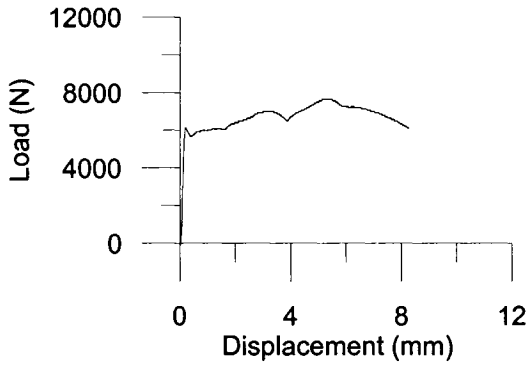

Figure D21: 122-N-I

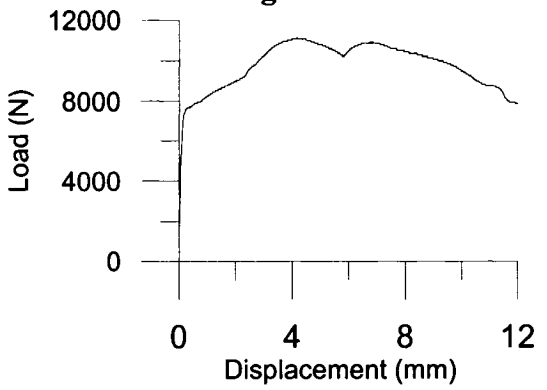

Figure D22: 151-N-A

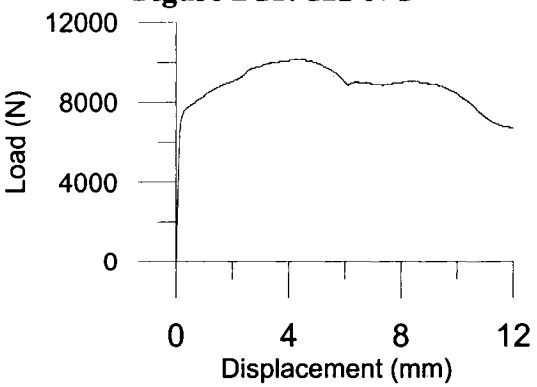

Figure D23: 151-N-B

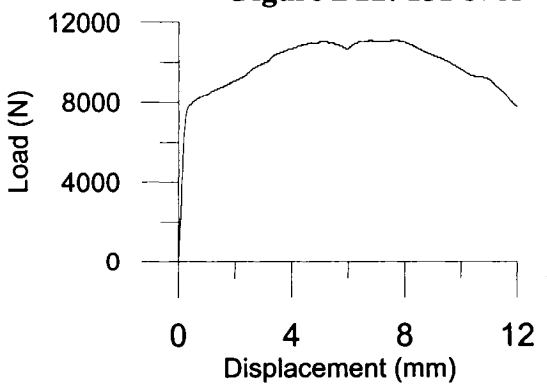

Figure D24: 151-N-C

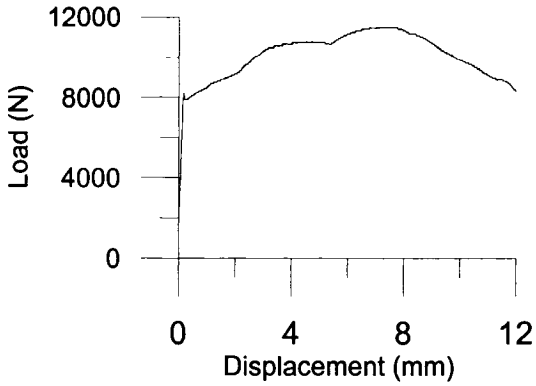

Figure D25: 151-N-D

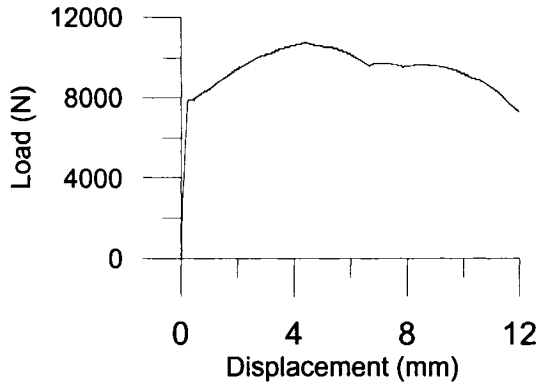

Figure D26: 151-N-E

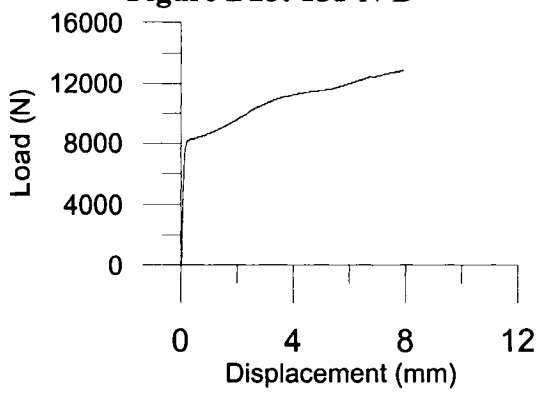

Figure D27: 151-N-H

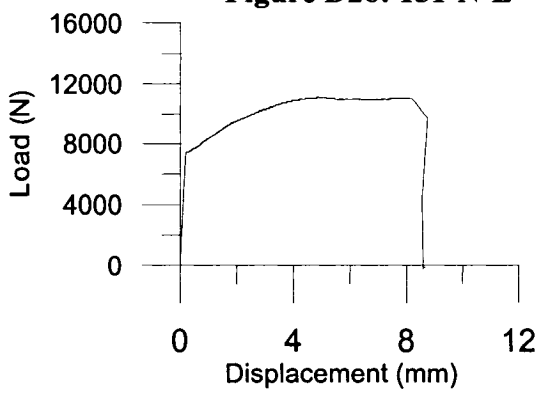

Figure D28: 151-N-I

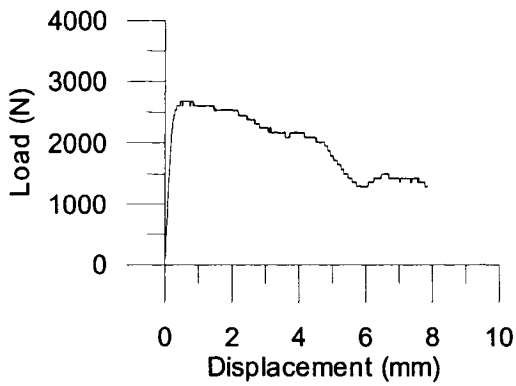

Figure D29: 076-S-A

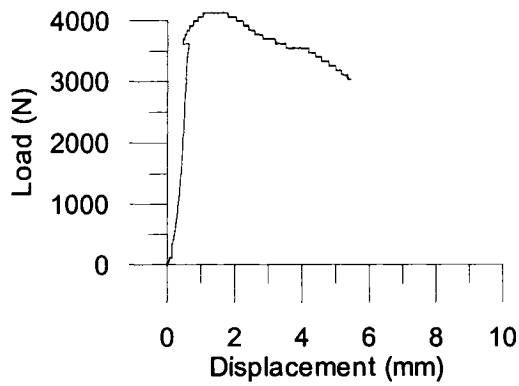

Figure D30: 076-S-B

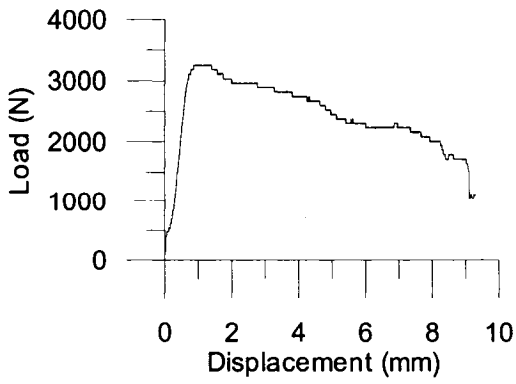

Figure D31: 076-S-C

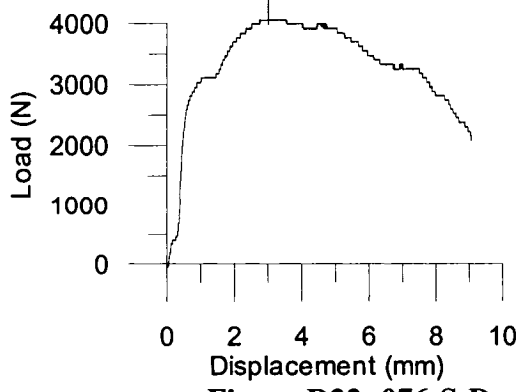

Figure D32: 076-S-D

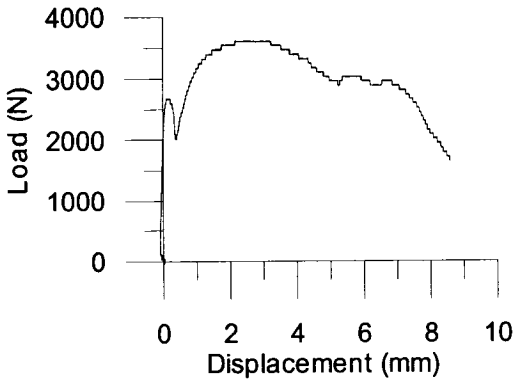

Figure D33: 076-S-E

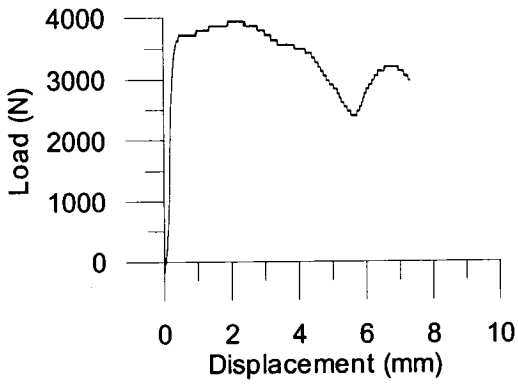

Figure D34: 076-S-H

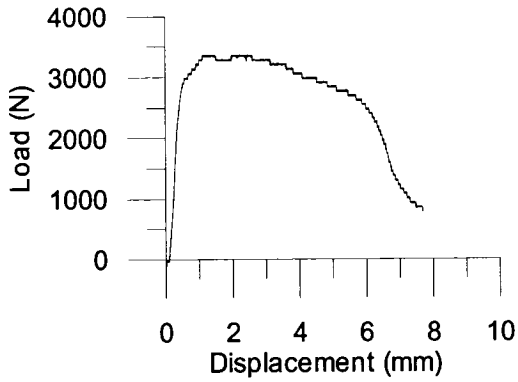

Figure D35: 076-S-I

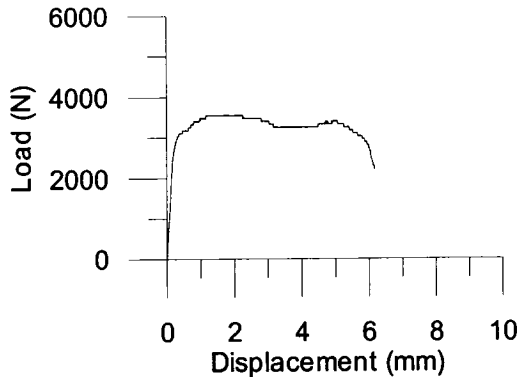

Figure D36: 091-S-A

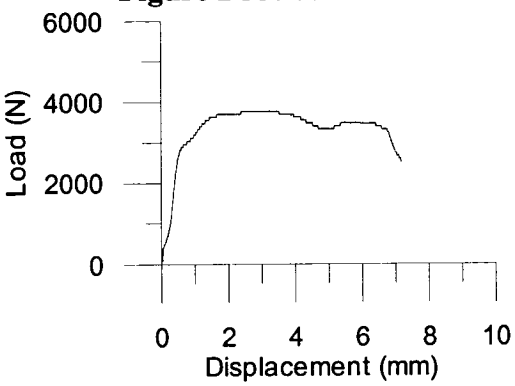

Figure D37: 091-S-B

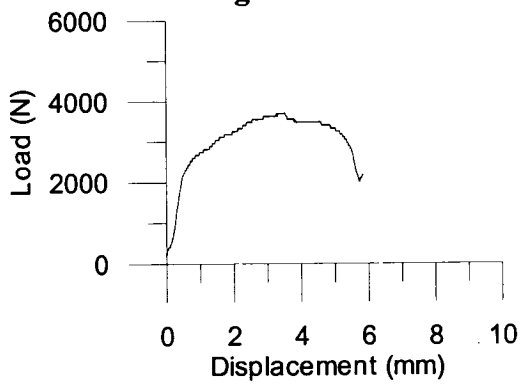

Figure D38: 091-S-C

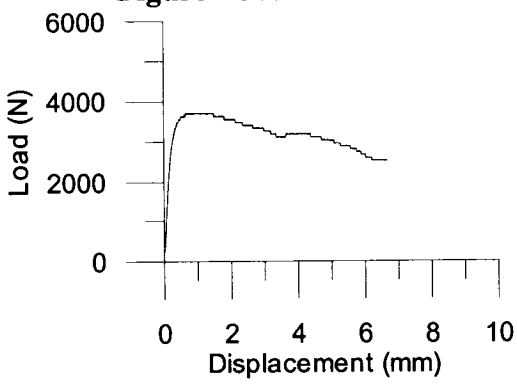

Figure D39: 091-S-D

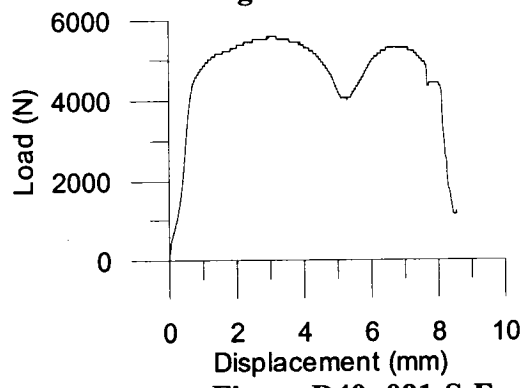

Figure D40: 091-S-E

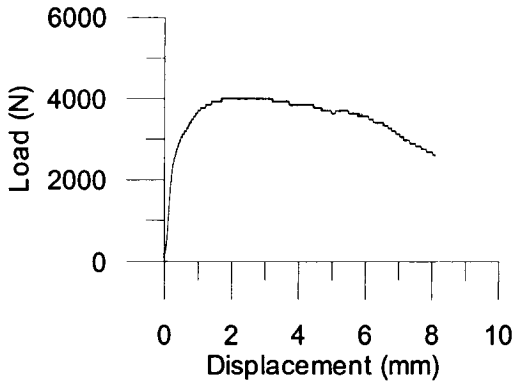

Figure D41: 091-S-H

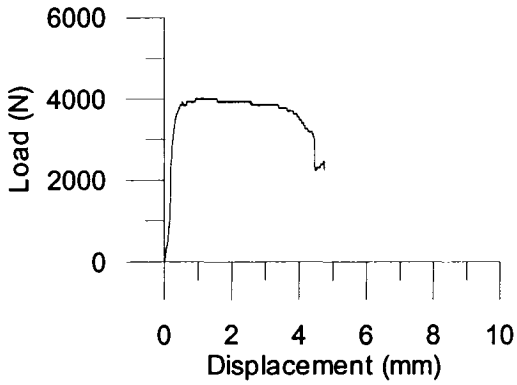

Figure D42: 091-S-I

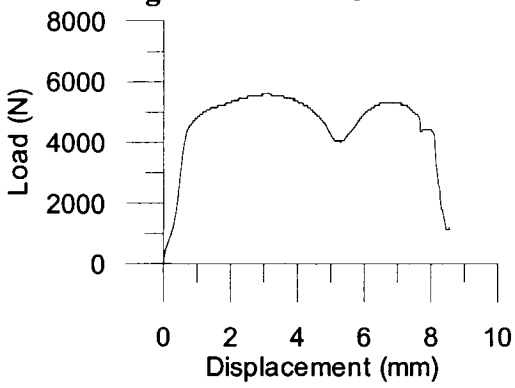

Figure D43: 122-S-A

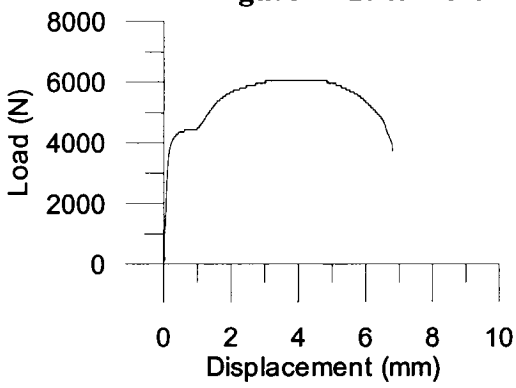

Figure D44: 122-S-B

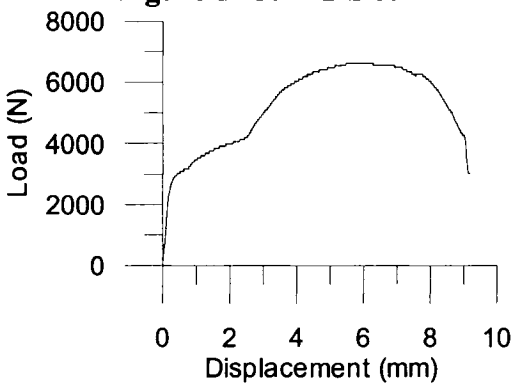

Figure D45: 122-S-C

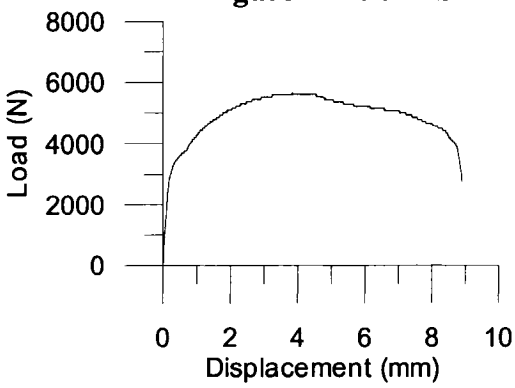

Figure D46: 122-S-D

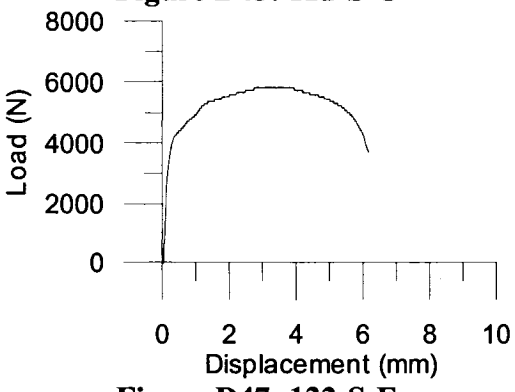

Figure D47: 122-S-E

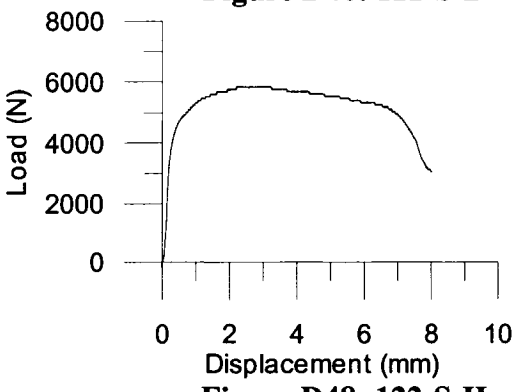

Figure D48: 122-S-H

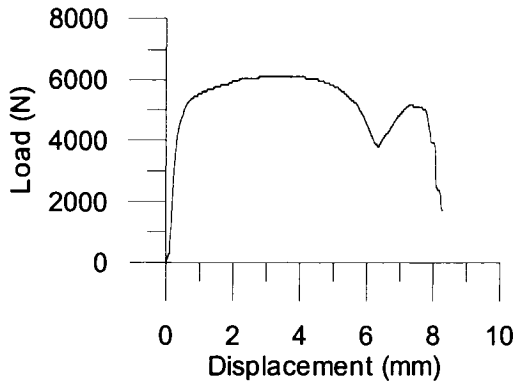

Figure D49: 122-S-I

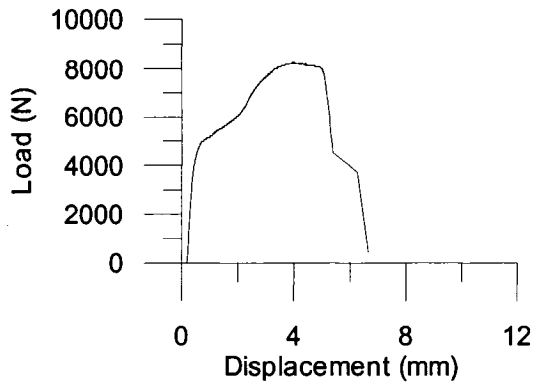

Figure D50: 151-S-A

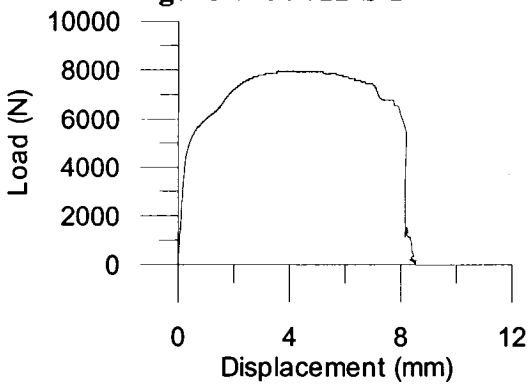

Figure D52: 151-S-B

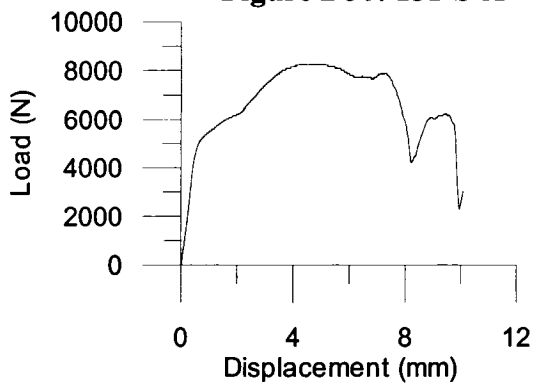

Figure D51: 151-S-C

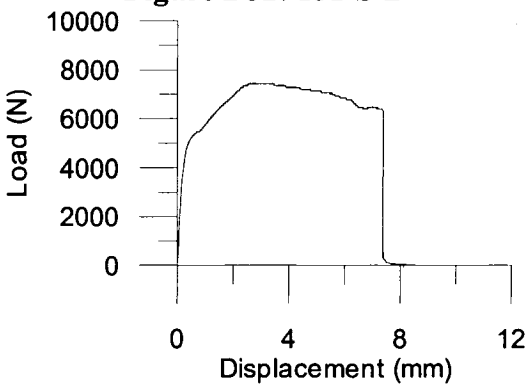

Figure D53: 151-S-D

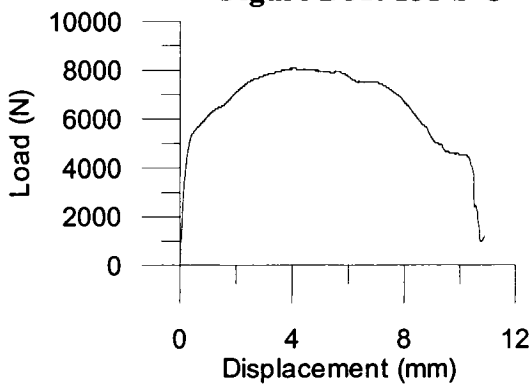

Figure D54: 151-S-E

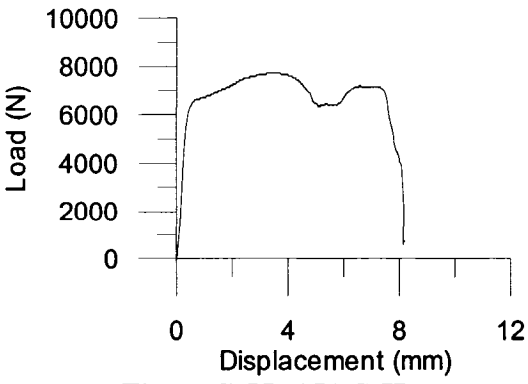

Figure D55: 151-S-H

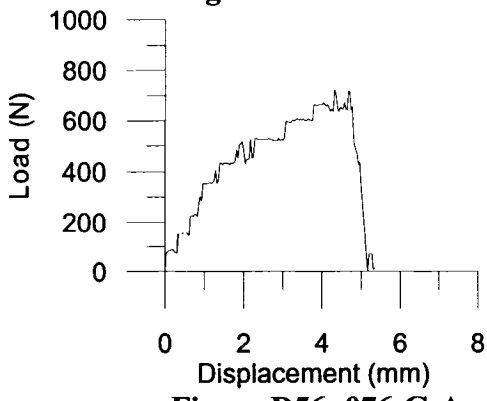

Figure D56: 076-G-A

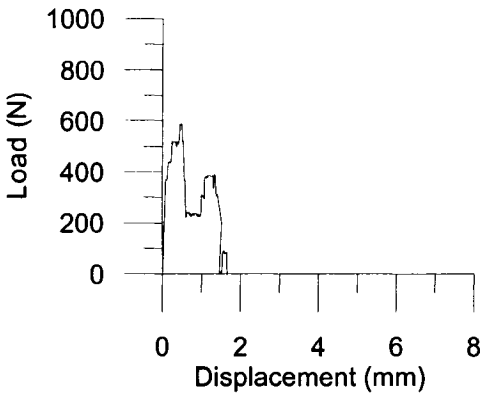

Figure D57: 076-G-B

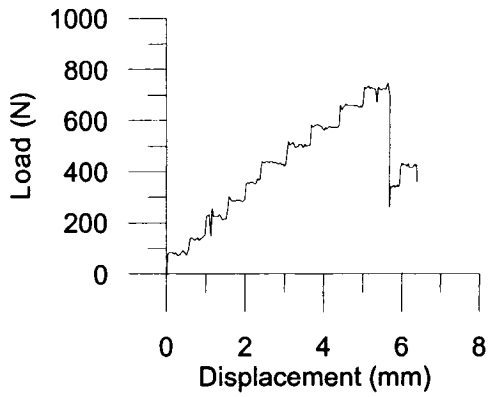

Figure D58: 076-G-C

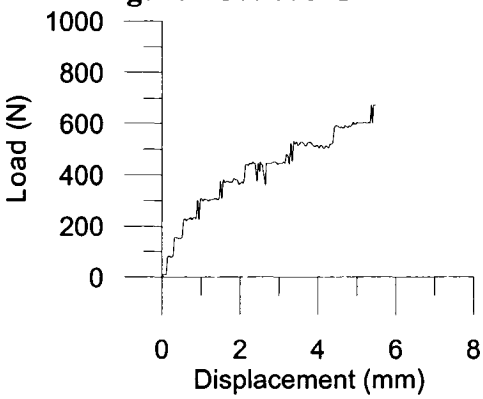

Figure D59: 076-G-D

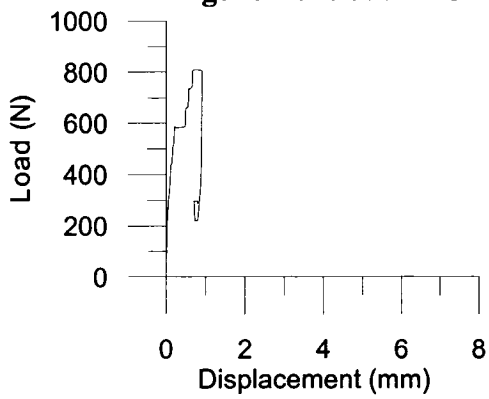

Figure D60: 076-G-E

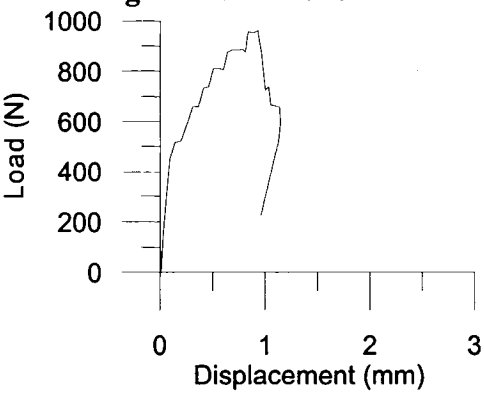

Figure D61: 091-G-A

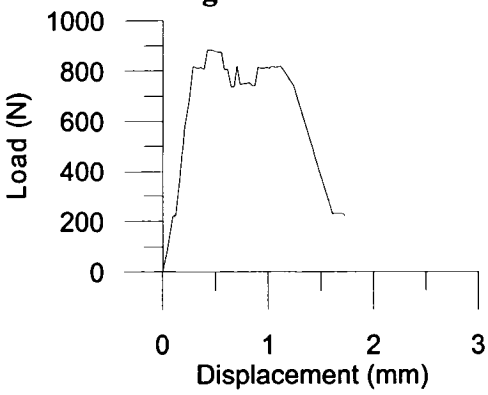

Figure D62: 091-G-B

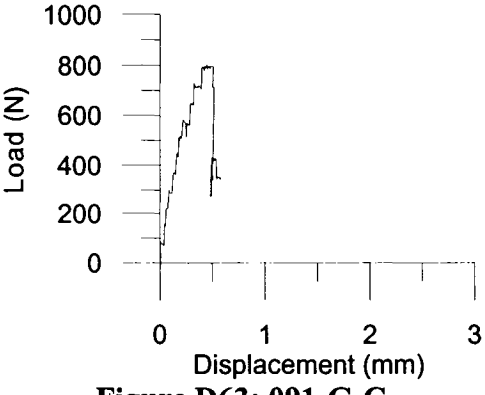

Figure D63: 091-G-C

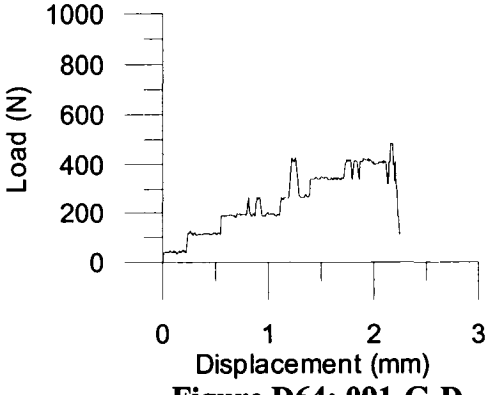

Figure D64: 091-G-D

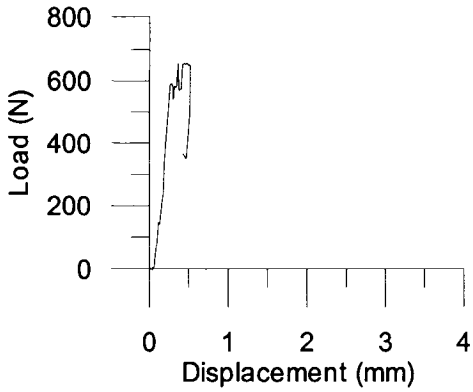

Figure D65: 122-G-A

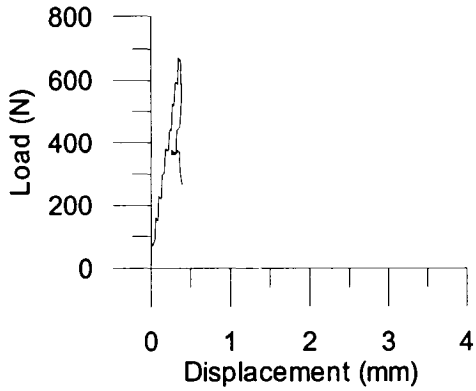

Figure D66: 122-G-B

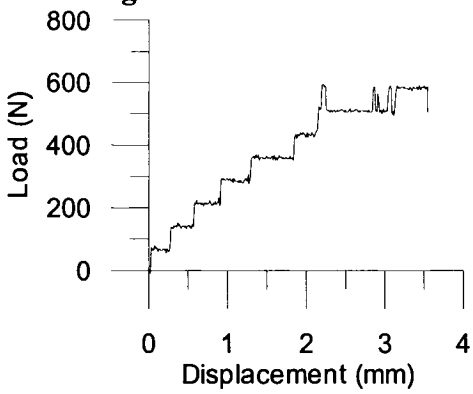

Figure D67: 122-G-C

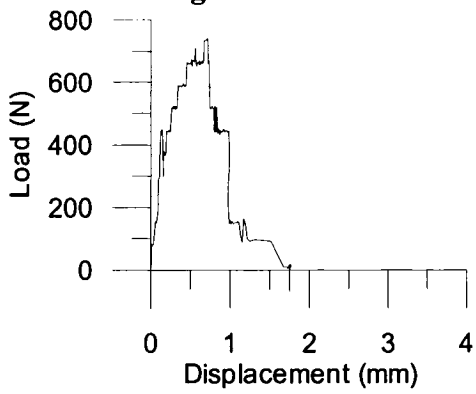

Figure D68: 122-G-D

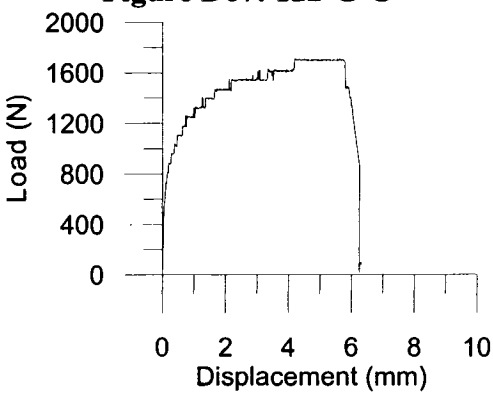

Figure D69: 151-G-A

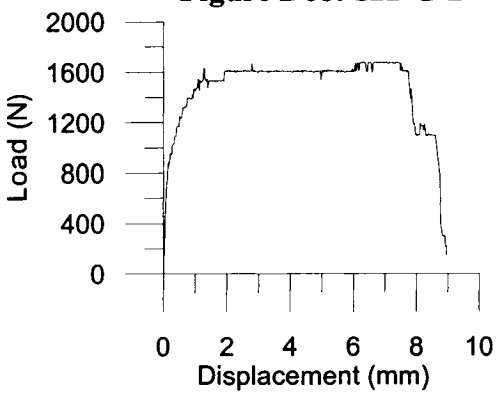

Figure D70: 151-G-B

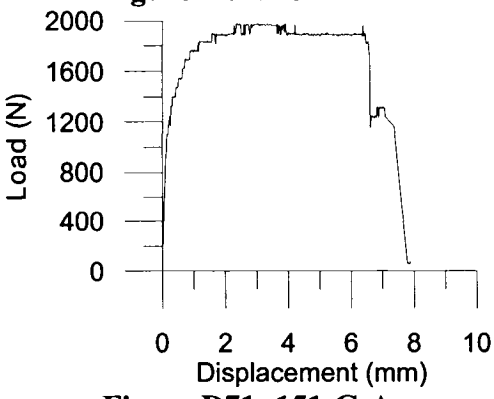

Figure D71: 151-G-A

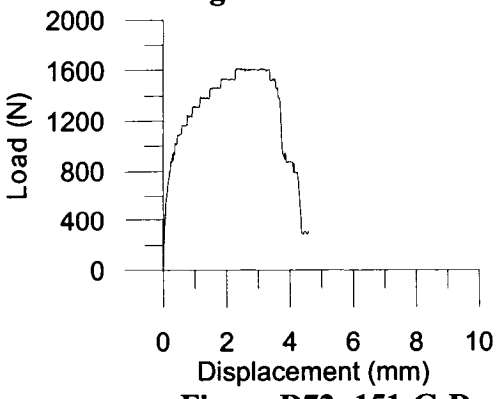

Figure D72: 151-G-D

APPENDIX E
SAP2000 INPUT/OUTPUT FILE EXCERPTS

The analytical results are presented in Chapter 4. Excerpts of the input and output files of the 38-76-6-NS-R-M models are shown in this Appendix. All input files and output files are similar therefore only this model's input and output files are shown.

The actual input file for the 38-76-6-NS-M model is 1009 pages long and the output file contains more than 5000 pages. Therefore, only excerpts of each section of the input and output files are presented in this Appendix. All tables are unformatted, therefore not included in the List of Tables.

For the input, sample node, element and link definitions are be presented.

For the output, some sample node deflections and element stresses are presented.

FOR MODEL 38-76-6-NS-R-M

INPUT:

```
File G:\Thesis\SAP\Finals\With Roofing\076\38-76-6-NS-R-M.$2k was saved
on 10/10/05 at 22:28:44

TABLE:  "JOINT COORDINATES"
Joint=1  CoordSys=GLOBAL CoordType=Cartesian XorR=482.6  Y=0     Z=0.5
Joint=2  CoordSys=GLOBAL CoordType=Cartesian XorR=514.35 Y=0     Z=38.1
Joint=3  CoordSys=GLOBAL CoordType=Cartesian XorR=482.6  Y=101.6 Z=0.5
Joint=4  CoordSys=GLOBAL CoordType=Cartesian XorR=558.8  Y=0     Z=38.1
Joint=5  CoordSys=GLOBAL CoordType=Cartesian XorR=603.25 Y=0     Z=38.1
Joint=6  CoordSys=GLOBAL CoordType=Cartesian XorR=615.95 Y=0     Z=0
Joint=7  CoordSys=GLOBAL CoordType=Cartesian XorR=635    Y=0     Z=0
Joint=8  CoordSys=GLOBAL CoordType=Cartesian XorR=654.05 Y=0     Z=0
Joint=9  CoordSys=GLOBAL CoordType=Cartesian XorR=666.75 Y=0     Z=38.1
Joint=10 CoordSys=GLOBAL CoordType=Cartesian XorR=711.2  Y=0     Z=38.1
Joint=11 CoordSys=GLOBAL CoordType=Cartesian XorR=755.65 Y=0     Z=38.1
Joint=12 CoordSys=GLOBAL CoordType=Cartesian XorR=768.35 Y=0     Z=0
Joint=13 CoordSys=GLOBAL CoordType=Cartesian XorR=787.4  Y=0     Z=0
Joint=14 CoordSys=GLOBAL CoordType=Cartesian XorR=806.45 Y=0     Z=0
Joint=15 CoordSys=GLOBAL CoordType=Cartesian XorR=819.15 Y=0     Z=38.1
Joint=967 CoordSys=GLOBAL CoordType=Cartesian XorR=25.4  Y=50.8  Z=-0.5


TABLE:  "CONNECTIVITY - FRAME/CABLE"
Frame=1   JointI=967   JointJ=968
Frame=2   JointI=968   JointJ=969
Frame=3   JointI=969   JointJ=970
Frame=4   JointI=970   JointJ=971
Frame=5   JointI=971   JointJ=972
Frame=6   JointI=972   JointJ=973
Frame=7   JointI=973   JointJ=974
Frame=8   JointI=974   JointJ=975
Frame=9   JointI=975   JointJ=742
Frame=10   JointI=742   JointJ=741
Frame=11   JointI=741   JointJ=724
Frame=12   JointI=724   JointJ=725
Frame=13   JointI=725   JointJ=726
Frame=14   JointI=726   JointJ=727
Frame=15   JointI=727   JointJ=728


TABLE:  "CONNECTIVITY - AREA"
Area=1    Joint1=460   Joint2=461   Joint3=946   Joint4=947
Area=2    Joint1=461   Joint2=462   Joint3=947   Joint4=948
Area=3    Joint1=462   Joint2=463   Joint3=948   Joint4=949
Area=4    Joint1=463   Joint2=465   Joint3=949   Joint4=950
Area=5    Joint1=465   Joint2=466   Joint3=950   Joint4=951
Area=6    Joint1=466   Joint2=951   Joint3=467   Joint4=952
Area=7    Joint1=467   Joint2=468   Joint3=952   Joint4=953
Area=8    Joint1=468   Joint2=469   Joint3=953   Joint4=954
Area=9    Joint1=469   Joint2=954   Joint3=470   Joint4=955
Area=10   Joint1=470   Joint2=471   Joint3=955   Joint4=956
Area=11   Joint1=471   Joint2=472   Joint3=956   Joint4=957
```

```
Area=12   Joint1=472   Joint2=473   Joint3=957   Joint4=958
Area=13   Joint1=473   Joint2=474   Joint3=958   Joint4=959
Area=14   Joint1=474   Joint2=475   Joint3=959   Joint4=960
Area=15   Joint1=475   Joint2=960   Joint3=476   Joint4=961

TABLE:  "CONNECTIVITY - LINK"
Link=1    JointI=36442   JointJ=36462
Link=2    JointI=25252   JointJ=25272
Link=3    JointI=947     JointJ=967
Link=4    JointI=14062   JointJ=14082
Link=5    JointI=47372   JointJ=47427
Link=6    JointI=36182   JointJ=36237
Link=7    JointI=462     JointJ=489
Link=8    JointI=460     JointJ=487
Link=9    JointI=461     JointJ=488
Link=10   JointI=24992   JointJ=25047
Link=11   JointI=13802   JointJ=13857
Link=12   JointI=687     JointJ=742
Link=13   JointI=467     JointJ=490
Link=14   JointI=468     JointJ=491
Link=15   JointI=469     JointJ=492
```

OUTPUT:

TABLE: Joint Displacements

Joint	U1	U2	U3	R1	R2	R3
Text	mm	mm	mm	Radians	Radians	Radians
1	0.002651	0.159839	-0.067455	0.001936	-0.003136	0.000103
2	-0.152346	0.161339	0.043962	-0.000021	-0.003429	-0.000078
24	0.002644	0.161902	-0.00839	0.000062	-0.003528	0.000113
59	0	0	0	0	0	0
60	0	0	0	0	0	0
460	0.000111	0.182053	-0.002402	0.000164	0.00063	-0.000002726
461	0.000099	0.182113	-0.011594	0.000488	0.000195	0.000007962
462	0.000086	0.182386	-0.006962	0.000049	-0.000687	0.000021
463	-0.037211	0.180956	0.005473	0.000021	-0.000572	-0.000035
465	-0.037223	0.179466	-0.006606	0.000073	0.000697	-0.000032
466	-0.037226	0.17793	-0.014007	-0.000045	-0.000918	-0.000036
467	0.005022	0.175509	0.000028	-0.000117	0.000061	0.000148
468	0.005044	0.177986	-0.012323	0.000604	0.000593	0.000112
469	0.005073	0.180324	-0.004656	0.000054	-0.001699	0.000131
470	-0.123909	0.180374	0.038321	-0.000036	-0.00334	-0.00007

TABLE: Element Forces - Frames

Frame	P	V2	V3	T	M2	M3
Text	KN	KN	KN	KN-mm	KN-mm	KN-mm
1	0.107	0	-0.048	0	0	0
2	0.107	0	-0.048	0	0.91	0
3	0.107	0	-0.048	0	6.4	0
4	0.135	0	-0.015	0	7.31	0
5	0.135	0	-0.015	0	7.6	0
6	0.135	0	-0.015	0	9.29	0
7	0.135	0	-0.015	0	9.58	0
8	0.135	0	-0.015	0	9.86	0
9	0.135	0	-0.015	0	11.56	0
10	0.167	0	0.011	0	11.84	0
11	0.167	0	0.011	0	11.64	0
382	-1.019	0	-0.099	0	-20.16	0
383	-1.019	0	-0.099	0	-15.12	0
384	-1.019	0	-0.099	0	-10.08	0
385	-1.019	0	-0.099	0	-5.04	0

TABLE: Element Forces - Area Shells									
Area	Joint	F11	F22	F12	M11	M22	M12	V13	V23
Text	Text	KN/mm	KN/mm	KN/mm	KN-mm/mm	KN-mm/mm	KN-mm/mm	KN/mm	KN/mm
1	460	-2.90E-04	-6.70E-04	7.12E-05	-4.93E-06	-3.55E-05	9.63E-05	-1.73E-05	2.38E-06
1	461	4.75E-05	4.70E-04	6.24E-05	3.39E-04	1.77E-05	5.04E-05	-1.73E-05	6.10E-06
1	947	3.10E-04	5.40E-04	9.78E-05	-3.59E-04	-1.70E-04	1.05E-05	1.97E-05	6.10E-06
1	946	-2.61E-05	-5.90E-04	1.10E-04	1.27E-06	-3.42E-05	5.63E-05	1.97E-05	2.38E-06
2	461	3.16E-05	4.60E-04	1.25E-05	3.43E-04	1.88E-05	-7.96E-05	-3.64E-06	5.03E-06
2	462	-1.60E-04	-1.70E-04	-1.33E-05	3.85E-04	1.13E-04	-1.04E-04	-3.64E-06	-7.23E-07
2	948	-1.10E-04	-1.50E-04	-1.10E-04	7.24E-04	2.15E-04	-3.14E-05	-5.84E-05	-7.23E-07
2	947	7.89E-05	4.70E-04	-8.73E-05	-3.62E-04	-1.71E-04	-6.91E-06	-5.84E-05	5.03E-06
3	462	-1.30E-04	-3.02E-05	1.78E-05	1.16E-04	4.01E-04	2.43E-05	2.64E-06	2.11E-05
3	463	3.80E-05	2.03E-05	-9.64E-06	-1.34E-04	-4.49E-04	-8.89E-06	4.23E-07	2.11E-05
3	949	2.31E-05	-2.94E-05	-3.69E-06	-1.54E-04	-5.16E-04	-1.12E-05	4.23E-07	3.04E-05
3	948	-1.50E-04	-7.99E-05	2.37E-05	2.09E-04	7.08E-04	2.20E-05	2.64E-06	3.04E-05
4	463	-3.53E-05	2.13E-05	7.51E-06	-4.63E-04	-1.38E-04	6.72E-06	-1.02E-05	3.32E-07
4	465	-4.23E-05	-2.11E-06	8.95E-06	-4.89E-06	-8.44E-06	2.80E-06	-1.02E-05	4.90E-08
4	950	-9.95E-06	7.59E-06	-1.28E-05	7.80E-06	-6.45E-06	-1.16E-06	-1.14E-05	4.90E-08
4	949	-2.92E-06	3.10E-05	-1.43E-05	-5.02E-04	-1.50E-04	2.76E-06	-1.14E-05	3.32E-07
5	465	-8.91E-06	7.90E-06	-2.38E-05	-1.06E-05	-1.01E-05	-1.73E-06	-1.38E-05	4.67E-07
5	466	1.00E-05	7.10E-05	-4.71E-05	6.01E-04	1.78E-04	-2.63E-05	-1.38E-05	1.63E-06
5	951	2.69E-05	7.61E-05	-5.29E-05	4.19E-04	1.24E-04	-2.37E-05	-9.24E-06	1.63E-06
5	950	7.94E-06	1.30E-05	-2.97E-05	1.01E-05	-5.77E-06	9.00E-07	-9.24E-06	4.67E-07
6	466	1.30E-04	2.10E-04	-6.30E-05	-1.88E-04	-6.30E-04	5.98E-05	-3.25E-07	4.12E-05
6	951	6.40E-05	-1.33E-05	-6.83E-05	-1.18E-04	-3.97E-04	5.60E-05	-3.25E-07	1.74E-05
6	952	-1.40E-04	-7.48E-05	-1.40E-04	8.68E-05	3.04E-04	-1.17E-05	-5.86E-06	1.74E-05
6	467	-7.26E-05	1.50E-04	-1.40E-04	2.99E-04	1.00E-03	-7.98E-06	-5.86E-06	4.12E-05
7	467	1.50E-04	-7.23E-05	9.58E-05	-1.10E-03	-3.10E-04	1.69E-04	-8.24E-05	-2.96E-06
7	468	2.94E-05	-4.90E-04	8.22E-05	5.57E-04	4.49E-05	1.41E-04	-8.24E-05	7.63E-06
7	953	1.88E-05	-4.90E-04	-9.61E-05	-6.32E-04	-2.66E-04	3.55E-05	2.04E-05	7.63E-06
7	952	1.40E-04	-7.55E-05	-8.25E-05	-2.83E-04	-8.38E-05	6.40E-05	2.04E-05	-2.96E-06
8	468	8.99E-05	-4.70E-04	1.70E-04	5.55E-04	4.41E-05	-8.07E-05	-4.46E-05	8.97E-06
8	469	4.10E-04	6.00E-04	3.00E-04	1.40E-03	4.06E-04	-1.35E-04	-4.46E-05	5.88E-07
8	954	-3.30E-04	3.80E-04	2.50E-04	1.70E-03	5.21E-04	-3.55E-05	-1.30E-04	5.88E-07
8	953	-6.50E-04	-6.90E-04	1.20E-04	-6.32E-04	-2.66E-04	1.89E-05	-1.30E-04	8.97E-06
9	469	5.00E-04	9.15E-05	-3.52E-05	-4.12E-04	-1.40E-03	4.37E-05	2.79E-06	-5.25E-05
9	954	4.60E-04	-5.77E-05	-9.96E-05	-5.19E-04	-1.70E-03	4.28E-05	2.79E-06	-6.41E-05
9	955	-1.60E-04	-2.40E-04	-5.22E-05	2.55E-04	8.55E-04	1.55E-05	-1.22E-07	-6.41E-05
9	470	-1.10E-04	-9.34E-05	1.21E-05	2.15E-04	7.22E-04	1.64E-05	-1.22E-07	-5.25E-05
10	470	-1.76E-05	-8.89E-05	-4.77E-05	-7.33E-04	-2.16E-04	-5.23E-05	-4.74E-06	3.54E-07
10	471	1.73E-06	-2.47E-05	-2.53E-05	-5.58E-04	5.74E-05	-4.03E-05	-4.74E-06	4.27E-06
10	956	-5.22E-05	-4.09E-05	-3.36E-05	-4.60E-04	-1.73E-04	-3.28E-07	-9.29E-06	4.27E-06
10	955	-7.15E-05	-1.10E-04	-5.60E-05	-8.38E-04	-2.48E-04	-1.24E-05	-9.29E-06	3.54E-07

TABLE: Element Deformations - Links							
Link	LinkElem	U1	U2	U3	R1	R2	R3
Text	Text	mm	mm	mm	Radians	Radians	Radians
3	1978	0.00015	0.00042	0.00151	-0.01640	-0.00001	-0.00027
7	1	0.00696	-0.00009	-0.18239	-0.00002	0.00005	0.00069
8	2	0.00240	-0.00011	-0.18205	0.00000	0.00016	-0.00063
9	3	0.01159	-0.00010	-0.18211	-0.00001	0.00049	-0.00020
12	1984	0.00023	0.00121	0.00031	-0.00018	-0.00080	-0.00188
13	4	-0.00003	-0.00502	-0.17551	-0.00015	-0.00012	-0.00006
14	5	0.01232	-0.00504	-0.17799	-0.00011	0.00060	-0.00059
15	6	0.00466	-0.00507	-0.18032	-0.00013	0.00005	0.00170
19	7	0.00399	0.21367	-0.17374	0.00018	0.00005	-0.00119
20	8	0.01392	0.21368	-0.17047	0.00016	0.00001	-0.00014
21	9	0.01959	0.21370	-0.16718	0.00018	-0.00015	-0.00071
22	10	-0.00002	0.00409	-0.16110	0.00004	-0.00004	0.00152
23	11	0.00839	0.00088	-0.16184	-0.00011	0.00006	0.00353
178	74	0.00492	0.00043	0.00047	-0.00005	0.00003	0.00018
179	75	-0.00001	0.00044	-0.18186	-0.00003	-0.00007	0.00011

APPENDIX F
SDI CALCULATION EXCEL WORKSHEETS

The computed values for the diaphragm stiffness using the SDI equations are presented in Chapter 4, Section 4.5.1. The calculation sheets used to compute the stiffness of the diaphragm are presented in this Appendix.

Calcul de la résistance et de la rigidité des diaphragmes selon le "SDI Diaphragm Design Manual 2nd ed.", par R. Tremblay, 4 février 2001								
Attention: les calculs sont faits en SI : se conformer aux unités spécifiées					SDI 38-76-6-NS-M			
Entrer les valeurs des paramètres en caractères gras de couleur bleue								
Des valeurs de résistance de connecteurs sont suggérées sur le côté (selon la valeur de t spécifiée)								
Des valeurs de I_x et de x_c sont aussi suggérées sur le côté								
Acier								
Épaisseur de l'acier	tt	0.72	mm			I_x (mm⁴/m)		
Limite élastique de l'acier (pour calcul de Q_f des vis selon SDI)	F_y	230	MPa		t (mm)	P3615	P2436	
Résistance ultime de l'acier (pour calcul de Q_f des soudures selon SDI)	F_u	310	MPa		0.76	214000	1001000	
Module d'Young	E	195520	MPa		0.91	258000	1189000	
Tablier					1.22	359000	1718000	
Profondeur du tablier	hh	38.1	mm		1.52	445000	2213000	
Largeur de l'âme (mesurée sur le plan incliné)	ww	40.16	mm					
Pas du tablier (pitch)	dd	152.4	mm					
Demi-largeur de la semelle inférieure	ee	19.05	mm			Connecteurs à la structure	Q_f (kN)	S_f (mm/kN)
Largeur de la semelle supérieure	ff	88.9	mm		Soudure	13 mm	5.89	0.0390
Projection horizontale de l'âme	gg	12.7	mm			16 mm	7.45	0.0390
Développée de l'acier par nervure	ss	207.32	mm			19 mm	9.01	0.0390
Largeur des feuilles de tablier	w_f	914	mm			Rond 1.52 x 10 mm - 410X0	12.61	0.0390
Longueur des feuilles de tablier	LL	6096	mm			Rond 1.52 x 10 mm - 480X0	13.67	0.0390
Nombre de poutrelles intermédiaires	np	3			Vis	#12 SDS14	4.38	0.0441
Espacement des poutrelles	Lv	1524	mm		Clous	HILTI DNP2-21 L15	6.83	0.0424
Moment d'inertie de la section effective (flexion sous charge de gravité)	I_x	214000	mm⁴/m			HILTI DNP3-21 L15	6.83	0.0424
Connecteurs						HILTI DNKC	6.00	0.0529
Résistance des connecteurs à la structure (voir ci-contre)	Q_f	0.0529	kN			Ramset 28SD	6.76	0.0848
Flexibilité des connecteurs à la structure (voir ci-contre)	S_f	0.0529	mm/kN					
Résistance des connecteurs de couture (voir ci-contre)	Q_s	2.37	kN			Connecteurs de couture	Q_s (kN)	S_s (mm/kN)
Flexibilité des connecteurs de couture (voir ci-contre)	S_s	0.1017	mm/kN		Soudure	16 mm	4.42	0.0424
Nombre de nervures entre les connecteurs à la structure aux bouts des feuilles	n_pas	2			Pincements		0.86	1.0175
$\Sigma(x_n/w)$ sur les poutrelles de bout (sur w, incluant les connecteurs en rive)	α_1	1.333			Vis	#8	2.37	0.1017
$\Sigma(x_n/w)$ sur les poutrelles intermédiaires (sur w, incluant les connecteurs en rive)	α_2	1.333				#10	2.71	0.1017
$\Sigma(x_n/w)^2$ sur les poutrelles de bout (sur w, incluant les connecteurs en rive)	$\Sigma(x_n/w)^2$	0.556				#12	3.06	0.1017
$\Sigma(x_n/w)^2$ sur les poutrelles intermédiaires (sur w, incluant les connecteurs en rive)	$\Sigma(x_n/w)^2$	0.556				#14	3.59	0.1017
Nombre de connecteurs de bout (sur w, incluant les connecteurs en rive)	n_v	3.5						
Nombre de connecteurs à la structure en rive (total sur LL, excluant ceux sur poutrelles int.)	n_s	16				Tablier - Connecteurs	$\Sigma(x_n/w)$	$\Sigma(x_n/w)^2$
Nombre de connecteurs de couture (total sur LL, excluant ceux sur poutrelles int.)	n_s	16				P3615 - 3/7	1.000	0.500
						P3615 - 4/7	1.333	0.556
Resistance						P3615 - 5/7	1.667	0.722
Facteur de coin	λ	0.814				P3615 - 7/7	2.000	0.778
Facteur B	B	722.270				P2436 - 3/5	1.000	0.500
Résistance du panneau de bout	S_u	0.20	kN/m			P2436 - 5/5	1.500	0.625
Résistance du panneau intermédiaire	S_u	6.27	kN/m					
Résistance basée sur le connecteur de coin	S_u	0.20	kN/m					
Résistance limitée sur le voilement du tablier	S_u	30.23	kN/m					
Résistance ultime	**min S_u**	**0.20**	**kN/m**					
F.S. = 2.0 pour S_u, et 2.35 (2.75 si soudures) pour S_u								
Flexibilité et rigidité								
Flexibilité due à la déformation en cisaillement de l'acier	Fs	0.0251	mm/kN	8%				
Flexibilité due au gauchissement du tablier (paramètre Dn)	Fn	0.2565	mm/kN	82%				
Flexibilité due à la déformation des connecteurs (paramètre C)	Fslip	0.0303	mm/kN	10%				
Flexibilité	**F**	**0.3120**	**mm/kN**					
Rigidité	**G'**	**3.206**	**kN/mm**					
	Calcul du paramètre Dn:							
	WT	4079953						
	WB	454412						
	PW	1.636821						
	AAA	0.428571						
	D_1	167912.6						
	D_2	83956.28						
	D_3	48422.05						
	C_1	0.000155						
	C_2	1.51E-05						
	C_3	7.91E-06						
	C_4	3.57E-06						
	C_5	1.79E-06						
	C_6	4.06E-06						
	D_41	34143.74						
	D_42	196398.2						
	D_43	318208.5						
	D_44	428521.6						
	D_45	720684.6						
	D_46	524895.3						
	G_41	34143.74						
	G_42	576448.5						
	G_43	1779042						
	C_41	1.19E-06						
	C_42	5.37E-06						
	C_43	8.93E-07						
	C_44	2.35E-06						
	D_441	976818						
	D-442	425791.2						
	D_443	1212042						
	D_444	791915.1						
	G_444	3792132						
	DW_1	32600.86						
	DW_2	275200.1						
	DW_3	566217.1						
	DW_4	905193.6						
	PHI	0.8						
	Dn	45.14437						
	CCC	4.263124						

Figure F1: SDI 38-76-6-NS-M calculation sheet

Calcul de la résistance et de la rigidité des diaphragmes selon le "SDI Diaphragm Design Manual 2ième ed.", par R. Tremblay, 4 février 2001										
Attention: les calculs sont faits en SI : se conformer aux unités spécifiées						SDI 38-91-6-NS-M				
Entrer les valeurs des paramètres en caractères gras de couleur bleue										
Des valeurs de résistance de connecteurs sont suggérées sur le côté (selon la valeur de t spécifiée)										
Des valeurs de I_x et de x_o sont aussi suggérées sur le côté										
Acier										
Épaisseur de l'acier	tt	0.905	mm				I_x (mm⁴/m)			
Limite élastique de l'acier (pour calcul de Q_t des vis selon SDI)	F_y	230	MPa			t (mm)	P3615	P2436		
Résistance ultime de l'acier (pour calcul de Q_t des soudures selon SDI)	F_u	310	MPa			0.76	214000	1001000		
Module d'Young	E	197000	MPa			0.91	258000	1189000		
Tablier						1.22	359000	1718000		
Profondeur du tablier	hh	38.1	mm			1.52	445000	2213000		
Largeur de l'âme (mesurée sur le plan incliné)	ww	40.16	mm							
Pas du tablier (pitch)	dd	152.4	mm							
Demi-largeur de la semelle inférieure	ee	19.05	mm			Connecteurs à la structure		Q_t (kN)	S_t (mm/kN)	
Largeur de la semelle supérieure	ff	88.9	mm			Soudure	13 mm	7.28	0.0348	
Projection horizontale de l'âme	gg	12.7	mm				16 mm	9.25	0.0348	
Développée de l'acier par nervure	ss	207.32	mm				19 mm	11.21	0.0348	
Largeur des feuilles de tablier	w_f	914	mm				Rond. 1.52 x 10 mm - 410XX	17.91	0.0348	
Longueur des feuilles de tablier	LL	6096	mm				Rond. 1.52 x 10 mm - 480XX	19.39	0.0348	
Nombre de poutrelles intermédiaires	np	3				Vis	#12 ou #14	5.51	0.0393	
Espacement des poutrelles	Lv	1524	mm			Clous	Hilti ENP2-21-L15	8.30	0.0378	
Moment d'inertie de la section effective (flexion sous charge de gravité)	I_x	214000	mm⁴/m				Hilti ENP3-21-L15	8.30	0.0378	
Connecteurs							Hilti ENICK	9.36	0.0472	
Résistance des connecteurs à la structure (voir ci-contre)	Q_t	6.41	kN				Ramset 26SD	8.14	0.0756	
Flexibilité des connecteurs à la structure (voir ci-contre)	S_t	0.0472	mm/kN							
Résistance des connecteurs de couture (voir ci-contre)	Q_s	2.37	kN			Connecteurs de couture		Q_s (kN)	S_s (mm/kN)	
Flexibilité des connecteurs de couture (voir ci-contre)	S_s	0.0908	mm/kN			Soudure	16 mm	5.46	0.0378	
Nombre de nervures entre les connecteurs à la structure aux bouts des feuilles	n_pas	2				Pincements		1.36	0.9075	
$\Sigma(x_e/w)$ sur les poutrelles de bout (sur w, incluant les connecteurs en rive)	α_1	1.333				Vis	#8	2.98	0.0908	
$\Sigma(x_e/w)$ sur les poutrelles intermédiaires (sur w, incluant les connecteurs en rive)	α_2	1.333					#10	3.40	0.0908	
$\Sigma(x_e/w)^2$ sur les poutrelles de bout (sur w, incluant les connecteurs en rive)	$\Sigma(x_e/w)^2$	0.556					#12	3.85	0.0908	
$\Sigma(x_e/w)^2$ sur les poutrelles intermédiaires (sur w, incluant les connecteurs en rive)	$\Sigma(x_e/w)^2$	0.556					#14	4.51	0.0908	
Nombre de connecteurs de bout (sur w, incluant les connecteurs en rive)	n_v	3.5								
Nombre de connecteurs à la structure en rive (total sur LL, excluant ceux sur poutrelles int.)	n_e	16					Tablier - Connecteurs	$\Sigma(x_e/w)$	$\Sigma(x_e/w)^2$	
Nombre de connecteurs de couture (total sur LL, excluant ceux sur poutrelles int.)	n_s	16					P3615 - 3/7	1.000	0.500	
							P3615 - 4/7	1.333	0.556	
Resistance							P3615 - 5/7	1.667	0.722	
Facteur de coin	λ	0.834					P3615 - 7/7	2.000	0.778	
Facteur B	B	11.476					P2436 - 3/5	1.000	0.500	
Résistance du panneau de bout	S_b	23.83	kN/m				P2436 - 5/5	1.500	0.625	
Résistance du panneau intermédiaire	S_m	11.72	kN/m							
Résistance basée sur le connecteur de coin	S_c	10.83	kN/m							
Résistance limitée sur le voilement du tablier	S_v	35.88	kN/m							
Résistance ultime	**min S_u**	**10.83**	**kN/m**							
F.S. = 2.0 pour S_v et 2.35 (2.75 si soudures) pour S_u										
Flexibilité et rigidité										
Flexibilité due à la déformation en cisaillement de l'acier	Fs	0.0198	mm/kN	10%						
Flexibilité due au gauchissement du tablier (paramètre Dn)	Fn	0.1437	mm/kN	75%						
Flexibilité due à la déformation des connecteurs (paramètre C)	Fslip	0.0270	mm/kN	14%						
Flexibilité	**F**	**0.1906**	**mm/kN**							
Rigidité	**G'**	**5.247**	**kN/mm**							
	Calcul du paramètre Dn:									
	WT	4079953								
	WB	454412								
	PW	1.161521								
	AAA	0.428571								
	D_1	167912.6								
	D_2	83956.28								
	D_3	48422.05								
	C_1	0.000155								
	C_2	1.51E-05								
	C_3	7.91E-06								
	C_4	3.57E-06								
	C_5	1.79E-06								
	C_6	4.06E-06								
	D_41	34143.74								
	D_42	196398.2								
	D_43	318208.5								
	D_44	428521.6								
	D_45	720684.6								
	D_46	524895.3								
	G_41	34143.74								
	G_42	576448.5								
	G_43	1779042								
	C_41	1.19E-06								
	C_42	5.37E-06								
	C_43	8.93E-07								
	C_44	2.35E-06								
	D_441	976818								
	D-442	425791.2								
	D_443	1212042								
	D_444	791915.1								
	G_444	3792132								
	DW_1	23134.23								
	DW_2	195287.5								
	DW_3	401799								
	DW_4	642343.5								
	PHI	0.8								
	Dn	32.03535								
	CCC	4.815718								

Figure F2: SDI 38-91-6-NS-M calculation sheet

Calcul de la résistance et de la rigidité des diaphragmes selon le "SDI Diaphragm Design Manual 2nd ed.", par R. Tremblay, 4 février 2001									
Attention: les calculs sont faits en SI ; se conformer aux unités spécifiées						SDI 38-122-6-NS-M			
Entrer les valeurs des paramètres en caractères gras de couleur bleue									
Des valeurs de résistance de connecteurs sont suggérées sur le côté (selon la valeur de t spécifiée)									
Des valeurs de I_x et de x_o sont aussi suggérées sur le côté									
Acier									
Épaisseur de l'acier	tt	1.22	mm				I_x (mm⁴/m)		
Limite élastique de l'acier (pour calcul de Q_f des vis selon SDI)	F_y	230	MPa			t (mm)	P3615	P2436	
Résistance ultime de l'acier (pour calcul de Q_f des soudures selon SDI)	F_u	310	MPa			0.76	214000	1001000	
Module d'Young	E	203000	MPa			0.91	258000	1189000	
Tablier						1.22	359000	1718000	
Profondeur du tablier	hh	38.1	mm			1.52	445000	2213000	
Largeur de l'âme (mesurée sur le plan incliné)	ww	40.16	mm						
Pas du tablier (pitch)	dd	152.4	mm						
Demi-largeur de la semelle inférieure	ee	19.05	mm			Connecteurs à la structure		Q_f (kN)	S_f (mm/kN)
Largeur de la semelle supérieure	ff	88.9	mm			Soudure	13 mm	9.56	0.0300
Projection horizontale de l'âme	gg	12.7	mm				16 mm	12.26	0.0300
Développée de l'acier par nervure	ss	207.32	mm				19 mm	14.85	0.0300
Largeur des feuilles de tablier	w_f	914	mm				Rond. 1.52 x 10 mm - 410XC	28.86	0.0300
Longueur des feuilles de tablier	LL	6096	mm				Rond. 1.52 x 10 mm - 480XC	31.91	0.0300
Nombre de poutrelles intermédiaires	np	3				Vis	#12 et #14	7.43	0.0339
Espacement des poutrelles	Lv	1524	mm			Clous	Hilti ENP2-21-L15	10.55	0.0336
Moment d'inertie de la section effective (flexion sous charge de gravité)	I_x	214000	mm⁴/m				Hilti ENP3-21-L15	10.55	0.0326
Connecteurs							Hilti ENDK	9.51	0.0406
Résistance des connecteurs à la structure (voir ci-contre)	Q_f	9.51	kN				Ramset 26SD	10.15	0.0651
Flexibilité des connecteurs à la structure (voir ci-contre)	S_f	0.0406	mm/kN						
Résistance des connecteurs de couture (voir ci-contre)	Q_s	2.37	kN			Connecteurs de couture		Q_s (kN)	S_s (mm/kN)
Flexibilité des connecteurs de couture (voir ci-contre)	S_s	0.0782	mm/kN			Soudure	16 mm	7.17	0.0326
Nombre de nervures entre les connecteurs à la structure aux bouts des feuilles	n_pas	2				Pincements		2.46	0.7816
$\Sigma(x_g/w)$ sur les poutrelles de bout (sur w, incluant les connecteurs en rive)	α_1	1.333				Vis	#8	4.02	0.0782
$\Sigma(x_g/w)$ sur les poutrelles intermédiaires (sur w, incluant les connecteurs en rive)	α_2	1.333					#10	4.59	0.0782
$\Sigma(x_g/w)^2$ sur les poutrelles de bout (sur w, incluant les connecteurs en rive)	$\Sigma(x_g/w)^2$	0.556					#12	5.19	0.0782
$\Sigma(x_g/w)^2$ sur les poutrelles intermédiaires (sur w, incluant les connecteurs en rive)	$\Sigma(x_g/w)^2$	0.556					#14	6.09	0.0782
Nombre de connecteurs de bout (sur w, incluant les connecteurs en rive)	n_v	3.5							
Nombre de connecteurs à la structure en rive (total sur LL, excluant ceux sur poutrelles int.)	n_s	16					Tablier - Connecteurs	$\Sigma(x_g/w)$	$\Sigma(x_g/w)^2$
Nombre de connecteurs de couture (total sur LL, excluant ceux sur poutrelles int.)	n_s	16					P3615 - 3/7	1.000	0.500
							P3615 - 4/7	1.333	0.556
Resistance							P3615 - 5/7	1.667	0.722
Facteur de coin	λ	0.857					P3615 - 7/7	2.000	0.778
Facteur B	B	9.548					P2436 - 3/5	1.000	0.500
Résistance du panneau de bout	S_u	35.35	kN/m				P2436 - 5/5	1.500	0.625
Résistance du panneau intermédiaire	S_u	14.45	kN/m						
Résistance basée sur le connecteur de coin	S_u	13.78	kN/m						
Résistance limitée sur le voilement du tablier	S_{cr}	44.89	kN/m						
Résistance ultime	min S_u	13.78	kN/m						
F.S. = 2.0 pour S_{cr} et 2.35 (2.75 si soudures) pour S_u									
Flexibilité et rigidité									
Flexibilité due à la déformation en cisaillement de l'acier	Fs	0.0143	mm/kN	14%					
Flexibilité due au gauchissement du tablier (paramètre Dn)	Fn	0.0661	mm/kN	64%					
Flexibilité due à la déformation des connecteurs (paramètre C)	Fslip	0.0233	mm/kN	22%					
Flexibilité	F	0.1037	mm/kN						
Rigidité	G'	9.647	kN/mm						
	Calcul du paramètre Dn:								
	WT	4079953							
	WB	454412							
	PW	0.742096							
	AAA	0.428571							
	D_1	167912.6							
	D_2	83956.28							
	D_3	48422.05							
	C_1	0.000155							
	C_2	1.51E-05							
	C_3	7.91E-06							
	C_4	3.57E-06							
	C_5	1.79E-06							
	C_6	4.06E-06							
	D_41	34143.74							
	D_42	196398.2							
	D_43	318208.5							
	D_44	428521.6							
	D_45	720684.6							
	D_46	524895.3							
	G_41	34143.74							
	G_42	576448.5							
	G_43	1779042							
	C_41	1.19E-06							
	C_42	5.37E-06							
	C_43	8.93E-07							
	C_44	2.35E-06							
	D_441	976818							
	D-442	425791.2							
	D_443	1212042							
	D_444	791915.1							
	G_444	3792132							
	DW_1	14780.47							
	DW_2	124769.2							
	DW_3	256709.5							
	DW_4	410393.5							
	PHI	0.8							
	Dn	20.4674							
	CCC	5.761645							

Figure F3: SDI 38-122-6-NS-M calculation sheet

Calcul de la résistance et de la rigidité des diaphragmes selon le "SDI Diaphragm Design Manual 2nd ed.", par R. Tremblay, 4 février 2001									
Attention: les calculs sont faits en SI : se conformer aux unités spécifiées						SDI 38-151-6-NS-M			
Entrer les valeurs des paramètres en caractères gras de couleur bleue									
Des valeurs de résistance de connecteurs sont suggérées sur le côté (selon la valeur de t spécifiée)									
Des valeurs de I_x et de x_g sont aussi suggérées sur le côté									
Acier									
Épaisseur de l'acier	tt	1.51	mm				I_x (mm⁴/m)		
Limite élastique de l'acier (pour calcul de Q_t des vis selon SDI)	F_y	230	MPa			t (mm)	P3615	P2436	
Résistance ultime de l'acier (pour calcul de Q_t des soudures selon SDI)	F_u	310	MPa			0.76	214000	1001000	
Module d'Young	E	203000	MPa			0.91	258000	1189000	
Tablier						1.22	359000	1718000	
Profondeur du tablier	hh	38.1	mm			1.52	445000	2213000	
Largeur de l'âme (mesurée sur le plan incliné)	ww	40.16	mm						
Pas du tablier (pitch)	dd	152.4	mm						
Demi-largeur de la semelle inférieure	ee	19.05	mm			Connecteurs à la structure		Q_t (kN)	S_t (mm/kN)
Largeur de la semelle supérieure	ff	88.9	mm			Soudure	13 mm	11.53	0.0269
Projection horizontale de l'âme	gg	12.7	mm				16 mm	14.80	0.0269
Développée de l'acier par nervure	ss	207.32	mm				19 mm	18.06	0.0269
Largeur des feuilles de tablier	w_f	914	mm				Rond. 1.52 x 10 mm - 410XC	41.10	0.0269
Longueur des feuilles de tablier	LL	6096	mm				Rond. 1.52 x 10 mm - 480XC	45.77	0.0269
Nombre de poutrelles intermédiaires	np	3				Vis	#12 et #14	9.19	0.0304
Espacement des poutrelles	Lv	1524	mm			Clous	Hilti ENP2-21-L15	12.32	0.0293
Moment d'inertie de la section effective (flexion sous charge de gravité)	I_s	214000	mm⁴/m				Hilti ENP3-21-L15	12.32	0.0293
Connecteurs							Hilti ENKK	11.30	0.0365
Résistance des connecteurs à la structure (voir ci-contre)	Q_t	6.41	kN				Ramset 26SD	11.61	0.0585
Flexibilité des connecteurs à la structure (voir ci-contre)	S_t	0.0365	mm/kN						
Résistance des connecteurs de couture (voir ci-contre)	Q_s	2.37	kN			Connecteurs de couture		Q_s (kN)	S_s (mm/kN)
Flexibilité des connecteurs de couture (voir ci-contre)	S_s	0.0703	mm/kN			Soudure	16 mm	8.65	0.0293
Nombre de nervures entre les connecteurs à la structure aux bouts des feuilles	n_pas	2				Pincements		3.77	0.7026
$\Sigma(x_g/w)$ sur les poutrelles de bout (sur w, incluant les connecteurs en rive)	α_1	1.333				Vis	#8	4.97	0.0703
$\Sigma(x_g/w)$ sur les poutrelles intermédiaires (sur w, incluant les connecteurs en rive)	α_2	1.333					#10	5.68	0.0703
$\Sigma(x_g/w)^2$ sur les poutrelles de bout (sur w, incluant les connecteurs en rive)	$\Sigma(x_g/w)^2$	0.556					#12	6.42	0.0703
$\Sigma(x_g/w)^2$ sur les poutrelles intermédiaires (sur w, incluant les connecteurs en rive)	$\Sigma(x_g/w)^2$	0.556					#14	7.53	0.0703
Nombre de connecteurs de bout (sur w, incluant les connecteurs en rive)	n_v	3.5							
Nombre de connecteurs à la structure en rive (total sur LL, excluant ceux sur poutrelles int.)	n_e	16					Tablier - Connecteurs	$\Sigma(x_g/w)$	$\Sigma(x_g/w)^2$
Nombre de connecteurs de couture (total sur LL, excluant ceux sur poutrelles int.)	n_s	16					P3615 - 3/7	1.000	0.500
							P3615 - 4/7	1.333	0.556
Resistance							P3615 - 5/7	1.667	0.722
Facteur de coin	λ	0.872					P3615 - 7/7	2.000	0.778
Facteur B	B	11.476					P2436 - 3/5	1.000	0.500
Résistance du panneau de bout	S_{u1}	23.83	kN/m				P2436 - 5/5	1.500	0.625
Résistance du panneau intermédiaire	S_{u2}	11.80	kN/m						
Résistance basée sur le connecteur de coin	S_{u3}	10.83	kN/m						
Résistance limitée sur le voilement du tablier	S_{uv}	52.68	kN/m						
Résistance ultime	**min S_u**	**10.83**	**kN/m**						
F.S. = 2.0 pour S_σ et 2.35 (2.75 si soudures) pour S_u									
Flexibilité et rigidité									
Flexibilité due à la déformation en cisaillement de l'acier	Fs	0.0115	mm/kN	16%					
Flexibilité due au gauchissement du tablier (paramètre Dn)	Fn	0.0388	mm/kN	54%					
Flexibilité due à la déformation des connecteurs (paramètre C)	Fslip	0.0209	mm/kN	29%					
Flexibilité	**F**	0.0712	mm/kN						
Rigidité	**G'**	14.036	kN/mm						
	Calcul du paramètre Dn:								
	WT	4079953							
	WB	454412							
	PW	0.538933							
	AAA	0.428571							
	D_1	167912.6							
	D_2	83956.28							
	D_3	48422.05							
	C_1	0.000155							
	C_2	1.51E-05							
	C_3	7.91E-06							
	C_4	3.57E-06							
	C_5	1.79E-06							
	C_6	4.06E-06							
	D_41	34143.74							
	D_42	196398.2							
	D_43	318208.5							
	D_44	428521.6							
	D_45	720684.6							
	D_46	524895.3							
	G_41	34143.74							
	G_42	576448.5							
	G_43	1779042							
	C_41	1.19E-06							
	C_42	5.37E-06							
	C_43	8.93E-07							
	C_44	2.35E-06							
	D_441	976818							
	D-442	425791.2							
	D_443	1212042							
	D_444	791915.1							
	G_444	3792132							
	DW_1	10734.02							
	DW_2	90611.2							
	DW_3	186430.2							
	DW_4	298040.2							
	PHI	0.8							
	Dn	14.86404							
	CCC	6.409956							

Figure F4: SDI 38-151-6-NS-M calculation sheet

Calcul de la résistance et de la rigidité des diaphragmes selon le "SDI Diaphragm Design Manual 2ième ed.", par R. Tremblay, 4 février 2001									
Attention: les calculs sont faits en SI : se conformer aux unités spécifiées						SDI* 38-76-6-NS-M			
Entrer les valeurs des paramètres en caractères gras de couleur bleue									
Des valeurs de résistance de connecteurs sont suggérées sur le côté (selon la valeur de t spécifiée)									
Des valeurs de I_x et de x_e sont aussi suggérées sur le côté									
Acier									
Épaisseur de l'acier	tt	0.72	mm				I_x (mm⁴/m)		
Limite élastique de l'acier (pour calcul de Q_t des vis selon SDI)	F_y	230	MPa			t (mm)	P3615	P2436	
Résistance ultime de l'acier (pour calcul de Q_t des soudures selon SDI)	F_u	310	MPa			0.76	214000	1001000	
Module d'Young	E	195520	MPa			0.91	258000	1189000	
Tablier						1.22	359000	1718000	
Profondeur du tablier	hh	38.1	mm			1.52	445000	2213000	
Largeur de l'âme (mesurée sur le plan incliné)	ww	40.16	mm						
Pas du tablier (pitch)	dd	152.4	mm						
Demi-largeur de la semelle inférieure	ee	19.05	mm			Connecteurs à la structure		Q_t (kN)	S_t (mm/kN)
Largeur de la semelle supérieure	ff	88.9	mm			Soudure	13 mm	5.89	0.0390
Projection horizontale de l'âme	gg	12.7	mm				16 mm	7.45	0.0390
Développée de l'acier par nervure	ss	207.32	mm				19 mm	9.01	0.0390
Largeur des feuilles de tablier	w_f	914	mm				Rond. 1.52 x 10 mm - 410XC	12.61	0.0390
Longueur des feuilles de tablier	LL	6096	mm				Rond. 1.52 x 10 mm - 480XC	13.67	0.0390
Nombre de poutrelles intermédiaires	np	3				Vis	#12 et #14	4.36	0.0441
Espacement des poutrelles	Lv	1524	mm			Clous	Hilti ENP2-21-L15	6.83	0.0424
Moment d'inertie de la section effective (flexion sous charge de gravité)	I_x	214000	mm⁴/m				Hilti ENP2-21-L15	6.83	0.0424
Connecteurs							Hilti ENCK	6.00	0.0529
Résistance des connecteurs à la structure (voir ci-contre)	Q_t	6.41	kN				Ramset 26SD	6.76	0.0848
Flexibilité des connecteurs à la structure (voir ci-contre)	S_t	0.0431	mm/kN						
Résistance des connecteurs de couture (voir ci-contre)	Q_s	2.37	kN			Connecteurs de couture		Q_s (kN)	S_s (mm/kN)
Flexibilité des connecteurs de couture (voir ci-contre)	S_s	0.7407	mm/kN			Soudure	16 mm	4.42	0.0424
Nombre de nervures entre les connecteurs à la structure aux bouts des feuilles	n_pas	2				Pincements		0.86	1.0175
$\Sigma(x_e/w)$ sur les poutrelles de bout (sur w, incluant les connecteurs en rive)	α_1	1.333				Vis	#8	2.37	0.1017
$\Sigma(x_e/w)$ sur les poutrelles intermédiaires (sur w, incluant les connecteurs en rive)	α_2	1.333					#10	2.71	0.1017
$\Sigma(x_e/w)^2$ sur les poutrelles de bout (sur w, incluant les connecteurs en rive)	$\Sigma(x_e/w)^2$	0.556					#12	3.06	0.1017
$\Sigma(x_e/w)^2$ sur les poutrelles intermédiaires (sur w, incluant les connecteurs en rive)	$\Sigma(x_e/w)^2$	0.556					#14	3.59	0.1017
Nombre de connecteurs de bout (sur w, incluant les connecteurs en rive)	n_v	3.5							
Nombre de connecteurs à la structure en rive (total sur LL, excluant ceux sur poutrelles int.)	n_e	16					Tablier - Connecteurs	$\Sigma(x_e/w)$	$\Sigma(x_e/w)^2$
Nombre de connecteurs de couture (total sur LL, excluant ceux sur poutrelles int.)	n_s	16					P3615 - 3/7	1.000	0.500
							P3615 - 4/7	1.333	0.556
Resistance							P3615 - 5/7	1.667	0.722
Facteur de coin	λ	0.814					P3615 - 7/7	2.000	0.778
Facteur B	B	11.476					P2436 - 3/5	1.000	0.500
Résistance du panneau de bout	S_v	23.83	kN/m				P2436 - 5/5	1.500	0.625
Résistance du panneau intermédiaire	S_v	11.68	kN/m						
Résistance basée sur le connecteur de coin	S_u	10.83	kN/m						
Résistance limitée sur le voilement du tablier	S_σ	30.23	kN/m						
Résistance ultime	**min S_u**	**10.83**	**kN/m**						
F.S. = 2.0 pour S_σ et 2.35 (2.75 si soudures) pour S_u									
Flexibilité et rigidité									
Flexibilité due à la déformation en cisaillement de l'acier	Fs	0.0251	mm/kN	7%					
Flexibilité due au gauchissement du tablier (paramètre Dn)	Fn	0.2565	mm/kN	73%					
Flexibilité due à la déformation des connecteurs (paramètre C)	Fslip	0.0674	mm/kN	19%					
Flexibilité	**F**	0.3491	**mm/kN**						
Rigidité	**G'**	2.864	**kN/mm**						
	Calcul du paramètre Dn:								
	WT	4079953							
	WB	454412							
	PW	1.636821							
	AAA	0.428571							
	D_1	167912.6							
	D_2	83956.28							
	D_3	48422.05							
	C_1	0.000155							
	C_2	1.51E-05							
	C_3	7.91E-06							
	C_4	3.57E-06							
	C_5	1.79E-06							
	C_6	4.06E-06							
	D_41	34143.74							
	D_42	196398.2							
	D_43	318208.5							
	D_44	428521.6							
	D_45	720684.6							
	D_46	524895.3							
	G_41	34143.74							
	G_42	576448.5							
	G_43	1779042							
	C_41	1.19E-06							
	C_42	5.37E-06							
	C_43	8.93E-07							
	C_44	2.35E-06							
	D_441	976818							
	D-442	425791.2							
	D_443	1212042							
	D_444	791915.1							
	G_444	3792132							
	DW_1	32600.86							
	DW_2	275200.1							
	DW_3	566217.1							
	DW_4	905193.6							
	PHI	0.8							
	Dn	45.14437							
	CCC	9.492152							

Figure F5: SDI* 38-76-6-NS-M calculation sheet

Calcul de la résistance et de la rigidité des diaphragmes selon le "SDI Diaphragm Design Manual 2ème ed.", par R. Tremblay, 4 février 2001										
Attention: les calculs sont faits en SI : se conformer aux unités spécifiées							SDI* 38-91-6-NS-M			
Entrer les valeurs des paramètres en caractères gras de couleur bleue										
Des valeurs de résistance de connecteurs sont suggérées sur le côté (selon la valeur de t spécifiée)										
Des valeurs de I_x et de x_e sont aussi suggérées sur le côté										
Acier										
Épaisseur de l'acier	tt	0.905	mm					I_x (mm⁴/m)		
Limite élastique de l'acier (pour calcul de Q_f des vis selon SDI)	F_y	230	MPa				t (mm)	P3615	P2436	
Résistance ultime de l'acier (pour calcul de Q_f des soudures selon SDI)	F_u	310	MPa				0.76	214000	1001000	
Module d'Young	E	197000	MPa				0.91	258000	1189000	
Tablier							1.22	359000	1718000	
Profondeur du tablier	hh	38.1	mm				1.52	445000	2213000	
Largeur de l'âme (mesurée sur le plan incliné)	ww	40.16	mm							
Pas du tablier (pitch)	dd	152.4	mm							
Demi-largeur de la semelle inférieure	ee	19.05	mm					Connecteurs à la structure	Q_s (kN)	S_s (mm/kN)
Largeur de la semelle supérieure	ff	88.9	mm				Soudure	13 mm	7.28	0.0348
Projection horizontale de l'âme	gg	12.7	mm					16 mm	9.25	0.0348
Développée de l'acier par nervure	ss	207.32	mm					19 mm	11.21	0.0348
Largeur des feuilles de tablier	w_f	914	mm					Rond. 1.52 x 10 mm - 410XX	17.91	0.0348
Longueur des feuilles de tablier	LL	6096	mm					Rond. 1.52 x 10 mm - 480XX	19.39	0.0348
Nombre de poutrelles intermédiaires	np	3					Vis	#12 et #14	5.51	0.0393
Espacement des poutrelles	Lv	1524	mm				Clous	Hilti ENP2-21-L15	8.30	0.0378
Moment d'inertie de la section effective (flexion sous charge de gravité)	I_x	214000	mm⁴/m					Hilti ENP3-21-L15	8.30	0.0378
Connecteurs								Hilti ENKK	7.36	0.0472
Résistance des connecteurs à la structure (voir ci-contre)	Q_f	6.41	kN					Ramset 26SD	8.14	0.0756
Flexibilité des connecteurs à la structure (voir ci-contre)	S_f	0.041841	mm/kN							
Résistance des connecteurs de couture (voir ci-contre)	Q_s	2.37	kN					Connecteurs de couture	Q_s (kN)	S_s (mm/kN)
Flexibilité des connecteurs de couture (voir ci-contre)	S_s	0.442478	mm/kN				Soudure	16 mm	5.46	0.0378
Nombre de nervures entre les connecteurs à la structure aux bouts des feuilles	n_pas	2					Pincements		1.36	0.9075
$\Sigma(x_e/w)$ sur les poutrelles de bout (sur w, incluant les connecteurs en rive)	α_1	1.333					Vis	#8	2.98	0.0908
$\Sigma(x_e/w)$ sur les poutrelles intermédiaires (sur w, incluant les connecteurs en rive)	α_2	1.333						#10	3.40	0.0908
$\Sigma(x_e/w)^2$ sur les poutrelles de bout (sur w, incluant les connecteurs en rive)	$\Sigma(x_e/w)^2$	0.556						#12	3.85	0.0908
$\Sigma(x_e/w)^3$ sur les poutrelles intermédiaires (sur w, incluant les connecteurs en rive)	$\Sigma(x_e/w)^3$	0.556						#14	4.51	0.0908
Nombre de connecteurs de bout (sur w, incluant les connecteurs en rive)	n_v	3.5								
Nombre de connecteurs à la structure en rive (total sur LL, excluant ceux sur poutrelles int.)	n_s	16						Tablier - Connecteurs	$\Sigma(x_e/w)$	$\Sigma(x_e/w)^2$
Nombre de connecteurs de couture (total sur LL, excluant ceux sur poutrelles int.)	n_s	16						P3615 - 3/7	1.000	0.500
								P3615 - 4/7	1.333	0.556
Resistance								P3615 - 5/7	1.667	0.722
Facteur de coin	λ	0.834						P3615 - 7/7	2.000	0.778
Facteur B	B	11.476						P2436 - 3/5	1.000	0.500
Résistance du panneau de bout	S_u	23.83	kN/m					P2436 - 5/5	1.500	0.625
Résistance du panneau intermédiaire	S_u	11.72	kN/m							
Résistance basée sur le connecteur de coin	S_u	10.83	kN/m							
Résistance limitée sur le voilement du tablier	S_{cr}	35.88	kN/m							
Résistance ultime	min S_u	**10.83**	kN/m							
F.S. = 2.0 pour S_{cr} et 2.35 (2.75 si soudures) pour S_u										
Flexibilité et rigidité										
Flexibilité due à la déformation en cisaillement de l'acier	Fs	0.0198	mm/kN	9%						
Flexibilité due au gauchissement du tablier (paramètre Dn)	Fn	0.1437	mm/kN	65%						
Flexibilité due à la déformation des connecteurs (paramètre C)	Fslip	0.0576	mm/kN	26%						
Flexibilité	F	0.2212	mm/kN							
Rigidité	G'	4.521	kN/mm							
	Calcul du paramètre Dn:									
	WT	4079953								
	WB	454412								
	PW	1.161521								
	AAA	0.428571								
	D_1	167912.6								
	D_2	83956.28								
	D_3	48422.05								
	C_1	0.000155								
	C_2	1.51E-05								
	C_3	7.91E-06								
	C_4	3.57E-06								
	C_5	1.79E-06								
	C_6	4.06E-06								
	D_41	34143.74								
	D_42	196398.2								
	D_43	318208.5								
	D_44	428521.6								
	D_45	720684.6								
	D_46	524895.3								
	G_41	34143.74								
	G_42	578448.5								
	G_43	1779042								
	C_41	1.19E-06								
	C_42	5.37E-06								
	C_43	8.93E-07								
	C_44	2.35E-06								
	D_441	976818								
	D_442	425791.2								
	D_443	1212042								
	D_444	791915.1								
	G_444	3792132								
	DW_1	23134.23								
	DW_2	195287.5								
	DW_3	401799								
	DW_4	642343.5								
	PHI	0.8								
	Dn	32.03535								
	CCC	10.26785								

Figure F6: SDI* 38-91-6-NS-M calculation sheet

Calcul de la résistance et de la rigidité des diaphragmes selon le "SDI Diaphragm Design Manual 2nd ed.", par R. Tremblay, 4 février 2001										
Attention: les calculs sont faits en SI : se conformer aux unités spécifiées						SDI** 38-76-6-NS-M				
Entrer les valeurs des paramètres en caractères gras de couleur bleue										
Des valeurs de résistance de connecteurs sont suggérées sur le côté (selon la valeur de t spécifiée)										
Des valeurs de I_x et de x_s sont aussi suggérées sur le côté										
Acier										
Épaisseur de l'acier	tt	0.72	mm				I_x (mm⁴/m)			
Limite élastique de l'acier (pour calcul de Q_t des vis selon SDI)	F_y	230	MPa			t (mm)	P3615	P2436		
Résistance ultime de l'acier (pour calcul de Q_t des soudures selon SDI)	F_u	310	MPa			0.76	214000	1001000		
Module d'Young	E	195520	MPa			0.91	258000	1189000		
Tablier						1.22	359000	1718000		
Profondeur du tablier	hh	38.1	mm			1.52	445000	2213000		
Largeur de l'âme (mesurée sur le plan incliné)	ww	40.16	mm							
Pas du tablier (pitch)	dd	152.4	mm							
Demi-largeur de la semelle inférieure	ee	19.05	mm				Connecteurs à la structure		Q_t (kN)	S_t (mm/kN)
Largeur de la semelle supérieure	ff	88.9	mm			Soudure	13 mm		5.89	0.0390
Projection horizontale de l'âme	gg	12.7	mm				16 mm		7.45	0.0390
Développée de l'acier par nervure	ss	207.32	mm				19 mm		9.01	0.0390
Largeur des feuilles de tablier	w_f	914	mm				Rond: 1.52 x 10 mm - 410XC		12.61	0.0390
Longueur des feuilles de tablier	LL	6096	mm				Rond: 1.52 x 10 mm - 480XC		13.67	0.0390
Nombre de poutrelles intermédiaires	np	3					Vis #12 x #14		4.38	0.0441
Espacement des poutrelles	Lv	1524	mm				Clous Hilti ENP2-21-L15		6.83	0.0424
Moment d'inertie de la section effective (flexion sous charge de gravité)	I_x	214000	mm⁴/m				Hilti ENP3-21-L15		6.83	0.0424
Connecteurs							Hilti ENRK		6.00	0.0529
Résistance des connecteurs à la structure (voir ci-contre)	Q_t	6.41	kN				Ramset 368D		6.76	0.0848
Flexibilité des connecteurs à la structure (voir ci-contre)	S_t	0.03125	mm/kN							
Résistance des connecteurs de couture (voir ci-contre)	Q_s	2.37	kN				Connecteurs de couture		Q_s (kN)	S_s (mm/kN)
Flexibilité des connecteurs de couture (voir ci-contre)	S_s	0.086207	mm/kN			Soudure	16 mm		4.42	0.0424
Nombre de nervures entre les connecteurs à la structure aux bouts des feuilles	n_pas	2				Pincements			0.86	1.0175
$\Sigma(x_s/w)$ sur les poutrelles de bout (sur w, incluant les connecteurs en rive)	α_1	1.333				Vis	#8		2.37	0.1017
$\Sigma(x_s/w)$ sur les poutrelles intermédiaires (sur w, incluant les connecteurs en rive)	α_2	1.333					#10		2.71	0.1017
$\Sigma(x_s/w)^2$ sur les poutrelles de bout (sur w, incluant les connecteurs en rive)	$\Sigma(x_s/w)^2$	0.556					#12		3.06	0.1017
$\Sigma(x_s/w)^2$ sur les poutrelles intermédiaires (sur w, incluant les connecteurs en rive)	$\Sigma(x_s/w)^2$	0.556					#14		3.59	0.1017
Nombre de connecteurs de bout (sur w, incluant les connecteurs en rive)	n_v	3.5								
Nombre de connecteurs à la structure en rive (total sur LL, excluant ceux sur poutrelles int.)	n_s	16					Tablier - Connecteurs		$\Sigma(x_s/w)$	$\Sigma(x_s/w)^2$
Nombre de connecteurs de couture (total sur LL, excluant ceux sur poutrelles int.)	n_s	16					P3615 - 3/7		1.000	0.500
							P3615 - 4/7		1.333	0.556
Resistance							P3615 - 5/7		1.667	0.722
Facteur de coin	λ	0.814					P3615 - 7/7		2.000	0.778
Facteur B	B	11.476					P2436 - 3/5		1.000	0.500
Résistance du panneau de bout	S_b	23.83	kN/m				P2436 - 5/5		1.500	0.625
Résistance du panneau intermédiaire	S_u	11.68	kN/m							
Résistance basée sur le connecteur de coin	S_u	10.83	kN/m							
Résistance limitée sur le voilement du tablier	S_{cr}	30.23	kN/m							
Résistance ultime	**min S_u**	**10.83**	**kN/m**							
F.S. = 2.0 pour S_{cr} et 2.35 (2.75 si soudures) pour S_u										
Flexibilité et rigidité										
Flexibilité due à la déformation en cisaillement de l'acier	Fs	0.0251	mm/kN	8%						
Flexibilité due au gauchissement du tablier (paramètre Dn)	Fn	0.2565	mm/kN	84%						
Flexibilité due à la déformation des connecteurs (paramètre C)	Fslip	0.0228	mm/kN	7%						
Flexibilité	**F**	0.3045	**mm/kN**							
Rigidité	**G'**	3.284	**kN/mm**							
	Calcul du paramètre Dn:									
	WT	4079953								
	WB	454412								
	PW	1.636821								
	AAA	0.428571								
	D_1	167912.6								
	D_2	83956.28								
	D_3	48422.05								
	C_1	0.000155								
	C_2	1.51E-05								
	C_3	7.91E-06								
	C_4	3.57E-06								
	C_5	1.79E-06								
	C_6	4.06E-06								
	D_41	34143.74								
	D_42	196396.2								
	D_43	318208.5								
	D_44	428521.6								
	D_45	720684.6								
	D_46	524895.3								
	G_41	34143.74								
	G_42	576448.5								
	G_43	1779042								
	C_41	1.19E-06								
	C_42	5.37E-06								
	C_43	8.93E-07								
	C_44	2.35E-06								
	D_441	976818								
	D-442	425791.2								
	D_443	1212042								
	D_444	791915.1								
	G_444	3792132								
	DW_1	32600.86								
	DW_2	275200.1								
	DW_3	566217.1								
	DW_4	905193.6								
	PHI	0.8								
	Dn	45.14437								
	CCC	3.212793								

Figure F7: SDI 38-76-6-NS-M calculation sheet**

Calcul de la résistance et de la rigidité des diaphragmes selon le "SDI Diaphragm Design Manual 2ième ed.", par R. Tremblay, 4 février 2001										
Attention: les calculs sont faits en SI : se conformer aux unités spécifiées						SDI** 38-91-6-NS-M				
Entrer les valeurs des paramètres en caractères gras de couleur bleue										
Des valeurs de résistance de connecteurs sont suggérées sur le côté (selon la valeur de t spécifiée)										
Des valeurs de I_x et de x_n sont aussi suggérées sur le côté										
Acier										
Épaisseur de l'acier	tt	0.905	mm				I_x (mm⁴/m)			
Limite élastique de l'acier (pour calcul de Q_t des vis selon SDI)	F_y	230	MPa			t (mm)	P3615	P2436		
Résistance ultime de l'acier (pour calcul de Q_t des soudures selon SDI)	F_u	310	MPa			0.76	214000	1001000		
Module d'Young	E	197000	MPa			0.91	258000	1189000		
Tablier						1.22	359000	1718000		
Profondeur du tablier	hh	38.1	mm			1.52	445000	2213000		
Largeur de l'âme (mesurée sur le plan incliné)	ww	40.16	mm							
Pas du tablier (pitch)	dd	152.4	mm							
Demi-largeur de la semelle inférieure	ee	19.05	mm				Connecteurs à la structure		Q_t (kN)	S_t (mm/kN)
Largeur de la semelle supérieure	ff	88.9	mm			Soudure	13 mm		7.28	0.0348
Projection horizontale de l'âme	gg	12.7	mm				16 mm		9.25	0.0348
Développée de l'acier par nervure	ss	207.32	mm				19 mm		11.21	0.0348
Largeur des feuilles de tablier	w_f	914	mm				Rond. 1.52 x 10 mm - 410XC		17.91	0.0348
Longueur des feuilles de tablier	LL	6096	mm				Rond. 1.52 x 10 mm - 480XC		19.59	0.0348
Nombre de poutrelles intermédiaires	np	3				Vis	#12 or #14		5.51	0.0393
Espacement des poutrelles	Lv	1524	mm			Clous	Hilti ENP2-21-L15		8.30	0.0378
Moment d'inertie de la section effective (flexion sous charge de gravité)	I_x	214000	mm⁴/m				Hilti ENP3-21-L15		8.30	0.0378
Connecteurs							Hilti ENKK		7.36	0.0472
Résistance des connecteurs à la structure (voir ci-contre)	Q_t	6.41	kN				Ramset 26SD		8.14	0.0756
Flexibilité des connecteurs à la structure (voir ci-contre)	S_t	0.03125	mm/kN							
Résistance des connecteurs de couture (voir ci-contre)	Q_s	2.37	kN				Connecteurs de couture		Q_s (kN)	S_s (mm/kN)
Flexibilité des connecteurs de couture (voir ci-contre)	S_s	0.068027	mm/kN			Soudure	16 mm		5.46	0.0378
Nombre de nervures entre les connecteurs à la structure aux bouts des feuilles	n_pas	2				Pincements			1.36	0.9075
$\Sigma(x_n/w)$ sur les poutrelles de bout (sur w, incluant les connecteurs en rive)	α_1	1.333				Vis	#8		2.98	0.0908
$\Sigma(x_n/w)$ sur les poutrelles intermédiaires (sur w, incluant les connecteurs en rive)	α_2	1.333					#10		3.40	0.0908
$\Sigma(x_n/w)^2$ sur les poutrelles de bout (sur w, incluant les connecteurs en rive)	$\Sigma(x_n/w)^2$	0.556					#12		3.85	0.0908
$\Sigma(x_n/w)^2$ sur les poutrelles intermédiaires (sur w, incluant les connecteurs en rive)	$\Sigma(x_n/w)^2$	0.556					#14		4.51	0.0908
Nombre de connecteurs de bout (sur w, incluant les connecteurs en rive)	n_r	3.5								
Nombre de connecteurs à la structure en rive (total sur LL, excluant ceux sur poutrelles int.)	n_e	16					Tablier - Connecteurs		$\Sigma(x_n/w)$	$\Sigma(x_n/w)^2$
Nombre de connecteurs de couture (total sur LL, excluant ceux sur poutrelles int.)	n_s	16					P3615 - 3/7		1.000	0.500
							P3615 - 4/7		1.333	0.556
Resistance							P3615 - 5/7		1.667	0.722
Facteur de coin	λ	0.834					P3615 - 7/7		2.000	0.778
Facteur B	B	11.476					P2436 - 3/5		1.000	0.500
Résistance du panneau de bout	S_u	23.83	kN/m				P2436 - 5/5		1.500	0.625
Résistance du panneau intermédiaire	S_u	11.72	kN/m							
Résistance basée sur le connecteur de coin	S_u	10.83	kN/m							
Résistance limitée sur le voilement du tablier	S_σ	35.88	kN/m							
Résistance ultime	**min S_u**	**10.83**	**kN/m**							
F.S. = 2.0 pour S_σ et 2.35 (2.75 si soudures) pour S_u										
Flexibilité et rigidité										
Flexibilité due à la déformation en cisaillement de l'acier	Fs	0.0198	mm/kN	11%						
Flexibilité due au gauchissement du tablier (paramètre Dn)	Fn	0.1437	mm/kN	79%						
Flexibilité due à la déformation des connecteurs (paramètre C)	Fslip	0.0195	mm/kN	11%						
Flexibilité	**F**	**0.1831**	**mm/kN**							
Rigidité	**G'**	**5.462**	**kN/mm**							
	Calcul du paramètre Dn:									
	WT	4079953								
	WB	454412								
	PW	1.161521								
	AAA	0.428571								
	D_1	167912.6								
	D_2	83956.28								
	D_3	48422.05								
	C_1	0.000155								
	C_2	1.51E-05								
	C_3	7.91E-06								
	C_4	3.57E-06								
	C_5	1.79E-06								
	C_6	4.06E-06								
	D_41	34143.74								
	D_42	196398.2								
	D_43	318208.5								
	D_44	428521.6								
	D_45	720684.6								
	D_46	524895.3								
	G_41	34143.74								
	G_42	576448.5								
	G_43	1779042								
	C_41	1.19E-06								
	C_42	5.37E-06								
	C_43	8.93E-07								
	C_44	2.35E-06								
	D_441	976818								
	D-442	425791.2								
	D_443	1212042								
	D_444	791915.1								
	G_444	3792132								
	DW_1	23134.23								
	DW_2	195287.5								
	DW_3	401799								
	DW_4	642343.5								
	PHI	0.8								
	Dn	32.03535								
	CCC	3.478489								

Figure F8: SDI 38-91-6-NS-M calculation sheet**

Calcul de la résistance et de la rigidité des diaphragmes selon le "SDI Diaphragm Design Manual 2ème ed.", par R. Tremblay, 4 février 2001										
Attention: les calculs sont faits en SI : se conformer aux unités spécifiées							SDI** 38-122-6-NS-M			
Entrer les valeurs des paramètres en caractères gras de couleur bleue										
Des valeurs de résistance de connecteurs sont suggérées sur le côté (selon la valeur de t spécifiée)										
Des valeurs de I_x et de x_o sont aussi suggérées sur le côté										
Acier										
Épaisseur de l'acier	tt	1.22	mm					I_x (mm⁴/m)		
Limite élastique de l'acier (pour calcul de Q_t des vis selon SDI)	F_y	230	MPa				t (mm)	P3615	P2436	
Résistance ultime de l'acier (pour calcul de Q_t des soudures selon SDI)	F_u	310	MPa				0.76	214000	1001000	
Module d'Young	E	203000	MPa				0.91	258000	1189000	
Tablier							1.22	359000	1718000	
Profondeur du tablier	hh	38.1	mm				1.52	445000	2213000	
Largeur de l'âme (mesurée sur le plan incliné)	ww	40.16	mm							
Pas du tablier (pitch)	dd	152.4	mm							
Demi-largeur de la semelle inférieure	ee	19.05	mm				Connecteurs à la structure		Q_t (kN)	S_t (mm/kN)
Largeur de la semelle supérieure	ff	88.9	mm				Soudure	13 mm	9.56	0.0300
Projection horizontale de l'âme	gg	12.7	mm					16 mm	12.20	0.0300
Développée de l'acier par nervure	ss	207.32	mm					19 mm	14.85	0.0300
Largeur des feuilles de tablier	w_f	914	mm					Rond. 1.52 x 10 mm - 410XX	28.86	0.0300
Longueur des feuilles de tablier	LL	6096	mm					Rond. 1.52 x 10 mm - 480XX	31.91	0.0300
Nombre de poutrelles intermédiaires	np	3					Vis	#12 et #14	7.43	0.0339
Espacement des poutrelles	Lv	1524	mm				Clous	Hilti ENP2-21-L15	10.55	0.0326
Moment d'inertie de la section effective (flexion sous charge de gravité)	I_x	214000	mm⁴/m					Hilti ENP3-21-L15	10.55	0.0326
Connecteurs								Hilti ENDK	9.51	0.0406
Résistance des connecteurs à la structure (voir ci-contre)	Q_t	6.41	kN					Ramset 26SD	10.15	0.0651
Flexibilité des connecteurs à la structure (voir ci-contre)	S_t	0.021459	mm/kN							
Résistance des connecteurs de couture (voir ci-contre)	Q_s	2.37	kN				Connecteurs de couture		Q_s (kN)	S_s (mm/kN)
Flexibilité des connecteurs de couture (voir ci-contre)	S_s	0.053763	mm/kN				Soudure	16 mm	7.17	0.0326
Nombre de nervures entre les connecteurs à la structure aux bouts des feuilles	n_pas	2					Pincements		2.46	0.7816
$\Sigma(x_o/w)$ sur les poutrelles de bout (sur w, incluant les connecteurs en rive)	α_1	1.333					Vis	#8	4.02	0.0782
$\Sigma(x_o/w)$ sur les poutrelles intermédiaires (sur w, incluant les connecteurs en rive)	α_2	1.333						#10	4.59	0.0782
$\Sigma(x_o/w)^2$ sur les poutrelles de bout (sur w, incluant les connecteurs en rive)	$\Sigma(x_o/w)^2$	0.556						#12	5.19	0.0782
$\Sigma(x_o/w)^2$ sur les poutrelles intermédiaires (sur w, incluant les connecteurs en rive)	$\Sigma(x_o/w)^2$	0.556						#14	6.09	0.0782
Nombre de connecteurs de bout (sur w, incluant les connecteurs en rive)	n_v	3.5								
Nombre de connecteurs à la structure en rive (total sur LL, excluant ceux sur poutrelles int.)	n_s	16						Tablier - Connecteurs	$\Sigma(x_o/w)$	$\Sigma(x_o/w)^2$
Nombre de connecteurs de couture (total sur LL, excluant ceux sur poutrelles int.)	n_s	16						P3615 - 3/7	1.000	0.500
								P3615 - 4/7	1.333	0.556
Résistance								P3615 - 5/7	1.667	0.722
Facteur de coin	λ	0.857						P3615 - 7/7	2.000	0.778
Facteur B	B	11.476						P2436 - 3/5	1.000	0.500
Résistance du panneau de bout	S_{ob}	23.83	kN/m					P2436 - 5/5	1.500	0.625
Résistance du panneau intermédiaire	S_{oi}	11.77	kN/m							
Résistance basée sur le connecteur de coin	S_v	10.83	kN/m							
Résistance limitée sur le voilement du tablier	S_o	44.89	kN/m							
Résistance ultime	**min S_u**	**10.83**	**kN/m**							
F.S. = 2.0 pour S_o, et 2.35 (2.75 si soudures) pour S_u										
Flexibilité et rigidité										
Flexibilité due à la déformation en cisaillement de l'acier	Fs	0.0143	mm/kN	15%						
Flexibilité due au gauchissement du tablier (paramètre Dn)	Fn	0.0661	mm/kN	70%						
Flexibilité due à la déformation des connecteurs (paramètre C)	Fslip	0.0147	mm/kN	15%						
Flexibilité	**F**	0.0951	**mm/kN**							
Rigidité	**G'**	10.513	**kN/mm**							
	Calcul du paramètre Dn:									
	WT	4079953								
	WB	454412								
	PW	0.742096								
	AAA	0.428571								
	D_1	167912.6								
	D_2	83956.28								
	D_3	48422.05								
	C_1	0.000155								
	C_2	1.51E-05								
	C_3	7.91E-06								
	C_4	3.57E-06								
	C_5	1.79E-06								
	C_6	4.06E-06								
	D_41	34143.74								
	D_42	196398.2								
	D_43	318208.5								
	D_44	428521.6								
	D_45	720684.6								
	D_46	524895.3								
	G_41	34143.74								
	G_42	576448.5								
	G_43	1779042								
	C_41	1.19E-06								
	C_42	5.37E-06								
	C_43	8.93E-07								
	C_44	2.35E-06								
	D_441	976818								
	D-442	425791.2								
	D_443	1212042								
	D_444	791915.1								
	G_444	3792132								
	DW_1	14780.47								
	DW_2	124769.2								
	DW_3	256709.5								
	DW_4	410393.5								
	PHI	0.8								
	Dn	20.4674								
	CCC	3.647183								

Figure F9: SDI 38-122-6-NS-M calculation sheet**

Des valeurs de résistance de connecteurs sont suggérées sur le côté (selon la valeur de t spécifiée)								
Des valeurs de I_x et de x_e sont aussi suggérées sur le côté								
Acier								
Épaisseur de l'acier	tt	1.51	mm			I_x (mm⁴/m)		
Limite élastique de l'acier (pour calcul de Q_f des vis selon SDI)	F_y	230	MPa		t (mm)	P3615	P2436	
Résistance ultime de l'acier (pour calcul de Q_f des soudures selon SDI)	F_u	310	MPa		0.76	214000	1001000	
Module d'Young	E	203000	MPa		0.91	258000	1189000	
Tablier					1.22	359000	1718000	
Profondeur du tablier	hh	38.1	mm		1.52	445000	2213000	
Largeur de l'âme (mesurée sur le plan incliné)	ww	40.16	mm					
Pas du tablier (pitch)	dd	152.4	mm					
Demi-largeur de la semelle inférieure	ee	19.05	mm			Connecteurs à la structure	Q_f (kN)	S_f (mm/kN)
Largeur de la semelle supérieure	ff	88.9	mm			Soudure 13 mm	11.53	0.0269
Projection horizontale de l'âme	gg	12.7	mm			16 mm	14.80	0.0269
Développée de l'acier par nervure	ss	207.32	mm			19 mm	18.08	0.0269
Largeur des feuilles de tablier	w_f	914	mm			Rond. 1.52 x 10 mm - 410XX	41.10	0.0269
Longueur des feuilles de tablier	LL	6096	mm			Rond. 1.52 x 10 mm - 480XX	45.77	0.0269
Nombre de poutrelles intermédiaires	np	3				Vis #12 et #14	9.19	0.0304
Espacement des poutrelles	Lv	1524	mm			Clous Hilti ENP2-21-L15	12.32	0.0293
Moment d'inertie de la section effective (flexion sous charge de gravité)	I_x	214000	mm⁴/m			Hilti ENP3-21-L15	12.32	0.0293
Connecteurs						Hilti ENKK	11.30	0.0365
Résistance des connecteurs à la structure (voir ci-contre)	Q_f	6.41	kN			Ramset 26SD	11.61	0.0585
Flexibilité des connecteurs à la structure (voir ci-contre)	S_f	0.019881	mm/kN					
Résistance des connecteurs de couture (voir ci-contre)	Q_s	2.37	kN			Connecteurs de couture	Q_s (kN)	S_s (mm/kN)
Flexibilité des connecteurs de couture (voir ci-contre)	S_s	0.04717	mm/kN		Soudure	16 mm	8.65	0.0293
Nombre de nervures entre les connecteurs à la structure aux bouts des feuilles	n_pas	2			Pincements		3.77	0.7026
$\Sigma(x_e/w)$ sur les poutrelles de bout (sur w, incluant les connecteurs en rive)	α_1	1.333			Vis	#8	4.97	0.0703
$\Sigma(x_e/w)$ sur les poutrelles intermédiaires (sur w, incluant les connecteurs en rive)	α_2	1.333				#10	5.68	0.0703
$\Sigma(x_e/w)^2$ sur les poutrelles de bout (sur w, incluant les connecteurs en rive)	$\Sigma(x_e/w)^2$	0.556				#12	6.42	0.0703
$\Sigma(x_e/w)^2$ sur les poutrelles intermédiaires (sur w, incluant les connecteurs en rive)	$\Sigma(x_e/w)^2$	0.556				#14	7.53	0.0703
Nombre de connecteurs de bout (sur w, incluant les connecteurs en rive)	n_v	3.5						
Nombre de connecteurs à la structure en rive (total sur LL, excluant ceux sur poutrelles int.)	n_e	16				Tablier - Connecteurs	$\Sigma(x_e/w)$	$\Sigma(x_e/w)^2$
Nombre de connecteurs de couture (total sur LL, excluant ceux sur poutrelles int.)	n_s	16				P3615 - 3/7	1.000	0.500
						P3615 - 4/7	1.333	0.556
Résistance						P3615 - 5/7	1.667	0.722
Facteur de coin	λ	0.872				P3615 - 7/7	2.000	0.778
Facteur B	B	11.476				P2436 - 3/5	1.000	0.500
Résistance du panneau de bout	S_u	23.83	kN/m			P2436 - 5/5	1.500	0.625
Résistance du panneau intermédiaire	S_u	11.80	kN/m					
Résistance basée sur le connecteur de coin	S_u	10.83	kN/m					
Résistance limitée sur le voilement du tablier	S_u	52.68	kN/m					
Résistance ultime	**min S_u**	**10.83**	**kN/m**					
F.S. = 2.0 pour S_u et 2.35 (2.75 si soudures) pour S_u								
Flexibilité et rigidité								
Flexibilité due à la déformation en cisaillement de l'acier	Fs	0.0115	mm/kN	18%				
Flexibilité due au gauchissement du tablier (paramètre Dn)	Fn	0.0388	mm/kN	61%				
Flexibilité due à la déformation des connecteurs (paramètre C)	Fslip	0.0132	mm/kN	21%				
Flexibilité	**F**	0.0635	**mm/kN**					
Rigidité	**G'**	15.750	**kN/mm**					
	Calcul du paramètre Dn:							
	WT	4079953						
	WB	454412						
	PW	0.538933						
	AAA	0.428571						
	D_1	167912.6						
	D_2	83956.28						
	D_3	48422.05						
	C_1	0.000155						
	C_2	1.51E-05						
	C_3	7.91E-06						
	C_4	3.57E-06						
	C_5	1.79E-06						
	C_6	4.06E-06						
	D_41	34143.74						
	D_42	196398.2						
	D_43	318208.5						
	D_44	428521.6						
	D_45	720684.6						
	D_46	524895.3						
	G_41	34143.74						
	G_42	576448.5						
	G_43	1779042						
	C_41	1.19E-06						
	C_42	5.37E-06						
	C_43	8.93E-07						
	C_44	2.35E-06						
	D_441	976818						
	D-442	425791.2						
	D_443	1212042						
	D_444	791915.1						
	G_444	3792132						
	DW_1	10734.02						
	DW_2	90611.2						
	DW_3	186430.2						
	DW_4	298040.2						
	PHI	0.8						
	Dn	14.86404						
	CCC	4.033796						

Figure F10: SDI 38-151-6-NS-M calculation sheet**